

The energy biology of European Mistletoe  
(*Viscum album*)

Von der Naturwissenschaftlichen Fakultät der  
Gottfried Wilhelm Leibniz Universität Hannover

zur Erlangung des Grades  
Doktorin der Naturwissenschaften (Dr. rer. nat.)

genehmigte Dissertation  
von

Lucie Schröder, M. Sc.

2023

Referent: Prof. Dr. rer. nat. Hans-Peter Braun

Korreferent: Prof. Dr. rer. nat. Helge Küster

Tag der Promotion: 07. September 2023

## Abstract

The hemiparasitic European mistletoe (*Viscum album*) is known for its extraordinary way of life. Not only its huge genome of about 90 Gbp is noticeable, but also the absence of mitochondrial complex I of the Oxidative Phosphorylation system. Since a large genome indicates a high energy demand during cellular division, absence of complex I, which strongly contributes to the proton gradient across the inner mitochondrial membrane and thus to ATP production, is to be considered remarkable. How can *V. album* accomplish its energy metabolism? This is the central research question of this thesis.

To this end, the transcriptome of *V. album* was first sequenced to provide the basis for efficient proteome analysis. RNA was isolated from mistletoe leaves, flowers, and stems harvested in summer and winter. The RNA was next transcribed into cDNA and sequenced as a pooled sample via the PacBio sequencing strategy. The resulting initial *Viscum album* Gene Space (VaGs) database showed 78% completeness based on Benchmarking Universal Single-Copy Orthologs (BUSCO) analysis. To further develop this database, additional Illumina sequencing of the individual samples (summer and winter) was performed. The resulting *Viscum album* Gene Space database II (VaGsII) has a completeness of 93% and contains sequences of 90,039 transcripts. Based on these sequences, a GC content of 50% could be calculated. This is an unusually high GC content, as in other dicotyledonous plants the GC content usually ranges between 43-45 %. Due to the resulting enhanced stability of the DNA, an increased energy requirement must also be anticipated for DNA replication and transcription. In addition to the absence of the mitochondrial genes encoding subunits of complex I, the absence of almost all nuclear genes encoding complex I subunits could be shown. Furthermore, by re-evaluating an existing complexome dataset of *V. album* mitochondria using the new VaGs II database, more than 1,000 additional mitochondrial proteins could be identified with respect to the original evaluation.

Besides the mitochondria, also the chloroplasts were examined in more detail to determine their contribution to the energy metabolism of *V. album* cells through photosynthesis and photophosphorylation. In the course of this examination, a complete absence of the NDH complex (NADH dehydrogenase-like complex, chloroplast pendant of mitochondrial complex I), which contributes to cyclic electron transport around photosystem I, was proven on the proteome level. In addition, PGR5 and PGRL1, two proteins which were shown to be alternatively involved in cyclic electron transport around photosystem I, were found to be of reduced abundance in *V. album* compared to the model plant *Arabidopsis thaliana*. Abundance of the chloroplast ATP synthase complex is comparable to *A. thaliana*; however, its stability clearly is increased in *V. album*. Also, the photosystem II is of similar abundance in *A. thaliana* and *V. album*, in contrast to the photosystem I, which is of comparatively low abundance in *V. album*. It can be concluded that both, linear and cyclic electron transport and thus ATP synthesis by photophosphorylation are comparatively low in *V. album*.

In summary, it can be concluded that: 1. *V. album* has an even higher energy demand than previously thought due to its high GC content. 2. ATP production in mitochondria and chloroplasts is limited due to the absence or reduced abundance of some of the involved proteins and protein complexes.

How sufficient amounts of ATP are provided in *V. album* cells is therefore still not entirely clear. It is hypothesized that the slow growth and reduced cell division rate of *V. album* might reduce its energy demand. In addition, sugar compounds transported in the host xylem in spring may be a source of energy for *V. album*. This may also explain the strong growth rate of *V. album* in spring.

Further research is needed to understand the way of life of this very particular plant.

keywords: energy biology, Gene Space, mitochondria, chloroplasts, proteomic, *Viscum album*

## Zusammenfassung

Die hemiparasitäre europäische Mistel (*Viscum album*) ist für ihre außergewöhnliche Lebensweise bekannt. Auffallend ist nicht nur ihr riesiges Genom von ca. 90 Gbp, sondern auch das Fehlen des mitochondrialen Komplex I des oxidativen Phosphorylierungssystems. Da ein großes Genom einen hohen Energiebedarf während der Zellteilung erfordert, ist die Abwesenheit von Komplex I, welcher stark zum Protonengradienten über die innere mitochondriale Membran und damit zur ATP-Produktion beiträgt, bemerkenswert. Wie kann *V. album* ihren Energiestoffwechsel bewerkstelligen? Dies ist die zentrale Forschungsfrage dieser Arbeit.

Zunächst wurde das Transkriptom von *V. album* sequenziert, um einen soliden Datenhintergrund für die Auswertung von Proteomanalysen zu schaffen. Dazu wurde RNA aus Mistelblättern, -blüten und -stielen, deren Ernte im Sommer oder Winter erfolgte, isoliert. Die RNA wurde dann in cDNA umgeschrieben und als gepoolte Probe mittels der PacBio-Sequenzierungsstrategie analysiert. Eine daraus resultierende erste Sequenzdatenbank, die „*Viscum album* Gene Space“ (VaGs) Datenbank, zeigte, basierend auf „Benchmarking Universal Single-Copy Orthologs“ (BUSCO) Analyse, eine Vollständigkeit von 78 %. Zur Weiterentwicklung dieser Datenbank wurde zusätzlich eine Sequenzierung mittels der Illumina-Technologie für die im Sommer bzw. Winter geernteten Organe der Mistel durchgeführt. Die so entstandene „*Viscum album* Gene Space“ (VaGsII) Datenbank II weist eine Vollständigkeit von 93 % auf und enthält Sequenzen von 90.039 Transkripten. Anhand dieser Sequenzen konnte ein GC-Gehalt von 50 % berechnet werden. Dieser GC-Gehalt ist ungewöhnlich hoch, da bei anderen zweikeimblättrigen Pflanzen der GC-Gehalt normalerweise zwischen 43-45 % liegt. Aufgrund der daraus resultierenden erhöhten Stabilität der DNA muss auch mit einem erhöhten Energiebedarf für die DNA Replikation und Transkription gerechnet werden. Zusätzlich zu dem Fehlen der mitochondrialen Gene, die für Untereinheiten des Komplexes I kodieren, konnte auch das Fehlen fast aller im Zellkern lokalisierten Gene, die für Untereinheiten des Komplexes I kodieren, nachgewiesen werden. Des Weiteren konnten durch eine erneute Auswertung eines bestehenden Complexom Datensets von *V. album* Mitochondrien mithilfe der neuen VaGsII Datenbank über 1.000 zusätzliche Proteine im Vergleich zu der ursprünglichen Auswertung identifiziert werden.

Neben den Mitochondrien wurden auch die Chloroplasten von *V. album* genauer untersucht, um ihren Beitrag zum Energiestoffwechsel der Zellen durch Photophosphorylierung und Photosynthese festzustellen. Dabei wurde die Abwesenheit vom NDH-Komplex (das chloroplastidäre Pendant des mitochondrialen Komplexes I), welcher in Verbindung mit Photosystem I zum zyklischen Elektronentransport beiträgt, auf der Proteomebene nachgewiesen. Zusätzlich wurde festgestellt, dass PGR5 und PGRL1, zwei Proteine, die alternativ am zyklischen Elektronentransport um das Photosystem I beteiligt sind, in *V. album* im Vergleich zur Modellpflanze *Arabidopsis thaliana* in geringerer Menge vorkommen. Die Abundanz des chloroplastidären ATP Synthase Komplex ist vergleichbar mit der in der Modellpflanze *A. thaliana*; seine Stabilität ist jedoch in *V. album* deutlich erhöht. Auch das Photosystem II ist in *A. thaliana* und *V. album* in ähnlicher Menge vorhanden, im Gegensatz zum Photosystem I, welches in *V. album* vergleichsweise wenig vorhanden ist. Daraus lässt sich schließen, dass sowohl der lineare als auch der zyklische Elektronentransport und damit die ATP-Synthese durch Photophosphorylierung in *V. album* vergleichsweise limitiert sind.

Zusammenfassend kann festgestellt werden, dass: 1. *V. album* einen noch höheren Energiebedarf hat als bisher angenommen, aufgrund ihres hohen GC-Gehalts. 2. Die ATP-Produktion in den Mitochondrien und Chloroplasten aufgrund des Fehlens oder der verminderten Häufigkeit einiger Proteine oder Proteinkomplexe limitiert ist.

Wie ATP in ausreichender Menge in den Zellen von *V. album* bereitgestellt wird, ist daher nicht vollständig verstanden. Es wird vermutet, dass das langsame Wachstum und die geringere Zellteilungsrate von *V. album* ihren Energiebedarf reduziert. Darüber hinaus könnten Zuckerverbindungen, die im Frühjahr im Xylem des Wirts transportiert werden, eine Energiequelle für *V. album* darstellen. Dies könnte auch das starke Wachstum von *V. album* im Frühjahr erklären.

Weitere Forschung ist erforderlich, um die Lebensweise dieser sehr besonderen Pflanze noch besser zu verstehen.

Schlagerworte: Energiebiologie, Gene Space, Mitochondrien, Chloroplasten, Proteomik, *Viscum album*

## Contributing publications

The following publications are part of this PhD thesis:

1. Schröder L, Rupp O, Senkler M, Rugen N, Hohnjec N, Goesmann A, Küster H, Braun HP (2023)  
The *Viscum album* Gene Space database  
Frontiers in Plant Science, 14  
<https://doi.org/10.3389/fpls.2023.1193122>
2. Schröder L, Hohnjec N, Senkler M, Senkler J, Küster H, Braun HP (2022)  
The gene space of European mistletoe (*Viscum album*)  
Plant Journal, 109(1), 278-294  
<https://doi.org/10.1111/tpj.15558>
3. Schröder L, Hegermann J, Pille P, Braun HP (2022)  
The photosynthesis apparatus of European mistletoe (*Viscum album*)  
Plant Physiology, 190(3), 1896–1914  
<https://doi.org/10.1093/plphys/kiac377>
4. Schröder L, Eubel H, Braun HP (2022)  
Complexome Profiling of Plant Mitochondrial Fractions  
Methods in Molecular Biology, 2363, 101-110  
[https://10.1007/978-1-0716-1653-6\\_9](https://10.1007/978-1-0716-1653-6_9)
5. Schröder L, Senkler J, Braun, HP (2020)  
Special features of cellular respiration in *Viscum album*  
In: Die Mistel in der Tumorthherapie 5, Scheer R, et al. (eds.), KVC Verlag, Essen, pp 3-13  
ISBN: 978-3-96562-030-8

## Abbreviations

<i>A. thaliana</i>	<i>Arabidopsis thaliana</i>
AOX	alternative oxidase
bp	base pairs
BUSCO	Benchmarking Universal Single-Copy Orthologs
CET	cyclic electron transport
cryoEM	cryoelectron microscopy
ETC	electron transfer chain
FNR	ferredoxin-NADP+ reductase
Gbp	giga base pairs
GLDH	L-galactono-1,4-lactone dehydrogenase
IMM	inner mitochondrial membrane
IMS	intermembrane space
IR	inverted-repeat region
kb	kilo bases
kDa	kilo dalton
LET	linear electron transport
LSC	large single-copy region
mb	mega bases
MDa	mega dalton
ML	mistletoe lectin
MPP	mitochondrial processing peptidase
ND	alternative NADH dehydrogenase
OMM	outer mitochondrial membrane
OXPPOS	oxidative phosphorylation
pg	picogram
PGR5	proton gradient regulation 5
PGRL1	PGR5 like phenotype 1
PSI	photosystem I
PSII	photosystem II
ROS	reactive oxygen species
RubisCO	ribulose-1,5-bisphosphate carboxylase/oxygenase
RuBP	ribulose-1,5-bisphosphate
SDH	succinate dehydrogenase
SSC	small single-copy region
ssp	subspecies
TCA	tricarboxylic acid cycle
<i>V. album</i>	<i>Viscum album</i>
<i>V. coloratum</i>	<i>Viscum coloratum</i>
VaGs	Viscum album Gene Space
VDAC	voltage-dependent anion channel
$\gamma$ CA	gamma carbonic anhydrase

# Contents

Abstract	I
Zusammenfassung	II
Contributing publications	III
Abbreviations	IV
<b>1 Introduction</b>	<b>1</b>
1.1 The Biology of <i>Viscum album</i>	1
1.1.1 General features	1
1.1.2 Lifecycle	3
1.1.3 Specific biochemical compounds of <i>Viscum album</i>	4
1.1.4 Adaptation to the seasons	6
1.2 The Genome of <i>Viscum album</i>	7
1.2.1 The general structure of genomes	7
1.2.2 Insights into <i>Viscum album</i> genetics	7
1.2.3 GC content	8
1.2.4 Sequencing status	8
1.3 The Mitochondrial energy metabolism of <i>Viscum album</i>	9
1.3.1 General structure and function of the OXPHOS system	10
1.3.2 Oligomeric protein complexes and protein supercomplexes	11
1.3.3 The OXPHOS system in <i>Viscum album</i>	11
1.3.4 Evolution of the mitochondrial genome in plant parasites	15
1.4 The Photosynthesis of <i>Viscum album</i>	16
1.4.1 The Photosynthesis in general	16
1.4.2 Photosynthesis of <i>Viscum album</i>	17
1.5 The research topics of this thesis	18
1.6 References	19
<b>2 Publications and Manuscripts</b>	<b>27</b>
2.1 The gene space of European mistletoe ( <i>Viscum album</i> )	28
2.2 The photosynthesis apparatus of European mistletoe ( <i>Viscum album</i> )	51
2.3 Complexome Profiling of Plant Mitochondrial Fractions	78
2.4 Special features of cellular respiration in <i>Viscum album</i>	89
2.5 The <i>Viscum album</i> Gene Space database	102
<b>3 Appendix</b>	<b>114</b>
3.1 Curriculum Vitae	116
3.2 List of Publications	117
3.3 Conference abstracts	118
3.4 Poster Presentations	118

# 1 Introduction

## 1.1 The Biology of *Viscum album*

### 1.1.1 General features

About 100 million years ago, the first flowering plants (angiosperms) developed (Leslie et al. 2021). During their evolution, various nutritional modes proved to be effective. A peculiar but still successful strategy is parasitism, which independently developed twelve times in angiosperms, resulting in over 270 genera and up to 4,500 species, thus accounting for about 1% of all angiosperms (Nickrent 2011, reviewed in Těšitel 2016). Instead of roots, parasitic plants possess haustoria, which are necessary for the connection to the host. Parasitic plants divide into holo- and hemiparasites. Most holoparasitic plants have reduced leaves, succulent stems, extreme modifications of flowers and do not carry out photosynthesis (reviewed in Těšitel 2016, Nickrent 2020).

Hemiparasitic plants, on the other hand, are able to carry out photosynthesis and to produce organic compounds. The efficiency of their photosynthetic activity depends on the host's vitality as well as environmental conditions and can vary within and between species (reviewed in Těšitel 2016).

The probably most prominent hemiparasitic plants are mistletoe species. Mistletoes are widespread nearly all over the world and belong to the order Santalales (derived from its type genus *Santalum*, sandalwood). They are divided into five clades: Misodendraceae, Loranthaceae, Santalaceae, Amphorogynaceae, and Viscaceae (Nickrent 2011). Within these clades, 88 genera and almost 1,600 species evolved. With approximately 1,000 and 550 species, respectively, Loranthaceae and Viscaceae show the highest species diversity (Nickrent 2011). The genus *Viscum*, which belongs to the Viscaceae family, includes the world's most common mistletoes. Species of this genus inhabit the temperate zones of Europe and Asia, as well as the tropical and subtropical regions of Africa, Asia, and Australia (Figure 1). In total, the genus *Viscum* contains about 120 species (Maul et al. 2019). The most prominent *Viscum* species is *Viscum album*, also called "weißbeerige Mistel" in German ("white berry mistletoe") and "European Mistletoe" in English. Its origin is in Europe. However, as a neophyte, *V. album* now is also spreading across Canada and the USA (Maul et al. 2019).

The species *V. album* is divided into four subspecies: *V. album album*, *V. album abietis*, *V. album austriacum*, and *V. album creticum*. Originally, this subspecies division was based on slightly altered morphology and host tree specificity. It was eventually confirmed after sequencing of nuclear ribosomal DNA segments. *V. album creticum* can only be found on the island of Crete and is restricted to the sole pine *Pinus halepensis* ssp. *brutia* as host. *V. album abietis* and *V. album austriacum* are widespread, using fir (*Abies* spp.) and pine (*Pinus* spp.) trees as hosts, respectively. The subspecies *V. album album* also is widespread and shows a remarkably broad host spectrum that includes a broad variety of deciduous trees (Escher 2004, Zuber 2004, Zuber & Widmer 2009).



The occurrence of *V. album* subspecies differs throughout Europe. It seems to not only depend on spreading via birds but also on climate factors. Accordingly, even though *V. album album* and *V. album austriacum* are both widely distributed, only *V. album album* can be found in the further northern regions. It was postulated that this distribution is influenced by the freezing tolerance of seeds, which was shown to be higher in *V. album album* (Tikkanen et al. 2021).

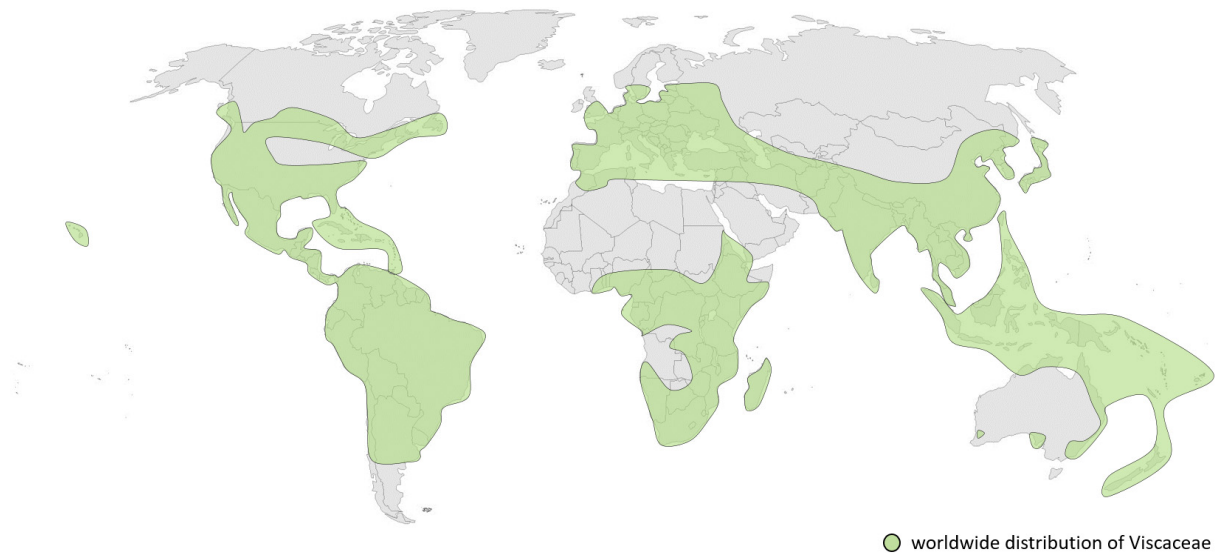


**Figure 1: Worldwide distribution of Viscaceae.**

The green shading on the world map illustrates the global distribution of Viscaceae, according to <https://parasiticplants.siu.edu/Viscaceae/index.html>. In North America, Viscaceae species are distributed throughout the continent, with notable concentrations in the United States, Mexico, and parts of Canada. Viscaceae can be found throughout South America with the exception of the southern parts of the continent. In Europe, Viscaceae species are widely distributed with the exception of the northern regions. Asia exhibits a diverse distribution of Viscaceae, with species occurring in countries like China, Japan, India, and Indonesia. In Africa, Viscaceae can be found mostly on the central and southeastern part of the continent. Australia and the Pacific Islands also have Viscaceae species. In Australia, they can be mainly found in the coastal regions.

Climate change and rising temperature therefore most probably will have a positive influence on further spreading of all *V. album* subspecies in the future. Especially colder regions, like Scandinavia and Russia, could be strongly affected (Tikkanen et al. 2021, Walas et al. 2022). Mistletoes can have negative effects on host trees, which mainly occur with a high population of mistletoe plants on one tree and water shortage, e.g., during summer. However, they should not generally be considered a pest. In fact, mistletoes can have beneficial effects on the ecosystem (Nickrent 2011, Hódar et al. 2018). For many birds, mistletoe berries are an important food source during winter. In addition, some mistletoe species, like *V. album*, are known to shed their leaves without resorbing nutrients. Fallen leaves therefore serve as natural fertilizers for surrounding plants. Consequently, a higher biodiversity in the vegetation beneath the host tree could be observed, associated with an increase in activity and diversity of animals (Hódar et al. 2018). The dwarf mistletoe (*Arceuthobium*) is considered a pathogen

as it deforms conifer host branches forming witches' brooms. Despite the negative effect on the host tree, these deformations provide valuable nesting sites for birds (Nickrent 2011). Since mistletoes are not dominant by biomass or number but still have a disproportionately high influence on the entire ecosystem, they are considered as keystone species (Nickrent 2011).

### 1.1.2 Lifecycle

The lifecycle of *V. album* begins with berry-like fruits, which ripen in winter (Figure 2). They are mainly spread by birds, for whom the fruit is a valuable winter food (Becker 1986, Escher 2004). As the "seeds" of *V. album* do not develop a true ovule, they are botanically defined as embryos (Becker 1986). Birds feeding from the fruits of *V. album* disperse the embryo unharmed (Becker 1986, Escher 2004, Gatzel & Geil 2009). The sticky viscin, a hemicellulose-based polymer in the mesocarp surrounding the embryo supports its attachment to tree branches.

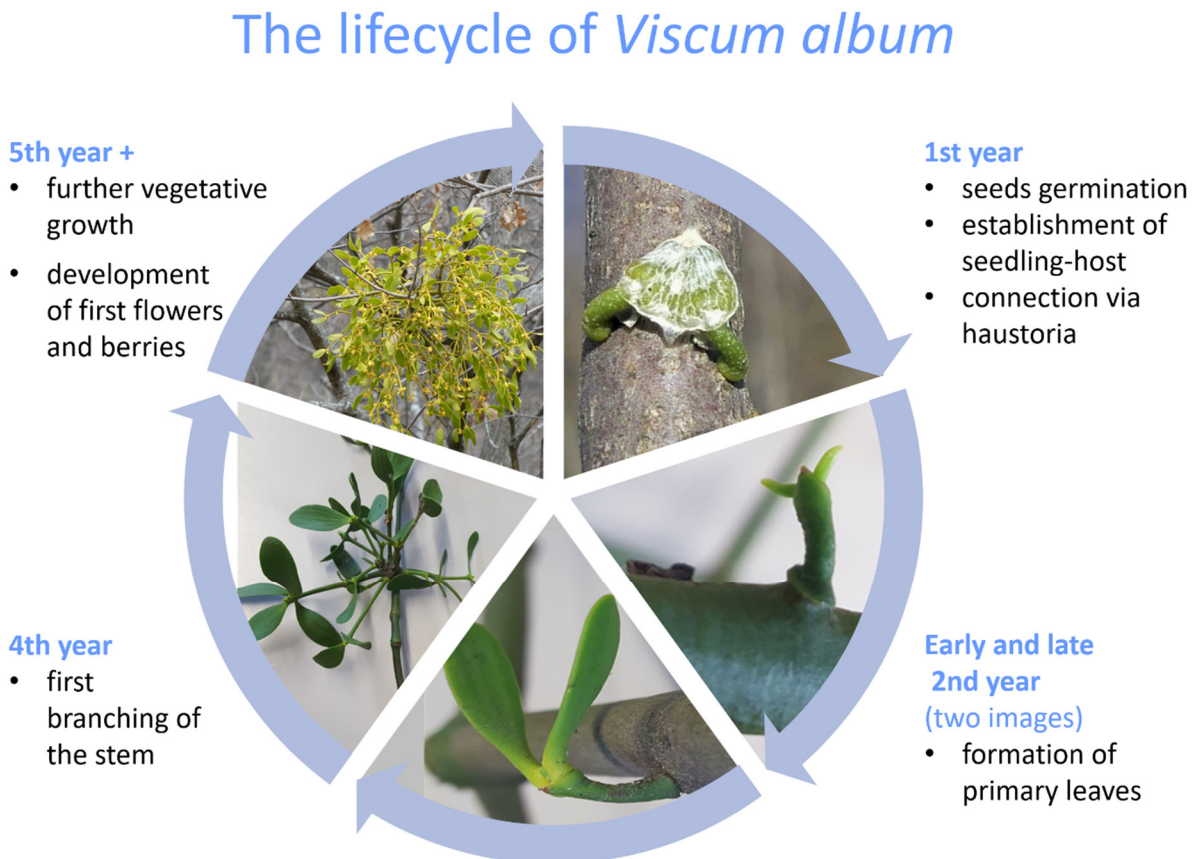


**Figure 2: The lifecycle of *V. album*.**

In the first year after the attachment of *V. album* berries to tree branches, the embryo forms haustoria, which connect to the host xylem. In the second year, primary leaves emerge. The first fork sprout is formed after three to four years. In the following years, flowers and berries develop and every year a new fork sprout is added to each shoot end. The embryos are spread through ornithochory (dispersal by birds). (Pictures: Prof. Dr. Hans-Peter Braun, Lucie Schröder)

In the first year after attachment, the embryo forms haustoria, whose growth is directed by negative phototropism to the branch's surface (**Figure 2**). The haustoria grow into the branch and get connected to the xylem of the tree to get access to water and minerals. In the second year, the first pair of leaves is formed. After three to four years, the first fork sprout is developed. Annually, one fork sprout is added to each shoot end. After approximately five years, mistletoes develop flowers for the first time. The dioecious mistletoe inherits only male or female flowers, which start flowering in the late winter/early spring. Fruit development takes time until the following winter. Overall, the growth rate of *V. album* is very low compared to other plants, most of which can complete their life cycle in less than a year ([Becker 1986](#), [Escher 2004](#), [Gatzel & Geil 2009](#)).

The major growth phase of *V. album* is in spring ([Escher et al. 2004](#), [Zuber 2004](#)). During this season, the host tree remobilizes energy-rich compounds, which were stored in roots and stem during winter. Sugars and amino acids are transported via the host xylem to the upper tree regions, thereby also supplying the connected mistletoes. Hence, new sprouts and leaves are formed during spring; latter remain on the plant for at least 1.5 years. Therefore, at least two generations of leaves are present between spring and August. Those of the past year(s) are recognizable due to their larger size.

During late summer, the leaves of the past year are discarded without recycling of nutrients or proteins, except for the viscotoxins (mistletoe-specific proteins, see chapter 1.1.3), which are remobilized ([Zuber 2004](#)). In some cases, the leaves of the previous years are not discarded but kept for another year ([Zuber 2004](#)).

While seeds of most mistletoe species are spread by birds, the lodgepole pine dwarf mistletoe *Arceuthobium americanum* has developed an alternative spreading mechanism ([deBruyn et al. 2015](#)). During ripening, the berries of this species build up a pressure, which, at a certain point triggered by thermogenesis, explosively discard the seeds. Thereby, the seeds can reach a speed of 100 km/h and can be spread up to 20 meters ([deBruyn et al. 2015](#)).

### 1.1.3 Specific biochemical compounds of *Viscum album*

Also at the molecular level, *V. album* is characterized by numerous peculiarities. Above all, *V. album* is known for very special biochemical compounds, in particular the mistletoe lectins, viscotoxins and viscin ([Zuber 2004](#), [Yousefvand et al. 2022](#)).

Viscin is mainly found in fruits and consists of hemicellulose and cellulose. It is responsible for the stickiness of the fruits and ensures an optimal attachment of the embryo to the host ([Azuma et al. 2000](#), [Horbelt et al. 2022](#)). Earlier in human history, the sticky fruits were used as a trap to catch birds. In fact, the word "viscous" was named after the sticky consistence of the viscin within the mistletoe fruits ([Azuma et al. 2000](#), [Whittingstall 2001](#)). Viscin also is considered as medical glue for injuries. This application is currently explored intensively ([Horbelt et al. 2022](#)).

Viscotoxins are small proteins that serve as protection against pathogens (Ochocka and Piotrowski 2002). Overall, seven different viscotoxins are known to date, termed A1, A2, A3, B, C1, 1-PS, and U-PS (Giudici et al. 2006). The viscotoxin U-PS is assumed to be a transformed variant of 1-PS (Ochocka & Piotrowski 2002). Viscotoxin C1 has not been found in *V. album*, but only in *V. coloratum* (Ochocka & Piotrowski 2002, Romagnoli et al. 2003, Yousefvand et al. 2022). All viscotoxins are composed of 46 amino acids and have a molecular mass of approximately 5 kDa. Their formation is initially based on the biosynthesis of precursors, which have a molecular mass of about 15 kDa. These precursors contain a thionon domain as signal peptide and an acidic domain, both of which are removed during subsequent processing steps (Ochocka & Piotrowski 2002). The concentrations of viscotoxins change during the seasons (Urech et al. 2006, Yousefvand et al. 2022). The highest viscotoxin content can be found in summer (Urech et al. 2006). During leaf senescence, they are the only proteins degraded for recycling of chemical groups, especially organic sulfur compounds (Zuber 2004). Due to the presence of three disulfide bridges, they are very tightly folded proteins, and therefore are extraordinary stable as well as highly resistant against proteolysis (Phytokodex: Pflanzliche Arzneispezialitäten in Österreich 2001/2002). They are also rich in Arginine and Lysin and hence have an isoelectric point in the range of 10, which enables them to interact with DNA in a histone-like manner. Their amphiphilic character can induce membrane disintegration and forms the basis of their cytotoxic properties (Phytokodex: Pflanzliche Arzneispezialitäten in Österreich 2001/2002).

Mistletoe lectins (ML) are glycoproteins. They recognize and bind specific sugars and therefore are able to agglutinate cells (Mohammed & Ferry 2021). Their structure consists of two polypeptide chains, termed A and B, which are connected via a disulfide bridge (Krauspenhaar et al. 1999, Wacker et al. 2004). Chain A is toxic and possesses enzymatic activity, whereas the slightly larger chain B exhibits carbohydrate binding properties (Mohammed & Ferry 2021). Based on their sugar specificity, mistletoe lectins are divided into the subtypes ML1, ML2, and ML3. ML1 exclusively binds D-galactose, ML2 D-galactose and N-acetyl-galactosamine, and ML3 N-acetyl-galactosamine (Mohammed & Ferry 2021, Yousefvand et al. 2022). Also, the molecular masses of the A and B chains differ between the subtypes (Table 1). Mistletoe lectins belong to the group of type 2 ribosome-inhibiting proteins (Franz et al. 1981, Mohammed & Ferry 2021). During their intracellular transport, the disulfide bridges connecting chains A and B can be reduced, leading to a dissociation of the two chains (Agapov et al. 1999). The monomeric A chain then acts as a potent ribosome-inactivating protein in the cytosol, causing irreversible inhibition of protein biosynthesis, thereby inducing apoptosis. The concentrations of the mistletoe lectins vary during the season. Highest levels occur in winter (Yousefvand et al. 2022). Additionally, the ML content seems to depend on the host tree. *V. album* growing on oaks, poplars and apple trees show the highest ML content (Büssing & Schietzel 1999). In complementary medicine, *V. album* harvested in summer and winter are combined. The resulting extracts are applied by injection. This treatment is used as an adjunct to conventional chemotherapy in the therapy of cancer (Büssing & Schietzel 1999, Urech et al. 2006).

**Table 1:** Molecular mass of chains A and B of the three different mistletoe lectins MLI, MLII and MLIII of *V. album* (based on data of [Mohammed & Ferry 2021](#)).

	Molecular mass chain A	Molecular mass chain B
MLI	29 kDa	34 kDa
MLII	27 kDa	32 kDa
MLIII	25 kDa	30 kDa

#### 1.1.4 Adaptation to the seasons

Sessile life forms like plants had to develop complex mechanisms to cope with the environmental influences of their habitats. Interactions with diverse abiotic and biotic factors take place at different levels, physiologically and metabolically. Plants have to deal with changing light conditions, pathogens, as well as water availability and soil composition. Besides the daily challenges, they also have to adapt to seasonal changes in order to survive.

Mistletoes have a particular way of life. As hemiparasitic plants with haustoria instead of roots, they are less affected by environmental constraints like water and nutrient restrictions and they do not interact with microorganisms present in the soil. Instead, they take up organic substances from the host xylem. To maintain a constant supply with water, nutrients and organic compounds, *V. album* mostly keeps its stomata (which are present on both leaf sides!) open to establish a constant transpirational suction ([Glatzel 1983](#), [Glatzel & Geil 2009](#), reviewed in [Zuber 2004](#)). This does not only increase water uptake but also gas exchange, creating optimal conditions for photosynthesis and carbon fixation (also see chapter 1.4). Hence, it is surprising to find severe changes in the energy systems of *V. album* chloroplasts, as well as mitochondria, pointing towards reduced metabolic activities (chapter 1.3 and 1.4, respectively).

As discussed in chapter 1.1.3, *V. album* contains viscotoxins and mistletoe lectins, which seem to be important in the context of its biotic stress response. This indicates that *V. album* is especially threatened by pathogens. Due to the slow growth of the plant, it needs to be especially resilient in order to complete its life cycle.

As an evergreen plant, *Viscum album* also needs to adapt to seasonal changes. In the temperate zone, which *V. album* predominantly inhabits, it has to cope with cold winters and warm summers. As a consequence, it is exposed to large differences in water and light availability, but also to varying pathogen populations.

*V. album* has been shown to develop cold resistance in winter (reviewed in [Zuber 2004](#)). Its leaves can withstand temperatures down to  $-20^{\circ}\text{C}$ . In contrast, during summer, it only can cope with temperatures above  $-5^{\circ}\text{C}$  (reviewed in [Zuber 2004](#)). A possible explanation could be decreased transpiration levels in the leaves in winter, accompanied by accumulation of osmotic cryoprotectants, like cyclitols, mistletoe lectins as well as proline ([Richter & Popp 1992](#), reviewed in [Zuber 2004](#)). Furthermore, photosynthesis rates are decreased in winter, as are chlorophyll a and b contents ([Lee 2015](#)).

## 1.2 The Genome of *Viscum album*

### 1.2.1 The general structure of genomes

The genetic material of an organism is preserved in form of DNA (deoxyribonucleic acid) in the nuclei of its cells (reviewed in [Goedings 2017](#)). DNA is a double helical molecule consisting of two intertwined polynucleotide chains, each consisting of an alternating sequence of four different nucleotides. A nucleotide consists of a phosphate group, a desoxyribose, and one of four nucleobases (adenine (A), thymine (T), cytosine (C), and guanine (G)). The nucleobases build the interconnection between the two polynucleotide chains by hydrogen bonds: A and T connect via two bonds, C and G via three. They also represent the genetic code. On a higher level, the DNA is organized into chromosomes, which contain protein-coding regions (exons), as well as non-coding regions (introns). Hence, chromosomes carry the genes of the organism. The number of expressed genes in animals and plants is relatively constant, ranging between 4,000 and 40,000 (reviewed in [Goedings 2017](#)). However, there is a significant variability in the size of non-coding regions among different species. The non-coding regions of some organisms can constitute as much as 98% of the genome, in others they only account for less than 50% (reviewed in [Goedings 2017](#)). The percentage of non-coding regions often correlates with the genome size: Organisms with smaller genomes have less non-coding DNA, those with larger genomes tend to have a higher proportion of non-coding DNA.

Furthermore, also the number of chromosomes differs between organisms (reviewed in [Goedings 2017](#)). The genome size is typically expressed as 1C, representing the haploid genome size of an organism. In most cases, organisms are diploid, meaning that they have two copies of their chromosome set. Also, higher ploidy levels are known, e.g., strawberries can be diploid (2C), tetraploid (4C), pentaploid (5C), hexaploid (6C), octoploid (8C), and even nonaploid (9C) ([Hummer et al. 2009](#)).

### 1.2.2 Insights into *Viscum album* genetics

*V. album* is a diploid plant. It is known for its exceptionally large chromosomes. It has a very low polyploidy rate and  $2n=20$  chromosomes ([Barlow 1981](#)). Several different chromosomal translocation complexes occur in *V. album*. During meiosis, they induce the formation of rings of chromosomes. The complexes and rings differ between genders. In male plants, chromosome rings usually consist of eight or ten chromosomes, sometimes twelve. The remaining chromosomes form bivalents. Female plants typically have ten bivalents. However, they also can be heterozygous for a distinct set of chromosome rings consisting of four or six chromosomes, which are not present in male plants. In addition, floating rings of four chromosomes can occur in both genders ([Barlow 1981](#), reviewed in [Thomas et al. 2023](#)).

In *V. album* not only the ring formation of chromosomes is special, but also the genome size. With an estimated number of 90-100 Gbp (1C), which corresponds to 102.90 pg (1C), the genome of *V. album* is one of the largest among angiosperms ([Zonneveld 2010](#), [Novák et al. 2020](#)). For comparison, the smallest genome of this clade was found in the species *Genlisea*

(~0.07 pg (1C)) (Fleischmann et al. 2014), the largest in *Paris japonica* (152.23 pg (1C)) (Pellicer et al. 2010). The average genome size of all 10,770 angiosperms taken from <https://cvalues.science.kew.org/search/angiosperm> (Leitch et al. 2019) adds up to 5.13 pg (1C). Compared to the model plant *Arabidopsis thaliana* with a size of 0.15 Gbp (Bennett et al. 2003), the genome of *V. album* is approximately 600 times larger (Novák et al. 2020). As already indicated above, large genomes in plants are not necessarily correlated with a higher number of genes, but rather include increased amounts of repetitive sequences. In *V. album*, only 0.03% of the genome consists of genes, while approximately 55% is occupied by repeats and 45% by non-repetitive sequences (Novák et al. 2020). However, large genomes are associated with higher biochemical and energy costs for both biosynthesis and maintenance, and require longer cell cycle times (Novák et al. 2020).

### 1.2.3 GC content

The GC content represents the amount of GC nucleobase pairs (see chapter 1.2.1) within the DNA of an organism. Several DNA properties can be related to this value. Primarily, DNA stability increases with a high GC content (Vinogradov 2003), especially in GC-rich areas (Yakovchuk et al. 2006). However, this also increases energy costs for DNA double helix separation, e.g., during DNA replication and transcription. Accordingly, exons often show a lower GC content than introns. The GC content also is involved in stress resistance. Species living in regions of extreme climates, like high temperatures, or at ecologically challenging conditions, have been shown to possess higher GC contents (Singh et al. 2016).

In eukaryotes, the GC content varies between 30% to 65% (Singh et al. 2016). Among dicotyledonous plants, the GC content of the coding regions is very similar, ranging from 43% to 45%. The GC content of *V. album* has been estimated to be between 39% and 40%, which is about average for angiosperms but rather low for dicotyledons (Marie & Brown 1993, Ko et al. 2014, Singh et al. 2016).

### 1.2.4 Sequencing status

To date, no complete genome of *V. album* has been sequenced. The large size and the large regions of repetitive sequences make such a project exceptional challenging (Novák et al. 2020). Nevertheless, the “Darwin Tree of life” consortium is currently working on a complete sequencing of the *V. album* genome (Date: 23.04.2023; [https://www.darwintreeof-life.org/news\\_item/2022-the-year-we-built-the-biggest-genome-in-britain-and-ireland/](https://www.darwintreeof-life.org/news_item/2022-the-year-we-built-the-biggest-genome-in-britain-and-ireland/)).

However, sequencing projects have been carried out for the mitochondrial and chloroplast genomes of *V. album* (Petersen et al. 2015a, Petersen et al. 2015b, Skippington et al. 2015, Skippington et al. 2017), as well as the chloroplast genome of *V. coloratum*, which is a close relative of *V. album* (Wei et al. 2019).

The chloroplast genome of *Viscum* species is divided in its typical regions: the large single-copy region (LSC), the small single-copy region (SSC), and several inverted-repeat regions (IRs).

The GC content within the chloroplast genome of *V. coloratum* varies between the regions (33.4% in LSC, 24.3% in SSC, and 43.1% in IR regions) resulting in an average chloroplast GC content of approximately 36.3%. In *V. album*, the GC content of the chloroplast genome is 36.4% (Petersen et al. 2015b). Most interestingly, sequencing of the chloroplast genome revealed absence of all genes encoding subunits of the NDH complex (the chloroplast pendant of mitochondrial complex I).

Mitochondrial genome size can vary extremely (208 kb to 11 mb) among seed plants. However, the number of protein-coding mitochondrial genes is in a very similar range (Petersen et al. 2015a). With 565,432 bp, the mitochondrial genome of *V. album* is about average in size, while the one of the closely related *V. scurruloideum*, comprising 65,873 bp, is one of the smallest mitochondrial genomes of all angiosperms (Skippington et al. 2015, Petersen et al. 2017).

The mitochondrial genomes of angiosperms contain a conserved set of 24 “core protein”-coding genes. However, only 15 of those could be identified in *V. album*, 13 of which are likely to be functional (Skippington et al. 2017). This means, that almost half of all mitochondrially encoded genes are absent in *V. album*. In detail, the mitochondrial genome sequencing project revealed absence of all nine mitochondrially encoded subunits (nad1, 2, 3, 4, 4L, 5, 6, 7, 9) of the NADH dehydrogenase complex (mitochondrial complex I) in *V. album*. Furthermore, these genes also were found to be missing in other species of the Viscaceae clades, namely *V. crassulae*, *V. minimum*, *V. scurruloideum*, and *Phoradendron liga* (Petersen et al. 2015a, Skippington et al. 2015, Zervas et al. 2019). In addition to the mitochondrially encoded complex I subunits, also two of the five mitochondrially encoded subunits of the ATP synthase complex (atp4, atp8) were initially assumed to be missing in *V. album* (Petersen et al. 2015a). However, these genes were finally identified but shown to be have highly derived sequences (Skippington et al. 2015, Petersen et al. 2020).

### 1.3 The Mitochondrial energy metabolism of *Viscum album*

The energy metabolism of a plant can be divided into biochemical processes generating ATP and other energy-rich compounds, particularly photosynthesis and cellular respiration, and processes that are driven by the energy-rich compounds, like protein biosynthesis, plant stress response and all biochemical reactions contributing to plant growth. In order to understand the energy metabolism of *V. album*, the chloroplast photosynthesis apparatus and the mitochondrial oxidative phosphorylation (OXPHOS) system have been investigated in detail as part of the studies for this dissertation. These systems are briefly introduced in the following two chapters (1.3 and 1.4).



### 1.3.1 General structure and function of the OXPPOS system

Although plant mitochondria maintain many important metabolic pathways (Scheffler 1999), their major function is the energy supply of the cell. The most prominent energy-related pathways in mitochondria are the tricarboxylic acid (TCA) cycle, which reduces the energy carriers NADH and FADH<sub>2</sub>, and the OXPPOS system, which oxidizes these carriers to generate ATP, a mobile energy source for the whole cell. Hence, the OXPPOS system directly influences the energy state of the cell and consequently, the entire organism. For efficient energy generation, not only the functional components of OXPPOS are important. Another major factor is the ultrastructure of mitochondria, which enables the formation of different subcompartments (Figure 3).

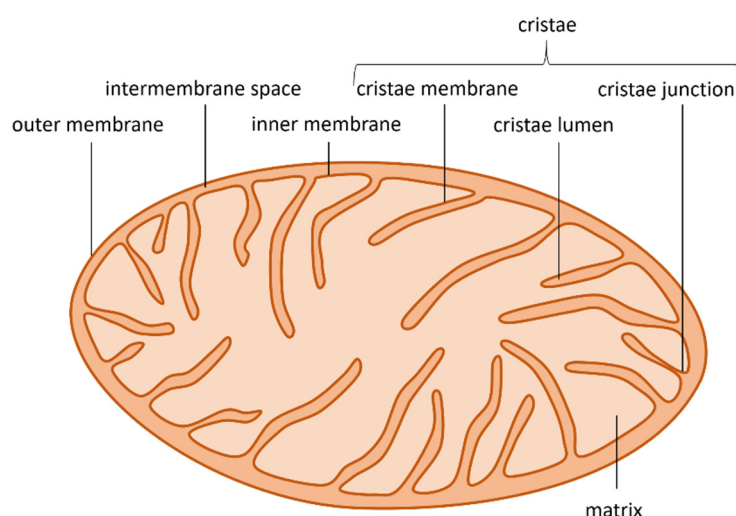


**Figure 3: Overview of mitochondrial compartments.**

The outer and inner membranes (both dark orange), serve as barriers that separate the cytosol from the intermembrane space (orange) and the intermembrane space from the matrix (light orange), respectively. Deep invaginations of the inner mitochondrial membrane are designated cristae. They are composed of the cristae membrane and the cristae lumen, which is separated from the intermembrane space by so-called cristae junctions.

Mitochondria consist of an outer mitochondrial membrane (OMM) and an inner mitochondrial membrane (IMM), separated by the inter membrane space (IMS) (Martinez et al. 2020). The OMM serves as separation from the cytosol and allows a defined transit of ions and metabolites via voltage-dependent anion channel (VDAC). It also hosts proteins involved in apoptosis, mitochondrial dynamics and tethering to other organelles. The IMM is further subdivided into the inner boundary membrane and the cristae membranes. Cristae are IMM folds that have an own lumen which is connected to the IMS only by cristae junctions (Figure 3), therefore representing another subcompartment. The OXPPOS system is located at the cristae membranes (Martinez et al. 2020).

Five protein complexes account for the classical OXPPOS system: the NADH dehydrogenase complex (complex I), succinate dehydrogenase complex (complex II), cytochrome c reductase complex (complex III), cytochrome c oxidase complex (complex IV), and the ATP synthase

(complex V). The first four complexes establish an electron transfer chain (ETC). Electrons are taken up from NADH and FADH<sub>2</sub> by complex I and complex II, respectively, and transferred to the membrane-soluble lipid ubiquinone, which is reduced to ubiquinol. Ubiquinol is then oxidized by complex III, which transfers the electrons to cytochrome c, a small protein present in the cristae lumen. Cytochrome c finally is oxidized by complex IV, which transfers the electrons to molecular oxygen, forming water (reviewed in [Braun 2020](#)). Coupled to the electron transfer, complexes I, III and IV translocate protons across the cristae membrane into the lumen, increasing the pH gradient across the membrane. The gradient is used by complex V, which allows flow of protons back into the mitochondrial matrix and thereby the formation of ATP from ADP and phosphate (reviewed in [Braun 2020](#)). ATP can be exported by mitochondria to provide energy for the entire cell.

### 1.3.2 Oligomeric protein complexes and protein supercomplexes

The protein complexes of the OXPHOS system can also exist as homo-oligomers (e.g., dimers) or, in combination with other complexes, as supercomplexes. The assembly into supercomplexes has not only been described for the OXPHOS complexes in plants, but also for those from mammals, fungi and bacteria ([Schägger & Pfeiffer 2000](#), [Eubel et al. 2003](#), [Stroh et al. 2004](#)).

Although the function of the respiratory supercomplexes is still a matter of debate, it is assumed that enzyme activities and structural stabilities are increased in supercomplexes ([Dudkina et al. 2010](#)). A special role was described for the dimers and oligomers of complex V, which are essential for cristae curvature and therefore play a key role for establishment of mitochondrial subcompartments. They also have been proposed to indirectly contribute to a more efficient ATP production ([Dudkina et al. 2010](#), [Anselmi et al. 2018](#), [Joubert & Puff 2021](#)).

### 1.3.3 The OXPHOS system in *Viscum album*

As mentioned above, the complete set of genes of the mitochondrial encoded complex I subunits is absent in *Viscum* species ([Petersen et al. 2015a](#), [Skippington et al. 2015](#), [Skippington et al. 2017](#)). This surprising discovery led to a closer investigation of the OXPHOS system on the proteome level. Two independent studies indeed revealed complete absence of complex I in *V. album* mitochondria ([Macleane et al. 2018](#), [Senkler et al. 2018](#)). Beyond that, other OXPHOS complexes are of reduced abundance and supercomplexes of special composition are formed (**Figure 4**). Compared to the model plant *A. thaliana*, less than 10% of complexes II and V are present, as well as approximately 30 % of complexes III and IV ([Senkler et al. 2018](#)). The exact structure and function of the OXPHOS complexes, as well as potential consequences of their absence or altered abundance in *V. album*, will be discussed in more detail below.

#### Complex I

Complex I of plants has a mass of ~1 MDa and consists of approximately 50 subunits. It is by far the largest complex of the OXPHOS system. Complex I has a major impact on the proton

gradient (it transfers four protons across the inner mitochondrial membrane per oxidized NADH) and consequently on ATP production (reviewed in [Braun 2020](#)). The structure of complex I from *A. thaliana* has recently been characterized by cryoEM ([Klusch et al. 2021](#)). It is L-shaped and possesses a peripheral, matrix exposed arm as well as a membrane arm embedded in the cristae membranes. The peripheral arm comprises the NADH oxidation (N) and ubiquinone reduction (Q) sites, which are connected by a chain of iron sulfur (FeS) clusters. The membrane arm contains the proton translocation sites. In plants, an additional module, designated the gamma carbonic anhydrase ( $\gamma$ CA) module, is attached to the membrane arm on its matrix side ([Klusch et al. 2021](#)).

To date, absence of mitochondrial complex I is known only for unicellular species like the dinoflagellate *Scrippsiella acuminata* ([Raven & Beardall 2017](#)), the yeast *Saccharomyces cerevisiae* ([Vitols & Linnane 1961](#), [Ohnishi et al. 1966](#), [Foury et al. 1998](#), [Gabaldón et al. 2005](#), [Malina et al. 2018](#)), and the malaria pathogen *Plasmodium falciparum* ([Evers et al. 2021](#)). In fact, *Viscum* species are the only multicellular species that can live without complex I. Recently, it was discovered that complex I is not formed in early human oocytes (which can remain dormant in this stage for decades), but is assembled during later developmental stages ([Adhikri & Carrol 2022](#), [Rodríguez-Nuevo et al. 2022](#)). It has been assumed that suppression of complex I assembly serves as protection against oxidative stress due to reactive oxygen species (ROS) accumulation. ROS production can be caused by electron leakage of the ETC. Especially complex I is considered to be a major ROS source. Therefore, suppression of complex I was assumed to increase longevity ([Adhikri & Carrol 2022](#), [Rodríguez-Nuevo et al. 2022](#)). Given the extraordinary size and subunit composition of complex I, which not only includes proteins but also several cofactors (like FeS clusters) and other organic compounds ([Klusch et al. 2021](#)), the energy costs for complex I assembly and maintenance can be considered to be high. Loss of complex I at some point during *Viscum* evolution possibly has been advantageous. Not only is the biosynthesis of complex I expensive, but also the maintenance of all of its genes requires energy. Finally, as complex I represents a major source for mitochondrial ROS production, additional energy is needed for ROS protection mechanisms. It seems that mistletoes rather are coping with reduced respiratory activity than investing the energy for biosynthesis and functioning of complex I.

Despite absence of complex I, two complex I subunits are present in *V. album*. These proteins are a  $\gamma$ CA subunit and the L-galactono-1,4-lactone dehydrogenase (GLDH) ([Senkler et al. 2018](#)). However, GLDH has not been identified in the mature structure of complex I in plants and therefore rather is considered an assembly factor ([Klusch et al. 2021](#)). Besides its role in complex I assembly, it catalyzes the terminal step of ascorbate synthesis. It has been shown that the  $\gamma$ CA subunits within the  $\gamma$ CA module of complex I include an intact active site in plants ([Klusch et al. 2021](#), [Klusch et al. 2023](#)), which should promote interconversion of CO<sub>2</sub> and H<sub>2</sub>O into bicarbonate and protons at basic pH. Therefore, the identified CA protein, just like GLDH, most probably has a complex I independent function in *V. album* mitochondria. In summary, remaining complex I subunits in *V. album* seem to be bifunctional.

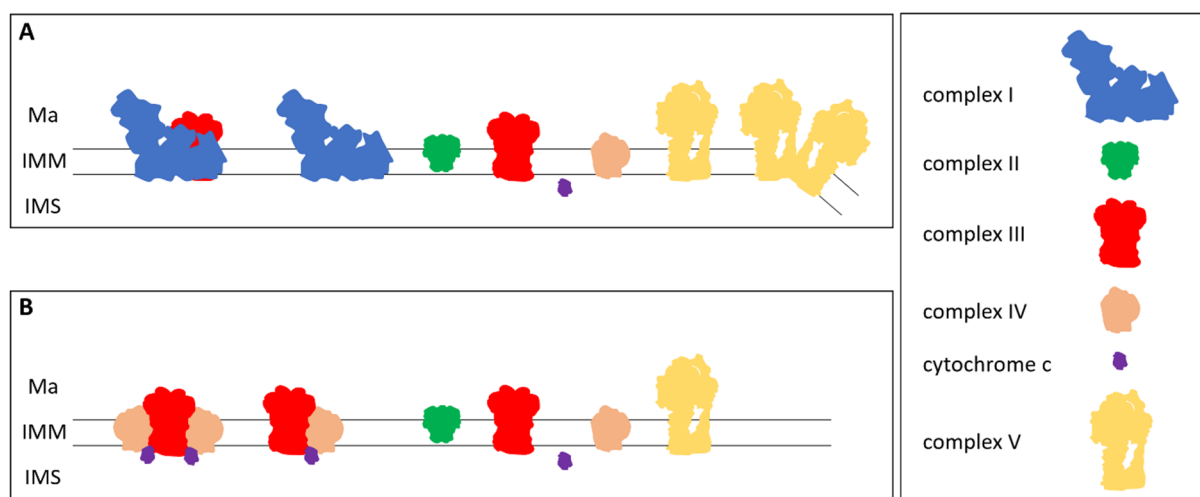


**Figure 4: Schematic model of OXPHOS complexes and supercomplexes for *A. thaliana* and *V. album*.**

In (A) the complexes and supercomplexes of the model plant *A. thaliana* are shown. In (B) the complexes and supercomplexes of *V. album* are shown. Ma: matrix; IMM: inner mitochondrial membrane; IMS: intermembrane space; blue: complex I; green: complex II; red: complex III; orange: complex IV; purple: cytochrome c; yellow: complex V. Alternative NAD(P)H dehydrogenases and alternative oxidases, which are part of the OXPHOS system in plants, are not shown in this scheme (Figure from [Senkler et al. 2018](#), modified).

### Complex II

The succinate dehydrogenase complex (SDH, also known as complex II) is not only part of the OXPHOS system but also of the TCA cycle. It catalyzes the interconversion of succinate and fumarate. Electrons are transferred onto a FAD group forming FADH<sub>2</sub>. From there, electrons are finally transferred onto ubiquinone, which is reduced to ubiquinol. In contrast to the other complexes of the ETC, complex II is not involved in the translocation of proton across the IMM ([Braun 2020](#)). In animal and fungal mitochondria, complex II consists of only 4 subunits (SDH1-4), whereas in plant mitochondria four additional subunits (SDH5-8) were identified. In plants, some of the subunits are present in isoforms. Compared to complex II of fungi and animals, the complex II of plants is relatively fragile (reviewed in [Braun 2020](#)). The reduction in amounts of complex II in *V. album* not only influences the ETC but also the TCA cycle.

### Complex III

The cytochrome c reductase, also called complex III, is the central enzyme of the OXPHOS system and catalyzes electron transport from ubiquinol to cytochrome c (reviewed in [Braun 2020](#)). In plants, the complex III has dual functions ([Maldonado et al. 2021](#)). On the one hand, it is part of the respiratory electron transfer chain, on the other it comprises the activity of the mitochondrial processing peptidase (MPP). The latter enzyme is composed of two subunits ( $\alpha$ ,  $\beta$ ) that are localized on the matrix side of complex III. The corresponding subunits are also present in animal and fungal complex III, but reduced in size and enzymically inactive (Braun and Schmitz 1995). In plants, MPP- $\alpha$  has an extension at its N-terminus, which wraps around MPP- $\beta$  and includes an extra  $\beta$  sheet. MPP- $\beta$  also has an extended N-terminus in plants, which

contacts MPP- $\alpha$  and the QCR7 subunit and additionally forms an extra  $\alpha$  helix. An extension of the Rieske or iron sulfur subunit contacts the MPP- $\beta$  anchor and provides extra stability to complex III in plants (Maldonado et al. 2021).

In *V. album*, the reduced abundance of complex III contributes to an overall limited capacity of OXPHOS. An efficient formation of supercomplexes may partially compensate this effect. In its basic form, complex III exists as a homodimer (III<sub>2</sub>). Besides, complex III of *V. album* forms two specific supercomplexes consisting of dimeric complex III and one or two copies of monomeric complex IV (III<sub>2</sub>IV<sub>1</sub>, III<sub>2</sub>IV<sub>2</sub> composition) (Senkler et al. 2018). Formation of these supercomplex may improve the efficiency of electron transfer, the stability of the involved complexes and reduce ROS production (Maldonado et al. 2021). The supercomplexes III<sub>2</sub>/IV<sub>1/2</sub> were also described in some other organisms, like *S. cerevisiae*, *P. falciparum* and mung bean (*Vigna radiata*) (Hartley et al. 2019, Rathore et al. 2019, Evers et al. 2021, Maldonado et al. 2021). However, in *V. album* these supercomplexes seem to be especially stable. In *V. radiata* the structure of supercomplex III<sub>2</sub>IV<sub>1</sub> revealed the arrangement of its 30 protein subunits, 10 of complex IV and 2x10 of complex III (Maldonado et al. 2021). The precise association of these supercomplexes in *S. cerevisiae* and *P. falciparum*, which lack complex I too, should also be interesting. Whether formation of supercomplexes III<sub>2</sub>/IV<sub>1/2</sub> is a consequence of complex I loss is not known. In *A. thaliana*, mutations causing complex I loss do not lead to increased formation of III<sub>2</sub>/IV<sub>1/2</sub> supercomplexes (Kühn et al. 2015, Fromm et al. 2016, Maldonado et al. 2021).

#### Complex IV

The cytochrome c oxidase (complex IV) is the terminal enzyme of the electron transport chain. From reduced cytochrome c it transfers electrons to O<sub>2</sub> generating H<sub>2</sub>O. In plants, this complex consists of up to 14 subunits. Eight of them are homologous to subunits of fungal and mammalian complex IV, but some others are discussed to be plant-specific (Millar et al. 2004, Klodmann et al. 2011, Senkler et al. 2017, Mansilla et al. 2018, Ghifari & Murcha 2020). The precise composition of this complex in plants is still unknown and also varies among different plant species. For instance, structural analysis has shown that the complex IV of *V. radiata* consists of only 10 subunits (Maldonado et al. 2021). In *V. album*, complex IV abundance is low compared to *A. thaliana*. It associates with complex III<sub>2</sub>.

#### Complex V

The mitochondrial ATP synthase consists of two parts termed F<sub>0</sub> and F<sub>1</sub>. The F<sub>0</sub> part is inserted into the IMM, while the spherical F<sub>1</sub> part protrudes into the mitochondrial matrix. The way complex V works is reminiscent of a turbine. Protons flow through the complex alongside the gradient from the IMS side of the IMM to the matrix. This flow causes rotation of a central oligomer of a small hydrophobic subunit (subunit c) within the F<sub>0</sub> part and of a connected central axis, which is anchored in F<sub>0</sub>. The other end of the axis protrudes into the F<sub>1</sub> part, which does not rotate, because it is fixed via a 'peripheral stalk' at F<sub>0</sub> subunits that are not involved

in the rotation. As a result of these molecular movements, the architecture of binding sites for ADP and phosphate within the  $F_1$  part are altered, enabling the generation of ATP (Wittig & Schägger 2008, reviewed in Braun 2020). Besides its role in ATP production, the ATP synthase complex also plays a role in the cristae formation of the IMM. The ATP synthase, in its dimeric form, causes bending of the IMM, which promotes generation of the IMM invaginations (Pau-mard et al. 2002, Minauro-Sanmiguel et al. 2005, Davies et al. 2012, reviewed in Braun 2020). In *V. album*, the abundance of ATP synthase is reduced in comparison to *A. thaliana*. Consequently, cristae formation takes place to a lesser extent, which has been revealed by electron microscopy analyses of *V. album* leaf cells. It can be anticipated that the reduced ultrastructure of *V. album* mitochondria further limits OXPHOS (Senkler et al. 2018).

#### Alternative enzymes

The abundance of alternative oxidoreductases, like the alternative oxidases (AOX) and alternative NADH dehydrogenases (NDs), which are prominent extra enzymes of the plant OXPHOS system, is increased in *V. album*. These enzymes participate in respiratory electron transport without contributing to the proton gradient across the IMM (Senkler et al. 2017). They are considered to play an important role in the regulation of the redox balance of the plant cell at high light conditions, and during diverse stress conditions (Rassmusson et al. 2008, Schertl & Braun 2014).

#### 1.3.4 Evolution of the mitochondrial genome in plant parasites

The mitochondrial OXPHOS system in *V. album* is reduced, which limits ATP synthesis by OXPHOS (Maclean et al. 2018, Senkler et al. 2018). The energy requirement of *V. album*, on the other side, should be significant, for instance due to replication costs of its extremely large genome (Zonneveld 2010, Novák et al. 2020). Nevertheless, the way of life of *Viscum* species is very successful, as they are widely distributed around the world (Maul et al. 2019). An explanation could be parasitic lifestyle. This raises the question of whether other parasitic plants also have a reduced OXPHOS system. A recent study of mitochondrial genomes of parasitic plants shows that this is not the case (Zervas et al. 2019). During this study, the mitochondrial genome of 10 other hemiparasitic and holoparasitic plant taxa were investigated. It was found that the massive loss of mitochondrial genes of *V. album*, *V. crassulae*, *V. minimum*, *V. scurruloideum* and *Phoradendron liga* of the taxa Viscaceae are unique among plant parasites (Zervas et al. 2019).

## 1.4 The Photosynthesis of *Viscum album*

### 1.4.1 The Photosynthesis in general

Mitochondria generate ATP by oxidation of organic compounds. In photoautotrophic organisms like plants, these are built by photosynthesis (Stirbet et al. 2020). Photosynthesis takes place in the chloroplasts. It can be divided into the light reaction which produces the energy-rich molecules ATP and NADPH, and the Calvin-Benson cycle, which uses these molecules to build up organic compounds.

The light reaction is based on an electron transport chain driven by light energy. It can either operate in a linear (linear electron transport, LET) or cyclic (cyclic electron transport, CET) mode. It takes place in the thylakoid membranes and involves the photosystems I and II (PSI and PSII), which are large protein-pigment complexes.

LET begins with the absorption of light energy by a chlorophyll-a dimer at the active site of PSII, which can donate an electron when it is in an excited state. An electron transport chain is started. PSII transfers electrons to plastoquinone present in the thylakoid membrane, which is reduced to plastoquinol. Plastoquinol can reduce the cytochrome  $b_6/f$  complex, which further transfers electrons to plastocyanin in the thylakoid lumen. Plastocyanin can finally replace electrons at the reaction center of PSI, which also can donate electrons, when the chlorophyll a-dimer at the active center is in an excited state. These electrons can be transferred via ferredoxin to onto NADP<sup>+</sup>, which leads to the formation of NADPH. Missing electrons at the PSII are replaced by electrons from water molecules. A so-called “water-splitting complex”, also termed “oxygen evolving complex”, is associated with PSII. Besides NADPH, LET also causes the formation of a proton gradient across the thylakoid membrane, which can be used by a chloroplast ATP synthase complex for ATP formation (reviewed in Johnson 2011).

In contrast to LET, CET does not involve PSII but only PSI. Electrons are transferred from PSI to ferredoxin and subsequently back to the PSI. Two ways have been characterized for the transfer of electrons from ferredoxin to PSI: (a) via a “mitochondrial NADH dehydrogenase-like complex” (NDH complex), which reduces plastoquinone to plastoquinol, and (b) via the “proton gradient regulation 5” (PGR5) or “PGR5 like phenotype 1” (PGRL1) proteins, which likewise allows formation of plastoquinol (Munekage et al. 2002, DalCorso et al. 2008, Hertle et al. 2013, Ma et al. 2021). In both ways, electrons from plastoquinol are subsequently transferred onto the cytochrome  $b_6/f$  complex, from there to plastocyanin and finally to PSI, which completes CET. During CET, ATP is formed, but no NADPH. Since the NDH complex transfer four protons into the thylakoid lumen per oxidation of two ferredoxins, its contribution to the proton gradient across the thylakoid membrane is substantial, allowing effective ATP formation (reviewed in Johnson 2011, Yamamoto et al. 2011, Shikanai 2014, Schuller et al. 2019).

In summary, CET exclusively results in ATP formation, whereas LET leads to the formation of both ATP and NADPH. Switching between the LET and the CET can adjust the ratio of ATP/NADPH. Furthermore, the ratio of LET and CET itself can be changed by altering the ratio of PSI and PSII. As PSII is exclusively involved in LET, a decrease in the number of PSII units would result in a reduced LET rate. Additionally, the ratio of LET to CET can be adjusted by the

modulation of the sizes of light-harvesting complexes, which associate with the two photosystems and which promote transfer of light energy to the active centers of the photosystems (Longoni and Goldschmidt-Clermont 2021).

ATP and NADPH formed by the light reaction are used in the second part of photosynthesis, the Calvin-Benson-cycle, to convert oxidized carbon (CO<sub>2</sub>) into reduced forms of carbon (carbohydrates). The Calvin-Benson-cycle can be divided into three phases: (i) the CO<sub>2</sub> fixation phase, (ii) the reduction phase, and (iii) the phase allowing regeneration of the CO<sub>2</sub> acceptor ribulose-1,5-bisphosphate (RuBP). During CO<sub>2</sub> fixation, ribulose-1,5-bisphosphate carboxylase/-oxygenase (RubisCO) catalyzes the binding of CO<sub>2</sub> to RuBP. As a result, two molecules of 3-phosphoglycerate are formed. In the reduction phase, 3-phosphoglycerate is reduced to glyceraldehyde 3-phosphate (triose phosphate), which requires energy provided in the form of ATP and NADPH. Glyceraldehyde 3-phosphate is either exported from the chloroplasts to allow sucrose formation in the cytoplasm, or used to regenerate the CO<sub>2</sub> acceptor molecule RuBP, enabling the cycle to start again (reviewed in Eberhard et al. 2008, Stirbet et al. 2020). Glyceraldehyde 3-phosphate also can be used inside chloroplasts for starch biosynthesis.

#### 1.4.2 Photosynthesis of *Viscum album*

As a hemiparasite, *V. album* possesses chlorophyll a and b and can perform photosynthesis. It belongs to the C<sub>3</sub>-plants. As in many other hemiparasitic plants, the photosynthesis rate in *V. album* is comparatively low within the group of C<sub>3</sub>-plants (Tuquet and Sallé 1996, reviewed in Zuber 2004). It also is much lower than in its host (Lee 2015). A specialty of *V. album* is to carry out photosynthesis during winter, even at temperatures as low as -20 °C (reviewed in Zuber 2004). The ratio of PSI/PSII changes seasonally. During summer, the leaves of *V. album* are partly covered by the host and its leaves. In winter, when the deciduous host trees lose their leaves, *V. album* is directly exposed to the sun light. As a consequence, the ratio of PSI/PSII is adapted in winter to avoid accumulation of electrons. However, all seasons exhibit distinct photosynthetic peculiarities. In spring, the ratio of PSI/PSII is approximately 0.66, while most seed plants have PSI/PSII ratios between 0.8 and 1.1 (Tuquet and Sallé 1996). Besides the PSI/PSII ratio, also the photosynthesis activity changes during the seasons and is highest in autumn. Photosynthesis activity of *V. album* in winter is reduced compared to the other seasons (Lee 2015).

Chloroplast genes encoding subunits of the NDH complex are absent in *V. album* (Petersen et al. 2015b). In most plant species, the NDH forms a supercomplex with PSI, which has an estimated molecular mass of 1600 kDa (Peng et al. 2008, Shen et al. 2022). Absence of this supercomplex in *V. album* and thereby reduced capacities to perform CET was tested in the frame of this thesis.



## 1.5 The research topics of this thesis

The aim of this thesis was to enhance our understanding of the energy biology of *V. album*. To achieve this, comprehensive sequence data were generated through PacBio and Illumina sequencing, which served as the foundation for efficient proteome analyses. Based on these sequences, two databases were established for the *V. album* Gene Space: VaGs (chapter 2.1) and its further developed version, VaGsII (chapter 2.5). During the sequence analyses, a GC content of the Gene Space was calculated to be in the range of 50%, which clearly is higher than the GC content of other dicotyledonous plants. This implied an increased DNA stability, but at the same time higher energy requirements for genome replication and transcription (chapter 2.1 and 2.5).

The current knowledge about the OXPHOS system in *V. album* (reviewed in chapter 2.4) was expanded through the utilization of the new databases VaGs and VaGsII. Especially the re-evaluation of a mitochondrial complexome profiling (method see chapter 2.3) dataset of *V. album* led to the identification of more than 1,000 additional mitochondrial proteins.

Furthermore, a detailed investigation of the photosynthesis apparatus of *V. album* was conducted (chapter 2.2). A thylakoid isolation of *V. album* coupled with blue native gel electrophoresis and complexome profiling revealed the absence of the NDH complex on the proteome level and comparatively low amounts of PSI. Overall, the investigation of the photosynthesis apparatus of *V. album* revealed a limited capacity for ATP production via photophosphorylation (chapter 2.2).

How this high energy demand of *V. album* is covered is still unclear. However, it is hypothesized that slow growth, reduced cell division rate, and sugar compounds transported in the host xylem may balance this energy demand.

## 1.6 References

- Adhikari, D. & Carroll, J. (2022). Eggs remodel energy production to protect themselves from harm. *Nature*, 607(7920), 664–665. <https://doi.org/10.1038/d41586-022-01642-x>
- Agapov, I. I., Tonevitsky, A. G., Moysenovich, M. M., Maluchenko, N. V., Weyhenmeyer, R., & Kirpichnikov, M. P. (1999). Mistletoe lectin dissociates into catalytic and binding subunits before translocation across the membrane to the cytoplasm. *FEBS Letters*, 452(3), 211–214. [https://doi.org/10.1016/S0014-5793\(99\)00639-0](https://doi.org/10.1016/S0014-5793(99)00639-0)
- Anselmi, C., Davies, K. M., Faraldo-Gómez, J. D. (2018). Mitochondrial ATP synthase dimers spontaneously associate due to a long-range membrane-induced force. *The Journal of General Physiology*, 150(5), 763–770. <https://doi.org/10.1085/jgp.201812033>.
- Azuma, J., Kim, N.-H., Heux, L., Vuong, R., & Chanzy, H. (2000). *Cellulose*, 7(1), 3–19. <https://doi.org/10.1023/A:1009223730317>
- Barlow, B. A. (1981). *Viscum album* in Japan: Chromosomal translocations, maintenance of heterozygosity and the evolution of dioecy. *The Botanical Magazine Tokyo*, 94(1), 21–34. <https://doi.org/10.1007/BF02490200>
- Becker, H. (1986). Botany of European mistletoe (*Viscum album* L.). *Oncology*, 43 Suppl 1, 2–7. <https://doi.org/10.1159/000226413>
- Bennett, M. D., Leitch, I. J., Price, H. J., & Johnston, J. S. (2003). Comparisons with *Caenorhabditis* (approximately 100 Mb) and *Drosophila* (approximately 175 Mb) using flow cytometry show genome size in *Arabidopsis* to be approximately 157 Mb and thus approximately 25% larger than the *Arabidopsis* genome initiative estimate of approximately 125 Mb. *Annals of Botany*, 91(5), 547–557. <https://doi.org/10.1093/aob/mcg057>
- Braun, H. P. & Schmitz, U. K. (1995). The bifunctional cytochrome c reductase/processing peptidase complex from plant mitochondria. *Journal of Bioenergetics and Biomembranes*, 27(4), 423–436. <https://doi.org/10.1007/BF02110005>
- Braun, H.-P. (2020). The Oxidative Phosphorylation system of the mitochondria in plants. *Mitochondrion*, 53, 66–75. <https://doi.org/10.1016/j.mito.2020.04.007>.
- Büssing, A. & Schietzel, M. (1999). Apoptosis-inducing properties of *Viscum album* L. Extracts from different host trees, correlate with their content of toxic mistletoe lectins. *Anticancer Research*, 19(1A), 23–28.
- DalCorso, G., Pesaresi, P., Masiero, S., Aseeva, E., Schünemann, D., Finazzi, G., Joliot, P., Barbato, R., Leister, D. (2008). A complex containing PGRL1 and PGR5 is involved in the switch between linear and cyclic electron flow in *Arabidopsis*. *Cell*, 132(2), 273–285. <https://doi.org/10.1016/j.cell.2007.12.028>
- Davies, K. M., Anselmi, C., Wittig, I., Faraldo-Gómez, J. D., & Kühlbrandt, W. (2012). Structure of the yeast F1Fo-ATP synthase dimer and its role in shaping the mitochondrial cristae. *Proceedings of the National Academy of Sciences of the United States of America*, 109(34), 13602–13607. <https://doi.org/10.1073/pnas.1204593109>
- DeBruyn, R. A. J., Paetkau, M., Ross, K. A., Godfrey, D. V., & Friedman, C. R. (2015). Thermogenesis-triggered seed dispersal in dwarf mistletoe. *Nature Communications*, 6, 6262. <https://doi.org/10.1038/ncomms7262>

- Dudkina, N. V., Kouril, R., Peters, K., Braun, H.-P., Boekema, E. J. (2010). Structure and function of mitochondrial supercomplexes. *Biochimica Et Biophysica Acta*, 1797(6-7), 664–670. <https://doi.org/10.1016/j.bbabi.2009.12.013>
- Eberhard, S., Finazzi, G., & Wollman, F.-A. (2008). The dynamics of photosynthesis. *Annual Review of Genetics*, 42, 463–515. <https://doi.org/10.1146/annurev.genet.42.110807.091452>.
- Escher, H. P. (2004): Untersuchungen zur C, N und S Akquisition durch *Viscum album*.
- Escher, P., Eiblmeier, M., Hetzger, I., Rennenberg, H. (2004). Seasonal and spatial variation of carbohydrates in mistletoes (*Viscum album*) and the xylem sap of its hosts (*Populus x euamericana* and *Abies alba*). *Physiologia Plantarum*, 120(2), 212–219. <https://doi.org/10.1111/j.0031-9317.2004.0230.x>
- Eubel, H., Jansch, L. Braun, H.-P. (2003). New insights into the respiratory chain of plant mitochondria. Supercomplexes and a unique composition of complex II. *Plant Physiology*, 133(1), 274–286. <https://doi.org/10.1104/pp.103.024620>
- Evers, F., Cabrera-Orefice, A., Dei Elurbe, M., Kea-Te Lindert, M., Boltryk, S. D., Voss, T. S., Huynen, M. A., Brandt U., Kooij, T. W. A. (2021). Composition and stage dynamics of mitochondrial complexes in *Plasmodium falciparum*. *Nature Communications*, 12(1), 3820. <https://doi.org/10.1038/s41467-021-23919-x>
- Fleischmann, A., Michael, T. P., Rivadavia, F., Sousa, A., Wang, W., Temsch, E. M., Greilhuber, J., Müller, K. F., Heubl, G. (2014). Evolution of genome size and chromosome number in the carnivorous plant genus *Genlisea* (Lentibulariaceae), with a new estimate of the minimum genome size in angiosperms. *Annals of Botany*, 114(8), 1651–1663. <https://doi.org/10.1093/aob/mcu189>
- Foury, F., Roganti, T., Lecrenier, N., Purnelle, B. (1998). The complete sequence of the mitochondrial genome of *Saccharomyces cerevisiae*. *FEBS Letters*, 440(3), 325–331. [https://doi.org/10.1016/s0014-5793\(98\)01467-7](https://doi.org/10.1016/s0014-5793(98)01467-7)
- Franz, H., Ziska, P., Kindt, A. (1981). Isolation and properties of three lectins from mistletoe (*Viscum album* L.). *The Biochemical Journal*, 195(2), 481–484. <https://doi.org/10.1042/bj1950481>
- Fromm, S., Braun, H. P., Peterhänsel, C. (2016). Mitochondrial gamma carbonic anhydrases are required for complex I assembly and plant reproductive development. *The New Phytologist*, 211(1), 194–207. <https://doi.org/10.1111/nph.13886>
- Gabaldón, T., Rainey, D., Huynen, M. A. (2005). Tracing the evolution of a large protein complex in the eukaryotes, NADH:Ubiquinone oxidoreductase (Complex I). *Journal of Molecular Biology*, 348(4), 857–870. <https://doi.org/10.1016/j.jmb.2005.02.067>
- Ghifari, A. S., Murcha, M. W. (2020) Plant Mitochondria. In *Encyclopedia of life sciences* (pp. 581–591). <https://doi.org/10.1002/9780470015902.a0029217>
- Giudici, M., Poveda, J. A., Molina, M. L., La Canal, L. de, González-Ros, J. M., Pfüller, K., Pfüller, U., Villalaín, J. (2006). Antifungal effects and mechanism of action of viscotoxin A3. *The FEBS Journal*, 273(1), 72–83. <https://doi.org/10.1111/j.1742-4658.2005.05042.x>
- Glatzel, G. (1983). Mineral nutrition and water relations of hemiparasitic mistletoes: A question of partitioning. Experiments with *Loranthus europaeus* on *Quercus petraea* and *Quercus robur*. *Oecologia*, 56(2-3), 193–201. <https://doi.org/10.1007/BF00379691>

- Glatzel, G., & Geils, B. W. (2009). Mistletoe ecophysiology: host–parasite. *Botany*, 87(1), 10–15. <https://doi.org/10.1139/B08-096>
- Goedings, P. (2017). Das Genom der weißbeerigen Mistel (*Viscum album*). *Der Merkurstab*, 70(3), 187–194. <https://doi.org/10.14271/DMS-20792-DE>
- Hartley, A. M., Lukoyanova, N., Zhang, Y., Cabrera-Orefice, A., Arnold, S., Meunier, B., Pinotsis, N., Maréchal, A. (2019). Structure of yeast cytochrome c oxidase in a supercomplex with cytochrome bc1. *Nature Structural & Molecular Biology*, 26(1), 78–83. <https://doi.org/10.1038/s41594-018-0172-z>
- Hertle, A. P., Blunder, T., Wunder, T., Pesaresi, P., Pribil, M., Armbruster, U., & Leister, D. (2013). Pgr1 is the elusive ferredoxin-plastoquinone reductase in photosynthetic cyclic electron flow. *Molecular Cell*, 49(3), 511–523. <https://doi.org/10.1016/j.molcel.2012.11.030>
- Hódar, J. A., Lázaro-González, A., & Zamora, R. (2018). Beneath the mistletoe: parasitized trees host a more diverse herbaceous vegetation and are more visited by rabbits. *Annals of Forest Science*, 75(3). <https://doi.org/10.1007/s13595-018-0761-3>
- Horbelt, N., Fratzl, P., & Harrington, M. J. (2022). Mistletoe viscin: A hygro- and mechano-responsive cellulose-based adhesive for diverse material applications. *PNAS Nexus*, 1(1), pgac026. <https://doi.org/10.1093/pnasnexus/pgac026>
- Hummer, K. E., Nathewet, P., & Yanagi, T. (2009). Decaploidy in *Fragaria iturupensis* (Rosaceae). *American Journal of Botany*, 96(3), 713–716. <https://doi.org/10.3732/ajb.0800285>
- Johnson, G. N. (2011). Physiology of PSI cyclic electron transport in higher plants. *Biochimica Et Biophysica Acta*, 1807(3), 384–389. <https://doi.org/10.1016/j.bbabi.2010.11.009>
- Joubert, F., & Puff, N. (2021). Mitochondrial Cristae Architecture and Functions: Lessons from Minimal Model Systems. *Membranes*, 11(7). <https://doi.org/10.3390/membranes11070465>
- Klodmann, J., Senkler, M., Rode, C., & Braun, H.-P. (2011). Defining the protein complex proteome of plant mitochondria. *Plant Physiology*, 157(2), 587–598. <https://doi.org/10.1104/pp.111.182352>
- Klusch, N., Senkler, J., Yildiz, Ö., Kühlbrandt, W., & Braun, H.-P. (2021). A ferredoxin bridge connects the two arms of plant mitochondrial complex I. *The Plant Cell*, 33(6), 2072–2091. <https://doi.org/10.1093/plcell/koab092>
- Klusch, N., Dreimann, M., Senkler, J., Rugen, N., Kühlbrandt, W., & Braun, H.-P. (2023). Cryo-EM structure of the respiratory I + III2 supercomplex from *Arabidopsis thaliana* at 2 Å resolution. *Nature Plants*, 9(1), 142–156. <https://doi.org/10.1038/s41477-022-01308-6>
- Ko, S. M., Kwon, Y. K., Kim, J. H., Song, I.-J., Lee, H.-Y., Choi, D.-W., Liu, J. R., Kim, S. W. (2014). Transcriptome analysis of mistletoe (*Viscum album*) haustorium development. *Horticulture, Environment, and Biotechnology*, 55(4), 352–361. <https://doi.org/10.1007/s13580-014-0033-6>
- Krauspenhaar, R., Eschenburg, S., Perbandt, M., Kornilov, V., Konareva, N., Mikailova, I., Stoeva, S., Wacker, R., Maier, T., Singh, T., Mikhailov, A., Voelter, W., Betzel, C. (1999). Crystal structure of mistletoe lectin I from *Viscum album*. *Biochemical and Biophysical Research Communications*, 257(2), 418–424. <https://doi.org/10.1006/bbrc.1999.0470>
- Kühn, K., Obata, T., Feher, K., Bock, R., Fernie, A. R., & Meyer, E. H. (2015). Complete Mitochondrial Complex I Deficiency Induces an Up-Regulation of Respiratory Fluxes That Is Abolished by Traces of Functional Complex I. *Plant Physiology*, 168(4), 1537–1549. <https://doi.org/10.1104/pp.15.00589>

- Lee, S. (2015). Seasonal Variation in Photosynthetic Characteristics and Chlorophyll Content of the *Loranthus tanakae*, *Viscum album* var. *coloratum* and its Hosts in Korea. *Journal of Korean Forest Society*, 104(1), 50–59. <https://doi.org/10.14578/jkfs.2015.104.1.50>
- Leitch IJ, Johnston E, Pellicer J, Hidalgo O, Bennett MD. (2019). Angiosperm DNA C-values database (release 9.0, Apr 2019) <https://cvalues.science.kew.org/>
- Leslie, A. B., Simpson, C., & Mander, L. (2021). Reproductive innovations and pulsed rise in plant complexity. *Science (New York, N.Y.)*, 373(6561), 1368–1372. <https://doi.org/10.1126/science.abi6984>
- Longoni, F. P., & Goldschmidt-Clermont, M. (2021). Thylakoid Protein Phosphorylation in Chloroplasts. *Plant & Cell Physiology*, 62(7), 1094–1107. <https://doi.org/10.1093/pcp/pcab043>
- Ma, M., Liu, Y., Bai, C., Yang, Y., Sun, Z., Liu, X., Zhang, S., Han, X., Yong, J. W. H. (2021). The Physiological Functionality of PGR5/PGRL1-Dependent Cyclic Electron Transport in Sustaining Photosynthesis. *Frontiers in Plant Science*, 12, 702196. <https://doi.org/10.3389/fpls.2021.702196>
- Maclean, A. E., Hertle, A. P., Ligas, J., Bock, R., Balk, J., & Meyer, E. H. (2018). Absence of Complex I Is Associated with Diminished Respiratory Chain Function in European Mistletoe. *Current Biology : CB*, 28(10), 1614-1619.e3. <https://doi.org/10.1016/j.cub.2018.03.036>
- Maldonado, M., Guo, F., & Letts, J. A. (2021). Atomic structures of respiratory complex III<sub>2</sub>, complex IV, and supercomplex III<sub>2</sub>-IV from vascular plants. *ELife*, 10. <https://doi.org/10.7554/eLife.62047>
- Malina, C., Larsson, C., & Nielsen, J. (2018). Yeast mitochondria: An overview of mitochondrial biology and the potential of mitochondrial systems biology. *FEMS Yeast Research*, 18(5). <https://doi.org/10.1093/femsyr/foy040>
- Mansilla, N., Racca, S., Gras, D. E., Gonzalez, D. H., & Welchen, E. (2018). The Complexity of Mitochondrial Complex IV: An Update of Cytochrome c Oxidase Biogenesis in Plants. *International Journal of Molecular Sciences*, 19(3). <https://doi.org/10.3390/ijms19030662>
- Marie, D., & Brown, S. C. (1993). A cytometric exercise in plant DNA histograms, with 2C values for 70 species. *Biology of the Cell*, 78(1-2), 41–51. [https://doi.org/10.1016/0248-4900\(93\)90113-S](https://doi.org/10.1016/0248-4900(93)90113-S).
- Martínez, J., Marmisolle, I., Tarallo, D., & Quijano, C. (2020). Mitochondrial Bioenergetics and Dynamics in Secretion Processes. *Frontiers in Endocrinology*, 11, 319. <https://doi.org/10.3389/fendo.2020.00319>.
- Maul, K., Krug, M., Nickrent, D. L., Müller, K. F., Quandt, D., & Wicke, S. (2019). Morphology, geographic distribution, and host preferences are poor predictors of phylogenetic relatedness in the mistletoe genus *Viscum* L. *Molecular Phylogenetics and Evolution*, 131, 106–115. <https://doi.org/10.1016/j.ympev.2018.10.041>
- Millar, A. H., Eubel, H., Jänsch, L., Kruff, V., Heazlewood, J. L., & Braun, H.-P. (2004). Mitochondrial cytochrome c oxidase and succinate dehydrogenase complexes contain plant specific subunits. *Plant Molecular Biology*, 56(1), 77–90. <https://doi.org/10.1007/s11103-004-2316-2>
- Minauro-Sanmiguel, F., Wilkens, S., & García, J. J. (2005). Structure of dimeric mitochondrial ATP synthase: Novel F<sub>0</sub> bridging features and the structural basis of mitochondrial cristae biogenesis. *Proceedings of the National Academy of Sciences of the United States of America*, 102(35), 12356–12358. <https://doi.org/10.1073/pnas.0503893102>

- Mohammed, S., & Ferry, N. (2021). Characterization of Sialic Acid Affinity of the Binding Domain of Mistletoe Lectin Isoform One. *International Journal of Molecular Sciences*, 22(15). <https://doi.org/10.3390/ijms22158284>
- Munekage, Y., Hojo, M., Meurer, J., Endo, T., Tasaka, M., & Shikanai, T. (2002). Pgr5 is involved in cyclic electron flow around photosystem I and is essential for photoprotection in Arabidopsis. *Cell*, 110(3), 361–371. [https://doi.org/10.1016/s0092-8674\(02\)00867-x](https://doi.org/10.1016/s0092-8674(02)00867-x)
- Nickrent, D. L. (2011). Santalales (Including Mistletoes). In eLS, (Ed.). <https://doi.org/10.1002/9780470015902.a0003714.pub2>
- Nickrent, D. L. (2020). Parasitic angiosperms: How often and how many? *TAXON*, 69(1), 5–27. <https://doi.org/10.1002/tax.12195>
- Novák, P., Guignard, M. S., Neumann, P., Kelly, L. J., Mlinarec, J., Koblížková, A., et al. (2020). Repeat-sequence turnover shifts fundamentally in species with large genomes. *Nature Plants*, 6(11), 1325–1329. <https://doi.org/10.1038/s41477-020-00785-x>
- Ochocka, J. R., & Piotrowski, A. (2002). Biologically active compounds from European mistletoe (*Viscum album* L.) 1. *Canadian Journal of Plant Pathology*, 24(1), 21–28. <https://doi.org/10.1080/07060660109506966>
- Ohnishi, T., Kawaguchi, K., & Hagihara, B. (1966). Preparation and some properties of yeast mitochondria. *The Journal of Biological Chemistry*, 241(8), 1797–1806.
- Paumard, P., Vaillier, J., Couлары, B., Schaeffer, J., Soubannier, V., Mueller, D. M., Brèthes, D., di Rago, J.-P., Velours, J. (2002). The ATP synthase is involved in generating mitochondrial cristae morphology. *The EMBO Journal*, 21(3), 221–230. <https://doi.org/10.1093/emboj/21.3.221>
- Pellicer, J., Fay, M. F., & Leitch, I. J. (2010). The largest eukaryotic genome of them all? *Botanical Journal of the Linnean Society*, 164(1), 10–15. <https://doi.org/10.1111/j.1095-8339.2010.01072.x>
- Peng, L., Shimizu, H., & Shikanai, T. (2008). The chloroplast NAD(P)H dehydrogenase complex interacts with photosystem I in Arabidopsis. *The Journal of Biological Chemistry*, 283(50), 34873–34879. <https://doi.org/10.1074/jbc.M803207200>
- Petersen, G., Cuenca, A., Møller, I. M., & Seberg, O. (2015). Massive gene loss in mistletoe (*Viscum*, Viscaceae) mitochondria. *Scientific Reports*, 5, 17588. <https://doi.org/10.1038/srep17588>
- Petersen, G., Anderson, B., Braun, H.-P., Meyer, E. H., & Møller, I. M. (2020). Mitochondria in parasitic plants. *Mitochondrion*, 52, 173–182. <https://doi.org/10.1016/j.mito.2020.03.008>
- Petersen, G., Cuenca, A., & Seberg, O. (2015). Plastome Evolution in Hemiparasitic Mistletoes. *Genome Biology and Evolution*, 7(9), 2520–2532. <https://doi.org/10.1093/gbe/evv165>
- Phytokodex: Pflanzliche Arzneyspezialitäten in Österreich (2001/2002) (2001). Wien, Ausg. 2001/2002: Österr. Apotheker-Verl.; Krause & Pachernegg. Retrieved from <https://permalink.obvsg.at/AC03298066>
- Rathore, S., Berndtsson, J., Marin-Buera, L., Conrad, J., Carroni, M., Brzezinski, P., & Ott, M. (2019). Cryo-EM structure of the yeast respiratory supercomplex. *Nature Structural & Molecular Biology*, 26(1), 50–57. <https://doi.org/10.1038/s41594-018-0169-7>

- Raven, J. A., & Beardall, J. (2017). Consequences of the genotypic loss of mitochondrial Complex I in dinoflagellates and of phenotypic regulation of Complex I content in other photosynthetic organisms. *Journal of Experimental Botany*, 68(11), 2683–2692. <https://doi.org/10.1093/jxb/erx149>
- Richter, A., & Popp, M. (1992). The physiological importance of accumulation of cyclitols in *Viscum album* L. *The New Phytologist*, 121(3), 431–438. <https://doi.org/10.1111/j.1469-8137.1992.tb02943.x>
- Rodríguez-Nuevo, A., Torres-Sanchez, A., Duran, J. M., Guirior, C. de, Martínez-Zamora, M. A., & Böke, E. (2022). Oocytes maintain ROS-free mitochondrial metabolism by suppressing complex I. *Nature*, 607(7920), 756–761. <https://doi.org/10.1038/s41586-022-04979-5>
- Romagnoli, S., Fogolari, F., Catalano, M., Zetta, L., Schaller, G., Urech, K., Giannattasio, M., Ragona, L., Molinari, H. (2003). Nmr solution structure of viscotoxin C1 from *Viscum album* species *Coloratum ohwi*: Toward a structure-function analysis of viscotoxins. *Biochemistry*, 42(43), 12503–12510. <https://doi.org/10.1021/bi034762t>
- Schägger, H., & Pfeiffer, K. (2000). Supercomplexes in the respiratory chains of yeast and mammalian mitochondria. *The EMBO Journal*, 19(8), 1777–1783. <https://doi.org/10.1093/emboj/19.8.1777>
- Scheffler, I.E. (1999). Metabolic Pathways Inside Mitochondria. In *Mitochondria*, I.E. Scheffler (Ed.). <https://doi.org/10.1002/0471223891.ch6>
- Schertl, P., Braun, H.P. (2014) Respiratory electron transfer pathways in plant mitochondria. *Front Plant Sci*. 5: 163. doi: 10.3389/fpls.2014.00163. PMID: 24808901; PMCID: PMC4010797.
- Schuller, J. M., Birrell, J. A., Tanaka, H., Konuma, T., Wulfhorst, H., Cox, N., et al. (2019). Structural adaptations of photosynthetic complex I enable ferredoxin-dependent electron transfer. *Science (New York, N.Y.)*, 363(6424), 257–260. <https://doi.org/10.1126/science.aau3613>
- Senkler, J., Rugen, N., Eubel, H., Hegermann, J., & Braun, H.-P. (2018). Absence of Complex I Implicates Rearrangement of the Respiratory Chain in European Mistletoe. *Current Biology : CB*, 28(10), 1606–1613.e4. <https://doi.org/10.1016/j.cub.2018.03.050>
- Senkler, J., Senkler, M., Eubel, H., Hildebrandt, T., Lengwenus, C., Schertl, P., Schwarzländer, M., Wagner, S., Wittig, I., Braun, H.-P. (2017). The mitochondrial complexome of *Arabidopsis thaliana*. *The Plant Journal: For Cell and Molecular Biology*, 89(6), 1079–1092. <https://doi.org/10.1111/tpj.13448>
- Shen, L., Tang, K., Wang, W., Wang, C., Wu, H., Mao, Z., et al. (2022). Architecture of the chloroplast PSI-NDH supercomplex in *Hordeum vulgare*. *Nature*, 601(7894), 649–654. <https://doi.org/10.1038/s41586-021-04277-6>
- Shikanai, T. (2014). Central role of cyclic electron transport around photosystem I in the regulation of photosynthesis. *Current Opinion in Biotechnology*, 26, 25–30. <https://doi.org/10.1016/j.copbio.2013.08.012>
- Singh, R., Ming, R., & Yu, Q. (2016). Comparative Analysis of GC Content Variations in Plant Genomes. *Tropical Plant Biology*, 9(3), 136–149. <https://doi.org/10.1007/s12042-016-9165-4>
- Skippington, E., Barkman, T. J., Rice, D. W., & Palmer, J. D. (2015). Miniaturized mitogenome of the parasitic plant *Viscum scurruloideum* is extremely divergent and dynamic and has lost all nad genes. *Proceedings of the National Academy of Sciences of the United States of America*, 112(27), E3515–24. <https://doi.org/10.1073/pnas.1504491112>

- Skippington, E., Barkman, T. J., Rice, D. W., & Palmer, J. D. (2017). Comparative mitogenomics indicates respiratory competence in parasitic *Viscum* despite loss of complex I and extreme sequence divergence, and reveals horizontal gene transfer and remarkable variation in genome size. *BMC Plant Biology*, 17(1), 49. <https://doi.org/10.1186/s12870-017-0992-8>
- Stirbet, A., Lazár, D., Guo, Y., & Govindjee, G. (2020). Photosynthesis: Basics, history and modelling. *Annals of Botany*, 126(4), 511–537. <https://doi.org/10.1093/aob/mcz171>
- Stroh, A., Anderka, O., Pfeiffer, K., Yagi, T., Finel, M., Ludwig, B., & Schägger, H. (2004). Assembly of respiratory complexes I, III, and IV into NADH oxidase supercomplex stabilizes complex I in *Paracoccus denitrificans*. *The Journal of Biological Chemistry*, 279(6), 5000–5007. <https://doi.org/10.1074/jbc.M309505200>
- Těšitel, J. (2016). Functional biology of parasitic plants: a review. *Plant Ecology and Evolution*, 149(1), 5–20. <https://doi.org/10.5091/plecevo.2016.1097>
- Thomas, P. A., Dering, M., Giertych, M. J., Iszkuło, G., Tomaszewski, D., & Briggs, J. (2023). Biological Flora of Britain and Ireland: *Viscum album*. *Journal of Ecology*, 111(3), 701–739. <https://doi.org/10.1111/1365-2745.14036>
- Tikkanen, O.-P., Kilpeläinen, J., Mellado, A., Hämäläinen, A., Hódar, J. A., Jaroszewicz, B., et al. (2021). Freezing tolerance of seeds can explain differences in the distribution of two widespread mistletoe subspecies in Europe. *Forest Ecology and Management*, 482, 118806. <https://doi.org/10.1016/j.foreco.2020.118806>
- Tuquet, C., & Sallé, G. (1996). Characteristics of chloroplasts isolated from two mistletoes originating from temperate (*Viscum album*) and tropical (*Tapinanthus dodoneifolius*) areas. *Plant physiology and biochemistry (Paris)*, 34(2), 283-292.
- Urech, K., Schaller, G., & Jäggy, C. (2006). Viscotoxins, mistletoe lectins and their isoforms in mistletoe (*Viscum album* L.) extracts Iscador. *Arzneimittel-Forschung*, 56(6A), 428–434. <https://doi.org/10.1055/s-0031-1296808>
- Vinogradov, A. E. (2003). Dna helix: The importance of being GC-rich. *Nucleic Acids Research*, 31(7), 1838–1844. <https://doi.org/10.1093/nar/gkg296>
- Vitols, E., & Linnane, A. W. (1961). Studies on the oxidative metabolism of *Saccharomyces cerevisiae*. II. Morphology and oxidative phosphorylation capacity of mitochondria and derived particles from baker's yeast. *The Journal of Biophysical and Biochemical Cytology*, 9(3), 701–710. <https://doi.org/10.1083/jcb.9.3.701>
- Wacker, R., Stoeva, S., Pfüller, K., Pfüller, U., & Voelter, W. (2004). Complete structure determination of the A chain of mistletoe lectin III from *Viscum album* L. Ssp. Album. *Journal of Peptide Science: An Official Publication of the European Peptide Society*, 10(3), 138–148. <https://doi.org/10.1002/psc.505>
- Walas, Ł., Kędziora, W., Ksepko, M., Rabska, M., Tomaszewski, D., Thomas, P. A., et al. (2022). The future of *Viscum album* L. in Europe will be shaped by temperature and host availability. *Scientific Reports*, 12(1), 17072. <https://doi.org/10.1038/s41598-022-21532-6>
- Wei, X., Guo, H., Che, P., Zhang, B., Liu, H., & Qi, Y. (2019). The complete chloroplast genome sequence of *Viscum coloratum* (Viscaceae), a semiparasitic medicinal plant. *Mitochondrial DNA. Part B, Resources*, 4(2), 2904–2905. <https://doi.org/10.1080/23802359.2019.1660923>



- Whittingstall, P. (2001). Overview of Viscosity and Its Characterization. *Current Protocols in Food Analytical Chemistry*, 00(1). <https://doi.org/10.1002/0471142913.fah0101s00>
- Wittig, I., & Schägger, H. (2008). Structural organization of mitochondrial ATP synthase. *Biochimica Et Biophysica Acta*, 1777(7-8), 592–598. <https://doi.org/10.1016/j.bbabi.2008.04.027>
- Yakovchuk, P., Protozanova, E., Frank-Kamenetskii, M.D. (2006) Base-stacking and base-pairing contributions into thermal stability of the DNA double helix. *Nucleic Acids Res.* 34(2):564-74. <https://doi.org/10.1093/nar/gkj454>
- Yamamoto, H., Peng, L., Fukao, Y., & Shikanai, T. (2011). An Src homology 3 domain-like fold protein forms a ferredoxin binding site for the chloroplast NADH dehydrogenase-like complex in Arabidopsis. *The Plant Cell*, 23(4), 1480–1493. <https://doi.org/10.1105/tpc.110.080291>
- Yousefvand, S., Fattahi, F., Hosseini, S. M., Urech, K., & Schaller, G. (2022). Viscotoxin and lectin content in foliage and fruit of *Viscum album* L. On the main host trees of Hyrcanian forests. *Scientific Reports*, 12(1), 10383. <https://doi.org/10.1038/s41598-022-14504-3>
- Zervas, A., Petersen, G., & Seberg, O. (2019). Mitochondrial genome evolution in parasitic plants. *BMC Evolutionary Biology*, 19(1), 87. <https://doi.org/10.1186/s12862-019-1401-8>
- Zonneveld, B. J. M. (2010). New Record Holders for Maximum Genome Size in Eudicots and Monocots. *Journal of Botany*, 2010, 1–4. <https://doi.org/10.1155/2010/527357>
- Zuber, D., & Widmer, A. (2009). Phylogeography and host race differentiation in the European mistletoe (*Viscum album* L.). *Molecular Ecology*, 18(9), 1946–1962. <https://doi.org/10.1111/j.1365-294x.2009.04168.x>
- Zuber, D. (2004). Biological flora of Central Europe: *Viscum album* L. *Flora - Morphology, Distribution, Functional Ecology of Plants*, 199(3), 181–203. <https://doi.org/10.1078/0367-2530-00147>

## 2 Publications and Manuscripts

## 2.1 The gene space of European mistletoe (*Viscum album*)

Lucie Schröder<sup>1</sup>, Natalija Hohnjec<sup>2</sup>, Michael Senkler<sup>1</sup>, Jennifer Senkler<sup>1</sup>, Helge Küster<sup>2</sup>, Hans-Peter Braun<sup>1</sup>

<sup>1</sup> Plant Proteomics, Institute of Plant Genetics, Leibniz Universität Hannover, Herrenhäuser Str. 2, 30419, Hannover, Germany.

<sup>2</sup> Plant Genomics, Institute of Plant Genetics, Leibniz Universität Hannover, Herrenhäuser Str. 2, 30419, Hannover, Germany.

Type of authorship:	First author
Type of article:	Research article
Share of the work:	60 %
Contribution to the publication:	Performed experiments, analyzed data, prepared figures, participated in writing the manuscript
Journal:	The Plant Journal
Impact factor:	7.091 (2022/2023)
Date of publication:	January 2022
Number of citations:	11
(Google Scholar, 20.09.2023)	
DOI:	10.1111/tpj.15558
PubMed-ID:	34713513

# *the plant journal*



VOLUME 109 | NUMBER 1 | JANUARY 2022  
<http://www.theplantjournal.com> | ISSN 1365-313X

WILEY

# the plant journal

CONTENTS OF VOL. 109, NO. 1, JANUARY 2022

## RESEARCH HIGHLIGHT

- 5 **From the redwood forest to the gulf stream waters – drought resistance in coast redwoods and giant sequoias.** L. Verhage (Research Highlights Editor)

## ORIGINAL ARTICLE

- 7 **Genome-wide association identifies candidate genes for drought tolerance in coast redwood and giant sequoia.** A. R. De La Torre, M. K. Sekhwal, D. Puiu, S. L. Salzberg, A. D. Scott, B. Allen, D. B. Neale, A. R. O. Chin and T. N. Buckley

## PERSPECTIVES

- 23 **Redesigning the photosynthetic light reactions to enhance photosynthesis – the *PhotoRedesign* consortium.** A. Hitchcock, C. N. Hunter, R. Sobotka, J. Komenda, M. Dann and D. Leister
- 35 **Combining novel technologies with interdisciplinary basic research to enhance horticultural crops.** X. Jiang, W. Zhang, A. R. Fernie and W. Wen

## ORIGINAL ARTICLES

- 47 **A mutation in the promoter of the arabinogalactan protein 7-like gene *PcAGP7-1* affects cell morphogenesis and brassinolide content in pear (*Pyrus communis* L.) stems.** X. Zheng, Y. Li, C. Ma, B. Chen, Z. Sun, Y. Tian and C. Wang
- 64 **Natural variation of *ZmCGT1* is responsible for isoorientin accumulation in maize silk.** X. Sun, X. Xue, X. Wang, C. Zhang, D. Zheng, W. Song, J. Zhao, J. Wei, Z. Wu and Z. Zhang
- 77 **Limiting factors for panicle photosynthesis at the anthesis and grain filling stages in rice (*Oryza sativa* L.).** Q. Zhang, W. Tang, S. Peng and Y. Li
- 92 **Acetylation of conserved lysines fine-tunes mitochondrial malate dehydrogenase activity in land plants.** M. Balparda, M. Elsässer, M. B. Badía, J. Giese, A. Bovdilova, M. Hüdig, L. Reinmuth, J. Eirich, M. Schwarzländer, I. Finkemeier, M. Schallenberg-Rüdinger and V. G. Maurino
- 112 **Gene targeting in polymerase theta-deficient *Arabidopsis thaliana*.** N. van Tol, R. van Schendel, A. Bos, M. van Kregten, S. de Pater, P. J. J. Hooykaas and M. Tijsterman
- 126 **MicroRNA840 (*MIR840*) accelerates leaf senescence by targeting the overlapping 3'UTRs of *PPR* and *WHIRLY3* in *Arabidopsis thaliana*.** Y. Ren, M. Li, W. Wang, W. Lan, D. Schenke, D. Cai and Y. Miao
- 144 **Oxidative stress response and programmed cell death guided by *NAC013* modulate pithiness in radish taproots.** N. V. Hoang, S. Park, C. Park, H. Suh, S.-T. Kim, E. Chae, B.-C. Kang and J.-Y. Lee
- 164 **Glucuronidation of type II arabinogalactan polysaccharides function in sexual reproduction of *Arabidopsis*.** O. O. Ajayi, M. A. Held and A. M. Showalter
- 182 **Alternative splicing triggered by the insertion of a CACTA transposon attenuates *LsGLK* and leads to the development of pale-green leaves in lettuce.** L. Zhang, J. Qian, Y. Han, Y. Jia, H. Kuang and J. Chen
- 196 **The *Arabidopsis* electron-transfer flavoprotein:ubiquinone oxidoreductase is required during normal seed development and germination.** P. da Fonseca-Pereira, P. A. Pham, J. H. F. Cavalcanti, R. P. Omena-Garcia, J. A. S. Barros, L. Rosado-Souza, J. G. Vallarino, M. Mutwil, T. Avin-Wittenberg, A. Nunes-Nesi, A. R. Fernie and W. L. Araújo
- 215 **The RanBP2 zinc finger domains of chloroplast RNA editing factor *OZ1* are required for protein–protein interactions and conversion of C to U.** A. B. Gipson, M. R. Hanson and S. Bentolila
- 227 ***DICER-LIKE1a* autoregulation based on intronic microRNA processing is required for stress adaptation in *Physcomitrium patens*.** M. A. Arif, O. Top, E. Csicsely, M. Lichtenstern, H. Beheshti, K. Adjabi and W. Frank
- 241 ***CIPK9* targets *VDAC3* and modulates oxidative stress responses in *Arabidopsis*.** P. Kanwar, S. K. Sanyal, S. Mahiwal, B. Ravi, K. Kaur, J. L. Fernandes, A. K. Yadav, I. Tokas, A. K. Srivastava, P. Suprasanna and G. K. Pandey

## RESOURCE

- 261 **Dynamic light- and acetate-dependent regulation of the proteome and lysine acetylome of *Chlamydomonas*.** M. Füll, A.-C. König, J. Eirich, M. Hartl, L. Kleinknecht, A.-V. Bohne, A. Harzen, K. Kramer, D. Leister, J. Nickelsen and I. Finkemeier
- 278 **The gene space of European mistletoe (*Viscum album*).** L. Schröder, N. Hohnjec, M. Senkler, J. Senkler, H. Küster and H.-P. Braun

## TECHNICAL ADVANCE

- 295 **A hybrid kinetic and constraint-based model of leaf metabolism allows predictions of metabolic fluxes in different environments.** S. Shameer, Y. Wang, P. Bota, R. G. Ratcliffe, S. P. Long and L. J. Sweetlove



**Front cover:** European mistletoe (*Viscum album*) at the Herrenhausen Gardens in Hannover, Germany. The photo shows a female mistletoe plant with yellow flowers and white berries. In this issue (page 278–294), Schröder *et al.* present the gene space of *V. album*. Transcripts were isolated from different *V. album* organs harvested in summer and winter and analysed via single-molecule real time sequencing. [Photo: Luisa Braun and Hans-Peter Braun, 2021].

## RESOURCE

The gene space of European mistletoe (*Viscum album*) 

Lucie Schröder<sup>1</sup> , Natalija Hohnjec<sup>2</sup>, Michael Senkler<sup>1</sup> , Jennifer Senkler<sup>1</sup> , Helge Küster<sup>2</sup>  and Hans-Peter Braun<sup>1\*</sup> 

<sup>1</sup>Plant Proteomics, Institute of Plant Genetics, Leibniz Universität Hannover, Herrenhäuser Str. 2, 30419, Hannover, Germany, and

<sup>2</sup>Plant Genomics, Institute of Plant Genetics, Leibniz Universität Hannover, Herrenhäuser Str. 2, 30419, Hannover, Germany

Received 28 July 2021; revised 28 September 2021; accepted 1 October 2021; published online 29 October 2021.

\*For correspondence (e-mail braun@genetik.uni-hannover.de).

## SUMMARY

European mistletoe (*Viscum album*) is a hemiparasitic flowering plant that is known for its very special life cycle and extraordinary biochemical properties. Particularly, *V. album* has an unusual mode of cellular respiration that takes place in the absence of mitochondrial complex I. However, insights into the molecular biology of *V. album* so far are very limited. Since the genome of *V. album* is extremely large (estimated 600 times larger than the genome of the model plant *Arabidopsis thaliana*) it has not been sequenced up to now. We here report sequencing of the *V. album* gene space (defined as the space including and surrounding genic regions, encompassing coding as well as 5' and 3' non-coding regions). mRNA fractions were isolated from different *V. album* organs harvested in summer or winter and were analyzed via single-molecule real-time sequencing. We determined sequences of 39 092 distinct open reading frames encoding 32 064 *V. album* proteins (designated *V. album* protein space). Our data give new insights into the metabolism and molecular biology of *V. album*, including the biosynthesis of lectins and viscotoxins. The benefits of the *V. album* gene space information are demonstrated by re-evaluating mass spectrometry-based data of the *V. album* mitochondrial proteome, which previously had been evaluated using the *A. thaliana* genome sequence. Our re-examination allowed the additional identification of nearly 200 mitochondrial proteins, including four proteins related to complex I, which all have a secondary function not related to respiratory electron transport. The *V. album* gene space sequences are available at the NCBI.

**Keywords:** SMRT sequencing, viscotoxins, lectins, mitochondria, oxidative phosphorylation, complex I, *Viscum album*, *Arabidopsis thaliana*.

## INTRODUCTION

European mistletoe (*Viscum album*) is an obligate hemiparasitic flowering plant that grows on branches of various trees. It is supplied with water, minerals and organic compounds from the host. At the same time, *V. album* carries out photosynthesis and produces energy-rich compounds. *Viscum album* is widely distributed in central and northern Europe. It nicely is visible from November to March because it belongs to the few angiosperms that do not discard their leaves in the European winter. In fact, *V. album* is photosynthetically active at temperatures below the freezing point. *Viscum album* can cause problems in tree vitality, especially in combination with water stress. However, under favorable growth conditions, host trees are only moderately affected and can well coexist with the

hemiparasite. European mistletoe has important ecological functions. Its flowers and berries ripe in winter and are a nutritional source for several insects and birds.

Compared to other flowering plants, the life cycle of *V. album* is characterized by numerous remarkable features (reviewed, e.g., in Glatzel and Geils, 2009): (i) *V. album* does not germinate in soil but on branches of trees, which requires particularly 'sticky' fruits (berries) that stably attach to tree bark; (ii) seeds consist of an embryo but lack a seed coat; (iii) embryos can germinate directly from the berry (without a dormancy phase); (iv) the direction of initial shoot growth is not determined by positive but rather negative phototropism, which guides the shoot onto the surface of the branch of the host tree; (v) the shoot

afterwards penetrates the branch and gets connected to the xylem of the vascular system, where it forms a haustorium for uptake of water, minerals and organic compounds; (vi) the dichotomous mistletoe plant, which afterwards develops, forms one pair of shoot segments per year per shoot apical meristem and two comparatively simply organized leaves, which resemble primary leaves; (vii) shoots grow into all directions, giving rise to the typical ball-like shape of the adult plant (overall, the growth rate of *V. album* is low); (viii) in contrast to the leaves of the host tree, mistletoe leaves do not close stomata during water shortage (which may dramatically increase water stress of host plants); (ix) older leaves of the previous growth periods are discarded in September without preceding chlorophyll recycling; (x) leaves of the current growth period are kept during winter and perform photosynthesis; and (xi) fruit ripening and seed dispersal take place in winter.

*Viscum album* also has a particular biochemical composition. It is known for its rich content in phenolic acids, phenylpropanoids, flavonoids, triterpenes and phytosterols (Jäger *et al.*, 2021; Urech and Baumgartner, 2015). It contains low-molecular-mass proteins designated viscotoxins as well as characteristic lectins (viscolectins), both of which contribute to its biotic defense system. The glue-like substances present in mistletoe berries mainly consist of hemicellulose compounds (Azuma *et al.*, 2000). It is clear but hardly addressed by scientific investigations that the development of mistletoe is based on a very unusual distribution of phytohormones. Extracts of *V. album* have cytotoxic and immune-stimulating effects and are used in medicine (Nazaruk and Orlikowski, 2016).

On a molecular scale, *V. album* has been less characterized to date. Its mitochondrial and chloroplast genomes have been sequenced (Petersen *et al.*, 2015a,b; Skiptington *et al.*, 2015, 2017) and were surprisingly found to lack some genes previously considered to be essential for multicellular eukaryotes, like genes encoding subunits of complex I of the mitochondrial respiratory chain. In contrast, the sequence of the nuclear genome has not been analyzed. The *V. album* genome consists of  $2n = 20$  chromosomes, is exceptionally large and is estimated to have a mass of 160 pg (80 pg for the haploid genome; average taken from the 'Plant DNA C-values Database', Pellicer and Leitch, 2019 [<https://cvalues.science.kew.org/search>]; original data from Nagl *et al.*, 1983 [53.5 pg], Ulrich *et al.*, 1988 [79.3 pg], Marie and Brown, 1993 [76 and 77.5 pg] and Zonneveld, 2010 [102.9 pg]). Indeed, the *V. album* genome is one of the largest genomes of any flowering plant known to date (Novák *et al.*, 2020; Zonneveld, 2010). Its size has been estimated to be in the range of  $88 \times 10^9$  base pairs (approximately 90 Gbp; Novák *et al.*, 2020), which is 600 times the size of the genome of the model plant *Arabidopsis thaliana* (approximately 0.15 Gbp). Correspondingly, chromosomes of *V. album* are very large. Structural

rearrangements in the chromosomes occur frequently and may cause large chromosome assemblies during meiosis (Barlow, 1981). The GC content is in the range of 39%, which is about average for flowering plants (Novák *et al.*, 2020). An initial transcriptome analysis of *V. album* haustorium tissue has been performed and yielded sequences of 3044 open reading frames (Ko *et al.*, 2014).

The gene content of seed plants (angiosperms and gymnosperms) is considered to be similar and amounts to approximately 0.03 Gbp (Novák *et al.*, 2020). This implies that the gene content of *V. album* only covers 0.03% of its genome (20% in *A. thaliana*) and that the size of the inter-gene space is enormous. In general, genome size of eukaryotes correlates with the amount of repetitive DNA (Elliott and Gregory, 2015). Interestingly, this does not hold true for especially large genomes of seed plants (>10 Gbp), which unexpectedly were found not to have a further increased amount of repetitive DNA. In *V. album*, the genome proportion of repeats (copy number > 20) is 55% (Novák *et al.*, 2020). This leaves much space for non-repetitive and low-copy DNA (excluding protein-coding genes).

Due to genome size and the amount of repetitive DNA, determination of the *V. album* genome sequence remains challenging. We therefore decided to firstly characterize the *V. album* gene space. The mRNA fraction was extracted from various organs of *V. album*, reverse-transcribed into cDNAs and subsequently used for systematic sequence determination by single-molecule real-time (SMRT) sequencing. We developed a database including >39 000 *V. album* gene sequences, which contain complete open reading frames encoding *V. album* proteins. Several new insights into the molecular biology of *V. album* are provided by an initial analysis of the deduced protein sequences and by re-evaluation of previously published *V. album* proteome data. The database is publicly available.

## RESULTS AND DISCUSSION

### SMRT sequencing of the *V. album* gene space

SMRT sequencing was used to analyze the full-length transcriptome of a pooled *V. album* RNA sample (representing stems, leaves and male and female flower buds; harvested in summer and winter). Quality control of our RNA was performed by gel electrophoresis, Qubit fluorometry and Nanodrop spectrophotometry (Table S1). The pooled RNA sample was reverse-transcribed into cDNA and subsequently converted into double-stranded cDNA. Two SMRTbell libraries (termed libraries A and B) were constructed for sequencing without size selection. SMRT sequencing was performed using both libraries. The analysis workflow is given in Figure 1 and a summary of the primary results is given in Table 1.

Overall, SMRT sequencing of libraries A and B revealed 321 472 and 343 119 circular consensus sequences (CCSs;

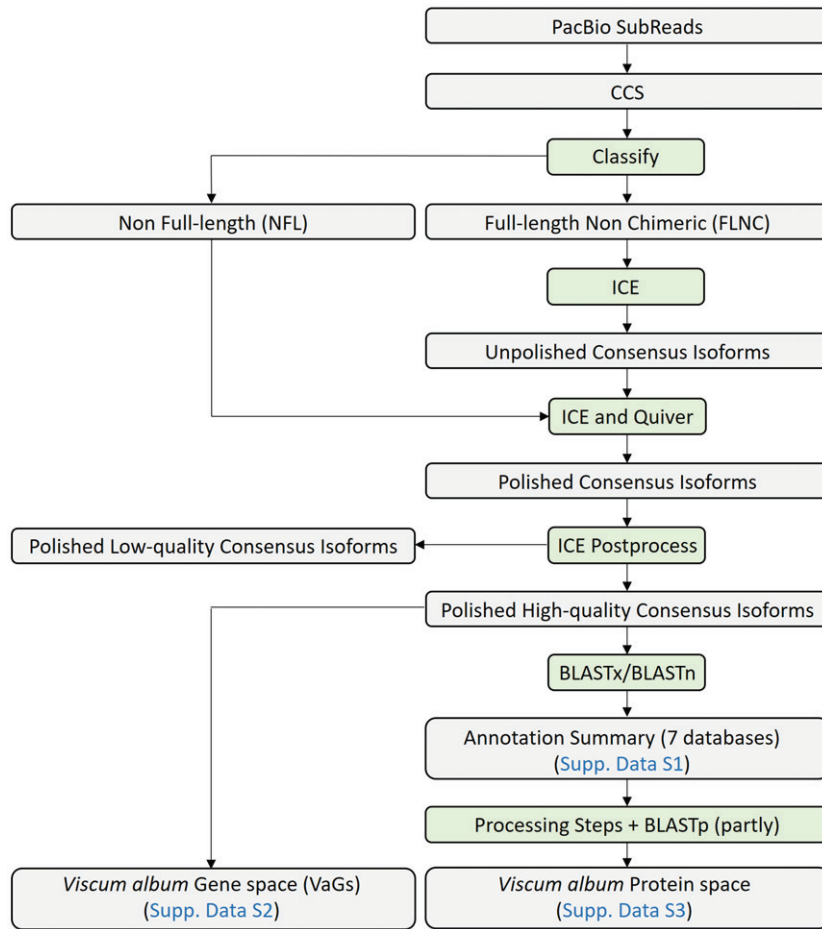


**Figure 1.** *Viscum album* gene space annotation summary. The different processing steps are shown in green. CCS, circular consensus sequence; ICE, Iterative Clustering for Error correction. For further information, see the Experimental Procedures section. Data are presented in Data S1–S3 (the Supplemental Data are highlighted in blue in the figure).

**Table 1** Summary of reads from PacBio SMRT sequencing (for analysis workflow see Figure 1)

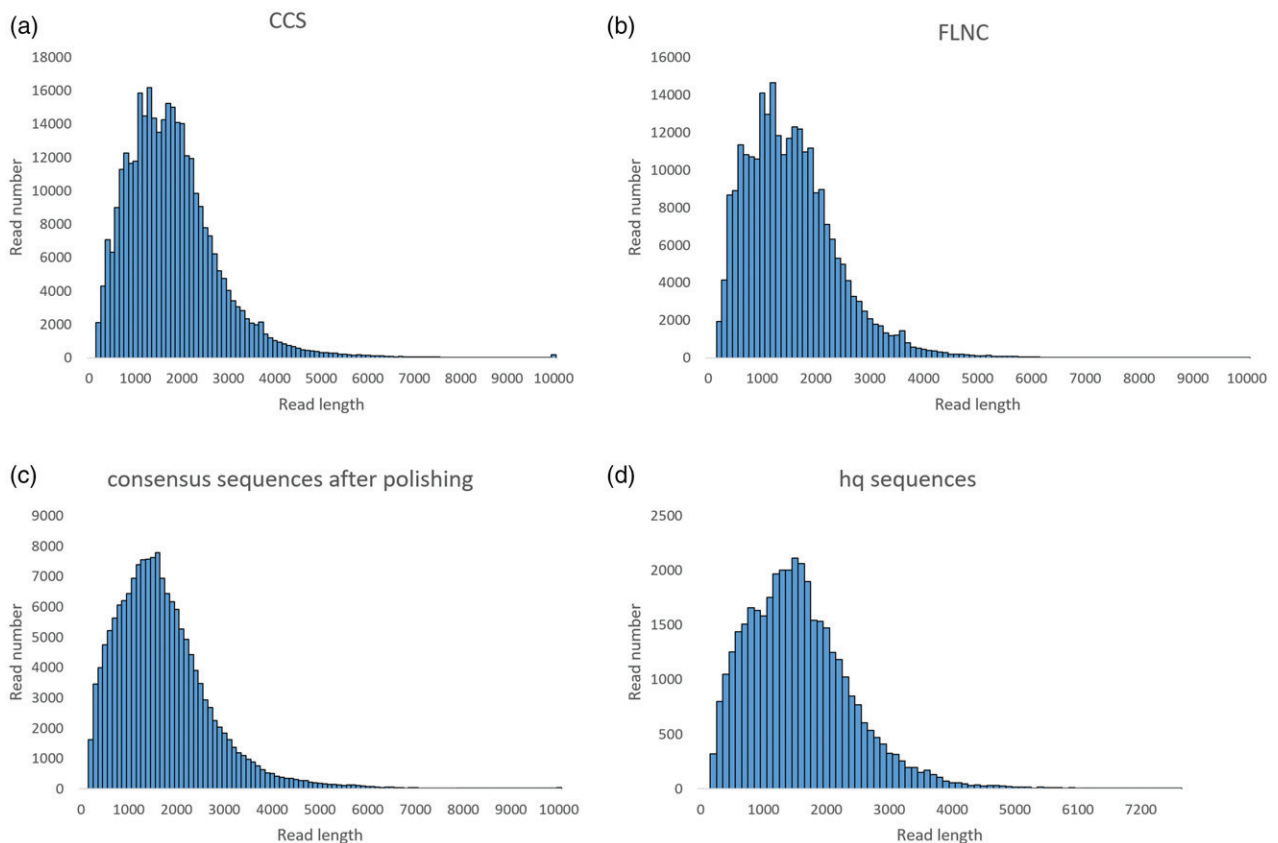
	Library A	Library B
Number of subreads	11 894 129	10 838 444
Circular consensus sequence (CCS) number	321 472	343 119
Average CCS length	1746	1846
Full-length reads	286 599	306 147
Non-full-length reads	27 518	30 762
Short reads	7355	6210
Full-length non-chimeric reads	253 284	268 386
Average length of full-length non-chimeric reads	1522	1595
Collected final consensus after polishing	161 841	
High-quality (hq) sequences	39 092	
Low-quality (lq) sequences	122 749	

Table 1). In total, 89% of the sequences were classified as full-length transcripts (including 5' and 3' adapters as well as poly(A) tails). In a next processing step, full-length

non-chimeric sequences were defined for both libraries. The Iterative Clustering for Error correction (ICE) algorithm was used to define unpolished consensus isoforms, which afterwards were polished using the Quiver algorithm. Based on sequence accuracy, resulting polished consensus sequences were divided into high- (hq) and low-quality (lq) sequences. As a result, 39 092 hq sequences were defined. Length profiles of the sequences at the different processing steps are given in Figure 2.

The coding domain sequences (CDSs) of the 39 092 hq sequences were predicted by BLAST and ESTscan analyses using the current releases of the Swiss-Prot (<https://www.uniprot.org/>) and NR (<https://www.ncbi.nlm.nih.gov/>) databases. Functional annotation of all sequences was carried out using seven databases (see the Experimental Procedures section; Data S1). Accession numbers were assigned to all sequences, which range from VaGs00001 to VaGs39092 (VaGs, *V. album* gene space). For ease of use, a table was prepared which includes all hq nucleotide sequences, their accession numbers, sequence length





**Figure 2.** Length profiles of *V. album* sequences defined along the different data processing steps. (a) Length profile of circular consensus (CCS) sequences. (b) Length profile of full-length non-chimeric (FLNC) sequences. (c) Length profile of the consensus sequences after polishing. (d) Length profile of the 39 092 high-quality (hq) sequences. See Table 1 and Figure 1 for information on the processing steps.

information and encoded amino acid sequences as well as information on functional predictions (*V. album* gene space, Data S2). For all accessions, the table also includes the most similar protein of the model plant *A. thaliana*. Finally, a more focused table is presented that lists all *V. album* proteins encoded by the 39 092 hq sequences (*V. album* protein space, Data S3). The overall number of distinct proteins is 32 064, because some of the hq DNA sequences slightly differ but encode proteins with identical amino acid sequences. This might indicate the presence of isogenes and/or allelic variation.

The completeness of the presented gene space with respect to the entire *V. album* transcriptome lies at approximately 78%, as revealed by an evaluation using the Benchmarking Universal Single-Copy Orthologs (BUSCO) software (Seppey *et al.*, 2019; Figure 3).

### Transcriptome properties in *V. album*

The sequences of the 39 092 full-length transcripts offer new insights into the transcriptome structure and composition of *V. album*. Overall, the GC content of the coding regions within *V. album* transcripts lies at 50.0%, which is

well above the 39.4% determined before by cytometric analyses of the entire *V. album* genome (Marie and Brown, 1993). An increased GC content in coding regions in comparison to intergenic regions is common in plants. For instance, the GC content of coding regions in *A. thaliana* is 44%, but it is only 34% in non-coding regions (Arabidopsis Genome Initiative, 2000). Similarly, the GC content of coding regions of several other dicotyledonous plants is in the range of 43–45% (Singh *et al.*, 2016). Within the clade of dicotyledonous plants, the GC content of *V. album* is strikingly high. A high GC content has positive effects on genome stability but comes at the price of increased energy demand for transcription and genome replication, which both require opening of the double helix.

The codon usage in *V. album* does not differ fundamentally from that in *A. thaliana*, with a few exceptions. For example, the CCC codon (which encodes proline) has a frequency of 12.9/1000 codons in *V. album* but only 5.2/1000 codons in *A. thaliana*; similarly, the GGG codon (which encodes glycine) has a frequency of 20.1/1000 codons in *V. album* but only 10.2/1000 codons in *A. thaliana* (Table S2). Overall, several codons of increased abundance in *V.*

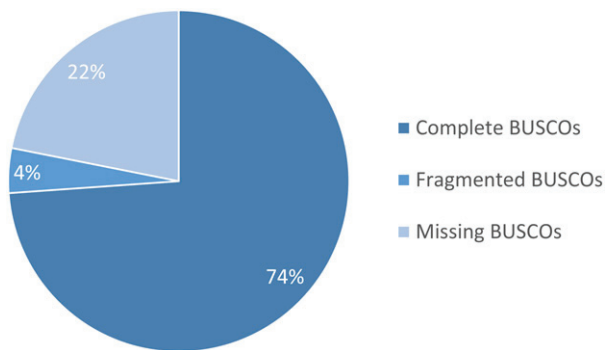


**Figure 3.** Completeness of the *V. album* gene space as revealed by ‘Benchmarking Universal Single-Copy Orthologs’ (BUSCO) analysis (Seppey *et al.*, 2019).

*album* are rich in G and/or C, which contributes to the increased GC content of transcripts in *V. album*.

#### Proteome properties in *V. album*

The proteins encoded by the *V. album* gene space have an average molecular mass of 40.4 kDa (Figure 4). The average molecular mass of proteins encoded by the *A. thaliana* genome has been reported to be 45.9 kDa based on evaluation of The Arabidopsis Information Resource (TAIR) 7 genome release (Baerenfaller *et al.*, 2008). Recalculation of the average molecular mass of proteins in *A. thaliana*

using the TAIR10 genome release revealed an average molecular mass of 45.8 kDa. Hence, the average molecular mass of *V. album* proteins is slightly lower. However, this result has to be treated with caution because we cannot rule out the possibility that a low percentage of transcripts in the *V. album* gene space code for incomplete proteins, which would affect our calculation. At the same time, the overall similar average molecular mass of the proteins in *V. album* and *A. thaliana* can be taken as evidence that a high percentage of our *V. album* transcripts can be considered to be complete.

The average isoelectric point (IEP) of *V. album* proteins encoded by our gene space is 7.43. However, a plot of IEPs of all *V. album* proteins encoded by our gene space shows a bimodal IEP distribution with two peaks at pH 5.8 and 9.2 and a prominent minimum at pH 7.5 (Figure 4). This IEP distribution has been reported before for several other species, including *A. thaliana* (Kiraga *et al.*, 2007; Schwartz *et al.*, 2001; van Wijk *et al.*, 2021), and is interpreted to reflect that solubility of proteins in aqueous solutions is low close to their isoelectric points. The hydrophobicity of the *V. album* proteins peaks at a GRAVY value of  $-0.2$ , which again is similar to the value calculated for *A. thaliana* ( $-0.3$  based on analyses using the TAIR10 genome release; Figure 4).

To estimate the average amino acid identity between proteins from *V. album* and *A. thaliana*, sequence comparisons were carried out for selected proteins (Table 2). As

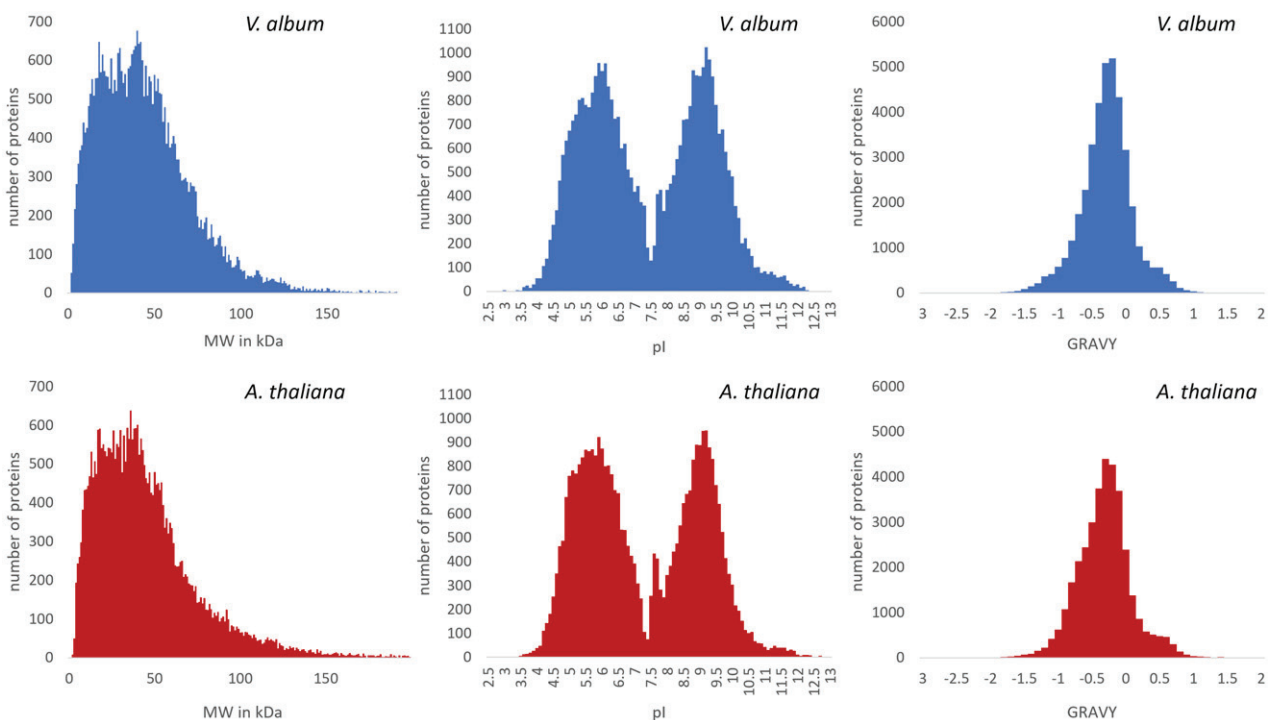


**Figure 4.** Physicochemical properties of proteins from *V. album* and *A. thaliana*.

expected, some proteins like histones are highly conserved (99%), whereas others are more divergent (e.g., the small subunit of ribulose biphosphate carboxylase/oxygenase, 65%). Proteins involved in cellular respiration like phosphofructokinase 5 (glycolysis), citrate synthase (tricarboxylic acid cycle) and cytochrome *c* (mitochondrial respiratory chain) exhibit approximately 80% sequence identity between *V. album* and *A. thaliana*. On average, sequence identity between the two plant species lies in the range of 75%.

#### Transcripts encoding lectins and viscotoxins

*Viscum album* contains characteristic lectins as well as amphiphilic micro-proteins called viscotoxins (Nazaruk and Orlikowski, 2016). Both classes of proteins are subjects of considerable attention because they contribute to cytotoxic and immune-stimulating effects of the mistletoe extracts used in medicine. Three types of *V. album* lectins were biochemically and structurally characterized, termed mistletoe lectins I, II and III (MLI, MLII and MLIII) (Krauspenhaar *et al.*, 2002; Niwa *et al.*, 2003). All three types of lectins are synthesized as precursor proteins and post-translationally cleaved into an alpha and a beta chain. The two chains are linked via a disulfide bridge. The beta chain has lectin activity and specifically binds to sugar residues of membrane proteins, thereby inducing its endocytic uptake by target cells. The alpha subunit has RNA glycosidase activity. It has been shown to cleave off the adenine of nucleotide A4325 of the 28S ribosomal RNA, thereby inactivating the ribosome and inducing apoptosis (Endo and Tsurugi, 1987).

The *V. album* gene space includes full-length sequences encoding the precursors of MLI (VaGs17673), MLII (VaGs17667) and MLIII (VaGs17674). Sequence conservation between the three proteins is in the range of 76–81% (Figure 5). They highly resemble sequences determined previously for MLI, MLII and MLIII (Kourmanova *et al.*, 2004; Sudarkina *et al.*, 2007) but are not identical (Table 3). Possibly, the previously determined *V. album* gene sequences are from a different *V. album* subspecies or regional variants, which is likely since these studies were not performed with a standardized model line. Alternatively, the *V. album* genome may contain isogenes and/or alleles encoding additional lectin isoforms. Indeed, our gene space includes five further transcripts, which all are highly similar to MLI but slightly shorter. More targeted investigations on the genomic level will be needed to fully characterize the *V. album* lectin gene family.

Viscotoxins have a molecular mass of about 5 kDa. Like the *V. album* lectins, they are synthesized as larger precursors, which are proteolytically processed. Their 3D structures are stabilized by the formation of disulfide bridges. Viscotoxins are functionally less defined but are considered to bind to bio-membranes. Five different transcripts encoding viscotoxin precursors are included in our gene space: VaGs38671, VaGs35165, VaGs38197, VaGs36524 and VaGs36525 (Figure 6). They resemble viscotoxin sequences determined previously (e.g., viscotoxin A3, Swiss-Prot entry P01538) but again are not identical to previously published sequences (Figure S1). Further genes encoding viscotoxins might be transcribed in *V. album* berries, which

**Table 2** Sequence identity of selected proteins from *Viscum album* and *Arabidopsis thaliana*

Protein <sup>a</sup>	Accession <sup>b</sup>	Sequence length <sup>c</sup>	Sequence range compared <sup>d</sup>	Identical amino acids <sup>e</sup>	Identity in % <sup>f</sup>
RuBisCO small chain	At1g67090 (At)	180	180	117	65.0
	VaGs21968 (Va)	191			
cytochrome <i>c</i>	At5g40810 (At)	307	273	217	79.5
	VaGs25594 (Va)	381			
phosphofructokinase 5	At2g22480 (At)	537	497	395	79.5
	VaGs15964 (Va)	547			
citrate synthase	At2g44350 (At)	474	470	376	80.0
	VaGs13003 (Va)	474			
histone H4	At1g07660 (At)	103	92	91	98.9
	VaGs37578 (Va)	92			
PsaD	At1g03130 (At)	204	202	144	71.3
	VaGs36078 (Va)	224			
Average (Ø)		310	286	223	79.0

<sup>a</sup>Protein names.

<sup>b</sup>Accession numbers according to our *Viscum album* gene space database or The Arabidopsis Information Resource (TAIR, www.arabidopsis.org); At, *A. thaliana*; Va, *V. album*.

<sup>c</sup>Sequence length of the entire protein (number of amino acids).

<sup>d</sup>Length of the sequences compared.

<sup>e</sup>Number of identical amino acids.

<sup>f</sup>Sequence identity.

© 2021 The Authors.

*The Plant Journal* published by Society for Experimental Biology and John Wiley & Sons Ltd., *The Plant Journal*, (2022), **109**, 278–294

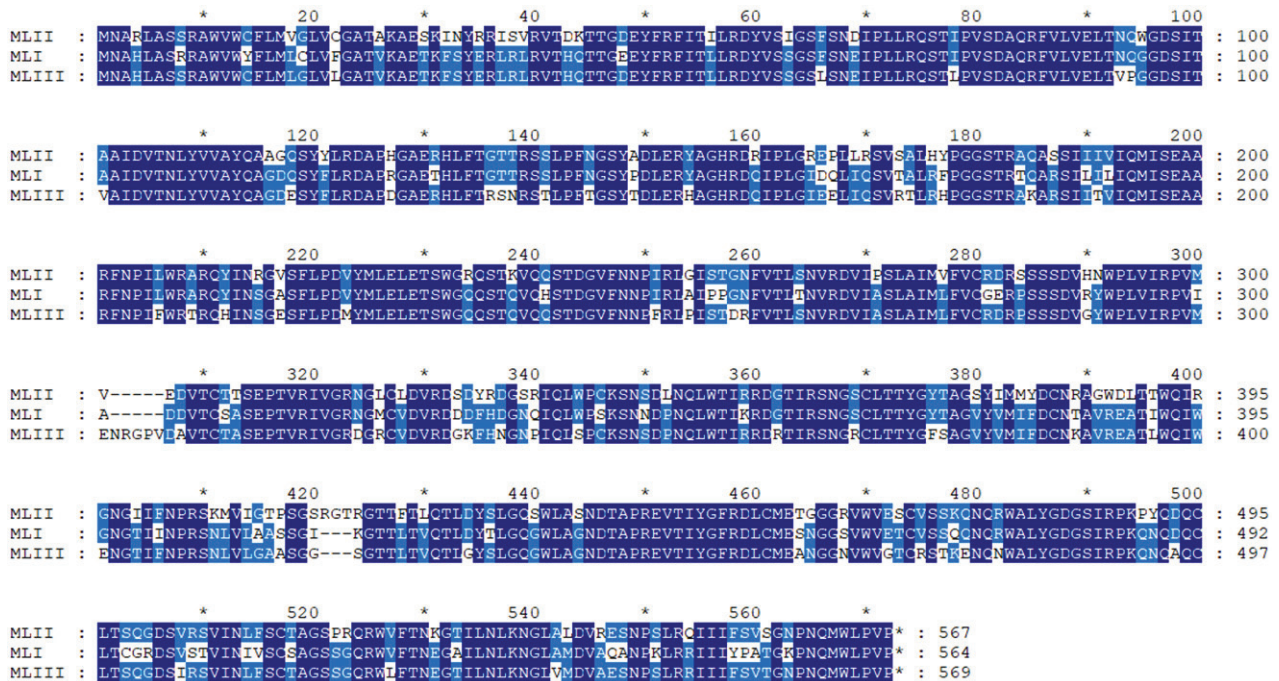


**Figure 5.** Alignment of the *V. album* lectins MLI (VaGs17673), MLII (VaGs17667) and MLIII (VaGs17674). Dark blue amino acid positions are conserved in all three sequences; medium blue amino acid positions are conserved in two of the three sequences.

**Table 3** *Viscum album* lectin sequences from the *V. album* gene space and from UniProt

Protein <sup>a</sup>	Accession <sup>b</sup>	Sequence length <sup>c</sup>	Sequence range compared <sup>d</sup>	Identical amino acids <sup>e</sup>	Identity in % <sup>f</sup>
MLI	VaGs17673	564	564	556	98.6%
	P81446	564			
MLII	VaGs17667	567	567	560	98.8%
	Q6H266	567			
MLIII	VaGs17674	569	569	502	88.2%
	P82683	569			

<sup>a</sup>Protein names. MLI, mistletoe lectin I; MLII, mistletoe lectin II; MLIII, mistletoe lectin III.

<sup>b</sup>Accession numbers according to our *V. album* gene space database or UniProt.

<sup>c</sup>Sequence length of the entire protein (number of amino acids).

<sup>d</sup>Length of the sequences compared.

<sup>e</sup>Number of identical amino acids.

<sup>f</sup>Sequence identity in percent.

were not included in our starting material for SMRT sequencing.

**Transcripts encoding *V. album* proteins localized in the mitochondria**

*Viscum album* has unusual mitochondria. Its mitochondrial genome lacks some genes encoding proteins considered to be essential for mitochondrial function, most notably subunits of the NADH dehydrogenase complex (complex I) of the respiratory chain (Petersen *et al.*, 2015a; Skippington *et al.*, 2015, 2017). While it initially could not be excluded

that the corresponding genes had been overlooked (due to far-going sequence alterations during evolution or translocation of sequences to the nuclear genome), it later became clear by proteome analyses of isolated mitochondria that complex I indeed is absent in *V. album* (Maclean *et al.*, 2018; Senkler *et al.*, 2018). This was a surprising finding, because it is the only known example of a multicellular eukaryote that can carry out cellular respiration in the absence of complex I (Busch, 2018; da Fonseca-Pereira *et al.*, 2018). In *V. album*, complexes III and IV of the respiratory chain form stable supercomplexes; furthermore,

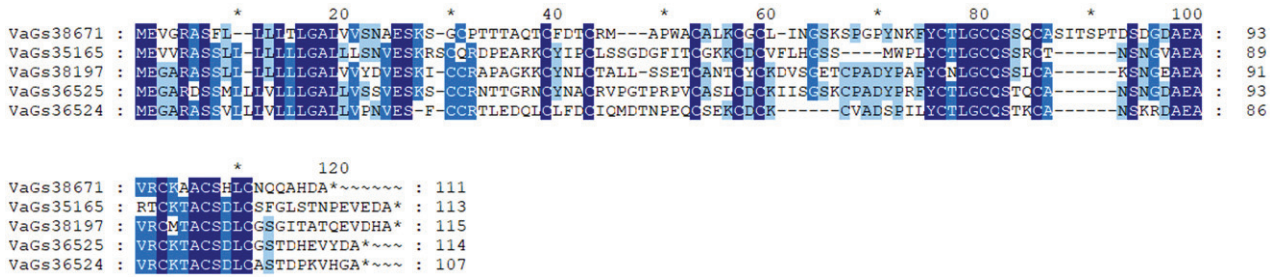


**Figure 6.** Alignment of the viscotoxin precursors encoded by VaGs38671, VaGs35165, VaGs38197, VaGs36525 and VaGs36524. Dark blue amino acid positions are conserved in all sequences; medium blue amino acid positions are conserved in four of the five sequences; light blue amino acid positions are conserved in three of the five amino acid positions.

numerous alternative oxidoreductases occur (Maclean *et al.*, 2018; Senkler *et al.*, 2018).

Proteome analyses of *V. album* mitochondria were so far greatly hindered due to the very limited genome sequence information for *V. album* or any other species of the *Viscum* genus or the Santalaceae family (which includes the *Viscum* genus and several related genera). Specifically, mass values of tryptic peptides from *V. album* proteins obtained by mass spectrometry could not be matched with peptide sequences encoded by the corresponding genes. In an attempt to evaluate the quality of our *V. album* gene space database, we therefore re-evaluated a mitochondrial proteome dataset from *V. album*. The following experiment has been carried out by Senkler *et al.* (2018):

Mitochondria were isolated from *V. album* leaves, mitochondrial membranes were solubilized with the detergent digitonin and the resulting protein fraction was separated by 2D Blue-native/SDS-PAGE. The result of the electrophoretic separation was visualized by staining the gel using Coomassie blue. The most prominent 182 protein spots were excised and trypsinized, and the masses of the tryptic peptides were subsequently determined by mass spectrometry. Due to the lack of *V. album* genome information, the data had to be evaluated using the genome sequence of the model plant *A. thaliana* (TAIR10 genome release) and the few *V. album* sequences available at NCBI in 2018. This evaluation was very restricted, because only few tryptic peptides are completely conserved between *V. album* and *A. thaliana* (considering about 75% sequence identity, on average 2.5 amino acids are exchanged per peptide of 10 amino acid length, which is about the average length of tryptic peptides). Overall, 3129 peptides could be defined, which were assigned to 427 different mitochondrial proteins (Senkler *et al.*, 2018). The obtained data are accessible as a web-based GelMap project (<https://gelmap.de/1327>), which offers protein identification information by simply clicking on protein spots of interest (Figure 7a).

Data evaluation of this experiment was now repeated using the sequences of the *V. album* gene space database (Table 4). The new data analysis allowed identification of

11 736 unique peptides (versus 3129 peptides based on TAIR evaluation; +257%). The number of identified proteins increased from 427 to 612 (+43%). Coverage of identified proteins by peptides increased from 7.3 to 19.2 peptides/protein (+163%). A new GelMap has been created (Figure 7b), which is accessible at <https://gelmap.de/2274>. Comparison of the two GelMaps nicely allows visualization of the much increased identification rate especially of small proteins, which, upon trypsinization, only account for few peptides.

For a more detailed comparison between TAIR10 and *V. album* gene space-based data evaluation, we specifically focused on the mitochondrial oxidative phosphorylation (OXPHOS) system (Figure 8). Blue-native/SDS-PAGE is especially suitable for separating subunits of the protein complexes involved in OXPHOS. Overall, based on the new evaluation, 163 out of 182 analyzed protein spots included at least one OXPHOS protein (75 out of 170 based on the TAIR10 evaluation). The five proteins involved in the ubiquinone biosynthesis pathway were exclusively identified by *V. album* gene space evaluation.

In another attempt to evaluate the completeness of our *V. album* gene space, we directly searched our database for genes encoding subunits of the OXPHOS complexes II, III, IV and V. In *A. thaliana*, these complexes have been characterized in depth and their subunit compositions are well defined (Braun, 2020). Amino acid sequences of all OXPHOS proteins from *A. thaliana* were used to probe the *V. album* gene space database. The gene space includes a close to complete set of nuclear genes encoding OXPHOS proteins (except those encoding subunits of complex I) (Table 5). Interestingly, we also found some OXPHOS sequences transcribed from mitochondrial genes. It originally was anticipated that transcripts of mitochondrial (and chloroplast) genes lack poly(A) tails and therefore are not present in cDNA libraries produced from mRNA (which usually is amplified using poly(T) primers at the 3' end). However, it later became clear that mitochondrial transcripts in plants can be polyadenylated and that polyadenylation targets organellar transcripts for degradation (Lang *et al.*, 2009; Schuster and Stern, 2009).

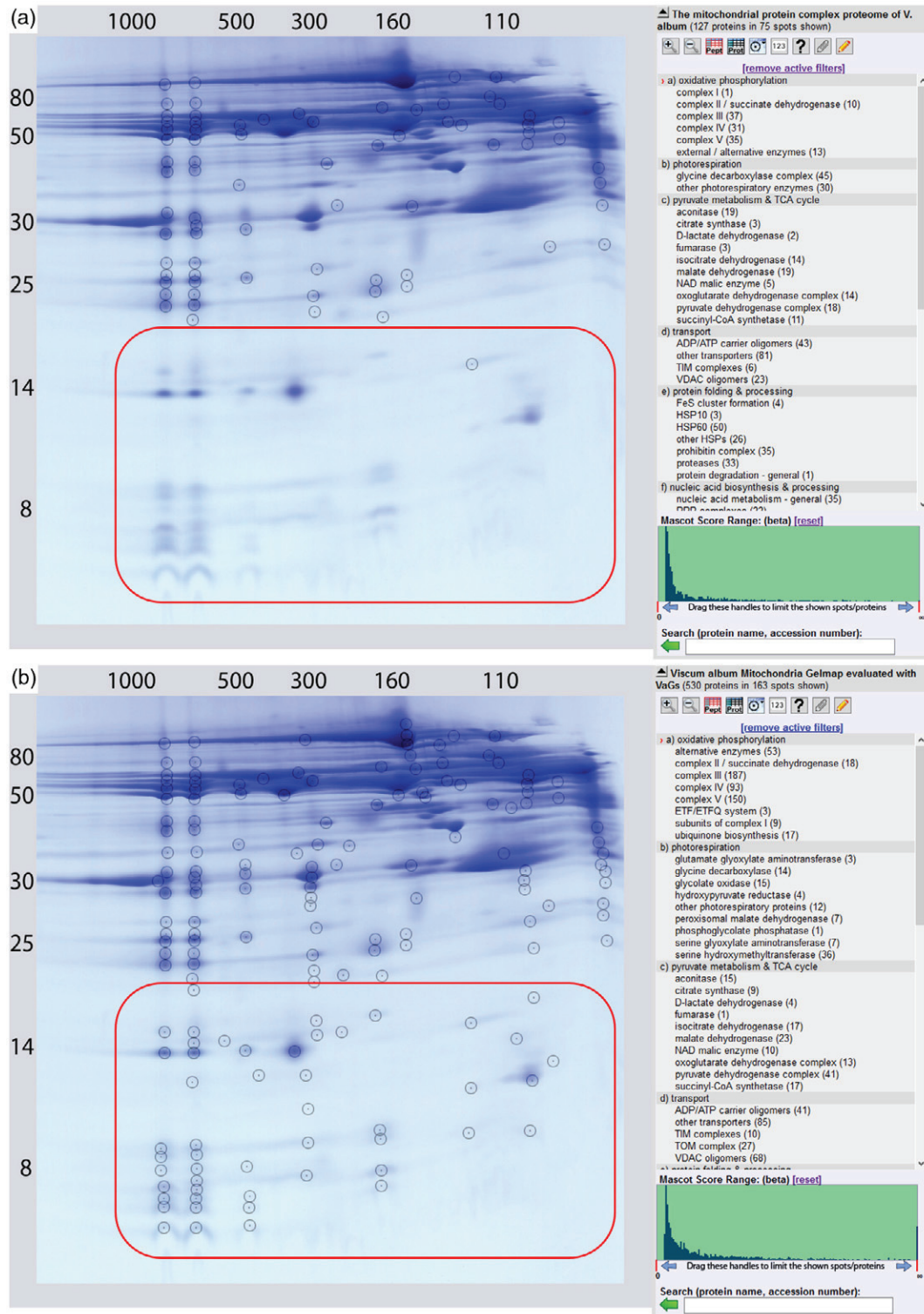


**Figure 7.** Identified OXPHOS proteins of *V. album* on a 2D Blue-native/SDS-PAGE gel (Senkler *et al.*, 2018). Mass spectrometry data were evaluated using the *A. thaliana* TAIR10 database (a) or the *V. album* gene space database (b). Interactive data presentations are available at <https://gelmap.de/1327> (TAIR evaluation) and <https://gelmap.de/2274> (*V. album* gene space evaluation). For both parts of the figure, displayed OXPHOS proteins were selected by using the filter menu given to the right. Black circles indicate identified OXPHOS proteins. The red frames on the two 2D gels highlight gel regions containing small proteins (<20 kDa).

**Table 4** Numbers of proteins and peptides identified for a mitochondrial fraction of *V. album* as revealed by TAIR10 evaluation (Senkler *et al.*, 2018) and evaluation using the *V. album* gene space (VaGs; this study)

	TAIR10 (2018) <sup>a</sup>	VaGs (2021) <sup>b</sup>
Successfully analyzed protein spots (out of 182)	170	182
Unique peptides	3129	11 736
Proteins identified	1245	2318
Average per spot	7.3	12.7
Unique proteins	427	612
Average number of peptides per protein	7.3	19.2
Protein spots with OXPHOS proteins	75	163

<sup>a</sup>Results published in 2018 using the TAIR10 database (<https://gelmap.de/1327>).

<sup>b</sup>Re-evaluated data using the *V. album* gene space database (this study; <https://gelmap.de/2274>).

**Transcripts encoding subunits of mitochondrial complex I**

*Arabidopsis thaliana* complex I consist of 48 subunits, 39 of which are encoded by the nuclear and nine by the mitochondrial genome (Klusch *et al.*, 2021). The mitochondrial genome of *V. album* lacks the nine genes encoding complex I subunits (Petersen *et al.*, 2015a; Skippington *et al.*, 2015, 2017) and the enzyme complex indeed is absent in the mitochondria as revealed by proteome investigations (Maclean *et al.*, 2018; Senkler *et al.*, 2018). It hence is

supposed that all nuclear complex I genes also are absent in *V. album*. This hypothesis was now tested by systematically probing the *V. album* gene space database using complex I sequences from *A. thaliana*.

In contrast to transcripts encoding subunits of complexes II, III, IV and V, transcripts encoding subunits of complex I indeed are absent in our *V. album* gene space. Only a few exceptions were found: a transcript that encodes a complex I-integrated gamma-type carbonic anhydrase (VaGs39093; Table 5) and two transcripts which encode two distinct mitochondrial acyl carrier proteins (VaGs37160/VaGs37159 and VaGs36982; Table 5), which are part of complex I in *A. thaliana* (Klusch *et al.*, 2021).

Peptides of the complex I-integrated gamma-type carbonic anhydrase were also identified in the mitochondrial proteome of *V. album* upon data evaluation using the *V. album* gene space (see GelMap at <https://gelmap.de/2274>). In plants, a carbonic anhydrase domain is attached to the membrane arm of complex I on its matrix-exposed side (Sunderhaus *et al.*, 2006). It is composed of three gamma-type carbonic anhydrase subunits. The domain binds a metal ion and is considered to be enzymatically active (Klusch *et al.*, 2021). Plant complex I cannot assemble if these proteins are absent (Fromm *et al.*, 2016). A direct role of the gamma-type carbonic anhydrase proteins for complex I function during OXPHOS so far is elusive, but it has been suggested that they might integrate a secondary function into plant complex I, which may be related to photorespiration (Soto *et al.*, 2015). The presence of a transcript of the complex I-integrated gamma-type carbonic anhydrase

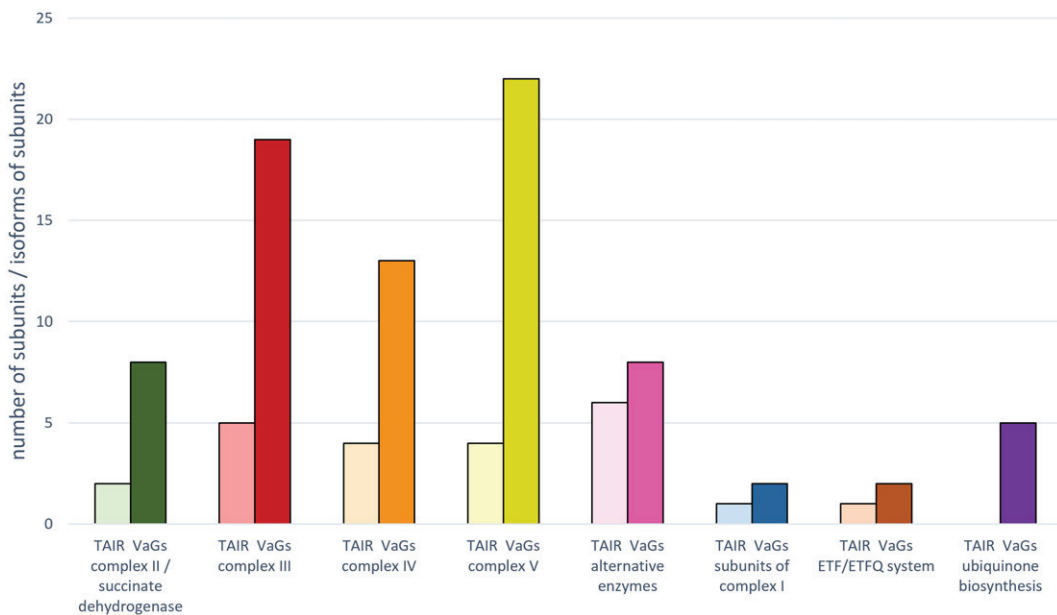


**Figure 8.** Number of identified OXPHOS components within the mitochondrial proteome dataset of Senkler *et al.*, 2018 upon data evaluation based on TAIR10 (light colors) and the *V. album* gene space (dark colors) database.

© 2021 The Authors.

*The Plant Journal* published by Society for Experimental Biology and John Wiley & Sons Ltd., *The Plant Journal*, (2022), 109, 278–294

**Table 5** Proteins involved in the mitochondrial OXPHOS system in *A. thaliana* and *V. album*. Amino acid sequences of all known OXPHOS proteins from *A. thaliana* were used to probe the *V. album* gene space database. Selection of proteins of *A. thaliana* is based on Braun, 2020, but was extended by recently identified additional OXPHOS proteins (Maldonado *et al.*, 2021 for complex IV, Zancani *et al.*, 2020 for complex V and Klusch *et al.*, 2021 for complex I). The data for *V. album* are based on the *V. album* protein space (this publication). Mitochondrially (mt) encoded proteins are partially not included in the *V. album* gene space (but supplemented from NCBI in cases they have been annotated previously)

Annotation	Functional category	No.	Accession(s) in <i>A. thaliana</i>	Accession(s) in <i>V. album</i>
<b>Complex II</b>				
SDH1	complex II	1	At5g66760, At2g18450	VaGs15504, VaGs18431, VaGs15593, VaGs15594, VaGs15446, VaGs15505
SDH2	complex II	2	At3g27380, At5g40650, At5g65165	VaGs29615, VaGs30174, VaGs34595
SDH3	complex II	3	At5g09600, At4g32210	(mt encoded)
SDH4	complex II	4	At2g46505	(mt encoded)
SDH5	complex II	5	At1g47420	VaGs33410, VaGs33411
SDH6	complex II	6	At1g08480	VaGs36736, VaGs34875, VaGs36436
SDH7	complex II	7	At3g47833, At5g62575	VaGs38038
SDH8	complex II	8	At2g46390	---
<b>Complex III</b>				
cytochrome <i>b</i>	complex III	9	AtMg00220	(mt encoded); YP_009220377.1
cytochrome <i>c1</i>	complex III	10	At5g40810, At3g27240	VaGs25595, VaGs25661, VaGs24535, VaGs24536, VaGs25594
FeS	complex III	11	At5g13430, At5g13440	VaGs24540, VaGs24539, VaGs24541, VaGs33119
MPPalpha	complex III	12	At1g51980, At3g16480	VaGs13131, VaGs29795, VaGs13256, VaGs00721
MPPbeta	complex III	13	At3g02090	VaGs04283, VaGs01538, VaGs04991
QCR10	complex III	14	At2g40765	VaGs17923
QCR6	complex III	15	At1g15120, At2g01090	VaGs23198, VaGs35349, VaGs23201
QCR7	complex III	16	At4g32470, At5g25450	VaGs39075, VaGs39072, VaGs38385
QCR8	complex III	17	At3g10860, At5g05370	VaGs35998
QCR9	complex III	18	At3g52730	VaGs36144, VaGs03304, VaGs36125, VaGs02923, VaGs39020, VaGs36037, VaGs36038
<b>Complex IV</b>				
COX1	complex IV	19	AtMg01360	VaGs08501, YP_009220376.1
COX2	complex IV	20	AtMg00160	VaGs31628, YP_009220375.1
COX3	complex IV	21	AtMg00730	(mt encoded); YP_009220379.1
COX4 (=COX-X2)	complex IV	22	At4g00860, At1g01170	VaGs37231
COX5b	complex IV	23	At3g15640, At1g80230	VaGs29247, VaGs29249, VaGs29246, VaGs29248
COX5c	complex IV	24	At2g47380, At3g62400, At5g61310	VaGs03020
COX6a	complex IV	25	At4g37830	VaGs37400
COX6b	complex IV	26	At1g22450	VaGs38369, VaGs33922, VaGs33924, VaGs35619, VaGs33923
COX7a (=COX-X4)	complex IV	27	At4g21105	VaGs34759, VaGs34760, VaGs36004
COX7b (=COX-X3)	complex IV	28	At1g72020	VaGs34763, VaGs34761
<b>Complex V (ATP Synthase)</b>				
alpha subunit	complex V	29	AtMg01190	VaGs21852, YP_009220384.1
beta subunit	complex V	30	At5g08670, At5g08680, At5g08690	VaGs14513, VaGs19745, VaGs15576, VaGs14512, VaGs15180, VaGs19744, VaGs14514
gamma subunit	complex V	31	At2g33040	VaGs09754, VaGs09752, VaGs36320
delta subunit	complex V	32	At5g47030	VaGs25731, VaGs25732
epsilon subunit	complex V	33	At1g51650	VaGs38057, VaGs38055, VaGs38056, VaGs38054
subunit a (=ATP6)	complex V	34	AtMg00410, AtMg01170	VaGs28647, YP_009220378.1

(continued)



Table 5. (continued)

Annotation	Functional category	No.	Accession(s) in <i>A. thaliana</i>	Accession(s) in <i>V. album</i>
subunit b	complex V	35	AtMg00640	(mt encoded)
subunit c (=ATP9)	complex V	36	AtMg01080	(mt encoded)
subunit d	complex V	37	At3g52300	VaGs20371, VaGs20376, VaGs20237
subunit e (=ATP21)	complex V	38	At5g15320	VaGs37459
subunit f (=ATP17)	complex V	39	At4g30010	VaGs34973, VaGs34978,
subunit g (=ATP20)	complex V	40	At2g19680, At4g26210, At4g29480	VaGs33118, VaGs38387, VaGs33861, VaGs38389, VaGs38808, VaGs33863, VaGs38388
FAD (24 kDa)	complex V	41	At2g21870	VaGs32332
Inhibitory factor	complex V	42	At2g27730, At5g04750	VaGs23857, VaGs36801
OSCP	complex V	43	At5g13450	VaGs25651, VaGs25474, VaGs25652, VaGs25473
subunit 8	complex V	44	AtMg00480	(mt encoded)
6 kDa subunit	complex V	45	At5g59613, At3g46430	VaGs37919, VaGs37922, VaGs37923, VaGs37590
<b>Complex I</b>				
13 kDa subunit	complex I	46	At3g03070	---
15 kDa subunit	complex I	47	At3g62790, At2g47690	---
18 kDa subunit	complex I	48	At5g67590	---
24 kDa subunit	complex I	49	At4g02580	---
39 kDa subunit	complex I	50	At2g20360	---
51 kDa subunit	complex I	51	At5g08530	---
75 kDa subunit	complex I	52	At5g37510	---
AGGG	complex I	53	At1g76200	---
ASHI	complex I	54	At5g47570	---
B12	complex I	55	At1g14450, At2g02510	---
B13	complex I	56	At5g52840	---
B14	complex I	57	At3g12260	---
B14.5a	complex I	58	At5g08060	---
B14.5b	complex I	59	At4g20150	---
B14.7	complex I	60	At2g42210	---
B15	complex I	61	At2g31490	---
B16.6	complex I	62	At1g04630, At2g33220	---
B17.2	complex I	63	At3g03100	---
B18	complex I	64	At2g02050	---
B22	complex I	65	At4g34700	---
B8	complex I	66	At5g47890	---
B9	complex I	67	At2g46540	---
CA1	complex I	68	At1g19580	VaGs39093
CA2	complex I	69	At1g47260	---
CA3	complex I	70	At5g66510	---
CAL1/CAL2	complex I	71	At5g63510, At3g48680	---
ESSS	complex I	72	At2g42310, At3g57785	---
C1-FDX	complex I	73	At3g07480	---
GLDH	complex I	74	At3g47930	VaGs17436, VaGs17437
KFYI	complex I	75	At4g00585	---
MNLL	complex I	76	At4g16450	---
MWFE	complex I	77	At3g08610	---
ND1	complex I	78	AtMg00516	---
ND2	complex I	79	AtMg00285	---
ND3	complex I	80	AtMg00990	---
ND4	complex I	81	AtMg00580	---
ND4L	complex I	82	AtMg00650	---
ND5	complex I	83	AtMg00665	---
ND6	complex I	84	AtMg00270	---
ND7	complex I	85	AtMg00510	---
ND9	complex I	86	AtMg00070	---

(continued)

Table 5. (continued)

Annotation	Functional category	No.	Accession(s) in <i>A. thaliana</i>	Accession(s) in <i>V. album</i>
P1	complex I	87	At1g67350	---
P2	complex I	88	At2g27730	VaGs23857
PDSW	complex I	89	At3g18410, At1g49140	---
PGIV	complex I	90	At3g06310, At5g18800	---
PSST	complex I	91	At5g11770	---
SDAP-1	complex I	92	At2g44620	VaGs37160, VaGs37159
SDAP-2	complex I	93	At1g65290	VaGs36982
SGDH1	complex I	94	At1g67785	---
TYKY	complex I	95	At1g79010, At1g16700	---
Alternative respiratory enzymes				
AOX1A, AOX1B, AOX1C, AOX1D, AOX2	AOX	96-100	At3g22370, At3g22360, At3g27620, At1g32350, At5g64210	VaGs06791, VaGs06681, VaGs06620, VaGs06230, VaGs06621
NDA1	altNDH	101	At1g07180	VaGs26116, VaGs27510
NDA2	altNDH	102	At2g29990	---
NDB1	altNDH	103	At4g28220	VaGs10450, VaGs10451, VaGs08998
NDB2	altNDH	104	At4g05020	VaGs18309, VaGs18311, VaGs19303, VaGs19304, VaGs19328, VaGs19364, VaGs19366, VaGs19369
NDB3	altNDH	105	At4g21490	---
NDB4	altNDH	106	At2g20800	---
NDC1	altNDH	107	At5g08740	VaGs17536, VaGs17959, VaGs17961, VaGs17962
Cytochrome <i>c</i>				
Cytc	Cytc	108	At4g10040, At1g22840	VaGs34883, VaGs34884
Other enzymes contributing electrons to the respiratory chain				
Electron transfer flavoprotein $\alpha$	ETF	109	At1g50940	VaGs28996, VaGs28997
Electron transfer flavoprotein $\beta$	ETF	110	At5g43430	VaGs31920
ETF:ubiquinone oxidoreductase	ETFQO	111	At2g43400	VaGs15522
D-Lactate dehydrogenase	D-LDH	112	At5g06580	VaGs18761
Proline dehydrogenase 1	ProDH	113	At3g30775, At5g38710	VaGs18295
Glyceraldehyde 3-phosphate dehydrogenase	GPDH	114	At3g10370	VaGs10872
Dihydroorotate dehydrogenase	DHODH	115	At5g23300	VaGs16765, VaGs16766

in *V. album* now strongly supports a secondary role of this protein in the mitochondria of plants.

Two distinct acyl carrier subunits are part of complex I in fungi and animals (Dobrynin *et al.*, 2010; Runswick *et al.*, 1991). They carry a fatty acid and are essential for assembly and stability of complex I. In *A. thaliana*, three acyl carrier proteins are present in the mitochondrial matrix and assumed to be involved in mitochondrial fatty acid biosynthesis (Meyer *et al.*, 2007). Two of them, termed SDAP-1 and SDAP-2 (or mtACP1 and mtACP2), were recently found to be subunits of plant complex I (Klusck *et al.*, 2021). The presence of homologous transcripts in *V. album* again indicates an essential secondary function of these complex I subunits, probably in mitochondrial fatty acid biosynthesis.

Finally, our *V. album* gene space includes a transcript encoding L-galactono-1,4-lactone dehydrogenase (GLDH). This protein is localized in the mitochondrial intermembrane space and catalyzes the terminal step of the

mitochondrial ascorbate biosynthesis pathway (Bartoli *et al.*, 2000). At the same time, this protein has been found to catalyze complex I assembly in plants (Pineau *et al.*, 2008; Schertl *et al.*, 2012; Schimmeyer *et al.*, 2016). However, GLDH is not considered to be a complex I subunit because it does not form part of the holo complex (Soufari *et al.*, 2020). In *V. album*, GLDH is considered to be in charge in ascorbic acid biosynthesis.

We conclude that transcripts encoding complex I subunits are absent in *V. album*, except for transcripts of a few bifunctional complex I components: a gamma-type carbonic anhydrase, two acyl carrier subunits and GLDH.

### Concluding remarks

We present a *V. album* gene space comprising 39 092 transcripts. This considerably extends our knowledge on the genome of *V. album*. Currently (July 12th, 2021), 270 *V. album* proteins are annotated at NCBI, in comparison to

35 386 proteins of the model plant *A. thaliana* (TAIR10 database; release July 11th, 2019). The *V. album* protein space now comprises 32 064 proteins. Coverage of the *V. album* gene space with respect to the total coding capacity is estimated to be in the range of 78% as revealed by BUSCO analysis. The more abundant enzymes related to primary metabolism should be covered almost completely, which is supported by the evaluation of transcripts encoding components of the OXPHOS system. The *V. album* gene space is accessible at NCBI (BioProject ID: PRJNA765163). Its further evaluation will offer new insights into the molecular biology of a very unusual flowering plant.

## EXPERIMENTAL PROCEDURES

### Plant material and sample preparation

Mistletoes (European mistletoe, *V. album*) grown on an apple tree (*Malus* sp.) on our university campus (Leibniz Universität Hannover, Herrenhäuser Str. 2, Hannover, Germany; Figure S2) were harvested in July 2019 (summer sample) and January 2020 (winter sample). Leaves, stems and flower buds of male and female plants were used. Directly after harvesting, the plant material was shock-frozen using liquid nitrogen and stored at  $-80^{\circ}\text{C}$  until use.

### RNA sample preparation

Frozen plant material (50  $\mu\text{g}$  per sample) was pulverized using a swinging mill pre-chilled with liquid nitrogen. Isolation of total RNA was carried out using the RNeasy Plant Mini Kit (Qiagen, Hilden, Germany), including DNase I treatment, as described by Hohnjec *et al.* (2015). In the final purification step, RNA fractions were eluted using 50  $\mu\text{l}$  RNase-free water. RNA samples were kept at  $-80^{\circ}\text{C}$  until use.

### RNA quality control

All RNA samples went through quality control procedures to determine the concentration, purity and integrity of the RNA. In addition to agarose gel electrophoresis, RNA quality control was based on Qubit fluorometer (Thermo Fischer, Waltham, MA, USA), Nanodrop spectrophotometer (Thermo Fischer), and Bioanalyzer measurements (Agilent, Santa Clara, CA, USA), all according to the manufacturers' instructions. The final quality values determined prior to cDNA synthesis are summarized in Table S1.

### cDNA synthesis

After quality control, RNA samples (summer/winter) were pooled at a ratio of 1:1. Five micrograms of the pooled RNA sample was used for cDNA synthesis using the Clontech SMARTer PCR cDNA Synthesis Kit (Takara Bio Inc., Kusatsu, Japan). At the final step, single-stranded cDNA was PCR-amplified to generate double-stranded cDNA, according to a protocol used by Novogene (Cambridge, UK).

### Library preparation and SMRT sequencing

Two SMRTbell libraries were constructed using the PacBio SMRTbell® Template Prep Kit 1.0 (Pacific Biosciences, Menlo Park, CA, USA). SMRT sequencing was performed with the PacBio Sequel System using the Sequel® Binding Kit 3.0 Insert Kit (Pacific Biosciences).

### Processing of SMRT reads

After SMRT sequencing, data analysis steps were carried out as outlined in Figure 1. Raw data processing was performed with SMRTlink (version 6.0.0.47841). Subread BAM files were used to generate CCSs by setting `minFullPasses = 2` and `minPredictedAccuracy = 0.9`. For this, the subreads from a single zero-mode waveguide (ZMW) were aligned to each other and afterwards self-corrected. Next, 5' and 3' adapters and the poly(A) tail of the CCSs were identified and on that basis they were classified into full-length (containing all three elements) and non-full-length reads. Out of the full-length reads the full-length non-chimeric reads were extracted. During the classification step the poly(A) tails, primers and artificial concatemers (caused by PCR amplification due to the low SMRT adapter concentration) were removed. Using the iterative clustering for error correction (ICE) algorithm, the consensus isoforms from the full-length non-chimeric sequences were identified. Subsequently, the consensus isoforms were polished with the non-full-length reads for a higher accuracy using the Quiver algorithm. The polished consensus isoforms were then divided during the ICE post-process into hq (accuracy > 99%; full-length coverage  $\geq 2$ ) and low quality (lq) consensus isoforms. For further processing steps (e.g., transcriptome database annotation and CDS prediction) the high quality (hq) consensus isoforms were used.

### Prediction of coding sequences – Data S1

BLAST and ESTscan were used for automated prediction of the CDSs of the 39 092 hq sequences. BLAST was used to search for matching consensus sequences of the NR (NCBI non-redundant protein sequences) (<https://www.ncbi.nlm.nih.gov/>) and Swiss-Prot databases (<https://www.uniprot.org/>). Matching nucleotide sequences were translated via the standard codon table into amino acid sequences. If BLAST analyses did not allow finding a matching consensus sequence, sequences were re-analyzed with ESTscan (3.0.3) to predict coding regions. For 243 hq sequences, neither the standard, automated BLAST searches nor EST Scan analyses predicted a CDS. In these cases, homology searches were carried out by BLAST searches of six-frame translated reading frames against the current release of the NCBI NR database using CLC Main Workbench (Qiagen Digital Insights, Aarhus, Denmark). However, the identified protein sequences were often very short because the corresponding open reading frames include multiple stop codons. We therefore decided to exclude these sequences from further evaluations, as they rather seem to be pseudogenes. The remaining 38 849 hq sequences of our *V. album* gene space were used to predict the *V. album* protein space.

### Functional annotation of transcripts

Functional annotation of all sequences was carried out using seven different databases: NR (NCBI non-redundant protein sequences), NT (NCBI nucleotide sequences), KO (KEGG ORTHO-LOG), Swiss-Prot, PFAM (Protein family), GO (Gene Ontology) and KOG (euKaryotic Orthologous Groups). The results of the functional annotation are compiled in Data S1. For defining the *V. album* gene space (see below), functional annotation is mainly based on Swiss-Prot. NR annotation was used to further complete our annotation. Sequences insufficiently defined were re-analyzed by comparison to Viridiplantae sequences at NCBI or further manual sequence evaluation.

### The *V. album* gene space – Data S2

The *V. album* gene space includes all hq sequences, GenIDs and gene length information. Novel accession numbers were assigned to all sequences starting with 'V. album gene space', which range from VaGs00001 to VaGs39092. Furthermore, the amino acid sequences encoded by all genes are given, as well as properties of the corresponding proteins (molecular mass, isoelectric point and hydrophobicity). Finally, functional annotation information is added, as well as information on the most similar protein of the model plant *A. thaliana*. In some cases, several slightly differing genes encode identical proteins. This information is given in column k of Data S2. The resulting number of physically distinct *V. album* protein sequences is 32 064.

### The *V. album* protein space – Data S3

The *V. album* protein space includes all 32 064 distinct *V. album* proteins deduced from the *V. album* gene space and information on their functional annotation.

### Re-evaluation of proteomic mass spectrometry data using the *V. album* gene and protein space

Mass spectrometry data evaluation and annotation was carried out with ProteinScape (Bruker Daltonics) using an in-house Mascot server (Matrix Science; <http://www.matrixscience.com/>) for searches of our *V. album* gene space database (for details see Senkler *et al.*, 2018). For selected proteins, searches were additionally carried out using the *V. album* database including polished lq consensus isoforms.

### ACKNOWLEDGMENTS

We thank Dr. Sabine Reichwein for project advice, Marius Schrader for taking care of the apple tree used for *V. album* cultivation and Matthias Döring for critical reading of the manuscript. PacBio SMRT sequencing was carried out by Novogene, Cambridge, UK. This research has been supported by the Deutsche Forschungsgemeinschaft (grant BR 1829/16-1 to HPB). Open access funding enabled and organized by Projekt DEAL.

### CONFLICT OF INTEREST

The authors declare no conflict of interest.

### AUTHOR CONTRIBUTIONS

HPB initiated the project with advice from HK. *Viscum album* was harvested by LS. RNA isolation and quality evaluation were carried out by NH. Data processing and database development were accomplished by LS with support from MS. Data annotation was performed by LS, JS and MS. HK and HPB supervised the project. LS and HPB wrote the manuscript.

### OPEN RESEARCH BADGES



This article has earned an Open Data badge for making publicly available the digitally shareable data necessary to reproduce the reported results. The data are available at <https://www.ncbi.nlm.nih.gov/bioproject> (BioProject ID:

PRJNA765163) and at the GelMap portal (<https://gelmap.de/2274>).

### DATA AVAILABILITY STATEMENT

*Viscum album* nucleotide sequences (raw data) are available at NCBI (<https://www.ncbi.nlm.nih.gov/bioproject>; BioProject ID: PRJNA765163). The coding sequences are available at the same BioProject at DDBJ/ENA/GenBank, accession GJLGG00000000. Primary protein identification data related to the 2D Blue-native/SDS-PAGE gel presented in Figure 7(b), which were obtained by mass spectrometry, are accessible at the GelMap portal at <https://gelmap.de/2274>.

### SUPPORTING INFORMATION

Additional Supporting Information may be found in the online version of this article.

**Figure S1.** Alignment of VaGs36525 with viscotoxin A3 from Swiss-Prot (P01538).

**Figure S2.** *Viscum album* growing on an apple tree at the campus of Leibniz University Hannover.

**Table S1.** Quality control of the pooled RNA sample, which was used for library preparation and SMRT sequencing.

**Table S2.** Codon usage in *V. album* and *A. thaliana* (frequency per 1000 codons).

**Table S3.** Proteins involved in the mitochondrial OXPHOS system in *A. thaliana* and *V. album*.

**Data S1.** Prediction of *V. album* coding sequences.

**Data S2.** The *V. album* gene space: nucleotide sequences of 39 093 *V. album* transcripts and their functional annotation.

**Data S3.** The *V. album* protein space: amino acid sequences of 32 064 *V. album* proteins and their functional annotation.

### REFERENCES

- Arabidopsis Genome Initiative.** (2000) Analysis of the genome sequence of the flowering plant *Arabidopsis thaliana*. *Nature*, **408**, 796–815.
- Azuma, Ji., Kim, NH., Heux, L., Vuong, R. & Chanzy, H.** (2000) The cellulose system in viscin from mistletoe berries. *Cellulose*, **7**, 3–19. <https://doi.org/10.1023/A:1009223730317>
- Baerenfaller, K., Grossmann, J., Grobei, M.A., Hull, R., Hirsch-Hoffmann, M., Yalovsky, S. et al.** (2008) Genome-scale proteomics reveals *Arabidopsis thaliana* gene models and proteome dynamics. *Science*, **320**(5878), 938–941. <https://doi.org/10.1126/science.1157956>
- Barlow, B.A.** (1981) *Viscum album* in Japan: Chromosomal translocations, maintenance of heterozygosity and the evolution of dioecy. *The Botanical Magazine Tokyo*, **94**, 21–34. <https://doi.org/10.1007/BF02490200>
- Bartoli, C.G., Pastori, G.M. & Foyer, C.H.** (2000) Ascorbate biosynthesis in mitochondria is linked to the electron transport chain between complexes III and IV. *Plant Physiology*, **123**(1), 335–344. <https://doi.org/10.1104/pp.123.1.335>
- Braun, H.P.** (2020) The Oxidative Phosphorylation system of the mitochondria in plants. *Mitochondrion*, **53**, 66–75. <https://doi.org/10.1016/j.mito.2020.04.007>
- Busch, K.B.** (2018) Respiration: life without complex I. *Current Biology*, **28**(10), R616–R618. <https://doi.org/10.1016/j.cub.2018.04.030>
- da Fonseca-Pereira, P., Silva, W.B., Araújo, W.L. & Nunes-Nesi, A.** (2018) How does European mistletoe survive without complex I? *Trends in Plant Science*, **23**(10), 847–850. <https://doi.org/10.1016/j.tplants.2018.07.008>

- Dobrynin, K., Abdrakmanova, A., Richers, S., Hunte, C., Kerscher, S. & Brandt, U. (2010) Characterization of two different acyl carrier proteins in complex I from *Yarrowia lipolytica*. *Biochimica Et Biophysica Acta*, **1797** (2), 152–159. <https://doi.org/10.1016/j.bbabi.2009.09.007>
- Elliott, T.A. & Gregory, T.R. (2015) What's in a genome? The C-value enigma and the evolution of eukaryotic genome content. *Philosophical Transactions of the Royal Society of London. Series B, Biological Sciences*, **370** (1678), 20140331. <https://doi.org/10.1098/rstb.2014.0331>
- Endo, Y. & Tsurugi, K. (1987) RNA N-glycosidase activity of ricin A-chain. *Journal of Biological Chemistry*, **262**, 8128–8130. PMID: 3036799.
- Fromm, S., Braun, H.P. & Peterhansel, C. (2016) Mitochondrial gamma carbonic anhydrases are required for complex I assembly and plant reproductive development. *New Phytologist*, **211**(1), 194–207. <https://doi.org/10.1111/nph.13886>
- Glatzel, G. & Geils, B.W. (2009) Mistletoe ecophysiology: host–parasite interactions. *Botany-Botanique*, **87**, 10–15. <https://doi.org/10.1139/B08-096>
- Hohnjec, N., Czaja-Hasse, L.F., Hagekamp, C. & Küster, H. (2015) Pre-announcement of symbiotic guests: transcriptional reprogramming by mycorrhizal lipochitooligosaccharides shows a strict co-dependency on the GRAS transcription factors NSP1 and RAM1. *BMC Genomics*, **16**, 994. <https://doi.org/10.1186/s12864-015-2224-7>
- Jäger, T., Holandino, C., Melo, M.N.O., Peñaloza, E.M.C., Oliveira, A.P., Garrett, R. et al. (2021) Metabolomics by UHPLC-Q-TOF reveals host tree-dependent phytochemical variation in *Viscum album* L. *Plants*, **10**(8), 1726. <https://doi.org/10.3390/plants10081726>
- Kiraga, J., Mackiewicz, P., Mackiewicz, D., Kowalczyk, M., Biecek, P., Polak, N. et al. (2007) The relationships between the isoelectric point and: length of proteins, taxonomy and ecology of organisms. *BMC Genomics*, **8**, 163. <https://doi.org/10.1186/1471-2164-8-163>
- Klusck, N., Senkler, J., Yildiz, Ö., Kühlbrandt, W. & Braun, H.P. (2021) A ferredoxin bridge connects the two arms of plant mitochondrial complex I. *The Plant Cell*, **33**, 2072–2091. <https://doi.org/10.1093/plcell/koab092>
- Ko, S.M., Kwon, Y.K., Kim, J.H., Song, I.J., Lee, H.Y., Choi, D.W. et al. (2014) Transcriptome analysis of mistletoe (*Viscum album*) haustorium development. *Horticulture, Environment, and Biotechnology*, **55**, 352–361. <https://doi.org/10.1007/s13580-014-0033-6>
- Kourmanova, A.G., Soudarkina, O.J., Olsnes, S. & Kozlov, J.V. (2004) Cloning and characterization of the genes encoding toxic lectins in mistletoe (*Viscum album* L). *European Journal of Biochemistry*, **271**(12), 2350–2360. <https://doi.org/10.1111/j.1432-1033.2004.04153.x>
- Krauspenhaar, R., Rypniewski, W., Kalkura, N., Moore, K., DeLucas, L., Stoeva, S. et al. (2002) Crystallisation under microgravity of mistletoe lectin I from *Viscum album* with adenine monophosphate and the crystal structure at 1.9 Å resolution. *Acta Crystallographica. Section D. Biological Crystallography*, **58**(Pt 10 Pt 1), 1704–1707. <https://doi.org/10.1107/s0907444902014270>
- Lang, H., Sement, F.M., Canaday, J. & Gagliardi, D. (2009) Polyadenylation-assisted RNA degradation processes in plants. *Trends in Plant Science*, **14**, 497–504. <https://doi.org/10.1016/j.tplants.2009.06.007>
- Macleane, A.E., Hertle, A.P., Ligas, J., Bock, R., Balk, J. & Meyer, E.H. (2018) Absence of complex I is associated with diminished respiratory chain function in European mistletoe. *Current Biology*, **28**(10), 1614–1619.e3. <https://doi.org/10.1016/j.cub.2018.03.036>
- Maldonado, M., Guo, F. & Letts, J.A. (2021) Atomic structures of respiratory complex III2, complex IV, and supercomplex III2-IV from vascular plants. *eLife*, **10**, e62047. <https://doi.org/10.7554/eLife.62047>
- Marie, D. & Brown, S.C. (1993) A cytometric exercise in plant DNA histograms, with 2C values for 70 species. *Biological Cell*, **78**, 41–51. [https://doi.org/10.1016/0248-4900\(93\)90113-s](https://doi.org/10.1016/0248-4900(93)90113-s)
- Meyer, E.H., Heazlewood, J.L. & Millar, A.H. (2007) Mitochondrial acyl carrier proteins in *Arabidopsis thaliana* are predominantly soluble matrix proteins and none can be confirmed as subunits of respiratory Complex I. *Plant Molecular Biology*, **64**(3), 319–327. <https://doi.org/10.1007/s11103-007-9156-9>
- Nagl, W., Jeanjour, M., Kling, H., Kuhner, S., Michels, I., Muller, T. et al. (1983) Genome and chromatin organization in higher plants. *Biologischen Zentralblatt*, **102**, 129–148.
- Nazaruk, J. & Orlikowski, P. (2016) Phytochemical profile and therapeutic potential of *Viscum album* L. *Natural Product Research*, **30**(4), 373–385. <https://doi.org/10.1080/14786419.2015.1022776>
- Niwa, H., Tonevitsky, A.G., Agapov, I.I., Seward, S., Pfüller, U. & Palmer, R.A. (2003) Crystal structure at 3 Å of mistletoe lectin I, a dimeric type-II ribosome-inactivating protein, complexed with galactose. *European Journal of Biochemistry*, **270**(13), 2739–2749. <https://doi.org/10.1046/j.1432-1033.2003.03646.x>
- Novák, P., Guignard, M.S., Neumann, P., Kelly, L.J., Mlinarec, J., Koblížková, A. et al. (2020) Repeat-sequence turnover shifts fundamentally in species with large genomes. *Nature Plants*, **6**(11), 1325–1329. <https://doi.org/10.1038/s41477-020-00785-x>
- Pellicer, J. & Leitch, I.J. (2019) The Plant DNA C-values database (release 7.1): an updated online repository of plant genome size data for comparative studies. *New Phytologist*, **226**, 301–305. <https://doi.org/10.1111/nph.16261>
- Petersen, G., Cuenca, A., Møller, I.M. & Seberg, O. (2015a) Massive gene loss in mistletoe (*Viscum*, Viscaceae) mitochondria. *Scientific Reports*, **5**, 17588. <https://doi.org/10.1038/srep17588>
- Petersen, G., Cuenca, A. & Seberg, O. (2015b) Plastome evolution in hemiparasitic mistletoes. *Genome Biology and Evolution*, **7**(9), 2520–2532. <https://doi.org/10.1093/gbe/evv165>
- Pineau, B., Layoune, O., Danon, A. & De Paepe, R. (2008) L-galactono-1,4-lactone dehydrogenase is required for the accumulation of plant respiratory complex I. *Journal of Biological Chemistry*, **283**(47), 32500–32505. <https://doi.org/10.1074/jbc.m805320200>
- Runswick, M.J., Fearnley, I.M., Skehel, J.M. & Walker, J.E. (1991) Presence of an acyl carrier protein in NADH:ubiquinone oxidoreductase from bovine heart mitochondria. *FEBS Letters*, **286**(1–2), 121–124. [https://doi.org/10.1016/0014-5793\(91\)80955-3](https://doi.org/10.1016/0014-5793(91)80955-3)
- Schertl, P., Sunderhaus, S., Klodmann, J., Grozoff, G.E., Bartoli, C.G. & Braun, H.P. (2012) L-galactono-1,4-lactone dehydrogenase (GLDH) forms part of three subcomplexes of mitochondrial complex I in *Arabidopsis thaliana*. *Journal of Biological Chemistry*, **287**(18), 14412–14419. <https://doi.org/10.1074/jbc.m111.305144>
- Schimmeyer, J., Bock, R. & Meyer, E.H. (2016) L-Galactono-1,4-lactone dehydrogenase is an assembly factor of the membrane arm of mitochondrial complex I in *Arabidopsis*. *Plant Molecular Biology*, **90**(1–2), 117–126. <https://doi.org/10.1007/s11103-015-0400-4>
- Schuster, G. & Stern, D. (2009) RNA polyadenylation and decay in mitochondria and chloroplasts. *Progress in Molecular Biology and Translational Science*, **85**, 393–422. [https://doi.org/10.1016/s0079-6603\(08\)00810-6](https://doi.org/10.1016/s0079-6603(08)00810-6)
- Schwartz, R., Ting, C.S. & King, J. (2001) Whole proteome pI values correlate with subcellular localizations of proteins for organisms within the three domains of life. *Genome Research*, **11**(5), 703–709. <https://doi.org/10.1101/gr-gr-1587r>
- Senkler, J., Rugen, N., Eubel, H., Hegermann, J. & Braun, H.P. (2018) Absence of complex I implicates rearrangement of the respiratory chain in European mistletoe. *Current Biology*, **28**(10), 1606–1613.e4. <https://doi.org/10.1016/j.cub.2018.03.050>
- Sepey, M., Manni, M. & Zdobnov, E.M. (2019) BUSCO: Assessing Genome Assembly and Annotation Completeness. In: Kollmar, M. (Ed.) *Gene prediction. Methods in molecular biology*, vol 1962. Humana, New York, NY. 227–245. [https://doi.org/10.1007/978-1-4939-9173-0\\_14](https://doi.org/10.1007/978-1-4939-9173-0_14)
- Singh, R., Ming, R. & Yu, Q. (2016) Comparative analysis of GC content variations in plant genomes. *Tropical Plant Biology*, **9**, 136–149. <https://doi.org/10.1007/s12042-016-9165-4>
- Skippington, E., Barkman, T.J., Rice, D.W. & Palmer, J.D. (2015) Miniaturized mitogenome of the parasitic plant *Viscum scurruloideum* is extremely divergent and dynamic and has lost all nad genes. *Proceedings of the National Academy of Sciences of the United States of America*, **112** (27), E3515–E3524. <https://doi.org/10.1073/pnas.1504491112>
- Skippington, E., Barkman, T.J., Rice, D.W. & Palmer, J.D. (2017) Comparative mitogenomics indicates respiratory competence in parasitic *Viscum* despite loss of complex I and extreme sequence divergence, and reveals horizontal gene transfer and remarkable variation in genome size. *BMC Plant Biology*, **17**(1), 49. <https://doi.org/10.1186/s12870-017-0992-8>
- Soto, D., Córdoba, J.P., Villarreal, F., Bartoli, C., Schmitz, J., Maurino, V.G. et al. (2015) Functional characterization of mutants affected in the carbonic anhydrase domain of the respiratory complex I in *Arabidopsis thaliana*. *The Plant Journal*, **83**(5), 831–844. <https://doi.org/10.1111/tpj.12930>

- Soufari, H., Parrot, C., Kuhn, L., Waltz, F. & Hashem, Y.** (2020) Specific features and assembly of the plant mitochondrial complex I revealed by cryo-EM. *Nature Communications*, **11**(1), 5195. <https://doi.org/10.1038/s41467-020-18814-w>
- Sudarkina, O.J., Kurmanova, A.G. & Kozlov, J.V.** (2007) Production and characterization of the B chains of mistletoe toxic lectins. *Molecular Biology*, **41**, 601–608. <https://doi.org/10.1134/S0026893307040127>
- Sunderhaus, S., Dudkina, N.V., Jänsch, L., Klodmann, J., Heinemeyer, J., Perales, M. et al.** (2006) Carbonic anhydrase subunits form a matrix-exposed domain attached to the membrane arm of mitochondrial complex I in plants. *Journal of Biological Chemistry*, **281**(10), 6482–6488. <https://doi.org/10.1074/jbc.m511542200>
- Ulrich, I., Fritz, B. & Ulrich, W.** (1988) Application of DNA fluorochromes for flow cytometric DNA analysis of plant protoplasts. *Plant Science*, **55**, 151–158. [https://doi.org/10.1016/0168-9452\(88\)90171-9](https://doi.org/10.1016/0168-9452(88)90171-9)
- Urech, K. & Baumgartner, S.** (2015) Chemical Constituents of *Viscum album* L.: Implications for the Pharmaceutical Preparation of Mistletoe. In: Zänker, K.S. & Kaveri, S.V. (Eds.), *Mistletoe: from mythology to evidence-based medicine*. Transl. Res. Biomed. Basel: Karger, vol 4, pp 11–23. <https://doi.org/10.1159/000375422>
- van Wijk, K.J., Leppert, T., Sun, O., Boguraev, S.S., Sun, Z., Mendoza, L. & Deutsch, E.W.** (2021) The Arabidopsis thaliana PeptideAtlas; harnessing world-wide proteomics data for a comprehensive community proteomics resource. *The Plant Cell*, **33**(11), 3421–3453. <https://doi.org/10.1093/plcell/koab211>
- Zancani, M., Braidot, E., Filippi, A. & Lippe, G.** (2020) Structural and functional properties of plant mitochondrial F-ATP synthase. *Mitochondrion*, **53**, 178–193. <https://doi.org/10.1016/j.mito.2020.06.001>
- Zonneveld, B.J.M.** (2010) New record holders for maximum genome size in eudicots and monocots. *Journal of Botany*, **2010**, 1–4. <https://doi.org/10.1155/2010/527357>

## Schröder et al. 2021, Supplementary Material

### Supplementary Figures

```

                *           20           *           40           *
VaGs36525 : MEGARDSSMILLVLLLGLLVSSVESKSCCRNTTGRNCCYNACRVECTPRP : 50
P01538    : MEVVRGSSLVLLLGLLVSSVESKSCCPNTTGRNCCYNACRLTCAPRE : 50

                60           *           80           *           100
VaGs36525 : VCAQLCDCKIISGSKCPADYERFYCTLGCGSTQCA-NSNGDAEAVRCKTA : 99
P01538    : TCAKLSGCKIISGSTCESDYERFYCTLGCESSQCATNSNGDAEAVRCKTA : 100

                *
VaGs36525 : CSDLGSGTDHEVYDA* : 114
P01538    : CSDLQQDVDDA~~~~~ : 111

```

Supplementary Figure S1: Alignment of VaGs36525 with viscotoxin A3 from Swissprot (P01538). Identical amino acid positions are indicated in dark blue.



Supplementary Figure S2: *V. album* growing on an apple tree at the campus of Leibniz University Hannover. Different *V. album* organs harvested from this tree in summer and in winter were used for our investigations. The photo was taken in winter (February).

## Supplementary Tables

**Supplementary Table S1:** Quality control of the pooled RNA sample, which was used for library preparation and SMRT sequencing

Sample name <sup>1</sup>	Qubit concentration (ng/μl) <sup>2</sup>	Volume (μl) <sup>3</sup>	Amount (μg) <sup>4</sup>	A260/280 <sup>5</sup>	A260/230 <sup>6</sup>	Nanodrop (ng/μl) <sup>7</sup>	RIN <sup>8</sup>
s7w8	656.6	13	8.5358	2.084	2.548	905	8.1

<sup>1</sup> Name of the pooled RNA sample

<sup>2</sup> RNA concentration determined using a Qubit fluorometer

<sup>3</sup> Volume of the pooled RNA sample

<sup>4</sup> Amount of the RNA in μg

<sup>5</sup> A260/A280 absorption ratio to assess the protein content

<sup>6</sup> A260/A230 absorption ratio to assess the presence of organic compounds

<sup>7</sup> RNA concentration determined using a Nanodrop spectrophotometer

<sup>8</sup> RNA Integrity number determined using a Bioanalyzer



**Supplementary Table S2:** Codon usage in *V. album* and *A. thaliana* (frequency per 1000 codons). The ratio in codon usage between *V. album* and *A. thaliana* is highlighted in red when > 1.5. (Tair10 dataset with 35386 cds; downloaded on July 11<sup>th</sup> 2019). The codon usage was analysed with [https://www.bioinformatics.org/sms2/codon\\_usage.html](https://www.bioinformatics.org/sms2/codon_usage.html) (Stothard P [2000] The Sequence Manipulation Suite: JavaScript programs for analyzing and formatting protein and DNA sequences. Biotechniques 28:1102-1104.)

Amino acid	Codon	<i>Viscum album</i>	<i>Arabid. thaliana</i>	Va / At
Ala	GCG	14.0	8.4	1.7
Ala	GCA	18.6	17.8	1.0
Ala	GCT	24.8	27.6	0.9
Ala	GCC	19.7	9.7	2.0
Cys	TGT	8.3	10.9	0.8
Cys	TGC	10.5	7.3	1.4
Asp	GAT	33.7	37.3	0.9
Asp	GAC	19.5	16.8	1.2
Glu	GAG	33.3	32.1	1.0
Glu	GAA	28.8	35.4	0.8
Phe	TTT	20.8	22.3	0.9
Phe	TTC	20.9	20.0	1.0
Gly	GGG	20.1	10.2	2.0
Gly	GGA	18.0	23.6	0.8
Gly	GGT	17.9	21.5	0.8
Gly	GGC	18.1	8.9	2.0
His	CAT	13.9	14.2	1.0
His	CAC	10.4	8.5	1.2
Ile	ATA	9.9	13.3	0.7
Ile	ATT	20.1	21.8	0.9
Ile	ATC	18.5	17.7	1.0
Lys	AAG	31.8	32.2	1.0
Lys	AAA	22.8	31.3	0.7
Leu	TTG	20.4	21.4	1.0
Leu	TTA	8.4	13.2	0.6
Leu	CTG	22.0	10.2	2.2
Leu	CTA	6.4	10.2	0.6
Leu	CTT	19.1	24.5	0.8
Leu	CTC	17.6	15.4	1.1
Met	ATG	23.2	24.5	0.9
Asn	AAT	20.8	23.3	0.9
Asn	AAC	16.8	20.4	0.8
Pro	CCG	11.9	8.0	1.5
Pro	CCA	13.8	16.3	0.8
Pro	CCT	16.8	18.7	0.9
Pro	CCC	12.9	5.2	2.5
Gln	CAG	20.4	15.4	1.3
Gln	CAA	14.0	19.9	0.7
Arg	AGG	15.6	11.0	1.4
Arg	AGA	12.5	19.3	0.6
Arg	CGG	10.6	4.9	2.2
Arg	CGA	7.0	6.4	1.1
Arg	CGT	7.0	8.7	0.8
Arg	CGC	7.7	3.7	2.1
Ser	AGT	10.8	14.7	0.7
Ser	AGC	13.5	11.5	1.2
Ser	TCG	10.8	9.1	1.2
Ser	TCA	15.6	19.0	0.8
Ser	TCT	19.6	25.6	0.8
Ser	TCC	16.9	11.0	1.5
Thr	ACG	8.5	7.4	1.1
Thr	ACA	11.4	16.1	0.7
Thr	ACT	12.6	17.4	0.7
Thr	ACC	13.2	9.8	1.3
Val	GTG	23.2	17.0	1.4
Val	GTA	7.2	10.3	0.7
Val	GTT	22.5	27.0	0.8
Val	GTC	14.1	12.2	1.2
Trp	TGG	13.1	12.4	1.1
Tyr	TAT	12.7	15.0	0.8
Tyr	TAC	12.3	13.1	0.9
Stop	TGA	1.6	1.1	1.4
Stop	TAG	0.7	0.5	1.4
Stop	TAA	0.7	0.9	0.8

## 2.2 The photosynthesis apparatus of European mistletoe (*Viscum album*)

Lucie Schröder<sup>1</sup>, Jan Hegermann<sup>2</sup>, Patrick Pille<sup>1</sup>, Hans-Peter Braun<sup>1</sup>




<sup>1</sup> Institut für Pflanzengenetik, Leibniz Universität Hannover, Herrenhäuser Str. 2, 30419 Hannover, Germany.

<sup>2</sup> Institut für Funktionelle und Angewandte Anatomie, Medizinische Hochschule Hannover, Carl-Neuberg-Straße 1, 30625 Hannover, Germany.

Type of authorship:	First author
Type of article:	Research article
Share of the work:	60 %
Contribution to the publication:	Performed experiments, analyzed data, prepared figures, participated in writing the manuscript
Journal:	Plant Physiology
Impact factor:	8.005 (2022/2023)
Date of publication:	03.11.2022
Number of citations:	3
(Google Scholar, 20.09.2023)	
DOI:	10.1093/plphys/kiac377
PubMed-ID:	35976139



# The photosynthesis apparatus of European mistletoe (*Viscum album*)

Lucie Schröder ,<sup>1</sup> Jan Hegemann ,<sup>2</sup> Patrick Pille<sup>1</sup> and Hans-Peter Braun <sup>1,\*</sup>

<sup>1</sup> Institut für Pflanzgenetik, Leibniz Universität Hannover, Herrenhäuser Str. 2, 30419 Hannover, Germany

<sup>2</sup> Institut für Funktionelle und Angewandte Anatomie, Medizinische Hochschule Hannover, Carl-Neuberg-Straße 1, 30625 Hannover, Germany

\*Author for correspondence: braun@genetik.uni-hannover.de

H.-P.B. initiated and supervised the project. Isolation of chloroplasts and gel electrophoresis procedures were carried out by L.S., electron microscopy analyses by J.H., mass spectrometry analysis by P.P. All authors were involved in data evaluation and interpretation. H.P.B. and L.S. wrote the manuscript.

The author responsible for distribution of materials integral to the findings presented in this article in accordance with the policy described in the Instructions for Authors (<https://academic.oup.com/plphys/pages/general-instructions>) is Hans-Peter Braun: (braun@genetik.uni-hannover.de).

## Abstract

European mistletoe (*Viscum album*) is known for its special mode of cellular respiration. It lacks the mitochondrial NADH dehydrogenase complex (Complex I of the respiratory chain) and has restricted capacities to generate mitochondrial adenosine triphosphate (ATP). Here, we present an investigation of the *V. album* energy metabolism taking place in chloroplasts. Thylakoids were purified from young *V. album* leaves, and membrane-bound protein complexes were characterized by Blue native polyacrylamide gel electrophoresis as well as by the complexome profiling approach. Proteins were systematically identified by label-free quantitative shotgun proteomics. We identified >1,800 distinct proteins (accessible at [https://complexomemap.de/va\\_leaves](https://complexomemap.de/va_leaves)), including nearly 100 proteins forming part of the protein complexes involved in the light-dependent part of photosynthesis. The photosynthesis apparatus of *V. album* has distinct features: (1) comparatively low amounts of Photosystem I; (2) absence of the NDH complex (the chloroplast pendant of mitochondrial Complex I involved in cyclic electron transport (CET) around Photosystem I); (3) reduced levels of the proton gradient regulation 5 (PGR5) and proton gradient regulation 5-like 1 (PGRL1) proteins, which offer an alternative route for CET around Photosystem I; (4) comparable amounts of Photosystem II and the chloroplast ATP synthase complex to other seed plants. Our data suggest a restricted capacity for chloroplast ATP biosynthesis by the photophosphorylation process. This is in addition to the limited ATP supply by the mitochondria. We propose a view on mistletoe's mode of life, according to which its metabolism relies to a greater extent on energy-rich compounds provided by the host trees.

## Introduction

European mistletoe (*Viscum album*) has been studied for more than 2,000 years (Luther and Becker, 1987). It is known for its very special life cycle (reviewed in Zuber, 2004). *Viscum album* is an obligate hemiparasitic evergreen plant that grows on branches of various trees. It is connected to the xylem of the host tree and is thus supplied with water, minerals, and to some degree with organic

compounds by the host. At the same time, *V. album* carries out photosynthesis for de novo biosynthesis of organic compounds.

Photosynthesis takes place in the chloroplasts. The chloroplast ultrastructure of *V. album* resembles one of the typical seed plants (Hudák and Lux, 1986; Tuquet and Sallé, 1996; Zuber, 2004). All pigments required for photosynthesis are

Received June 07, 2022. Accepted July 19, 2022. Advance access publication August 17, 2022

© The Author(s) 2022. Published by Oxford University Press on behalf of American Society of Plant Biologists.

This is an Open Access article distributed under the terms of the Creative Commons Attribution License (<https://creativecommons.org/licenses/by/4.0/>), which permits unrestricted reuse, distribution, and reproduction in any medium, provided the original work is properly cited.

Open Access

present (Becker, 1986) but the amounts of chlorophyll *a* as well as chlorophyll *b* are comparatively low (Hudák and Lux, 1986). The photosynthesis rate of *V. album* is comparatively low (Tuquet and Sallé, 1996; Zuber, 2004). The molecular composition of the photosynthesis apparatus of *V. album* has not been characterized so far.

In plants, photosynthesis is tightly linked to cellular respiration, which takes place in the mitochondria. Numerous metabolic pathways in leaf cells involve both the mitochondria and the chloroplasts, like photorespiration, nitrogen assimilation, heme biosynthesis, or the regulation of the redox state of the plant cell (Møller et al., 2021). The respiratory electron transfer chain is similarly composed in plants and other clades of multicellular eukaryotes: It is based on the presence of four enzyme complexes termed Complexes I, II, III, and IV; Electron transfer by Complexes I–IV is linked to the formation of a proton gradient across the inner mitochondrial membrane; the proton motive force is used by the ATP synthase complex (also designated Complex V) to generate ATP from ADP and phosphate; ATP is finally provided by the mitochondria to the entire cell and drives numerous molecular functions. However, in contrast to several other clades of multicellular eukaryotes, the mitochondria of plants comprise a series of additional so-called “alternative” respiratory enzymes, like alternative NAD(P)H dehydrogenases, or an alternative oxidase, AOX (reviewed in Schertl and Braun, 2014). These alternative enzymes take part in respiratory electron transport but do not contribute to the proton gradient across the inner mitochondrial membrane and therefore not to the formation of ATP. Their physiological roles are still under debate but seem to be relevant for keeping the redox state of the plant cell in a balance, particularly when photosynthesis takes place.

Surprisingly, it was found that cellular respiration follows unique routes in *V. album* and related species of the *Viscum* genus. Initially, it was reported that several genes are absent in the mitochondrial genomes of *Viscum* species, which code for subunits of the NADH dehydrogenase complex (Complex I) of the respiratory chain (Petersen et al., 2015a; Skippington et al., 2015; Skippington et al., 2017). It was later shown that the entire enzyme complex, which is composed of close to 50 protein subunits in plants (Klusck et al., 2021), is absent in *V. album* (MacLean et al., 2018; Senkler et al., 2018; Petersen et al., 2022; Schröder et al., 2022a). Currently, mistletoe species are the only examples of multicellular organisms that can carry out cellular respiration in the absence of Complex I (Petersen et al., 2020). To compensate for Complex I deficiency, the respiratory chain of *V. album* is elaborately rearranged: numerous alternative respiratory enzymes are present and two of the “classical” complexes of the respiratory chain, Complexes III and IV, form an especially stable supercomplex, which has been suggested to promote efficient electron transport in the terminal half of the respiratory electron transfer chain. Still, the capacity of synthesizing mitochondrial ATP is considered to be limited in *V. album*.

How can *V. album* cope with a reduced capacity for generating mitochondrial ATP? This question has been intensively discussed (Busch, 2018; da Fonseca-Pereira et al., 2018; Maclean et al., 2018; Senkler et al., 2018). One of the most ATP-consuming processes in the cytosol of *V. album* leaf cells is the synthesis of sucrose from UDP-glucose and fructose (formation of UDP glucose requires UTP, which is synthesized by UDP phosphorylation using ATP). Provision of sucrose and other sugars by the host trees, especially in spring, should lessen the ATP requirement of *V. album*. Furthermore, the growth rate of *V. album* is extremely low, which may further reduce its ATP requirement. Finally, ATP biosynthesis could be increased in other subcellular compartments in *V. album*; particularly, ATP biosynthesis by glycolysis in the cytosol or by the photophosphorylation process of the chloroplasts might be enhanced. The latter two processes have not been characterized in *V. album* on a molecular scale. Sequencing of the chloroplast genome of *V. album* revealed absence of genes encoding subunits of the chloroplast NDH complex (the chloroplast pendant of mitochondrial NADH dehydrogenase complex), which is involved in cyclic electron transport (CET) around Photosystem I (Petersen et al., 2015b). This protein complex additionally is composed of nuclear-encoded subunits, which also might be absent.

To further investigate the energy metabolism of *V. album*, we report a molecular characterization of the photosynthesis apparatus of its chloroplasts. Thylakoids were isolated from young *V. album* leaves and membrane-bound protein complexes solubilized by mild nonionic detergents. The protein complex composition of the thylakoid fraction was subsequently analyzed by 2D Blue native (BN)/SDS polyacrylamide gel electrophoresis (PAGE) and by the complexome profiling approach (van Strien et al., 2021; Wittig and Malacarne, 2021) in combination with systematic protein identifications by mass spectrometry (MS). We define a close to complete set of proteins involved in the light reaction of photosynthesis and photophosphorylation. The photosynthesis apparatus of *V. album* turned out to be very special. Photosystem II amounts are similar to those reported for other seed plants, but Photosystem I amounts are reduced. The ATP synthase complex of *V. album* is remarkably stable. We present evidence that *V. album* lacks the entire NDH complex, which should limit CET around Photosystem I. However, based on alternative enzymes, ATP formation by CET can still take place, but capacity for photophosphorylation should be restricted. Furthermore, redox regulation in the chloroplasts and mitochondria of *V. album* seems to be limited. These findings further demonstrate that molecular processes in *V. album* follow particular routes.

## Results

### Isolation of thylakoid membranes

*Viscum album* leaves were used as starting material for thylakoid preparations. For reference, thylakoids were isolated from the model plant *Arabidopsis* (*Arabidopsis thaliana*).

For both species, actively growing leaves were chosen (see “Materials and methods” section). In *V. album*, new leaves emerge in late winter and have maximal growth rates in spring (Urech et al., 2004). The *V. album* leaves were harvested before the host tree developed leaves to avoid shading effects. Leaves include mostly oval-shaped chloroplasts as evaluated by transmission electron microscopy analysis (Figure 1). Thylakoids either are single-layered or stacked in grana with up to ten individual layers. For *A. thaliana*, rosette leaves were harvested in the middle of their growth period at 4 weeks after germination (Boyes et al., 2001). *Arabidopsis thaliana* as a reference system offers the most detailed background on the composition of the plant photosynthesis apparatus. The procedure for thylakoid isolation was identical for both species and included differential centrifugation steps and Percoll gradient centrifugation (see “Materials and methods” section). Resulting fractions were highly enriched in chloroplast proteins, especially in proteins present in the thylakoids (for purity evaluation of the fractions see below).

### Separation of thylakoid protein complexes

Thylakoid fractions from *V. album* and *A. thaliana* were solubilized using dodecylmaltoside (DDM) and protein complexes were separated by BN-PAGE. For *A. thaliana*, protein complexes are visible in the 120–1,500 kDa range (Figure 2). They were identified by comparison with reference gels (Järvi et al., 2011) and by analysis using a second gel dimension (see below). For *V. album*, protein complexes are visible in the 120–1,000 kDa range.

### Subunit composition of thylakoid protein complexes in *V. album* and *A. thaliana*

Two-dimensional (2D) separation of thylakoid fractions from *A. thaliana* and *V. album* by BN/SDS-PAGE allowed visualizing the subunit compositions of separated protein complexes, further facilitating their identification (Figure 3). For *A. thaliana*, both photosystems, monomeric Photosystem I and the dimeric reaction center complex of Photosystem II, run at about 550 kDa. Supermolecular assemblies of Photosystem II can be detected in the 1,000 kDa range. The

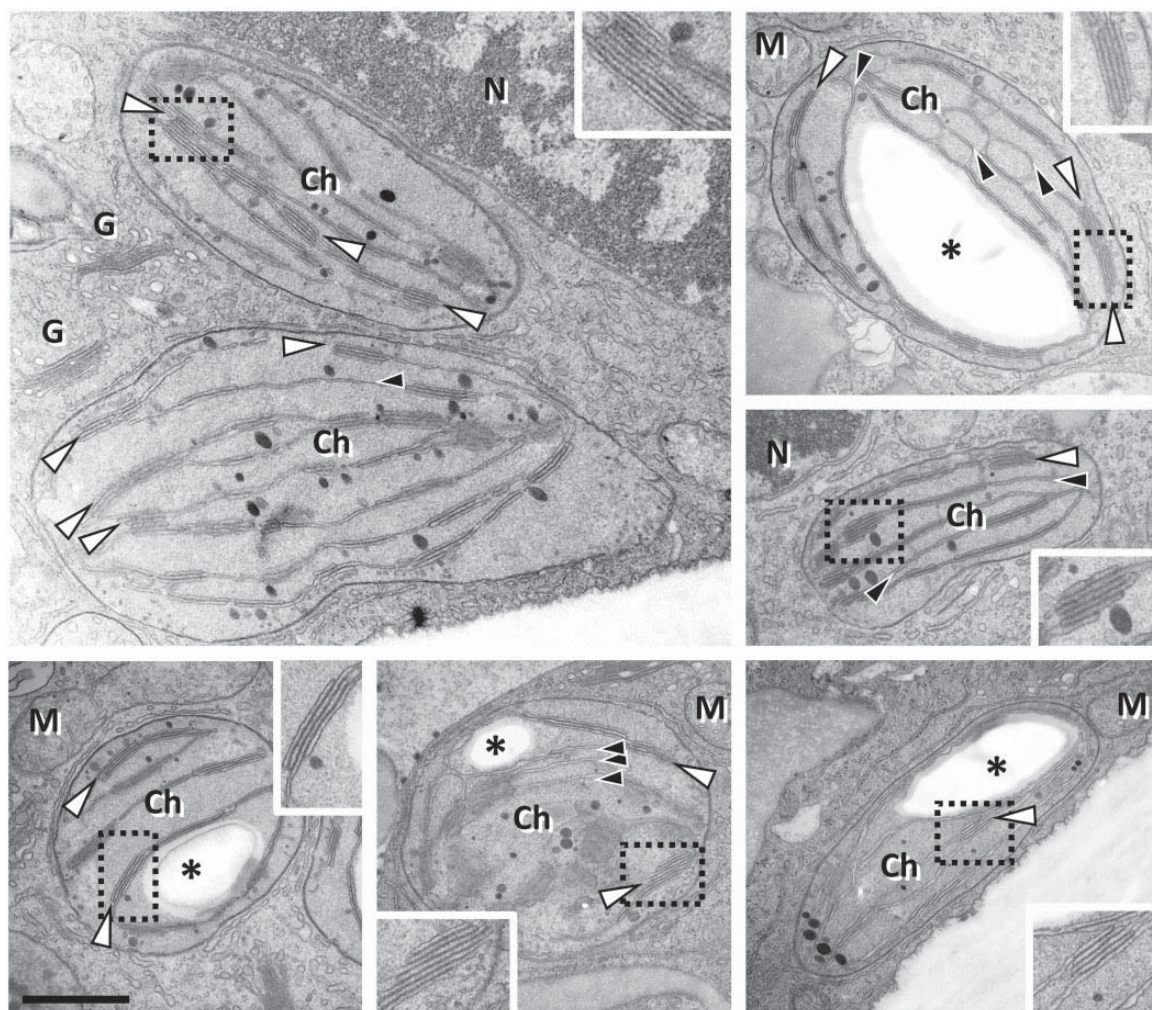


**Figure 1** Chloroplasts in *V. album* leaf cells as revealed by transmission electron microscopy. Chloroplasts (Ch) contain single layered thylakoids (black arrowheads), lipid droplets (black dots) as well as grana (white arrowheads) consisting of stacked thylakoids. In some sections a single starch granule (asterisks) is visible. The boxed areas are shown in the insets in double magnification. N, nucleus; M, mitochondria; G, Golgi. Scale bar: 1  $\mu\text{m}$  for all images; 0.5  $\mu\text{m}$  for all insets.

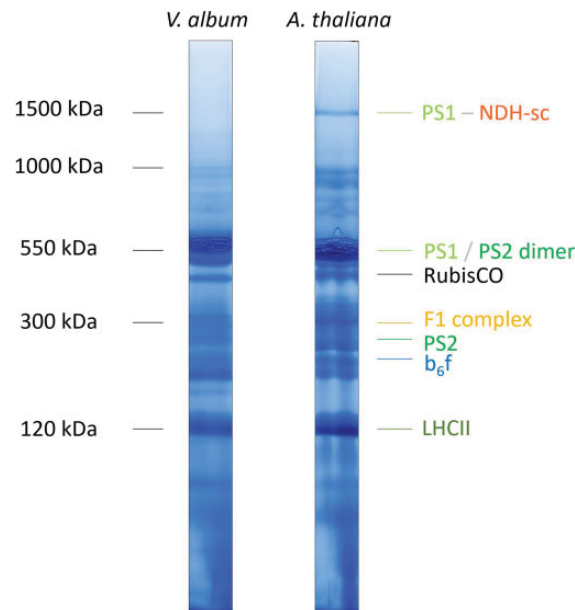


**Figure 2** Analysis of chloroplast protein complexes from *A. thaliana* and *V. album* by 1D BN-PAGE. Thylakoid membranes were solubilized using DDM and 1D BN-PAGE was carried out as described in “Materials and methods” section. Gel lanes were Coomassie-stained. The molecular masses of standard protein complexes are given to the left of the gel lanes (in kDa) and the identity of the chloroplast protein complexes from *A. thaliana* to the right (protein complex identification is based on comparison with reference gels, Järvi et al., 2011). Designations: PS1, Photosystem I; PS2, Photosystem II; NDH, chloroplast Complex I (chloroplast NADH dehydrogenase-like complex); RubisCO, Ribulose-1,5-bisphosphate-carboxylase/oxygenase; F<sub>1</sub> complex, F<sub>1</sub> part of the chloroplast ATP synthase; b<sub>6</sub>f, cytochrome b<sub>6</sub>f complex; LHCII, Light-harvesting Complex II; PS1-NDH-sc, supercomplex (sc) of NDH and two copies of monomeric PS1. The colors correspond to those given in Figures 2, 6, 8, 10, and Supplemental Figures 2 and 3.

largest protein complex of the *A. thaliana* fraction (1,500 kDa) includes, besides Photosystem I, the chloroplast NDH complex (NADH dehydrogenase-like complex). This complex represents a homolog of the mitochondrial NADH dehydrogenase complex (Complex I of the respiratory chain); the chloroplast NDH complex therefore also is termed “chloroplast complex I.” In contrast to mitochondrial Complex I, however, the chloroplast NDH complex does not use NADH but reduced ferredoxin as an electron donor (Yamamoto et al., 2011; Schuller et al., 2019). In *A. thaliana* and other angiosperms, it has been demonstrated that the NDH complex forms a supercomplex of 1,500 kDa together with two copies of Photosystem I, which is stable upon DDM solubilization (Peng et al., 2008; Shen et al., 2022). The chloroplast NDH complex is involved in CET around Photosystem I, which contributes to the proton gradient across the thylakoid membrane and thereby to the formation of ATP (Shikanai et al., 1998; Peltier et al., 2016). In addition to monomeric Photosystem I (550 kDa), the dimeric reaction center complex of Photosystem II (550 kDa), and the Photosystem I-NDH supercomplex (1,500 kDa), the 2D BN/SDS gel of the *A. thaliana* thylakoid fraction displays the cytochrome b<sub>6</sub>f complex, the F<sub>1</sub> part of the chloroplast ATP synthase complex, the monomeric reaction center complex of Photosystem II, the trimeric LHCII complex and some traces of RubisCO (indicating that the analyzed thylakoid fraction also includes some stromal proteins; Figure 3). Since the Photosystem I-NDH supercomplex of *A. thaliana* is of

low abundance, its correct identification was verified by MS (Supplemental Figure S1).

Two-dimensional separation of thylakoid fractions from *V. album* by BN/SDS-PAGE revealed protein complexes of similar composition (Figure 3): Photosystem I and the dimeric reaction center complex of Photosystem II at 550 kDa, the cytochrome b<sub>6</sub>f complex, the F<sub>1</sub> part of the chloroplast ATP synthase as well as the intact F<sub>0</sub>F<sub>1</sub> ATP synthase complex, the monomeric reaction center complex of Photosystem II, the RubisCO complex and the LHCII complex. However, the Photosystem I-NDH supercomplex and the Photosystem II supercomplexes are not visible. To test if the supercomplexes might be present but of low abundance, 2D gels of the *V. album* and *A. thaliana* thylakoid fractions were repeated and silver stained (Supplemental Figure S2). Again, the Photosystem I-NDH supercomplex and the Photosystem II supercomplexes were only detectable in *A. thaliana*. Additionally, we repeated experiments using digitonin-solubilized thylakoid protein fractions. Digitonin is an especially mild detergent for thylakoid membrane solubilization (Järvi et al., 2011). In our *A. thaliana* membrane fraction, the Photosystem I-NDH supercomplex is not visible (it forms part of extremely large protein assemblies not entering the BN gel). The Photosystem II supercomplexes are nicely retained. In contrast, the Photosystem II supercomplexes and the Photosystem I-NDH supercomplex were not detectable in *V. album* (Supplemental Figure S3). We conclude that these supercomplexes are of very low abundance or absent in *V. album*.

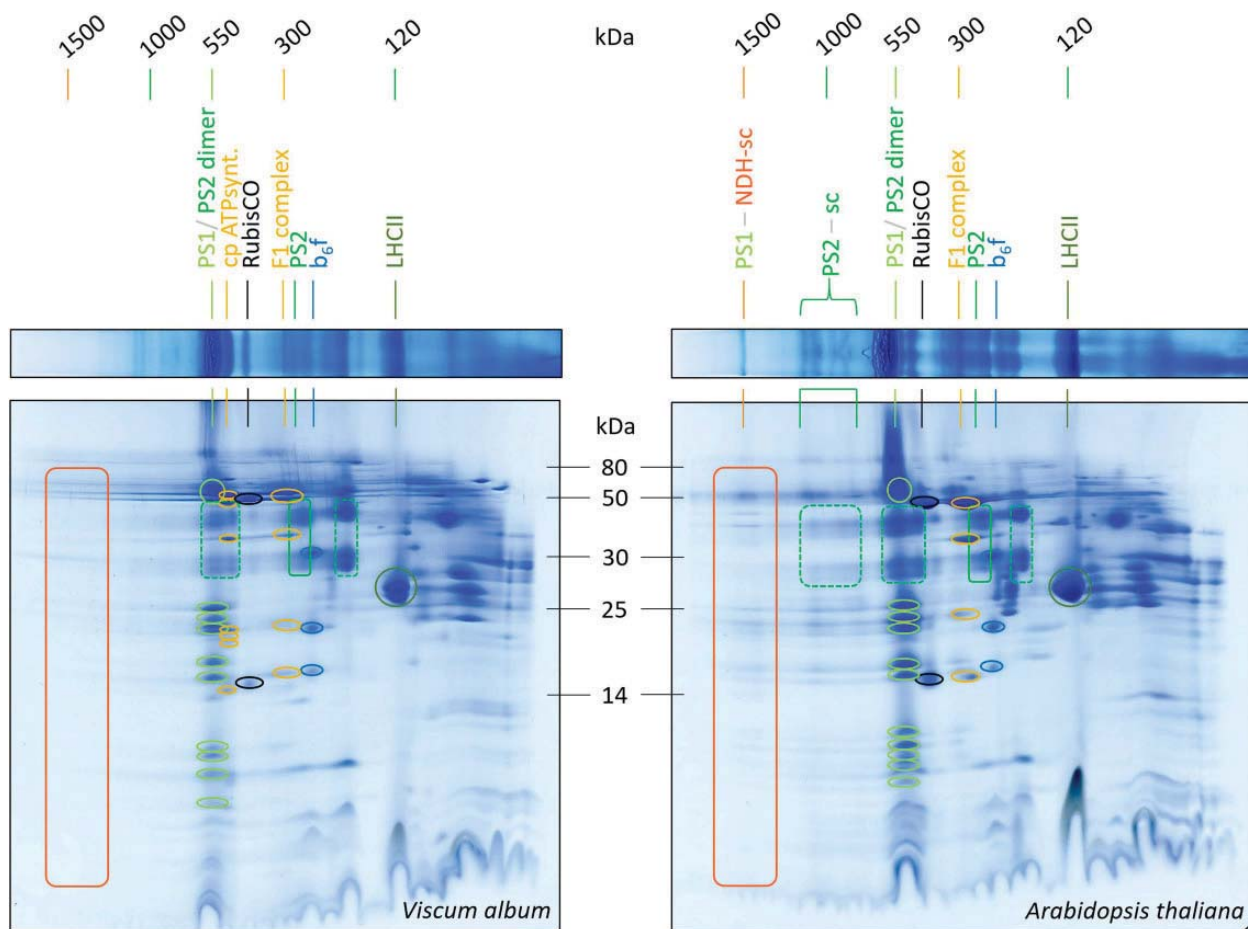


**Figure 3** Analyses of chloroplast protein complexes from *V. album* and *A. thaliana* by 2D BN/SDS-PAGE. Lanes of 1D BN gels (Figure 2) were transferred horizontally onto SDS gels for electrophoresis in orthogonal direction (see “Materials and methods” section for details). Two-dimensional gels were Coomassie-stained. Molecular masses of standard protein complexes are given above the gels (in kDa); molecular masses of monomeric standard proteins in between the 2D gels (in kDa). The identities of protein complexes are indicated above the gels (identifications based on reference gels, see <https://www.gelmap.de/Arabidopsis-chloro/> and Behrens et al., 2013). For designations see legend of Figure 2. PS2-sc, super-complexes (sc) consisting of Photosystem II. Boxes and circles on the 2D gels indicate subunits of defined protein complexes; the color code corresponds to the colors of the names of the protein complexes given above the gels. Note that the Photosystem I-NDH supercomplex and the Photosystem II supercomplexes are present in *A. thaliana* but not detectable in *V. album*.

### Analyses of thylakoid protein complexes of *V. album* and *A. thaliana* by complexome profiling

The complexome profiling approach (van Strien et al., 2021; Wittig and Malacarne, 2021) was used to obtain deeper insights into the protein complex composition of thylakoids from *V. album*. A corresponding thylakoid fraction of *A. thaliana* was analyzed in parallel for reference. Complexome profiling allows sensitive and systematic characterization of protein complexes in cellular or subcellular fractions. It is based on protein separation by one-dimensional (1D) BN-PAGE, subsequent dissection of a BN gel lane into horizontal slices, and finally systematic protein identification in all slices by label-free quantitative shotgun proteomics. We used 44 gel slices for the thylakoid fractions from *V. album* and *A. thaliana*, respectively (Supplemental Figure S4). Data from MS were evaluated using the Araport11 database (<https://www.arabidopsis.org/>) for *A. thaliana* and the *V. album* gene space database (<https://viscumalbum.pflanzenproteomik.de/>,

Schröder et al., 2022a) for *V. album*. Table 1 summarizes our results: For both species, about 400–600 proteins were detected per gel fraction (Figure 4; Supplemental Figure S5). The sum of identified proteins in the 44 fractions was 24,852 for *V. album* and 18,322 for *A. thaliana*. On average, each individual protein was identified in 13 different gel fractions (gel slices) for *V. album* and *A. thaliana*. The number of unique proteins is 1,833 for *V. album* and 1,374 for *A. thaliana*. Normalized (max) intensity profiles were calculated for all proteins along the two BN gel lanes and converted into heatmaps. In a final step, abundance profiles were aligned based on similarity using the Nova software tool (Giese et al., 2015). On the resulting figure, proteins forming part of protein complexes form clusters (Supplemental Figure S6, Supplemental Data Set S1, Supplemental Data Set S2). Evaluation of the complexome profiling data allowed defining all major protein complexes present in the thylakoids of *V. album* and *A. thaliana* (see below).

**Table 1** Results of complexome profiling analyses for thylakoid fractions from *V. album* and *A. thaliana*

	<i>Viscum album</i>	<i>Arabidopsis thaliana</i>
Number of analyzed fractions (gel slices)	44	44
Number of identified peptides (sum of all peptides in all fractions)	136,953	99,438
Average number of peptides per fraction	3,113	2,260
Number of identified proteins (sum of all proteins in all fractions)	24,852	18,322
Average number of proteins per fraction	565	416
Number of unique peptides	12,365	10,612
Number of unique proteins	1,833	1,374
Average coverage of proteins by peptides (unique peptides / unique protein)	6.74	7.72
Average frequency of protein detection (average number of fractions, in which individual proteins were detected)	13.56	13.33

### Evaluation of the purity of the thylakoid fractions

The MS data were also used to evaluate the purity of our thylakoid fractions. We calculated intensity-based absolute quantification (iBAQ) scores for all proteins of all complexome fractions. The iBAQ scores can be used as a quantitative estimate for each identified protein (Arike et al., 2012). In a second step, all identified proteins of all complexome profiling fractions were assigned to subcellular compartments based on the *A. thaliana* SUBAcon database (Hooper et al., 2014). This database integrates all available information on subcellular localization of all proteins for *A. thaliana*. Finally, iBAQ values of all proteins of all complexome fractions were summed up per subcellular compartment. In *A. thaliana*, >99% of the cumulated iBAQ values were assigned to the chloroplast compartment. Since the SUBAcon database only includes subcellular localization information of *A. thaliana* proteins, the same calculation could not directly be carried out for *V. album*. However, we systematically determined *A. thaliana* homologs for the identified *V. album* proteins and used these homologs for SUBAcon evaluation. >83% of the cumulated iBAQ scores of the homologs were assigned to the chloroplast compartment (Figure 5). Mitochondrial proteins represented another 15% of the cumulated iBAQ values in *V. album*. We conclude that the isolation procedure for chloroplasts, which has been optimized for *A. thaliana*, does lead to excellent results for *A. thaliana* and still very reasonable results for *V. album*. We cannot estimate the enrichment of thylakoid proteins with respect to proteins of other chloroplast sub-compartments (the envelope membranes, the chloroplast stroma), since proteins of these subfractions are not defined in the SUBAcon database. However, most identified proteins clearly form part of known thylakoid protein complexes (see below).

### Subunit composition of the thylakoid protein complexes of *V. album*

The protein complexes of the thylakoids of *A. thaliana*, Photosystems I and II, the cytochrome  $b_6/f$  complex, the

chloroplast ATP synthase complex, and the NDH complex, all are well defined (Shikanai, 2016; Berger et al., 2020; Malone et al., 2021). Nearly all subunits of these protein complexes were identified in the course of our complexome profiling analysis (Figure 6; Supplemental Data Set S2). Subunits of the individual protein complexes form distinct clusters on the maps. The complexome profiling map for the thylakoids of *V. album* resembles the one of the *A. thaliana* but also shows clear differences. Clusters for Photosystem I, Photosystem II, and the cytochrome  $b_6/f$  complex are similar (Figure 6; Supplemental Data Set S1, Supplemental Data Set S2). Photosystem II supercomplexes are visible in *A. thaliana* and, using the more sensitive complexome profiling approach, also in *V. album*. Compared to *A. thaliana*, the  $F_0F_1$  ATP synthase complex of *V. album* is clearly more stable. Upon DDM solubilization, this complex largely is dissected into the  $F_0$  and  $F_1$  parts in *A. thaliana* (Figure 6). In *V. album*, the  $F_0F_1$  holocomplex largely remains intact. This difference also is visible on the 2D BN/SDS gels for DDM-treated (Figure 3) and digitonin-treated (Supplemental Figure S3) thylakoid fractions of *V. album* and *A. thaliana*. The protein cluster of the Photosystem I-NDH supercomplex is completely absent in *V. album* (Figure 6). Subunits of the NDH complex were not detected in any *V. album* complexome fractions with the exception of the PnsL5 subunit (see below). The NDH complex of *A. thaliana* is composed of about 30 subunits (see Shikanai, 2016 and Shikanai and Aro, 2016 for review). Besides complexome profiling analyses, we systematically searched for homologs of the *A. thaliana* NDH complex in the *V. album* gene space database (<https://viscumalbum.pflanzenproteomik.de/>; Schröder et al., 2022a). Of the 30 subunits of the *A. thaliana* NDH complex, only one subunit, the PnsL5 protein, is present in *V. album*. This protein is an auxiliary subunit of the NDH complex (Sirpiö et al., 2009; Shikanai and Aro, 2016) and has been shown to exhibit peptidyl-prolyl isomerase activity (Edvardsson et al., 2003; Shapiguzov et al., 2006). In the *A. thaliana* complexome, PnsL5 forms part of the 1,500 kDa Photosystem I-NDH complex cluster. In contrast, in *V. album*, it clusters with monomeric proteins in the < 100 kDa range (Figure 7).

### Photosystem I has reduced abundance in *V. album*

To estimate the abundance and stoichiometry of the protein complexes involved in photosynthesis, summed up iBAQ values were calculated for selected protein complexes and related to the total iBAQ values of the analyzed thylakoid membrane fraction (Table 2). As expected, Photosystem II, which consists of the reaction center complex, the oxygen-evolving complex, and light-harvesting complexes, and which is responsible for thylakoid membrane stacking, constitutes a major part of the proteins in our thylakoid fraction (49% in *A. thaliana* and 43% in *V. album*). The cytochrome  $b_6/f$  complex represents about 3% of the total thylakoid protein in *A. thaliana* and *V. album* (it has fewer subunits and is much smaller than Photosystem II) and the ATP synthase complex constitutes about 12% of



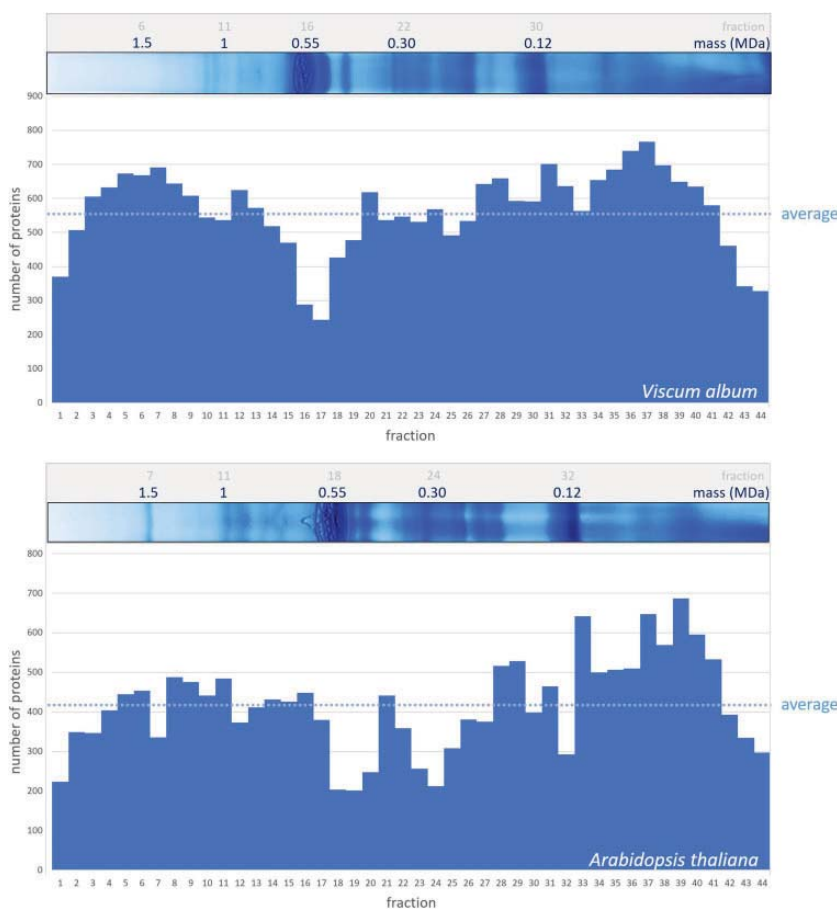


**Figure 4** Number of proteins identified in the complexome profiling fractions of *V. album* and *A. thaliana*. BN gel lanes were each horizontally dissected into 44 gel slices, and subjected to label-free quantitative shotgun proteomics (Supplemental Figure 4). Top: Identified proteins per gel slice fraction in *V. album*; evaluation of MS data was based on the *V. album* gene space database; <https://viscumalbum.pflanzenproteomik.de/>, Schröder et al. (2022a). Bottom: Identified proteins per gel slice fraction in *A. thaliana*; evaluation of MS data was based on the Araport11 database (<https://www.arabidopsis.org/>). The lanes of the 1D BN gel used for complexome profiling are shown above the diagrams (same gel images as shown in Figure 2). MS data of *V. album* were additionally evaluated using the Araport11 database (Supplemental Figure 5).

the thylakoid proteins in both species. In contrast to the three discussed complexes, the abundance of Photosystem I differs in *A. thaliana* and *V. album* (21% versus 12%). This result also is visible on the 2D BN/SDS gels (Figure 3; Supplemental Figures S2 and S3). We conclude that *V. album* has comparatively low amounts of Photosystem I and a reduced Photosystem I/Photosystem II ratio.

## Discussion

### Insights into the subunit composition and stoichiometry of the thylakoid protein complexes in *V. album*

Our complexome profiling analyses allowed identification of close to 100 distinct *V. album* proteins involved in the light reaction of photosynthesis. Overall, we identified > 1,800 proteins in the *V. album* thylakoid fraction, which is more than the > 1,300 proteins that were identified in parallel for the thylakoid fraction of the model plant *A. thaliana*. This, however, might partially reflect that the thylakoid fraction of *V. album* had a lower purity (it included some proteins of

the mitochondria). Besides complexome profiling, we additionally used the amino acid sequences of the proteins involved in the light reaction of photosynthesis in *A. thaliana* to systematically probe the *V. album* gene space database (Table 3). The table includes a close to complete set of proteins involved in the light reaction in *A. thaliana* and *V. album*, most of which also were identified by complexome profiling. Several of the involved proteins occur in isoforms, especially in *V. album*.

Photosystems I and II, together with the cytochrome  $b_6/f$  complex, are involved in linear electron transport (LET) from  $H_2O$  to  $NADP^+$ . As a result, NADPH and ATP are produced. Additionally, Photosystem I and the cytochrome  $b_6/f$  complex are involved in CET, which only generates ATP. The ratio of LET and CET can be adjusted by the numeric ratio of the two photosystems, but also by modulation of the antenna sizes associated with the photosystems (regulated, besides others, by the STN7 and STN8 protein kinases; see Longoni and Goldschmidt-Clermont, 2021 for review) and by regulation of photosystem activities. Interestingly, the amount of Photosystem I is comparatively low in

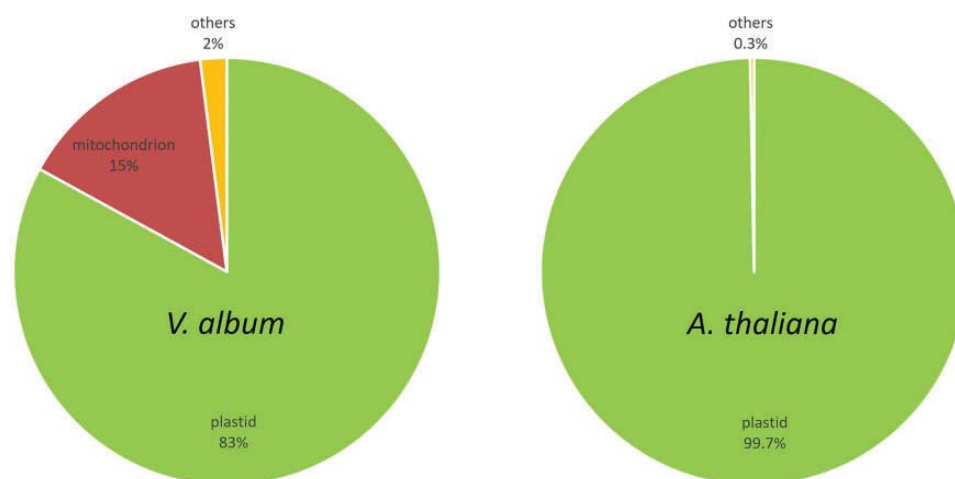


**Figure 5** Evaluation of the purity of the thylakoid fractions from *A. thaliana* and *V. album* by cumulated protein quantities (iBAQ values) assigned to subcellular compartments according to SUBAcon (<https://suba.live/>). iBAQ values of all proteins identified in all complexome profiling fractions were included in this evaluation. For *V. album*, the evaluation was based on *A. thaliana* homologs of the identified proteins because SUBAcon only includes subcellular localization information for *A. thaliana*.

*V. album*. Shading effects, which result in relative enrichment of far-red light and which are known to also cause a reduction of Photosystem I (reviewed in Schöttler and Tóth, 2014), can be excluded since *V. album* was harvested in spring before leaves of the host tree developed. Since Photosystem II amounts are similar in *A. thaliana* and *V. album* (Table 2), the Photosystem I–Photosystem II ratio is reduced in *V. album*, which should affect both LET and CET. This is in line with previous reports that *V. album* has a reduced Photosystem I to Photosystem II activity (Tuquet and Sallé, 1996). As a result, the overall photosynthesis rate in *V. album* is reduced (Tuquet and Sallé, 1996; Zuber, 2004). This also should affect photophosphorylation.

Photophosphorylation, the formation of ATP by phosphorylation of ADP using the proton gradient across the thylakoid membrane build up by LET and CET, is catalyzed by the chloroplast ATP synthase complex. In the chloroplasts of *A. thaliana* and *V. album*, amounts of chloroplast ATP synthase complexes are similar. This might reflect the importance of the chloroplast ATP synthase complex in regulating the pH in the thylakoid lumen (Trinh and Masuda, 2022). The chloroplast ATP synthase complex has been found to be especially stable in *V. album* (Figures 3 and 6). However, decreased LET and CET should reduce the proton gradient across the thylakoid membrane and thereby diminish the capacity to produce ATP. The proton gradient may be further reduced by the activity of the plastid terminal oxidase (PTOX), which catalyzes plastoquinol oxidation using oxygen as a direct electron acceptor. Interestingly, by our complexome profiling analysis, PTOX was identified in *A. thaliana* but not in *V. album*.

#### Absence of the NDH complex and the Photosystem I-NDH supercomplex

The chloroplast NDH complex is absent in *V. album*. This protein complex, which is homologous to mitochondrial

Complex I, includes about 30 subunits. It catalyzes ferredoxin-plastoquinone oxidoreduction and is involved in CET around the Photosystem I. Most of the subunits of this protein complex are encoded by the nuclear genome in plants, but some are encoded in the plastidic genome (reviewed in Shikanai, 2016). It has been reported previously that the plastidic genes encoding subunits of the NDH complex are absent in *Viscum* species (Petersen et al., 2015b). We here report that the entire NDH complex including the nuclear-encoded subunits is absent in *V. album* (Figure 8). Only one NDH subunit is retained in *V. album*, the PnsL5 protein. This protein is considered to be bifunctional since it exhibits peptidyl-prolyl isomerase activity and at the same time is necessary for the assembly of the NDH complex (Sirpiö et al., 2009; Shikanai and Aro, 2016). Similarly, bifunctional subunits of mitochondrial Complex I were recently reported to be retained in *V. album* despite the loss of this respiratory protein complex (Petersen et al., 2022; Schröder et al., 2022a). In the *A. thaliana* thylakoid complexome, PnsL5 forms part of the 1,500 kDa Photosystem I-NDH complex cluster. In contrast, in *V. album*, it clusters with monomeric proteins in the <100 kDa range (Figure 7). Since the NDH complex is absent in *V. album*, Photosystem I only is present as a monomer. Absence of the NDH complex should affect chloroplast capacity to re-oxidize ferredoxin and thereby CET.

#### CET around Photosystem I may be mediated by the PGR5/PGRL1 proteins in *V. album*

In plants, CET also can be carried out by an alternative pathway involving the PGR5/PGRL1 proteins (Munekage et al., 2002; DalCorso et al., 2008; Hertle et al., 2013; reviewed in Shikanai, 2014; Ma et al., 2021). These proteins are likewise present in *A. thaliana* and *V. album*, but, compared to *A. thaliana*, amounts of these proteins are reduced in *V. album* (Figure 9). We conclude that CET can take place

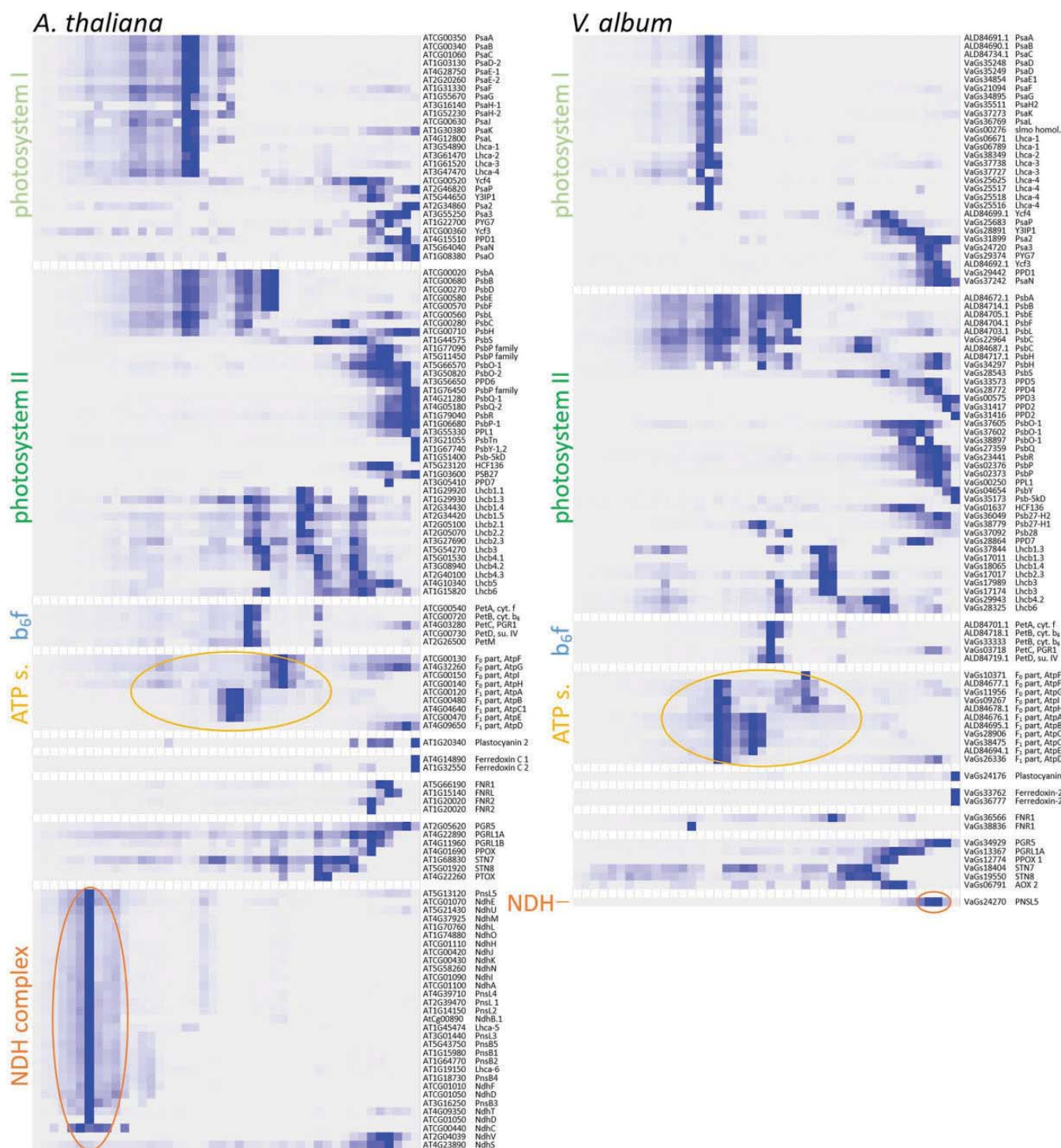


**Figure 6** Selective display of the complexome profiling data for subunits of the Photosystem I, the Photosystem II, the cytochrome  $b_6f$  complex, the chloroplast ATP synthase complex, the NDH complex, and some further monomeric proteins involved in photosynthesis from *A. thaliana* (left) and *V. album* (right). Relative quantities of all proteins (125 proteins in *A. thaliana* and 96 of *V. album* along two BN gel lanes (44 fractions, respectively; Supplemental Figure 4) are displayed as heatmap (dark blue stands for high quantity, light blue/white for low quantity/no detection). For complete complexome profiling maps (1,374 proteins in *A. thaliana* and 1,833 proteins in *V. album*) see Supplemental Figure 6. Accession numbers of the proteins in the Araport11 (<https://www.arabidopsis.org/>) and *V. album* gene space databases (<https://visucumalbum.pflanzenproteomik.de/>, Schröder et al., 2022a) are given to the right of the maps; in addition, names/abbreviations of the protein names are displayed. Subunits of the chloroplast ATP synthase and the NDH complex are indicated by circles. For complete complexome profiling data see Supplemental Data Sets S1 and S2. Data also can be accessed and probed at the ComplexomeMap portal at [https://complexomemap.de/va\\_chloroplasts](https://complexomemap.de/va_chloroplasts) and [https://complexomemap.de/at\\_chloroplasts](https://complexomemap.de/at_chloroplasts).



**Figure 7** Abundance profiles of PnsL5 from *V. album* and *A. thaliana* upon complexome profiling. The molecular masses of standard protein complexes (in MDa) are given above the profiles.

**Table 2** Summed up iBAQ values of individual thylakoid protein complexes in relation to the total iBAQ value of the corresponding thylakoid membrane fraction (summed up iBAQ values of all proteins of the analyzed fraction in percent)

	<i>Arabidopsis thaliana</i>	<i>Viscum album</i>
Photosystem I	20.7	12.0
Photosystem II	49.5	43.4
Cytochrome b <sub>6</sub> f complex	3.2	3.0
ATP synthase	11.7	12.5

in *V. album* (Figure 10). However, reduced amounts of Photosystem I together with the absence of one of the two CET pathways around Photosystem I both indicate that the capacity for chloroplast ATP formation based on photophosphorylation might be restricted in *V. album*. The degree of restriction is difficult to predict because further CET pathways were suggested to occur, which so far could not be precisely defined (Nawrocki et al., 2019). Also, the molecular functions of the PGR5/PGRL1 proteins might go beyond CET (Kanazawa et al., 2017; Shimakawa and Miyake, 2018) and have to be further defined.

### Life without mitochondrial and chloroplast Complex I

*Viscum album* and some other related species of the *Viscum* and *Phoradendron* genera of the *Santalaceae* family are the only multicellular species that can carry out cellular respiration without mitochondrial Complex I (Petersen et al., 2015a; Skippington et al., 2015; Maclean et al., 2018; Senkler et al., 2018; Zervas et al., 2019; Petersen et al., 2022; Schröder et al., 2022a). In addition, *V. album* now has been shown to completely lack chloroplast Complex I, the NDH complex. Absence of NDH is less an exception than absence of mitochondrial Complex I. Indeed, loss of chloroplast Complex I has been reported for a few clades of plants (Wakasugi et al., 1994; Wicke et al., 2011; Lin et al., 2017; Silva et al., 2018; reviewed in Sabater, 2021). In general, the NDH complex is found in mosses, ferns, and seed plants, but there are exceptions that concern some aquatic plants, plant parasites, and a few further plant species that grow under comparatively mild conditions. In contrast, most algae lack the NDH complex. It has been concluded that the NDH complex is beneficial in stressful terrestrial environments to maintain efficient photosynthesis (Sabater, 2021). However, its biosynthesis requires substantial amounts of energy for protein synthesis and for assembly of the protein complex. Under mild conditions, it might be advantageous to save this energy.

The *Viscum* species are another group of organisms that do not require the NDH complex. Most remarkably, they are the only known clade of plants that simultaneously lack both the mitochondrial and the chloroplast Complex I. The absence of mitochondrial Complex I reduces the mitochondrial capacity to produce ATP. Reduced amounts of Photosystem I together with the absence of chloroplast Complex I simultaneously limits the capacity for chloroplast ATP formation. *V. album* might tolerate low ATP formation because its growth rate is low. Furthermore, the host trees provide energy-rich organic compounds, including glucose, fructose, and sucrose, especially in spring (Escher et al., 2004). Sucrose biosynthesis in the cytosol requires substantial amounts of mitochondrial ATP, which can be saved if the sucrose is provided by the host. Indeed, maximal growth of *V. album* takes place in spring, when deciduous trees supply organic compounds to their developing organs of the new growing season (Urech et al., 2004). The importance of the host trees supplying *V. album* with carbohydrates may have been underestimated so far.

### The *V. album* way of life

*Viscum album* and related species are known for their very special life cycle (Luther and Becker, 1987; Zuber, 2004). Already von Tubeuf (1922) concluded on *V. album* “Nothing about this plant is normal.” Several regulatory mechanisms seem to be diminished in *V. album*: It has no polar axis but grows in all directions resulting in the spherical shape of the adult plant; stomata are at both sides of the leaves and not (much) regulated; seed dormancy does not take place; and senescence processes are very reduced as green leaves are discarded. Meanwhile increasing information is available on the molecular biology of *V. album* at the levels of its gene space, transcriptome, proteome, and metabolome (Novák et al., 2020; Jäger et al., 2021; Schröder et al., 2022a). Mechanisms to limit an increase in genome size were obviously weak during evolution, leading to one of the largest plant genomes ever described (Zonneveld, 2010). Mitochondria lack Complex I, have decreased amounts of the mitochondrial ATP synthase complex and fewer cristae. The amounts of Photosystem I are reduced and chloroplast Complex I is absent, restricting CET at Photosystem I. Besides limited organellar ATP generation, the absence of chloroplast and mitochondrial Complex I also should affect the capacity of *V. album* to regulate its cellular redox balance. Reduced levels of regulation in general means reduced energy costs, which, however, comes with the price of reduced molecular coordination and safeguard. Overall, the *V.*

**Table 3** Proteins of the photosynthesis apparatus of *V. album* and *A. thaliana* detected by complexome profiling and searches in proteome databases

Protein Name (Abbreviation)	Protein Complex/ Full Protein Name	Accession in <i>A. thaliana</i>	Identified in the Complexome in <i>A. thaliana</i>	Accessions in <i>V. album</i> (Accessions Identified in the <i>V. album</i> Complexome [Next Column] Are Indicated in Bold)	Identified in the Complexome in <i>V. album</i>
Photosystem I					
Lhca-1	Photosystem I	At3g54890	X	VaGs05700; VaGs05736; VaGs05756; VaGs05759; VaGs05818; VaGs05838; VaGs06232; <b>VaGs06671</b> ; VaGs06787; <b>VaGs06789</b>	X
Lhca-2	Photosystem I	At3g61470	X	VaGs38348; <b>VaGs38349</b>	X
Lhca-3	Photosystem I	At1g61520	X	VaGs37725; <b>VaGs37727</b> ; <b>VaGs37738</b> ; VaGs37739; VaGs37740; VaGs37741	X
Lhca-4	Photosystem I	At3g47470	X	VaGs24169; VaGs24170; VaGs24171; VaGs24240; VaGs24241; VaGs24242; VaGs24243; <b>VaGs25516</b> ; <b>VaGs25517</b> ; <b>VaGs25518</b> ; VaGs25519; VaGs25621; VaGs25623; VaGs25624; <b>VaGs25625</b>	X
Lhca-5	Photosystem I	At1g45474	X		
Lhca-6	Photosystem I	At1g19150	X		
PPD1	Photosystem I	At4g15510	X	VaGs29436; VaGs29437; VaGs29438; VaGs29439; VaGs29440; VaGs29441; <b>VaGs29442</b>	X
Psa2	Photosystem I	AT2G34860	X	VaGs31638; VaGs31897; VaGs31898; <b>VaGs31899</b> ; VaGs32548	X
Psa3	Photosystem I	At3g55250	X	<b>VaGs24720</b> ; VaGs25455	X
PsaA	Photosystem I	AtCg00350	X	VaGs09326; VaGs09330; VaGs09568; VaGs09860; VaGs10294; VaGs10458; VaGs10648; <b>ALD84691.1</b>	X
PsaB	Photosystem I	AtCg00340	X	VaGs09565; VaGs09569; VaGs09633; VaGs09861; VaGs10079; VaGs10295; VaGs10297; VaGs10456; VaGs10461; <b>ALD84690.1</b>	X
PsaC	Photosystem I	AtCg01060	X	<b>ALD84734.1</b>	X
PsaD-1	Photosystem I	At4g02770	X	<b>VaGs35249</b> ; VaGs36309	X
PsaD-2	Photosystem I	At1g03130	X	VaGs35247; <b>VaGs35248</b> ; VaGs35250; VaGs35312; VaGs36078; VaGs36310	X
PsaE-1	Photosystem I	At4g28750	X		
PsaE-2	Photosystem I	At2g20260	X	VaGs34853; <b>VaGs34854</b>	X
PsaF	Photosystem I	At1g31330	X	<b>VaGs21094</b> ; VaGs22312; VaGs22313; VaGs22314	X
PsaG	Photosystem I	At1g55670	X	VaGs34894; <b>VaGs34895</b> ; VaGs34896; VaGs34898; VaGs35931	X
PsaH-1	Photosystem I	At3g16140	X	<b>VaGs35511</b> ; VaGs35660; VaGs35716; VaGs35717	X
PsaH-2	Photosystem I	At1g52230	X	VaGs35510	
PsaI	Photosystem I	AtCg00510		ALD84698.1	
PsaJ	Photosystem I	AtCg00630	X	ALD84708.1	
PsaK	Photosystem I	At1g30380	X	<b>VaGs37273</b> ; VaGs37274	X
PsaL	Photosystem I	At4g12800	X	<b>VaGs36769</b> ; VaGs36770; VaGs36771; VaGs37857; VaGs37858; VaGs38059; VaGs38955	X
PsaN	Photosystem I	At5g64040	X	VaGs37238; VaGs37239; <b>VaGs37242</b>	X
PsaO	Photosystem I	At1g08380	X	VaGs22666; VaGs22667; VaGs22668; VaGs23530	
PsaP	Photosystem I	At2g46820	X	<b>VaGs25683</b> ; VaGs25686	X
PYG7	Photosystem I	At1g22700	X	VaGs29373; <b>VaGs29374</b> ; VaGs29375	X
Y3IP1	Photosystem I	At5g44650	X	<b>VaGs28891</b> ; VaGs28893; VaGs28894; VaGs30114	X
Ycf3	Photosystem I	AtCg00360	X	VaGs09567; VaGs23339; <b>ALD84692.1</b>	X
Ycf4	Photosystem I	AtCg00520	X	VaGs24236; VaGs24598; VaGs24858; VaGs24860; VaGs26085; VaGs26335; <b>ALD84699.1</b>	X
Photosystem II					
Lhcb1.1	Photosystem II	At1g29920	X		
Lhcb1.2	Photosystem II	At1g29910			
Lhcb1.3	Photosystem II	At1g29930	X	<b>VaGs17011</b> ; VaGs17018; VaGs17021; VaGs18064; VaGs18184; VaGs20794; <b>VaGs37844</b>	X
Lhcb1.4	Photosystem II	At2g34430	X	<b>VaGs18065</b> ; VaGs36420; VaGs36421; VaGs37845; VaGs37847; VaGs38519	X
Lhcb1.5	Photosystem II	At2g34420	X	VaGs37848	
Lhcb2.1	Photosystem II	At2g05100	X		
Lhcb2.2	Photosystem II	At2g05070	X		
Lhcb2.3	Photosystem II	At3g27690	X	VaGs17010; VaGs17016; <b>VaGs17017</b> ; VaGs17020; VaGs17022; VaGs17173; VaGs17988	X
Lhcb3	Photosystem II	At5g54270	X	VaGs17015; VaGs17145; <b>VaGs17174</b> ; <b>VaGs17989</b>	X

(continued)

Table 3 Continued

Protein Name (Abbreviation)	Protein Complex/ Full Protein Name	Accession in <i>A. thaliana</i>	Identified in the Complexome in <i>A. thaliana</i>	Accessions in <i>V. album</i> (Accessions Identified in the <i>V. album</i> Complexome [Next Column] Are Indicated in Bold)	Identified in the Complexome in <i>V. album</i>
Lhcb4.1	Photosystem II	At5g01530	X	VaGs29945; VaGs30342	
Lhcb4.2	Photosystem II	At3g08940	X	VaGs29942; <b>VaGs29943</b> ; VaGs29944; VaGs30341	X
Lhcb4.3	Photosystem II	At2g40100	X		
Lhcb5	Photosystem II	At4g10340	X		
Lhcb6	Photosystem II	At1g15820	X	<b>VaGs28325</b> ; VaGs28326	X
PPD6	Photosystem II	At3g56650	X		
PPL1	Photosystem II	At3g55330	X	<b>VaGs00250</b>	X
PPL2	Photosystem II	At2g39470	X		
Psb-5kD	Photosystem II	At1g51400	X	<b>VaGs35173</b>	X
PsbA	Photosystem II	AtCg00020	X	<b>ALD84672.1</b>	X
PsbB	Photosystem II	AtCg00680	X	VaGs34213; VaGs34217; <b>ALD84714.1</b>	X
PsbC	Photosystem II	AtCg00280	X	VaGs22823; VaGs22824; VaGs22877; VaGs22878; VaGs22879; VaGs22956; VaGs22957; <b>VaGs22964</b> ; VaGs23152; VaGs23233; VaGs23899; VaGs24088; <b>ALD84687.1</b>	X
PsbD	Photosystem II	AtCg00270	X	VaGs22880; ALD84686.1	
PsbE	Photosystem II	AtCg00580	X	VaGs24601; VaGs38380; <b>ALD84705.1</b>	X
PsbF	Photosystem II	AtCg00570	X	VaGs37226; <b>ALD84704.1</b>	X
PsbH	Photosystem II	AtCg00710	X	VaGs33255; <b>VaGs34297</b> ; <b>ALD84717.1</b>	X
PsbI	Photosystem II	AtCg00080		ALD84675.1	
PsbJ	Photosystem II	AtCg00550		ALD84702.1	
PsbK	Photosystem II	AtCg00070		VaGs00341; VaGs00769; ALD84674.1	
PsbL	Photosystem II	AtCg00560	X	<b>ALD84703.1</b>	X
PsbM	Photosystem II	AtCg00220		VaGs09191; ALD84685.1	
PsbN	Photosystem II	AtCg00700		ALD84716.1	
PsbO-1	Photosystem II	At5g66570	X	VaGs36809; VaGs36810; <b>VaGs37602</b> ; VaGs37604; <b>VaGs37605</b> ; <b>VaGs38897</b>	X
PsbO-2	Photosystem II	At3g50820	X		
PsbP family	Photosystem II	At1g76450	X	<b>VaGs00575</b> ; VaGs00577	X
PsbP family	Photosystem II	At1g69680			
PsbP family	Photosystem II	At1g77090	X	<b>VaGs28772</b>	X
PsbP family	Photosystem II	At5g11450	X	<b>VaGs33573</b>	X
PsbP family	Photosystem II	At3g05410	X	<b>VaGs28864</b>	X
PsbP-1	Photosystem II	At1g06680	X	VaGs02374; VaGs02375; <b>VaGs02376</b>	X
PsbP-2	Photosystem II	At2g30790		<b>VaGs02373</b> ; VaGs03329; VaGs03330	X
PsbQ-1	Photosystem II	At4g21280	X	VaGs27356; VaGs27357; VaGs27358; <b>VaGs27359</b> ; VaGs27654; VaGs28561	X
PsbQ-2	Photosystem II	At4g05180	X		
PsbR	Photosystem II	At1g79040	X	VaGs22618; VaGs23098; VaGs23099; VaGs23265; VaGs23267; VaGs23438; <b>VaGs23441</b>	X
PsbS	Photosystem II	At1g44575	X	VaGs27026; VaGs27027; VaGs27028; VaGs27030; VaGs27031; VaGs27173; VaGs28072; VaGs28170; VaGs28171; VaGs28349; <b>VaGs28543</b> ; VaGs28544; VaGs28545	X
PsbT	Photosystem II	AtCg00690		ALD84715.1	
PsbTn	Photosystem II	At3g21055	X	VaGs36194; VaGs36532	
PsbW	Photosystem II	At2g30570		VaGs31144; VaGs32081; VaGs32110; VaGs32305; VaGs32438; VaGs32481	
PsbX	Photosystem II	At2g06520		VaGs38401; VaGs38404	
PsbY-1,2	Photosystem II	At1g67740	X	VaGs04653; <b>VaGs04654</b> ; VaGs05309; VaGs05482; VaGs05483; VaGs05484; VaGs34835	X
PsbZ	Photosystem II	AtCg00300		VaGs23703; ALD84688.1	
cyt b6f complex					
PetA, cyt. f	cyt b6f complex	ATCG00540	X	VaGs37147; VaGs37223; <b>ALD84701.1</b>	X
PetB, cyt. b <sub>6</sub>	cyt b6f complex	ATCG00720	X	<b>VaGs33333</b> ; VaGs34157; VaGs34706; <b>ALD84718.1</b>	X
PetC, PGR1	cyt b6f complex	AT4G03280	X	VaGs03572; VaGs03573; VaGs03574; <b>VaGs03718</b>	X
PetD, su. IV	cyt b6f complex	ATCG00730	X	VaGs33222; VaGs33251; VaGs33339; VaGs34489; <b>ALD84719.1</b>	X
PetG	cyt b6f complex	ATCG00600		VaGs24596; VaGs25230; VaGs25801; VaGs37142; ALD84707.1	
PetL	cyt b6f complex	ATCG00590		ALD84706.1	

(continued)

Table 3 Continued

Protein Name (Abbreviation)	Protein Complex/ Full Protein Name	Accession in <i>A. thaliana</i>	Identified in the Complexome in <i>A. thaliana</i>	Accessions in <i>V. album</i> (Accessions Identified in the <i>V. album</i> Complexome [Next Column] Are Indicated in Bold)	Identified in the Complexome in <i>V. album</i>
PetM	cyt b6f complex	AT2G26500	X	VaGs38214; VaGs38215	
PetN	cyt b6f complex	ATCG00210		VaGs02857; ALD84684.1	
ND complex					
NdhA	ND complex	ATCG01100	X		
NdhB.1	ND complex	AtCg00890	X		
NdhB.2	ND complex	ATCG01250			
NdhC	ND complex	ATCG00440	X		
NdhD	ND complex	ATCG01050	X		
NdhE	ND complex	ATCG01070	X		
NdhF	ND complex	ATCG01010	X		
NdhG	ND complex	ATCG01080			
NdhH	ND complex	ATCG01110	X		
NdhI	ND complex	ATCG01090	X		
NdhJ	ND complex	ATCG00420	X		
NdhK	ND complex	ATCG00430	X		
NdhL	ND complex	AT1G70760	X		
NdhM	ND complex	AT4G37925	X		
NdhN	ND complex	AT5G58260	X		
NdhO	ND complex	AT1G74880	X		
NdhS	ND complex	AT4G23890	X		
NdhT	ND complex	AT4G09350	X		
NdhU	ND complex	AT5G21430	X		
NdhV	ND complex	AT2G04039	X		
PnsB1	ND complex	AT1G15980	X		
PnsB2	ND complex	AT1G64770	X		
PnsB3	ND complex	AT3G16250	X		
PnsB4	ND complex	AT1G18730	X		
PnsB5	ND complex	AT5G43750	X		
PnsL1	ND complex	AT2G39470	X		
PnsL2	ND complex	AT1G14150	X		
PnsL3	ND complex	AT3G01440	X		
PnsL4	ND complex	AT4G39710	X		
PnsL5	ND complex	AT5G13120	X	<b>VaGs24270</b> ; VaGs25386; VaGs25641; VaGs25642; VaGs25643	X
atp-synthase					
F <sub>0</sub> part, AtpI	atp-synthase	ATCG00150	X	<b>VaGs09267</b> ; VaGs10676; ALD84679.1	X
F <sub>0</sub> part, AtpF	atp-synthase	ATCG00130	X	VaGs09265; VaGs09681; <b>VaGs10371</b> ; VaGs10673; <b>ALD84677.1</b>	X
F <sub>0</sub> part AtpG	atp-synthase	AT4G32260	X	VaGs10779; <b>VaGs11956</b> ; VaGs12030; VaGs12031; VaGs35192; VaGs35193	X
F <sub>0</sub> part, AtpH	atp-synthase	ATCG00140	X	VaGs09832; VaGs10218; <b>ALD84678.1</b>	X
F <sub>1</sub> part, AtpA	atp-synthase	ATCG00120	X	VaGs09205; VaGs09268; VaGs09285; VaGs09379; VaGs09387; VaGs09593; VaGs09762; VaGs09807; VaGs09808; VaGs09828; VaGs09979; VaGs10066; <b>ALD84676.1</b>	X
F <sub>1</sub> part AtpB	atp-synthase	ATCG00480	X	VaGs27798; VaGs27799; AAK72868.1; <b>ALD84695.1</b>	X
F <sub>1</sub> part AtpD	atp-synthase	AT4G09650	X	VaGs24411; VaGs24412; VaGs25113; VaGs25114; <b>VaGs26336</b> ; VaGs26369	X
F <sub>1</sub> part AtpE	atp-synthase	ATCG00470	X	<b>ALD84694.1</b>	X
F <sub>1</sub> part AtpC1	atp-synthase	AT4G04640	X	<b>VaGs28906</b> ; <b>VaGs38475</b> ; VaGs38476	X
F <sub>1</sub> part AtpC2	atp-synthase	AT1G15700			
plastocyanin 1	plastocyanin	AT1G76100		VaGs24175; VaGs25830	
plastocyanin 2	plastocyanin	AT1G20340	X	<b>VaGs24176</b> ; VaGs26370	X
ferredoxin					
ferredoxin C 1	ferredoxin	AT4G14890	X	VaGs36776; <b>VaGs36777</b>	X
ferredoxin C 2	ferredoxin	AT1G32550	X	VaGs24838; VaGs37132	
ferredoxin 1	ferredoxin	AT1G10960		<b>VaGs33762</b>	X
ferredoxin 2	ferredoxin	At1g60950		VaGs33666; VaGs34701; VaGs35670; VaGs36681	
ferredoxin 3	ferredoxin	AT2G27510		VaGs36222	
ferredoxin 4	ferredoxin	AT5G10000			
ferredoxin- NADP + OR					

(continued)

Table 3 Continued

Protein Name (Abbreviation)	Protein Complex/ Full Protein Name	Accession in <i>A. thaliana</i>	Identified in the Complexome in <i>A. thaliana</i>	Accessions in <i>V. album</i> (Accessions Identified in the <i>V. album</i> Complexome [Next Column] Are Indicated in Bold)	Identified in the Complexome in <i>V. album</i>
FNR1	ferredoxin-NADP + OR	AT5G66190	X	VaGs38832; VaGs38833	
FNR2	ferredoxin-NADP + OR	AT1G20020	X	<b>VaGs36566</b> ; <b>VaGs38836</b> ; VaGs38841	X
FNRL	ferredoxin-NADP + OR	AT1G15140	X		
others					
AOX1a	others	At3g22370		VaGs06230; VaGs06620; VaGs06621; VaGs06681; <b>VaGs06791</b> ; UER43485.1	X
AOX2	others	At5g64210			
PGR5	others	AT2G05620	X	<b>VaGs34929</b> ; VaGs36763	X
PGRL1A	others	AT4G22890	X	<b>VaGs13367</b> ; VaGs13368; VaGs14105; VaGs14106; VaGs14107; VaGs14108; VaGs14110	X
PGRL1B	others	AT4G11960	X		
PPOX	others	AT4G01690	X	<b>VaGs12774</b> ; VaGs13625	X
PTOX	others	AT4G22260	X		
STN7	others	AT1G68830	X	<b>VaGs18404</b>	X
STN8	others	AT5G01920	X	<b>VaGs19550</b> ; VaGs19552	X

Notes: List of proteins forming part of the two photosystems, the cytochrome  $b_6f$  complex, the chloroplast ATP synthase complex, the NDH complex, and further proteins involved in thylakoid electron transfer processes and their regulation. The known proteins from *A. thaliana* (Shikanai, 2016; Berger et al., 2020; Malone et al., 2021) were used to probe the *V. album* gene space database (<https://viscumsalbus.pflanzenproteomik.de/>; Schröder et al., 2022a). Accessions are either from Araport (<https://www.arabidopsis.org/>), The *V. album* gene space database (<https://viscumsalbus.pflanzenproteomik.de/>) or NCBI (<https://www.ncbi.nlm.nih.gov/>).

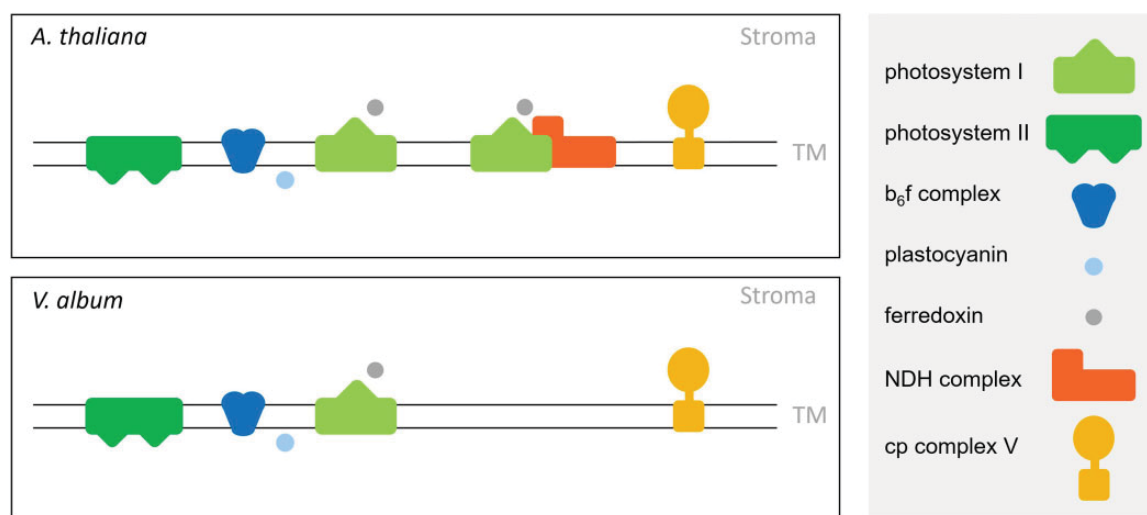


**Figure 8** Chloroplast protein complexes involved in photosynthesis in *A. thaliana* and *V. album*. Yellow, chloroplast (cp) complex V; orange, cp Complex I (NDH complex); dark blue, cytochrome  $b_6f$  complex; light green, Photosystem I; dark green, Photosystem II; light blue, plastocyanin; grey, ferredoxin. TM, thylakoid membrane.

*album* way of life seems to be characterized by a sophisticated system of controlled deregulation.

## Materials and methods

### Plant material

European Mistletoe (*V. album*) grown on an apple (*Malus domestica*) tree on our university campus (Leibniz Universität Hannover, Herrenhäuserstr. 2 in Hannover/Germany) was harvested in spring 2019. During the period of harvesting, the apple tree started to bloom but still was without leaves. The thylakoid preparation for the complexome profiling experiment was performed on April 25, 2019. Leaves were harvested at 9 am. Local weather data for

Herrenhäuser Str. 2/Hannover in April 2019 are provided by the Institute of Meteorology of Leibniz Universität Hannover at [https://www1.muk.uni-hannover.de/hp-design2020/wetter\\_archiv\\_frame.html](https://www1.muk.uni-hannover.de/hp-design2020/wetter_archiv_frame.html). Leaves for electron microscopy analyses were harvested at 9 am. Arabidopsis (*A. thaliana*; ecotype Columbia 0) was cultivated in parallel in a phyto chamber under long-day conditions (16-h light/8-h dark; 22°C). PAR intensity was 110  $\mu\text{mol s}^{-1} \text{m}^{-2}$ ; light source: Philips F25T8/TL841 lamps. Plants were harvested 4 weeks after germination. Leaves were used for experimental analyses.

### Transmission electron microscopy

Transmission electron microscopy of *V. album* leaf cells was carried out as described previously (Senkler et al., 2018). In



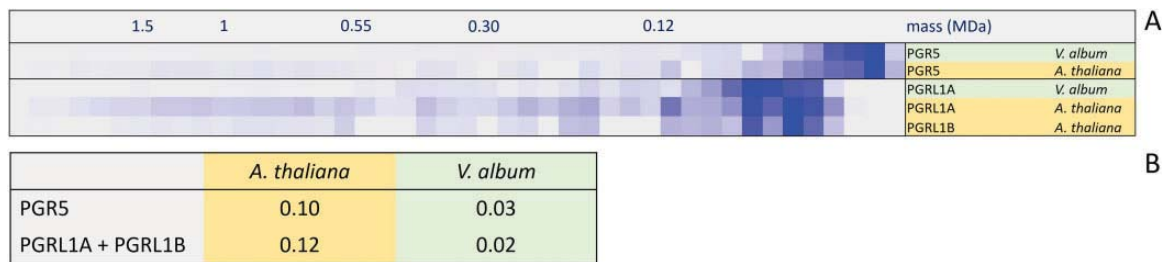


**Figure 9** Complexome profiling results for PGR5- and PGR5-like proteins (PGRL1) of *V. album* and *A. thaliana*. A, Relative abundances of the proteins along the 1D BN gel lane used for complexome profiling. The molecular masses of standard protein complexes (in MDa) are given above the abundance profiles. B, Summed up iBAQ values of the PGR5 and PGRL1 proteins in relation to the total iBAQ values of the corresponding thylakoid fraction (percent of total protein).

brief: Freshly harvested *V. album* leaves were cut into 1 mm pieces. The pieces were fixed in 150 mM HEPES, pH 7.35, containing 1.5% [v/v] formaldehyde and 1.5% glutaraldehyde [v/v] and washed with water. Afterward, the samples were incubated for 2 h in 1% [w/v] OsO<sub>4</sub> solution containing 1.5% [w/v] hexacyanoferrat II, subsequently washed with water and stored in 1% [w/v] aqueous uranyl acetate solution overnight. On the next day, the samples were washed again with water, dehydrated in acetone, and finally embedded in Low Viscosity Resin (Agar Scientific, Essex, UK). Ultrathin sections (60 nm) were mounted on formvar-coated copper grids and poststained with uranyl acetate and lead citrate (Reynolds, 1963). Samples were examined using a Morgagni Transmission Electron Microscope (FEI).

### Isolation of thylakoid membranes

*Viscum album* and *A. thaliana* leaves (30 g each) were used as starting material for the preparation of thylakoid membranes. All the following steps were carried out at 4°C. Homogenization of leaves was performed in 400 mL chilled homogenization buffer (50 mM HEPES, 2 mM EDTA, 1 mM MgCl<sub>2</sub>, 5 mM sodium ascorbate, 330 mM sorbitol, 0.5% [w/v] BSA, pH 8.0 [KOH]) using a Waring blender (one pulse of 3 s at high speed, two pulses of 3 s at low speed; breaks of 30 s in between the pulses). Resulting homogenates were filtered through 2 layers of Miracloth. Filtrates were centrifuged at 300 g at 4°C for 5 min. Supernatants were removed and the pellets carefully resuspended in 2 mL of homogenization buffer using a brush. Subsequently, 10 mL chilled Percoll medium (50 mM HEPES, 330 mM sorbitol, 35% [v/v] Percoll, pH 8.0 [KOH]) was transferred into tubes for gradient centrifugation. Two to three milliliter of the resuspended samples were carefully loaded on top of the Percoll medium, respectively. Centrifugation took place at 90.000 g for 20 min at 4°C. The upper (thylakoid) band was transferred to new tubes with sorbitol-HEPES (SH) buffer (50 mM HEPES, 330 mM sorbitol, pH 8.0 [KOH]). Washing steps (at least 4) were performed in SH buffer at 1.000 g for 5 min. Supernatants were discarded after the centrifugations, respectively, and pellets were carefully dissolved in SH buffer and collected. After the last centrifugation step, pellets were dissolved in 2 mL SH buffer and divided into aliquots of 200 µL, which

were either directly used for biochemical analyses (see below) or shock frozen in liquid nitrogen and stored at –80°C.

### Gel electrophoresis procedures

Isolated thylakoid fractions (200 µL) were centrifuged and pellets resuspended in 90 µL solubilization buffer DDM (25 mM BisTris/HCl pH 7.0, 20% [v/v] glycerol, 3% [w/v] dodecyl maltoside [DDM]). For digitonin solubilization, the pellets were resuspended in solubilization buffer digitonin (30 mM HEPES/HCl, pH 7.4, 150 mM potassium acetate, 10% [v/v] glycerol, 5% [w/v] digitonin). Further sample preparation and performance of 1D BN-PAGE and 2D BN/SDS-PAGE was carried out as described previously (Wittig et al., 2006). Gels were stained using the Coomassie colloidal staining procedure (Neuhoff et al., 1988). To increase staining sensitivity, selected gels were silver-stained using a modified version of a protocol published previously (Heukeshoven and Dernick, 1988). In short, gels were fixed in fixing solution (50% [v/v] ethanol, 10% [v/v] acetic acid) for 2 h. Gels were next treated with incubation solution (30% [v/v] ethanol, 0.2% [w/v] sodiumthiosulfate, 0.8 M NaAc) for 2 h and subsequently washed 3 times with ddH<sub>2</sub>O. Binding of silver to proteins was achieved by incubating gels with silver nitrate solution (0.1% [w/v] AgNO<sub>3</sub>) for 30 min. Gels were rinsed briefly with ddH<sub>2</sub>O and afterward washed thoroughly with a washing solution (2.5% [w/v] Na<sub>2</sub>CO<sub>3</sub>) for 1 min. Protein visualization took place in a fresh box using developing solution (2.5% [w/v] Na<sub>2</sub>CO<sub>3</sub>, 0.01% [v/v] formaldehyde). The time of development may differ and depends on the amount of protein separated within a gel (on average 10–30 min). As soon as the desired staining result has been achieved, the development process is stopped by transferring gels into stopping solution (0.05 EDTA).

### Protein identifications after gel electrophoresis

Proteins of interest were cut from the 2D gels and identified by MS as described previously (Senkler et al., 2018). For *A. thaliana*, MS data were evaluated using the *A. thaliana* Araport11 protein database (<https://www.arabidopsis.org/>).

### Complexome profiling

Complexome profiling is based on the separation of a complex protein sample under native conditions and the

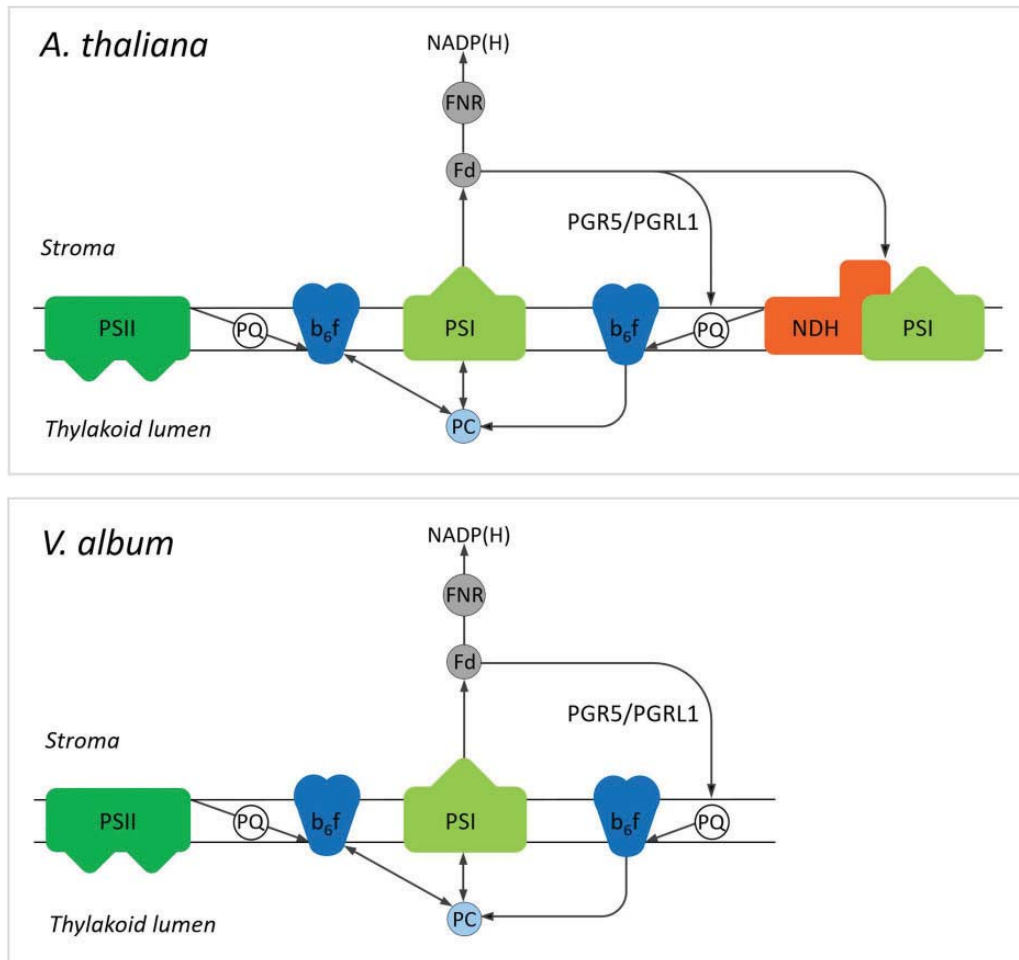


**Figure 10** Model of the linear and CET pathways in *V. album* and *A. thaliana*. In LET, electrons originate from Photosystem II (PSII). They are transferred via plastoquinol (PQ) to the cytochrome  $b_6f$  complex ( $b_6f$ ) and via plastocyanin (PC) from the cytochrome  $b_6f$  complex to Photosystem I (PSI). LET terminates by electron transfer from PSI to ferredoxin (Fd) and from Fd to NADP<sup>+</sup>, which is reduced to NADPH (the latter step is catalyzed by ferredoxin-NADP<sup>+</sup> reductase (FNR)). In contrast, in CET, electrons originate from Photosystem I. They are transferred onto Fd, but afterward not further transferred to NADP<sup>+</sup>, but to the cytochrome  $b_6f$  complex. In *A. thaliana*, this electron transfer requires either the PGR5/PGRL1 proteins or the NDH complex, which forms a supercomplex with the Photosystem I. CET is completed by transfer of electrons from the cytochrome  $b_6f$  complex via PC back to PSI. In *V. album*, electron transport from Fd to  $b_6f$  depends entirely on PGR5/PGRL1, since the NDH complex is absent. The colors of the involved components correspond to those introduced in Figure 2. Note that further CET pathways were suggested to occur but so far could not be precisely defined (Nawrocki et al., 2019). The figure is based on Figure 1 in Johnson (2011).

subsequent systematic analysis of several gel fractions along the native separation matrix by label-free quantitative shotgun proteomics (Arnold and Braun, 2022). We performed 1D BN-PAGE for protein separation and used 44 fractions for proteome analyses, respectively. The procedure has been described previously (Schröder et al., 2022b). We used an Ultimate 3000 UPLC/Q Exactive Orbitrap mass spectrometer (Thermo Fisher Scientific, Dreieich, Germany) for label-free quantitative shotgun proteomics. For MS data evaluation the Araport11 protein database (<https://www.arabidopsis.org/>) was used for *A. thaliana* and the *V. album* gene space (VaGs) database at <https://viscumalbum.pflanzenproteomik.de/>, Schröder et al., 2022a) for *V. album*. The following parameters were used for MS data analyses: Digestions mode: Specific; Enzyme: Trypsin/P; Maximum missed cleavage sites: 2; Variable modifications: Oxidation (M) and Acetyl (Protein N-term); Maximum number of modifications

per peptide: 5. Global parameters were set to: minimal peptide length: 7; maximum peptide mass: 4,600 Da; fixed modification: Carbamidomethyl (C). The peptide-to-spectrum match and the false discovery rates were set to 1% for protein identification. The default value of 1 was used for minimum number of peptides, razor peptides, and unique peptides (0) of the protein group identification. iBAQ values (Schwanhäusser et al., 2011) were determined for all proteins in all fractions and used for the calculation of abundance profiles of proteins along the 1D BN gel dimension.

### Generation of ComplexomeMaps

Normalized (max) intensity profiles for all proteins along the two BN gel lanes were converted into heatmaps (Schröder et al., 2022b). In a final step, abundance profiles were aligned based on hierarchical clustering using the Nova software tool (Giese et al., 2015). Complexome profiling data were

displayed in the form of ComplexomeMaps (<https://complexomemap.de/>) as described previously (Senkler et al., 2018). The *V. album* thylakoid ComplexomeMap is accessible at [https://complexomemap.de/va\\_chloroplasts](https://complexomemap.de/va_chloroplasts) and the *A. thaliana* thylakoid ComplexomeMaps at [https://complexomemap.de/at\\_chloroplasts](https://complexomemap.de/at_chloroplasts).

## Accession numbers

Sequence data of this article can be found in the *V. album* gene space (VaGs) database (Schröder et al., 2022a) at <https://viscumalbum.pflanzenproteomik.de/>.

## Data availability Statement

Primary data of the complexome profiling experiments can be accessed at the ComplexomeMap portal at [https://complexomemap.de/va\\_chloroplasts](https://complexomemap.de/va_chloroplasts) (*V. album*) and [https://complexomemap.de/at\\_chloroplasts](https://complexomemap.de/at_chloroplasts) (*A. thaliana*).

Primary data of the complexome profiling experiments also can be accessed in [Supplemental data Sets S1 and S2](#).

The mass spectrometry proteomics data have been deposited to the ProteomeXchange Consortium via the PRIDE (Perez-Riverol et al., 2022) partner repository with the dataset identifier PXD035825 and PXD035871.

## Supplemental data

The following materials are available in the online version of this article.

**Supplemental Figure S1.** Analyses of the Photosystem I-NDH supercomplex from *A. thaliana*.

**Supplemental Figure S2.** Two-dimensional analysis of thylakoid fractions from *V. album* and *A. thaliana* by BN/SDS-PAGE in combination with silver staining.

**Supplemental Figure S3.** Two-dimensional analysis of digitonin-treated thylakoid fractions from *V. album* and *A. thaliana* by 2D BN/SDS-PAGE.

**Supplemental Figure S4.** BN gel lanes of separated thylakoid protein complexes from *V. album* and *A. thaliana* used for complexome profiling.

**Supplemental Figure S5.** Number of proteins identified in the complexome profiling fractions of *V. album* from the database used for data evaluation.

**Supplemental Figure S6.** Heatmap of normalized (max) abundance profiles of thylakoid proteins from *V. album* leaves.

**Supplemental Data Set S1.** Heatmap of intensity profiles of the proteins included in the complexome dataset for thylakoids of *V. album*.

**Supplemental Data Set S2.** Heatmap of intensity profiles of the proteins included in the complexome dataset for thylakoids of *A. thaliana*.

## Acknowledgments

We thank Marianne Langer, Jennifer Senkler, and Holger Eubel for support with sample preparation for MS and MS analyses. We are grateful to Michael Senkler for IT support and to Noah Ditz for critically reading the manuscript.

## Funding

This research has been supported by the Deutsche Forschungsgemeinschaft, grant BR 1829/16-1, to HPB.

*Conflict of interest statement.* The authors declare no conflict of interest.

## References

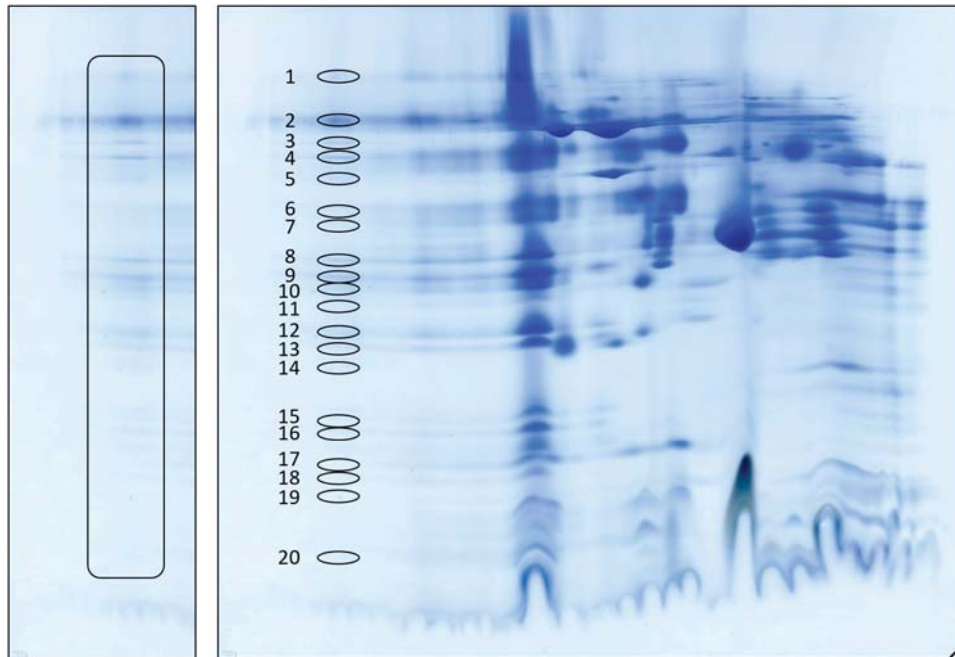
- Arike L, Valgepea K, Peil L, Nahku R, Adamberg K, Vilu R (2012) Comparison and applications of label-free absolute proteome quantification methods on *Escherichia coli*. *J Proteomics* **75**: 5437–5448
- Arnold S, Braun HP (2022) The complexome profiling approach for direct biochemical analysis of multiprotein assemblies. *Biochim Biophys Acta Bioenerg* **1863**: 148522
- Becker H (1986) Botany of European mistletoe (*Viscum album* L.). *Oncology* **43** Suppl 1: 2–7
- Behrens C, Blume C, Senkler M, Eubel H, Peterhänsel C, Braun HP (2013) The ‘protein complex proteome’ of chloroplasts in *Arabidopsis thaliana*. *J Proteomics* **91**: 73–83
- Berger N, Vignols F, Touraine B, Taupin-Broggini M, Rofidal V, Demolombe V, Santoni V, Rouhier N, Gaymard F, Dubos C (2020) A global proteomic approach sheds new light on potential iron-sulfur client proteins of the chloroplastic maturation factor NFU3. *Int J Mol Sci* **21**: 8121
- Boyes DC, Zayed AM, Ascenzi R, McCaskill AJ, Hoffman NE, Davis KR, Görlach J (2001) Growth stage-based phenotypic analysis of *Arabidopsis*: a model for high throughput functional genomics in plants. *Plant Cell* **13**: 1499–1510
- Busch KB (2018) Respiration: life without Complex I. *Curr Biol* **28**: R616–R618
- da Fonseca-Pereira P, Silva WB, Araújo WL, Nunes-Nesi A (2018) How does European mistletoe survive without Complex I? *Trends Plant Sci* **23**: 847–850
- DalCorso G, Pesaresi P, Masiero S, Aseeva E, Schünemann D, Finazzi G, Joliot P, Barbato R, Leister D (2008) A complex containing PGRL1 and PGR5 is involved in the switch between linear and cyclic electron flow in *Arabidopsis*. *Cell* **132**: 273–285
- Edvardsson A, Eshaghi S, Vener AV, Andersson B (2003) The major peptidyl-prolyl isomerase activity in thylakoid lumen of plant chloroplasts belongs to a novel cyclophilin TLP20. *FEBS Lett* **542**: 137–141
- Escher P, Eiblmeier M, Hetzger I, Rennenberg H (2004) Seasonal and spatial variation of carbohydrates in mistletoes (*Viscum album*) and the xylem sap of its hosts (*Populus x euamericana* and *Abies alba*). *Physiol Plant* **120**: 212–219
- Giese H, Ackermann J, Heide H, Bleier L, Dröse S, Wittig I, Brandt U, Koch I (2015) NOVA: a software to analyze complexome profiling data. *Bioinformatics* **31**: 440–441
- Hertle AP, Blunder T, Wunder T, Pesaresi P, Pribil M, Armbruster U, Leister D (2013) PGRL1 is the elusive ferredoxin-plastoquinone reductase in photosynthetic cyclic electron flow. *Mol Cell* **49**: 511–523
- Heukeshoven J, Dernick R (1988) Improved silver staining procedure for fast staining in PhastSystem Development Unit. I. Staining of sodium dodecyl sulfate gels. *Electrophoresis* **9**: 28–32
- Hooper CM, Tanz SK, Castleden IR, Vacher MA, Small ID, Millar AH (2014) SUBAcon: a consensus algorithm for unifying the sub-cellular localization data of the *Arabidopsis* proteome. *Bioinformatics* **30**: 3356–3364
- Hudák J, Lux A (1986) Chloroplast ultrastructure of semiparasitic *Viscum album* L. *Photosynthetica* **20**: 223–224
- Jäger T, Holandino C, Melo MNO, Peñaloza EMC, Oliveira AP, Garrett R, Glauser G, Grazi M, Ramm H, Urech K, et al. (2021)

- Metabolomics by UHPLC-Q-TOF Reveals Host Tree-Dependent Phytochemical Variation in *Viscum album* L. *Plants (Basel)* **10**: 1726
- Järvi S, Suorsa M, Paakkarinen V, Aro EM (2011) Optimized native gel systems for separation of thylakoid protein complexes: novel super- and mega-complexes. *Biochem J* **439**: 207–214
- Johnson GN (2011) Physiology of PSI cyclic electron transport in higher plants. *Biochim Biophys Acta* **1807**: 384–389
- Klusch N, Senkler J, Yildiz Ö, Kühlbrandt W, Braun HP (2021) A ferredoxin bridge connects the two arms of plant mitochondrial complex I. *Plant Cell* **33**: 2072–2091
- Kanazawa A, Ostendorf E, Kohzuma K, Hoh D, Strand DD, Sato-Cruz M, Savage L, Cruz JA, Fisher N, Froehlich JE, et al. (2017) Chloroplast ATP synthase modulation of the thylakoid proton motive force: implications for Photosystem I and Photosystem II photoprotection. *Front Plant Sci* **8**: 719
- Lin CS, Chen JJW, Chiu CC, Hsiao HCW, Yang CJ, Jin XH, Leebens-Mack J, de Pamphilis CW, Huang YT, Yang LH, et al. (2017) Concomitant loss of NDH complex-related genes within chloroplast and nuclear genomes in some orchids. *Plant J* **90**: 994–1006
- Longoni FP, Goldschmidt-Clermont M (2021) Thylakoid protein phosphorylation in chloroplasts. *Plant Cell Physiol* **62**: 1094–1107
- Luther P, Becker H (1987) Die Mistel. Botanik, Lektine, medizinische Anwendung. Springer-Verlag Berlin Heidelberg. DOI: 10.1007/978-3-642-71257-9
- Macleán AE, Hertle AP, Ligas J, Bock R, Balk J, Meyer EH (2018) Absence of Complex I is associated with diminished respiratory chain function in European mistletoe. *Curr Biol* **28**: 1614–1619.e3
- Ma M, Liu Y, Bai C, Yang Y, Sun Z, Liu X, Zhang S, Han X, Yong JWH (2021) The physiological functionality of PGR5/PGRL1-dependent cyclic electron transport in sustaining photosynthesis. *Front Plant Sci* **12**: 702196
- Malone LA, Proctor MS, Hitchcock A, Hunter CN, Johnson MP (2021) Cytochrome  $b_6/f$  - orchestrator of photosynthetic electron transfer. *Biochim Biophys Acta Bioenerg* **1862**: 148380
- Møller IM, Rasmusson AG, Van Aken O (2021) Plant mitochondria - past, present and future. *Plant J* **108**: 912–959
- Munekage Y, Hojo M, Meurer J, Endo T, Tasaka M, Shikanai T (2002) PGR5 is involved in cyclic electron flow around photosystem I and is essential for photoprotection in Arabidopsis. *Cell* **110**: 361–371
- Nawrocki WJ, Bailleul B, Picot D, Cardol P, Rappaport F, Wollman FA, Joliot P (2019) The mechanism of cyclic electron flow. *Biochim Biophys Acta Bioenerg* **1860**: 433–438
- Neuhoff V, Arold N, Taube D, Ehrhardt W (1988). Improved staining of proteins in polyacrylamide gels including isoelectric focusing gels with clear background at nanogram sensitivity using Coomassie Brilliant Blue G-250 and R-250. *Electrophoresis* **6**: 255–262
- Novák P, Guignard MS, Neumann P, Kelly LJ, Mlinarec J, Koblížková A, Dodsworth S, Kovařík A, Pellicer J, Wang W, et al. (2020) Repeat-sequence turnover shifts fundamentally in species with large genomes. *Nat Plants* **6**: 1325–1329
- Peltier G, Aro EM, Shikanai T (2016) NDH-1 and NDH-2 plastoquinone reductases in oxygenic photosynthesis. *Annu Rev Plant Biol* **67**: 55–80
- Peng L, Shimizu H, Shikanai T (2008) The chloroplast NAD(P)H dehydrogenase complex interacts with photosystem I in Arabidopsis. *J Biol Chem* **283**: 34873–34879
- Perez-Riverol Y, Bai J, Bandla C, Hewapathirana S, García-Seisdedos D, Kamatchinathan S, Kundu D, Prakash A, Frericks-Zipper A, Eisenacher M, et al. (2022). The PRIDE database resources in 2022: a Hub for mass spectrometry-based proteomics evidences. *Nucleic Acids Res* **50**: D543–D552 (PubMed ID: 34723319)
- Petersen G, Cuenca A, Møller IM, Seberg O (2015a) Massive gene loss in mistletoe (*Viscum*, Viscaceae) mitochondria. *Sci Rep* **5**: 17588
- Petersen G, Cuenca A, Seberg O (2015b) Plastome evolution in hemiparasitic mistletoes. *Genome Biol Evol* **7**: 2520–2532
- Petersen G, Anderson B, Braun HP, Meyer EH, Møller IM (2020) Mitochondria in parasitic plants. *Mitochondrion* **52**: 173–182
- Petersen G, Shyama Prasad Rao R, Anderson B, Zervas A, Seberg O, Rasmusson AG, Max Møller I (2022) Genes from oxidative phosphorylation complexes II-V and two dual-function subunits of complex I are transcribed in *Viscum album* despite absence of the entire mitochondrial holo-complex I. *Mitochondrion* **62**: 1–12
- Reynolds, E. S. (1963). The use of lead citrate at high pH as an electron-opaque stain in electron microscopy. *J Cell Biol* **17**: 208–212
- Sabater B (2021) On the edge of dispensability, the chloroplast NDH genes. *Int J Mol Sci* **22**: 12505
- Scherl P, Braun HP (2014) Respiratory electron transfer pathways in plant mitochondria. *Front Plant Sci* **5**: 163
- Schöttler MA, Tóth SZ (2014) Photosynthetic complex stoichiometry dynamics in higher plants: environmental acclimation and photosynthetic flux control. *Front Plant Sci* **5**: 188
- Schröder L, Hohnjec N, Senkler M, Senkler J, Küster H, Braun HP (2022a) The gene space of European mistletoe (*Viscum album*). *Plant J* **109**: 278–294
- Schröder L, Eubel H, Braun HP (2022b) Complexome profiling of plant mitochondrial fractions. *Methods Mol Biol* **2363**: 101–110
- Schuller JM, Birrell JA, Tanaka H, Konuma T, Wulffhorst H, Cox N, Schuller SK, Thiemann J, Lubitz W, Sétif P, et al. (2019) Structural adaptations of photosynthetic complex I enable ferredoxin-dependent electron transfer. *Science* **363**: 257–260
- Schwanhäusser B, Busse D, Li N, Dittmar G, Schuchhardt J, Wolf J, Chen W, Selbach M (2011) Global quantification of mammalian gene expression control. *Nature* **473**: 337–342
- Senkler J, Rugen N, Eubel H, Hegermann J, Braun HP (2018) Absence of Complex I implicates rearrangement of the respiratory chain in European mistletoe. *Curr Biol* **28**: 1606–1613.e4
- Shen L, Tang K, Wang W, Wang C, Wu H, Mao Z, An S, Chang S, Kuang T, Shen JR, et al. (2022) Architecture of the chloroplast PSI-NDH supercomplex in *Hordeum vulgare*. *Nature* **601**: 649–654
- Shapiguzov A, Edvardsson A, Vener AV (2006) Profound redox sensitivity of peptidyl-prolyl isomerase activity in Arabidopsis thylakoid lumen. *FEBS Lett* **580**: 3671–3676
- Shikanai T, Endo T, Hashimoto T, Yamada Y, Asada K, Yokota A (1998) Directed disruption of the tobacco *ndhB* gene impairs cyclic electron flow around photosystem I. *Proc Natl Acad Sci USA* **95**: 9705–9709
- Shikanai T (2014) Central role of cyclic electron transport around photosystem I in the regulation of photosynthesis. *Curr Opin Biotechnol* **26**: 25–30
- Shikanai T (2016) Chloroplast NDH: a different enzyme with a structure similar to that of respiratory NADH dehydrogenase. *Biochim Biophys Acta* **1857**: 1015–1022
- Shikanai T, Aro EM (2016) Evolution of photosynthetic NDH-1: structure and physiological function. In W Cramer, T Kallas, eds, *Cytochrome Complexes: Evolution, Structures, Energy Transduction, and Signaling. Advances in Photosynthesis and Respiration (Including Bioenergy and Related Processes)*, Vol **41**. Springer, Dordrecht, pp 51–70
- Shimakawa G, Miyake C (2018) Oxidation of P700 ensures robust photosynthesis. *Front Plant Sci* **9**: 1617
- Silva SR, Michael TP, Meer EJ, Pinheiro DG, Varani AM, Miranda VFO (2018) Comparative genomic analysis of Genlisea (corkscrew plants-Lentibulariaceae) chloroplast genomes reveals an increasing loss of the *ndh* genes. *PLoS One* **13**: e0190321
- Sirpiö S, Holmström M, Battchikova N, Aro EM (2009) AtCYP20-2 is an auxiliary protein of the chloroplast NAD(P)H dehydrogenase complex. *FEBS Lett* **583**: 2355–2358
- Skippington E, Barkman TJ, Rice DW, Palmer JD (2015) Miniaturized mitogenome of the parasitic plant *Viscum*

- scurruloideum is extremely divergent and dynamic and has lost all nad genes. *Proc Natl Acad Sci USA* **112**: E3515–E3524
- Skippington E, Barkman TJ, Rice DW, Palmer JD** (2017) Comparative mitogenomics indicates respiratory competence in parasitic *Viscum* despite loss of complex I and extreme sequence divergence, and reveals horizontal gene transfer and remarkable variation in genome size. *BMC Plant Biol* **17**: 49
- Trinh MDL, Masuda S** (2022) Chloroplast pH homeostasis for the regulation of photosynthesis. *Front Plant Sci* **13**: 919896
- Tuquet C, Sallé G** (1996) Characteristics of chloroplasts isolated from two mistletoes originating from temperate (*Viscum album*) and tropical (*Tapinanthus dodoneifolius*) areas. *Plant Physiol Biochem* **34**: 283–292
- Urech K, Jäggy C, Schaller G, Baumgartner S** (2004) Giftsubstanzbildung und Wachstumsdynamik der Mistel (*Viscum album* L.) im Jahreslauf. *Mistilteinn* **5**: 20–35. <https://www.vfk.ch/informationen/broschueren/mistilteinn/>
- van Strien J, Haupt A, Schulte U, Braun HP, Cabrera-Orefice A, Choudhary JS, Evers F, Fernandez-Vizarra E, Guerrero-Castillo S, Kooij TWA, et al.** (2021) CEDAR, an online resource for the reporting and exploration of complexome profiling data. *Biochim Biophys Acta Bioenerg* **1862**: 148411
- von Tubeuf KF** (1922) *Monographie der Mistel*. R. Oldenbourg Verlag München und Berlin
- Wakasugi T, Tsudzuki J, Ito S, Nakashima K, Tsudzuki T, Sugiura M** (1994) Loss of all ndh genes as determined by sequencing the entire chloroplast genome of the black pine *Pinus thunbergii*. *Proc Natl Acad Sci USA* **91**: 9794–9798
- Wicke S, Schneeweiss GM, dePamphilis CW, Müller KF, Quandt D** (2011) The evolution of the plastid chromosome in land plants: gene content, gene order, gene function. *Plant Mol Biol* **76**: 273–297
- Wittig I, Braun HP, Schägger H** (2006). Blue-native PAGE. *Nat Protoc* **1**: 418–428
- Wittig I, Malacarne PF** (2021) Complexome profiling: assembly and remodeling of protein complexes. *Int J Mol Sci* **22**: 7809
- Yamamoto H, Peng L, Fukao Y, Shikanai T** (2011) An Src homology 3 domain-like fold protein forms a ferredoxin binding site for the chloroplast NADH dehydrogenase-like complex in Arabidopsis. *Plant Cell* **23**: 1480–1493
- Zervas A, Petersen G, Seberg O** (2019) Mitochondrial genome evolution in parasitic plants. *BMC Evol Biol* **19**: 87
- Zonneveld BJM** (2010) New record holders for maximum genome size in eudicots and monocots. *J Bot* **527357**. <https://doi.org/10.1155/2010/527357>
- Zuber D** (2004) *Biological flora of Central Europe: Viscum album L.* *Flora* **199**: 181–203

## Supplemental Material

Supp. Fig. S1

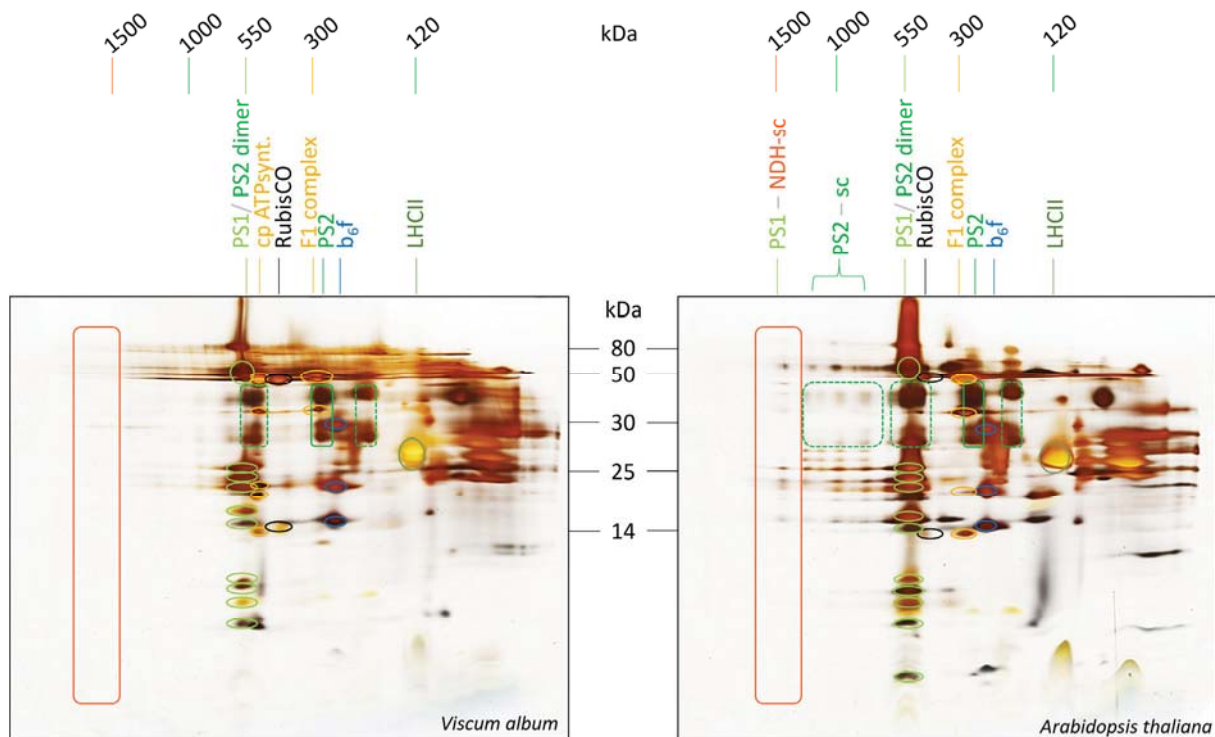


ID	Accession	Name	MW [kDa]	Mascot Score
1		not identified		
2	ATCG00350.1	PSAA	83.2	248
2	ATCG00340.1	PSAB	82.4	45
2	ATCG01010.1	NDHF	85.2	41
3	AT1G15980.1	PNSB1	51.0	146
4	ATCG01110.1	NDHH	45.5	173
5		not identified		
6	ATCG00270.1	PSBD	39.5	51
7		not identified		
8	AT1G61520.1	LHCA3	29.2	86
8	AT1G19150.1	LHCA6	29.9	50
8	AT3G01810.1	EEIG1/EHBP1 protein amino-terminal domain protein	101.6	35
9	AT1G45474.1	LHCA5	27.8	113
9	AT1G03130.1	PSAD-2	22.3	105
10	AT1G03130.1	PSAD-2	22.3	162
10	AT2G39470.1	PNSL1	26.9	46
11	AT2G39470.1	PNSL1	26.9	153
12	AT1G31330.1	PSAF	24.2	236
12	AT4G12800.1	PSAL	23.0	134
12	AT3G01440.1	PNSL3	24.8	87
13		not identified		
14	AT1G14150.1	PNSL2	22.1	114
15	AT1G52230.1	PSAH2	15.3	66
15	AT4G11400.1	ARID/BRIGHT DNA-binding domain	65.6	31
16	AT1G55670.1	PSAG	17.1	157
16	ATCG01070.1	NDHE	11.3	43
17		not identified		
18	AT1G30380.1	PSAK	13.2	40
19		not identified		
20		not identified		

### Supp. Figure S1: Analyses of the photosystem I-NDH supercomplex from *A. thaliana*.

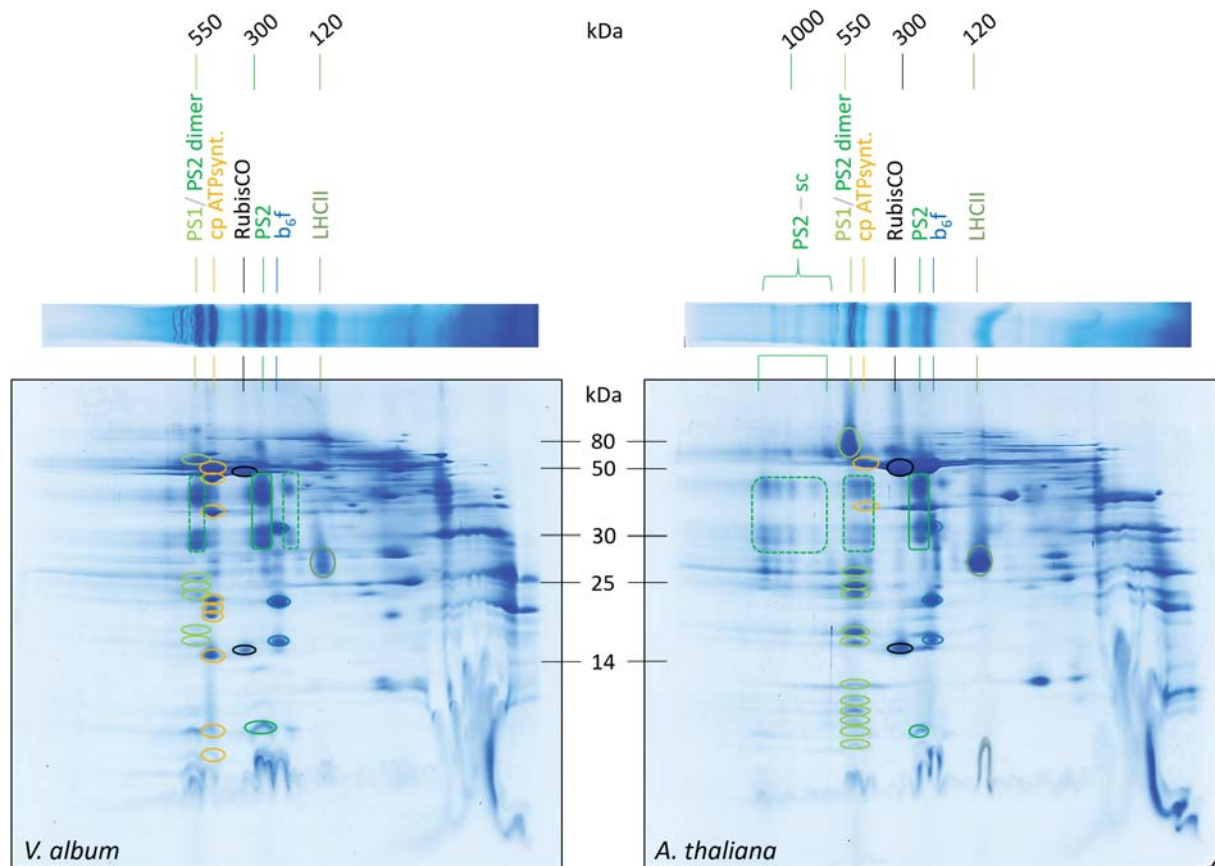
Thylakoid membranes were solubilized using DDM and protein complexes resolved by 2D Blue native PAGE (the gel image is the same as shown in Fig. 3) The subunits of the PS I-NDH supercomplex were analyzed by mass spectrometry. Green: subunits of photosystem I; orange: subunits of the NDH complex.

Supp. Fig. S2



**Supp. Figure S2: Two-dimensional analysis of thylakoid fractions from *V. album* and *A. thaliana* by Blue native / SDS PAGE in combination with silver staining.** Thylakoid membranes were solubilized using DDM. Molecular masses of standard protein complexes are given above the gels (in kDa); molecular masses of monomeric standard proteins in between the 2D gels (in kDa). The identities of protein complexes are indicated above the gels (identifications based on reference gels; Järvi et al. 2011). Designations: PS1: photosystem I; PS2: photosystem II; NDH: chloroplast complex I (chloroplast NADH dehydrogenase-like complex); cp ATP Synthase: chloroplast ATP synthase; RubisCO: Ribulose-1,5-bisphosphat-carboxylase/-oxygenase; F<sub>1</sub> complex: F<sub>1</sub> part of the cp ATP synthase; b<sub>6</sub>f: cytochrome b<sub>6</sub>f complex; LHClI: light harvesting complex II; sc: supercomplex. PS1-NDH-sc: supercomplex of NDH and two copies of monomeric PS1. PS2-sc: photosystem II supercomplexes.

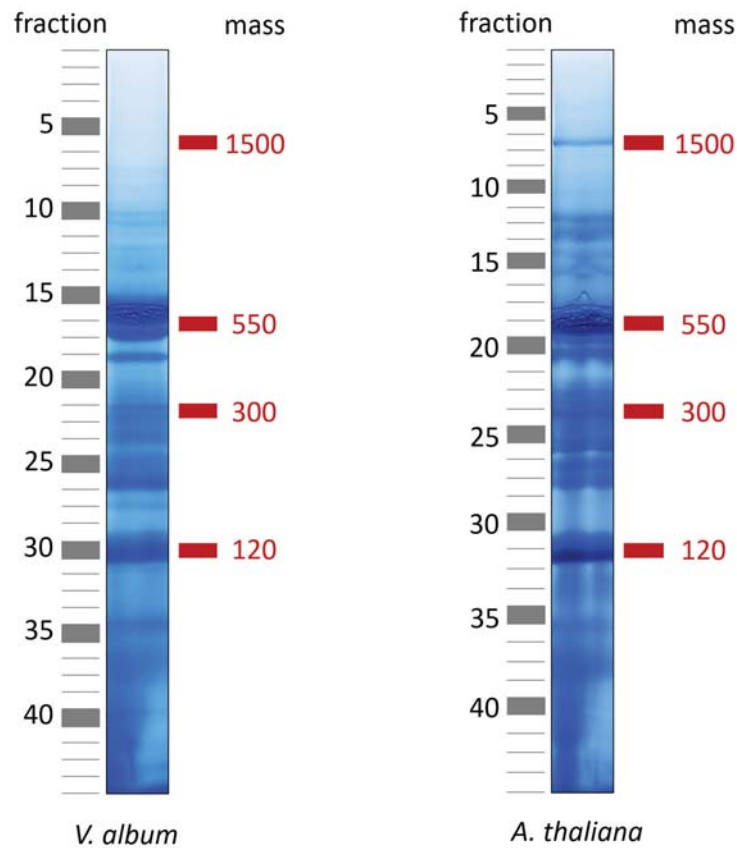
Supp. Fig. S3



**Supp. Figure S3: Two-dimensional analysis of digitonin-treated thylakoid fractions from *V. album* and *A. thaliana* by 2D Blue native / SDS PAGE.** Thylakoid membranes were solubilized using 5% digitonin. The gels were Coomassie-stained. Molecular masses of standard protein complexes are given above the gels (in kDa); molecular masses of monomeric standard proteins in between two 2D gels (in kDa). The identities of protein complexes are indicated above the gels (identifications based on reference gels; [Järvi et al. 2011](#)). Designations: PS1: photosystem I; PS2: photosystem II; cp ATP Synthase: chloroplast ATP synthase; RubisCO: Ribulose-1,5-bisphosphat-carboxylase/-oxygenase; F<sub>1</sub> complex: F<sub>1</sub> part of the cp ATP synthase; b<sub>6f</sub>: cytochrome b<sub>6f</sub> complex; LHCII: light harvesting complex II; sc: supercomplex; PS2-sc: photosystem II supercomplexes.

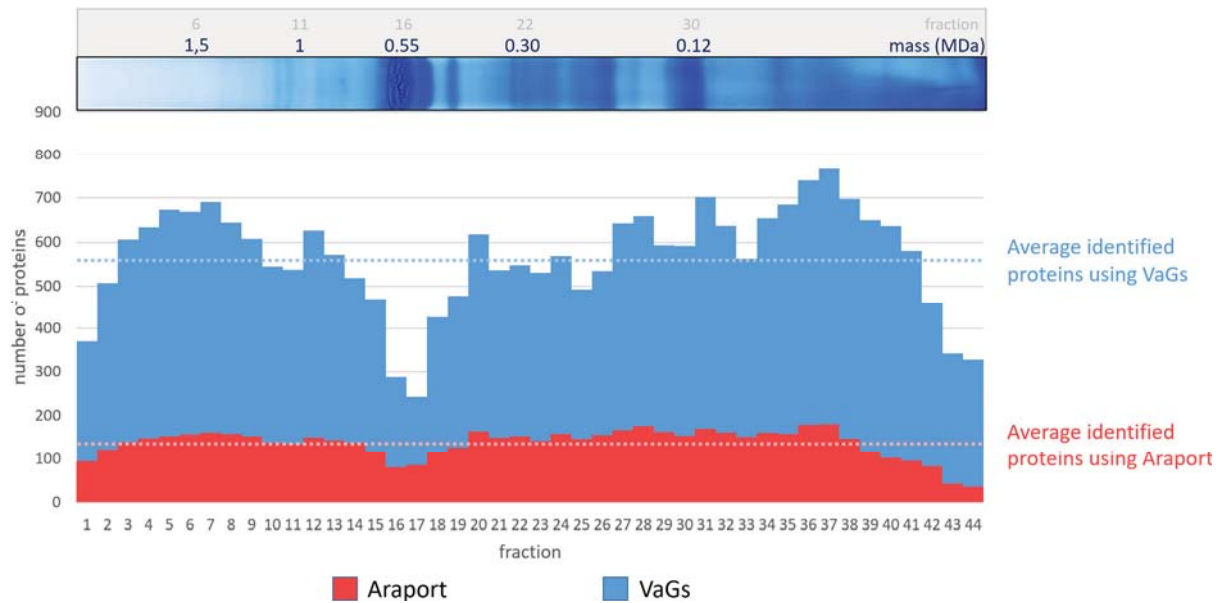


Supp. Fig. S4:

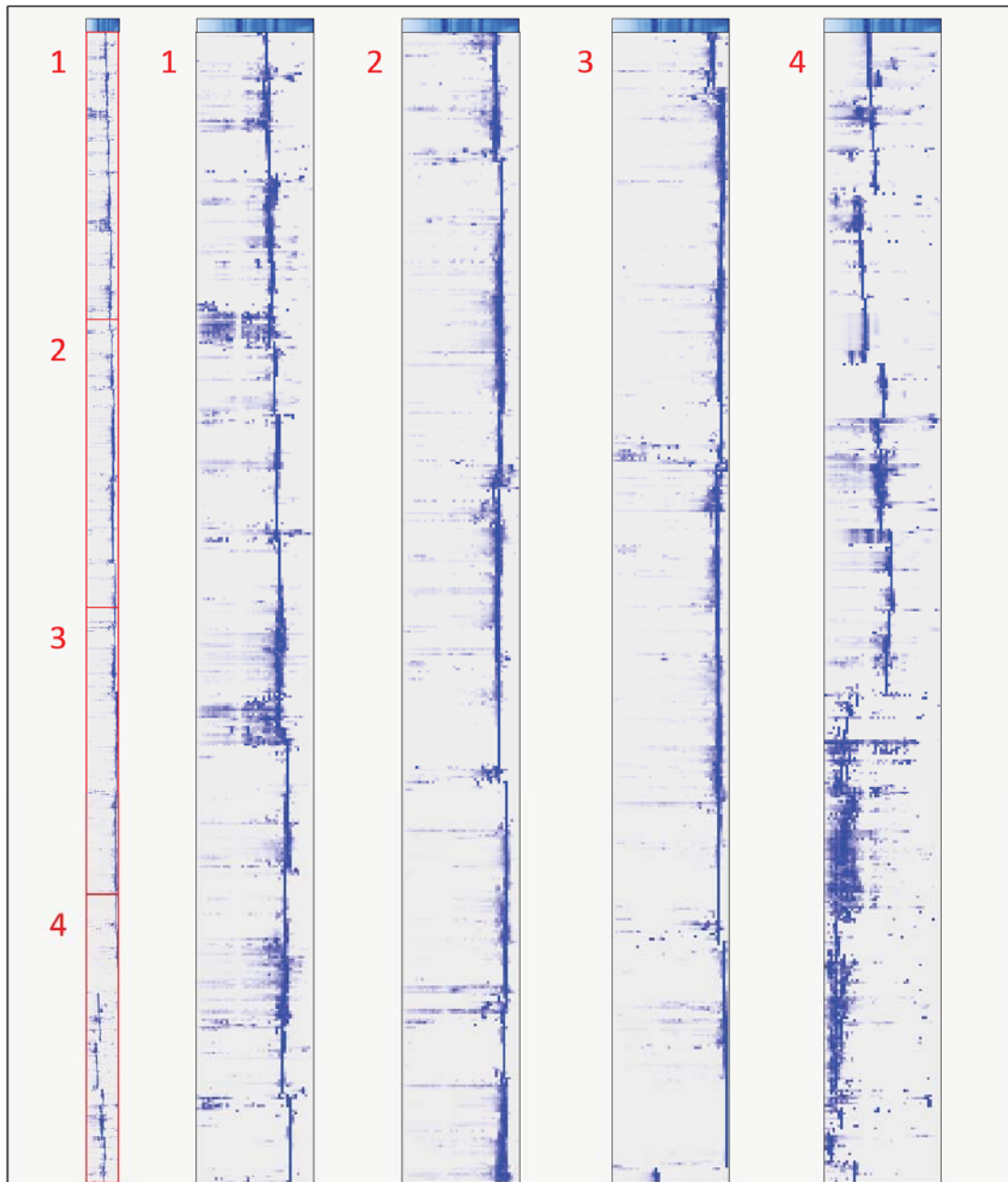


**Supp. Figure S4: BN gel lanes of separated thylakoid protein complexes from *V. album* and *A. thaliana* used for complexome profiling.** The molecular masses of standard protein complexes are given to the right of the gel lanes (in kDa). Both lanes were dissected into 44 gel slices, respectively, which are indicated to the left of the gel lanes. Finally, all 2 x 44 gel slices were subjected to analyses by label free quantitative mass spectrometry for systematic protein identifications. The gel images shown are the same as in Fig. 2.

Supp. Fig. S5



**Supp. Figure S5: Number of proteins identified in the complexome profiling fractions of *V. album* in dependence of the database used for data evaluation.** The BN gel lane is shown above the diagram (same gel image as the one shown in Fig. 2 for *V. album*). The lane was dissected in 44 gel slices (= fractions), which all were subjected to label free quantitative mass spectrometry (MS). Finally, MS data were evaluated using (i) the *A. thaliana* Araport11 gene database (<https://www.arabidopsis.org/>) (red columns) or (ii) the *V. album* protein space database (<https://viscumalbum.pflanzenproteomik.de/>, Schröder et al. 2022a) (blue columns). Note that the average number of identified proteins is only 134 based on Araport11 evaluation. Evaluation using the novel *V. album* gene space database on average revealed 565 (Table 1) proteins per fraction.



**Supp. Fig. S6: Heat map of normalized (max) abundance profiles of thylakoid proteins from *V. album* leaves.** The profiles were aligned by hierarchical clustering using the NOVA software (Giese et al. 2015). Left: entire heat map. The map consists of 44 columns corresponding to the 44 gel slices (left: fraction of largest molecular mass, right: fraction of lowest molecular mass) and 1,833 lines corresponding to the 1,833 identified unique proteins. Relative protein quantity is indicated by shades of blue (dark blue stands for high quantity, light blue/white for low quantity). Four figure parts to the right: enlarged sections of the entire map (the numbers correspond to the sections indicated in the entire map). The original BN gel is shown on top of all parts of the figure. For complete complexome profiling data see [Supp. Data 1 \(\*V. album\*\)](#) and [Supp data 2 \(\*A. thaliana\*\)](#). The map can be accessed in full detail at [https://complexomemap.de/va\\_chloroplasts](https://complexomemap.de/va_chloroplasts). A corresponding map has been generated for a *A. thaliana* thylakoid fraction and can be accessed at [https://complexomemap.de/at\\_chloroplasts](https://complexomemap.de/at_chloroplasts).



## Plant Physiology: Author Profiles

### Lucie Schröder: Plant Physiology First Author

October 7, 2022 / in [Plant Physiology: Author Profiles](#) / by Linda Palmer

*Plant Physiology*<sup>®</sup>



Lucie Schröder, first author of “The photosynthesis apparatus of European mistletoe (*Viscum album*)”

**Current Position:**

PhD student, Institute of Plant Genetics, Leibniz University Hannover

**Education:**

BSc and MSc in Plant Biotechnology, Leibniz University Hannover, Germany

**Non-scientific Interests:** plants, travelling, gaming

**Brief bio:**

After completing my BSc degree, I started a research project in the Plant Biochemistry laboratory of Hans-Peter Braun. The department’s research is mainly related to the model organism *Arabidopsis thaliana*; however, a new project at that time was related to the semi-parasitic flowering plant *Viscum album* (European Mistletoe), which grows on numerous trees in Europe. There were indications that the metabolism of this plant, which is used as an ornamental plant and source for the extraction of active substances but otherwise little studied, is very unusual. Hans-Peter Braun’s department was able to show at the time that the respiratory chain of *V. album* is reduced and that the mitochondria consequently produce only limited amounts of ATP. I was able to contribute to this project. As part of my doctoral thesis, I decided to further investigate the unusual energy metabolism of *V. album*. If the mitochondria only provide little ATP, could the missing ATP perhaps be produced by the chloroplasts? The results of this project are included in our current publication. We show that the chloroplasts also have only limited possibilities to produce ATP and propose a new view of the metabolism of mistletoe, according to which the supply of this plant must be ensured to a much greater extent by the host plant than was previously assumed. How exactly this works, however, still needs to be investigated further. In the meantime, I am very fascinated by this plant and hope to make further contributions to clarifying its way of life.

## 2.3 Complexome Profiling of Plant Mitochondrial Fractions

Lucie Schröder<sup>1</sup>, Holger Eubel<sup>1</sup>, Hans-Peter Braun<sup>1</sup>

<sup>1</sup> Institute of Plant Genetics, Plant Proteomics Group, Leibniz University Hannover, Hannover, Germany.

Type of authorship:	First author
Type of article:	book article
Share of the work:	40 %
Contribution to the publication:	Performed experiments, analyzed data, prepared figures, participated in writing the manuscript
Journal:	Methods in Molecular Biology
Impact factor:	0.368 (2022/2023)
Date of publication:	01.01.2022
Number of citations:	2
(Google Scholar, 20.09.2023)	
DOI:	10.1007/978-1-0716-1653-6_9
PubMed-ID:	34545489



# Chapter 9

## Complexome Profiling of Plant Mitochondrial Fractions

Lucie Schröder, Holger Eubel, and Hans-Peter Braun

### Abstract

Most molecular functions depend on defined associations of proteins. Protein–protein interactions may be transient or long-lasting; they may lead to labile assemblies or more stable particles termed protein complexes. Studying protein–protein interactions is of prime importance for understanding molecular functions in cells. The complexome profiling approach allows to systematically analyze protein assemblies of cells or subcellular compartments. It combines separation of intact protein fractions by blue native (BN) polyacrylamide gel electrophoresis (PAGE) and protein identification as well as quantification by mass spectrometry. Complexome profiling has been successfully applied to characterize mitochondrial fractions of plants. In a typical experiment, more than 1000 mitochondrial proteins are identified and assigned to defined protein assemblies. It allows discovering so far unknown protein complexes, studying assembly pathways of protein complexes and even characterizing labile super- and megacomplexes in the >10 mega-Dalton range. We here present a complexome profiling protocol for the straightforward definition of the protein complex inventory of mitochondria or other subcellular compartments from plants.

**Key words** Plant mitochondria, Blue native polyacrylamide gel electrophoresis, Mass spectrometry, Complexome profiling, Respiration, *Arabidopsis thaliana*, *Viscum album*

---

### 1 Introduction

Mitochondria provide ATP for driving cellular functions. They include the enzymes of the citric acid cycle and numerous additional metabolic pathways. The inner mitochondrial membrane harbors the enzyme complexes of the respiratory electron transfer chain and the ATP synthase complex. Mitochondria contain ribosomes for protein biosynthesis and enzymes for synthesizing prosthetic groups to be attached to proteins. In plants, mitochondria carry out additional functions, which are linked to photosynthesis, for example, the oxidation of glycine and the formation of serine in the photorespiration pathway and oxidation of surplus photosynthetic reduction equivalents [1]. It is estimated that mitochondria of the model plant *Arabidopsis thaliana* include >2000 types of

proteins [2]. Abundance of the mitochondrial protein species varies from only a few to several thousand copies per organelle and an average mitochondrion of *Arabidopsis* includes about 1.4 million protein molecules [3]. To fulfil their functions, most of these proteins specifically interact with other proteins forming transient protein assemblies or more stable protein complexes. Systematic characterization of protein–protein interactions (PPIs) therefore is of central importance for understanding mitochondrial functions.

The complexome profiling strategy, introduced by Wessels et al. [4] and Heide et al. [5], is a powerful approach for systematically analyzing PPIs. It combines protein separation by blue native (BN) polyacrylamide gel electrophoresis (PAGE) and protein identification by high-resolution, quantitative shotgun proteomics. The starting point is purified subcellular compartments (e.g., isolated mitochondria) (Fig. 1). Organellar membranes are solubilized using a mild non-ionic detergent and subsequently proteins in native state are separated according to their molecular masses by one-dimensional BN PAGE (Fig. 1). A lane of the BN gel is next dissected into 40–70 horizontal fractions from bottom (low molecular mass range) to top (high molecular mass range). All gel fractions are finally submitted to in-gel tryptic digestion and liquid chromatography coupled to tandem mass spectrometry. Typically, a hundred or even several hundreds of proteins are identified and quantified per gel fraction. From the MS-data, abundance profiles of all identified proteins along the BN gel lane can be produced. These abundance profiles are converted into a heatmap by hierarchical clustering [6]. On the resulting map, clusters of proteins become visible, which can be considered to correspond to defined protein assemblies (Fig. 1).

In the frame of an initial complexome profiling project dedicated to the mitochondria of the model plant *Arabidopsis thaliana*, 1359 proteins were identified, which could be assigned to >30 protein complexes, some of which were described for the first time [7]. In a parallel investigation, 1264 mitochondrial proteins of *Arabidopsis thaliana* were identified and assigned to protein complexes [8]. The method meanwhile also has been applied for mitochondrial fractions from other plants (e.g., European mistletoe) [9, 10]. Furthermore, it was used for following assembly of *Arabidopsis* mitochondrial complex I [11]. Larger protein assemblies can be characterized if large-pore BN gels are used [12]. By this approach, the subunit composition of mitochondrial ribosomes of *Arabidopsis thaliana* could recently be defined [13].

The following protocol includes instructions on how to analyze mitochondrial fractions from plants by complexome profiling. This procedure, however, can also be adopted for other plant and non-plant organelle fractions.

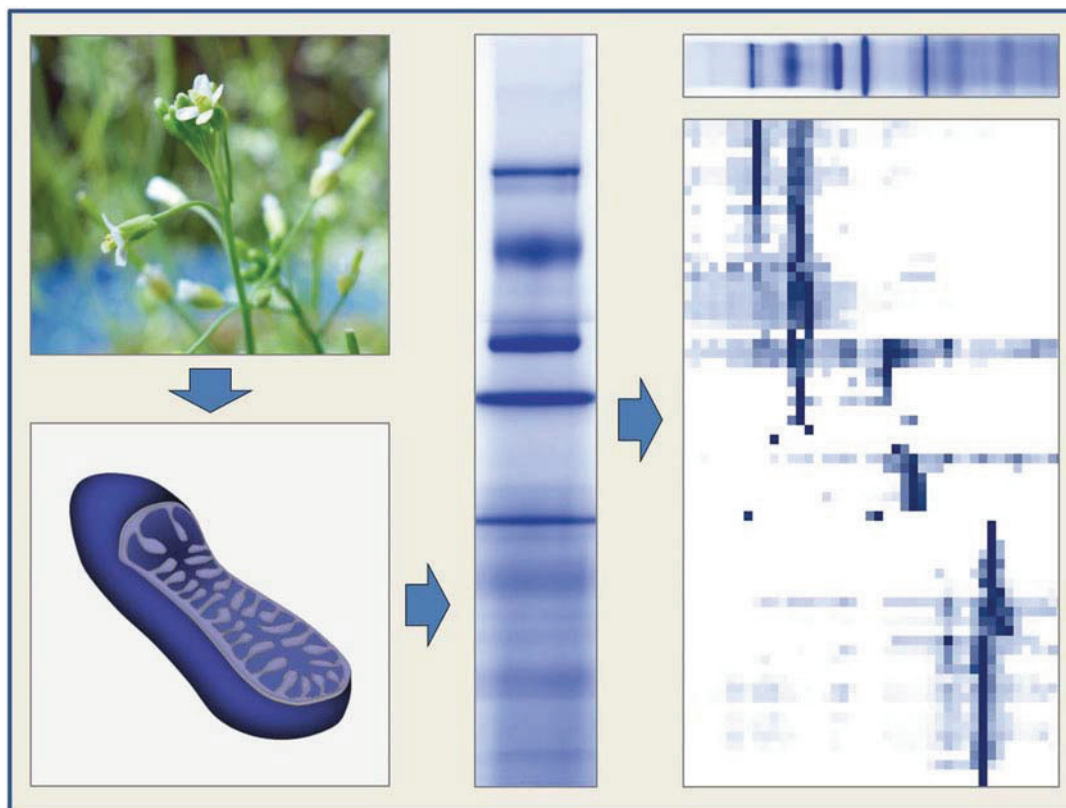


**Fig. 1** Complexome profiling workflow for plant mitochondria. Starting from plant organs, tissues or cell cultures (top left panel) mitochondria are isolated (bottom left panel). Mitochondrial membranes are next solubilized using a mild, nonionic detergent. Native proteins and protein complexes are subsequently separated by one-dimensional blue native (BN) polyacrylamide gel electrophoresis (PAGE; center panel). Finally, the corresponding gel lane is dissected into a defined number of horizontal fractions, and proteins within the slices are identified and quantified by label-free quantitative mass spectrometry. Abundance profiles of individual proteins along the BN gel lane, displayed as heat map, are clustered according to similarity (right panel)

## 2 Materials

### 2.1 Components for Casting and Running a BN Gel

All buffers are prepared from analytical grade reagents and with ultrapure water. Stock solutions should be used for limited time. All other solutions are prepared freshly.

1. 40% (w/v) acrylamide–bisacrylamide (32:1).
2. 6× BN gel buffer: 1.5 M aminocaproic acid, 150 mM bis-Tris (bis(2-hydroxyethyl)-amino-tris(hydroxymethyl)-methane), pH 7.0 (adjust at 4 °C).
3. 100% glycerol.



4. 99% (w/v) *N*, *N*, *N'*, *N'*-Tetramethylethylenediamine (TEMED).
5. 10% (w/v) ammonium persulfate (APS).
6. 5× BN cathode buffer: 250 mM tricine, 75 mM bis-Tris (Bis(2-hydroxyethyl)-amino-tris(hydroxymethyl)-methane), 0.1% (w/v) Coomassie G-250, pH 7.0 (adjust at 4 °C).
7. 6× BN anode buffer: 300 mM bis-Tris (bis(2-hydroxyethyl)-amino-tris(hydroxymethyl)-methane), pH 7.0 (adjust at 4 °C).
8. Gradient caster (for example: Model 485 Gradient Former #165–4120; Bio-Rad, Feldkirchen, Germany).
9. Peristaltic pump (e.g., EP-1 Econo Pump, Bio-Rad, Feldkirchen, Germany).
10. Gel electrophoresis unit (e.g., PROTEAN® II gel unit, Bio-Rad, Feldkirchen, Germany).

**2.2 Components  
for Solubilization  
of Mitochondrial  
Proteins and Protein  
Complexes**

1. 5% (w/v) digitonin solubilization buffer: 30 mM HEPES, 150 mM potassium acetate, 10% (v/v) glycerol, 5% (w/v) digitonin (*see Note 1*), pH 7.4. Buffer is stored at –20 °C.
2. Solubilization buffer: 30 mM HEPES, 150 mM potassium acetate, 10% (v/v) glycerol, pH 7.4. Buffer is stored at –20 °C.
3. 20× BN loading buffer: 750 mM aminocaproic acid, 5% (w/v) Coomassie G-250, stored at 4 °C.

**2.3 Components  
for Protein Analyses by  
Mass Spectrometry**

1. 100% acetonitrile (ACN).
2. 20 mM dithiothreitol (DTT).
3. 55 mM iodoacetamide (IAA).
4. 0.1 M  $\text{NH}_4\text{HCO}_3$ .
5. Trypsin solution: 2 µg trypsin (V5111) per mL resuspension buffer [Promega GmbH, Walldorf, Germany] in 0.1 M  $\text{NH}_4\text{HCO}_3$  (*see Note 2*).
6. 5% formic acid (FA), 50% ACN.
7. 1% FA, 50% ACN.
8. Transfer solution: 5% [v/v] acetonitrile, 0.1% trifluoroacetic acid (TFA).
9. Liquid chromatography (LC) system coupled to a tandem mass spectrometry (MS/MS) system.
10. C18 reverse phase trapping column, length 2 cm, ID 75 µm, particle diameter 3 µm, pore size 100 Å.
11. C18 reverse phase analytical column, length 50 cm, ID 75 µm, particle diameter 3 µm, pore size 100 Å.

### 3 Methods

#### 3.1 BN Gel Preparation

The following instructions refer to a gel with dimension of  $0.15 \times 16 \times 20$  cm. If other dimensions are used, volumes of solutions have to be adapted accordingly.

1. Mix 2.4 mL of acrylamide with 3.5 mL of BN gel buffer and 15.1 mL deionized water to prepare the 4.5% acrylamide separation gel solution (volume: 21 mL).
2. Mix 7.4 mL of acrylamide with 3 mL of BN gel buffer, 4.6 mL deionized water and 3.5 mL glycerol to prepare the 16% acrylamide separation gel solution (volume: 18.5 mL).
3. Transfer both acrylamide separation gel solutions and all necessary equipment to a cold room ( $\sim 4$  °C). Subsequent gel casting should take place in the cold to avoid early polymerization.
4. The separation phase of BN gels consists of a gradient gel, which is usually cast from the bottom. For this, a gradient caster is attached to suitable peristaltic pump tubing, which ends in a hypodermic needle. This needle is plunged through the rubber seal at the bottom of the gel casting assembly, its end now sitting between the two glass plates just above the seal. Before casting the gradient gel, pour in ultra-pure water (about 5 mL) into the space between the two glass plates (overlay solution for allowing formation of a sharp upper border of the gel). Make sure that the valve between the two chambers and the outlet valve of the gradient caster are closed. Place a magnetic stirring rod in each of the chambers. Transfer the 4.5% acrylamide separation gel solution into the first chamber of the gradient caster (connected to the outlet of the caster) and the 16% acrylamide separation gel solution into the second chamber, respectively. In case the gradient is cast from the top, the 16% acrylamide gel solution has to be transferred into the first chamber while the 4.5% acrylamide solution goes into the second chamber.
5. Add 95  $\mu$ L 10% APS and 9.5  $\mu$ L TEMED to the 4.5% separation gel solution and 61  $\mu$ L 10% APS and 6.1  $\mu$ L TEMED to the 16% separation gel solution. Mix solutions of each chamber using a magnetic stirrer. Afterward, remove the magnetic stirrer rod from the second chamber. The solution in the first chamber should be mixed continuously during gel casting. Open the outlet valve but keep the valve between the two chambers closed. Start the peristaltic pump for gel casting. Overall, gel casting should last about 30 min (average flow rate of 1.3 mL gel solutions per minute). However, use a slightly lower flow rate in the very first beginning of gradient

casting to allow formation of a sharp interface of the gel solution and the overlay (water) solution. When the gel solution in the first chamber of the gradient mixer has reached the same level as the one in the second chamber, open the valve between them. At the end of the gel casting, stop the pump in time to avoid pumping air into the gel. Remove the needle and transfer the gel either to room temperature or to a 37 °C chamber until polymerization is completed (45–70 min).

6. After gel polymerization, discard the ultra-pure water from the top of the separation gel (residual water can be removed by a strip of Whatman paper inserted between the glass plates).
7. Mix 1.5 mL of acrylamide with 2.5 mL of BN gel buffer and 11 mL of ultra-pure water to prepare the stacking gel.
8. Add 65 µL 10% APS and 6.5 µL TEMED to the stacking gel solution, mix thoroughly and cast it on top of the separation gel. Insert a comb suitable for your number of samples and their volume. Wait (approx. 30 min) for the gel to polymerize.
9. Dilute the corresponding stock solutions to prepare 1× BN cathode buffer and 1× BN anode buffer (*see Note 3*).
10. Carefully remove the comb before assembling the gel unit and add the BN anode buffer and cathode buffer to the lower and upper chambers. Rinse the gel pockets with cathode buffer before loading the samples. Store at 4 °C for at least 1 h before loading the sample and running the gel.

### 3.2 BN-PAGE Sample Preparation

The samples should be stored in buffers suitable to maintain their native conformation (avoiding high salt concentration, ionic detergents, urea, etc.). To avoid degradation during sample preparation, all steps are carried out on ice or at 4 °C. The BN gel should be ready and stored at 4 °C before commencing sample preparation.

The following steps describe sample preparation for isolated mitochondria of *Arabidopsis thaliana* cell cultures but mitochondria from any other source can be used accordingly (*see Chapters 1–4 in this volume*).

1. Spin-down mitochondria (corresponding to approximately 500 µg mitochondrial protein) at 14,300 × *g* for 10 min at 4 °C.
2. Resuspend the mitochondrial pellet in 100 µL of 5% (w/v) digitonin solubilization buffer pH 7.4 and incubate for 15 min on ice.
3. Remove insoluble material by centrifuging samples for 10 min, 4 °C, at 18,300 × *g*.
4. Mix the supernatant, which contains solubilized proteins and protein complexes, with 5 µL of 20× BN loading buffer.

### 3.3 Running the BN Gel

Load samples into the gel pockets. Empty pockets should be filled with the same volume of solubilization buffer (without digitonin) supplemented with BN loading buffer (1  $\mu$ l 20 $\times$  BN loading buffer per 20  $\mu$ L solubilization buffer). Electrophoresis takes place at 4 °C. Start with 100 V and max. 8 mA for 45 min and continue with 15 mA and max. 500 V for another 11–16 h.

### 3.4 Fractionation of BN Gel Lanes and in Gel Tryptic Digestion

A BN gel lane of about 140 mm length (only the separating gel is used) is cut into 40 to 70 horizontal gel slices of 2 mm each using a sharp scalpel blade. Dice the gel slices into blocks of 2 mm edge length to increase surface area and transfer the pieces of each single fraction to a 1.5 ml reaction tube for tryptic digestion. Rinse the blade after each slide with ethanol and deionized water to avoid cross contamination.

1. Dehydrate gel slices with 500  $\mu$ L acetonitrile for 5 min. Discard supernatant.
2. Incubate gel slices with 70  $\mu$ L of 20 mM DTT for 30 min at 56 °C. Discard supernatant.
3. Dehydrate gel slices with 500  $\mu$ L acetonitrile for 5 min. Discard supernatant.
4. Incubate gel slices in 200  $\mu$ L of 55 mM iodoacetamide (IAA) at room temperature for 30 min in the dark.
5. Dehydrate gel slices with 500  $\mu$ L acetonitrile for 5 min. Discard supernatant.
6. Incubate gel slices in 500  $\mu$ L of 0.1 M  $\text{NH}_4\text{HCO}_3$  for 15 min at room temperature. Discard supernatant.
7. Dehydrate gel slices with 500  $\mu$ L acetonitrile for 5 min. Discard supernatant.
8. Dry gel slices in a vacuum concentrator for 5 min.
9. Incubate gel slices in 70–200  $\mu$ L of trypsin solution (*see Note 4*). Incubate overnight at 37 °C in an oven (not a heating block; *see Note 5*).
10. To extract peptides from the gel pieces, incubate in 5% FA, 50% ACN for 20 min at 37 °C and 800 rpm in a heated shaker. Use a volume corresponding to that of the trypsin solution.
11. Transfer supernatants, which already contain extracted peptides, in a new low-binding reaction tube and start drying the peptides in a vacuum concentrator.
12. Repeat **steps 10** and **11** with the gel pieces except for using 1% FA, 50% ACN instead. Transfer the supernatants to the corresponding reaction tubes already containing the supernatants of **step 11**. Continue with drying the peptides and repeat these steps again.

13. Incubate gel pieces for 20 min in 200  $\mu$ L ACN. The gel pieces will turn white. Add supernatants to those of **steps 11** and **12**.
14. Continue drying the extracts in a vacuum concentrator and store them at  $-20^{\circ}\text{C}$  until use.
15. Dissolve extracted peptides in 20  $\mu$ L of transfer solution and transfer to 0.25 ml glass insert vials for LC- MS/MS analyses.
16. Keep the vials at  $8^{\circ}\text{C}$  in the sample compartment.

### **3.5 Liquid Chromatography Coupled Tandem Mass Spectrometry (LC-MS/MS)**

It is difficult to give detailed settings for this section of the protocol since these depend strongly on the layout of mass spectrometer and its performance but also on the expectations in terms of proteome coverage or time constraints. We usually employ a 5–31% ACN gradient (1 h) for eluting peptides from a C18 reverse phase column (length, 2 cm; ID, 75  $\mu$ m; particle diameter, 5  $\mu$ m; pore size, 100 Å) connected to a 50 cm analytical column (ID, 75  $\mu$ m; particle diameter, 3  $\mu$ m; pore size, 100 Å) and a Top10 MS/MS duty cycle. Basically, any established shotgun-MS protocol is compatible with complexome profiling. To improve coverage, 5  $\mu$ L of sample are loaded onto the column. Please note that the presence of proteins in several neighboring fractions abolishes the need for running blanks in-between gel fractions if the analytical sequence mirrors the sequence of fractions within the gel lane.

### **3.6 Database Search and Heat Map Building**

Raw files are searched against the Arabidopsis TAIR10 or TAIR11 database using MaxQuant [14]. The software allows for calculation and expression of protein abundance as iBAQ (intensity based absolute quantitation) values [15]. These values are then used to build protein abundance profiles of proteins by the NOVA software [6]. Hierarchical clustering of the profiles is also accomplished by the software.

1. Upload the MS raw files into MaxQuant and select “No fractions.”
2. Select the appropriate database (FASTA file path).
3. Apply the following search parameters: enzyme specificity trypsin, up to two missed cleavages, minimum peptide length of seven amino acids, error tolerance in MS and in MS/MS are to be selected according to the specifications of the MS instrument.
4. Choose as fixed modification carbamidomethylation (C) and as variable modification acetylation (N-term), oxidation (M) and deamination (D, Q).
5. Set the False discovery rate to 1%.
6. Run the search. Depending on the computer hardware, the number of fractions and the size of each MS file, this may take several hours.

7. Open the output txt file “proteingroups” in Excel.
8. Copy the columns “Majority protein IDs,” “Fasta headers” and all “IBAQ” columns (number of IBAQ columns matches the numbers of fractions) into a new Excel file.
9. Use the Excel command =A1&"|"&B1 to combine the columns “Majority protein IDs” and “Fasta headers”.
10. Copy and paste the combined column and the IBAQs in a new Excel file.
11. Save the file in xlsx or txt format.
12. Open the file with NOVA [6].
13. To normalize values, use “Edit,” “Normalization” and choose “Maximum Normalization.”
14. For clustering use “Methods,” “Clustering” and cluster with the Pearson Correlation distance function to produce a hierarchical clustering.

Well defined protein complexes can be used to calibrate the molecular mass of the complexome fractions. For this:

1. Double-click on the area just above the heat map.
2. Choose a suitable unit (e.g., kDa).
3. Press the “+” field and choose the fraction number and add the molecular mass of the complex found in this fraction.
4. Repeat this step for other protein complexes with known masses and save.

NOVA allows free selection of various settings, for example color coding and sample sequence (high mass range to the left or to the right). Also, normalization and clustering methods can be adjusted to personal needs. We here provide only the basic settings and readers are asked to familiarize themselves with the software to explore its full potential.

---

## 4 Notes

1. Digitonin is used for the solubilization of membrane bound protein complexes of cellular or organellar fractions. Solubilization buffer with digitonin should be heated to the boiling point for quantitatively dissolving the digitonin powder. The solution can afterward be cooled down and is stable for approximately 1 h.
2. Add 100  $\mu\text{L}$  of the supplied trypsin (V5111) resuspension buffer to a vial of trypsin and incubate for 15 min at 30 °C to activate the enzyme. Afterward, add 900  $\mu\text{L}$  of 0.1 M  $\text{NH}_4\text{HCO}_3$  and mix thoroughly. Store aliquots of 50  $\mu\text{L}$  at  $-20$  °C.

3. It is recommended to use cold water for dilution of the anode and cathode buffer for instant use.
4. It is important that the gel slices are fully covered by the trypsin solution but that it is not added in excess. Check the reaction tubes at the beginning of the tryptic digestion and add digestion solution if necessary. Repeat until full saturation of gel pieces is achieved.
5. In a heat block the water in the trypsin solution will evaporate and condensate in the cap. Gel pieces at the top may then be left dehydrated, producing poor digestion efficiency.

## References

1. Braun H-P (2020) The oxidative phosphorylation system of the mitochondria in plants. *Mitochondrion* 53:66–75. <https://doi.org/10.1016/j.mito.2020.04.007>
2. Rao RSP, Salvato F, Thal B et al (2017) The proteome of higher plant mitochondria. *Mitochondrion* 33:22–37. <https://doi.org/10.1016/j.mito.2016.07.002>
3. Fuchs P, Rugen N, Carrie C et al (2020) Single organelle function and organization as estimated from Arabidopsis mitochondrial proteomics. *Plant J* 101:420–441. <https://doi.org/10.1111/tbj.14534>
4. Wessels HJCT, Vogel RO, van den Heuvel L et al (2009) LC-MS/MS as an alternative for SDS-PAGE in blue native analysis of protein complexes. *Proteomics* 9:4221–4228. <https://doi.org/10.1002/pmic.200900157>
5. Heide H, Bleier L, Steger M et al (2012) Complexome profiling identifies TMEM126B as a component of the mitochondrial complex I assembly complex. *Cell Metab* 16:538–549. <https://doi.org/10.1016/j.cmet.2012.08.009>
6. Giese H, Ackermann J, Heide H et al (2015) NOVA: a software to analyze complexome profiling data. *Bioinformatics* 31:440–441. <https://doi.org/10.1093/bioinformatics/btu623>
7. Senkler J, Senkler M, Eubel H et al (2017) The mitochondrial complexome of Arabidopsis thaliana. *Plant J* 89:1079–1092. <https://doi.org/10.1111/tbj.13448>
8. Takabayashi A, Takabayashi S, Takahashi K et al (2017) PCoM-DB update: a protein co-migration database for photosynthetic organisms. *Plant Cell Physiol* 58:e10. <https://doi.org/10.1093/pcp/pcw219>
9. Senkler J, Rugen N, Eubel H et al (2018) Absence of complex I implicates rearrangement of the respiratory chain in European mistletoe. *Curr Biol* 28:1606–1613.e4. <https://doi.org/10.1016/j.cub.2018.03.050>
10. Maclean AE, Hertle AP, Ligas J et al (2018) Absence of complex I is associated with diminished respiratory chain function in European mistletoe. *Curr Biol* 28:1614–1619.e3. <https://doi.org/10.1016/j.cub.2018.03.036>
11. Ligas J, Pineau E, Bock R et al (2019) The assembly pathway of complex I in Arabidopsis thaliana. *Plant J* 97:447–459. <https://doi.org/10.1111/tbj.14133>
12. Strecker V, Wumaier Z, Wittig I et al (2010) Large pore gels to separate mega protein complexes larger than 10 MDa by blue native electrophoresis: isolation of putative respiratory strings or patches. *Proteomics* 10:3379–3387. <https://doi.org/10.1002/pmic.201000343>
13. Rugen N, Straube H, Franken LE et al (2019) Complexome profiling reveals association of PPR proteins with ribosomes in the mitochondria of plants. *Mol Cell Proteomics* 18:1345–1362. <https://doi.org/10.1074/mcp.RA119.001396>
14. Cox J, Mann M (2008) MaxQuant enables high peptide identification rates, individualized p.p.b.-range mass accuracies and proteome-wide protein quantification. *Nat Biotechnol* 26:1367–1372. <https://doi.org/10.1038/nbt.1511>
15. Schwanhäusser B, Busse D, Li N et al (2011) Global quantification of mammalian gene expression control. *Nature* 473:337–342. <https://doi.org/10.1038/nature10098>

## 2.4 Special features of cellular respiration in *Viscum album*

Lucie Schröder<sup>1</sup>, Jennifer Senkler<sup>1</sup>, Hans-Peter Braun<sup>1</sup>

<sup>1</sup> Plant Proteomics, Institute of Plant Genetics, Leibniz Universität Hannover, Herrenhäuser Str. 2, 30419, Hannover, Germany.

Type of authorship:	First author
Type of article:	Research article
Share of the work:	25 %
Contribution to the publication:	Performed experiments, analyzed data, prepared figures
Journal:	Die Mistel in der Tumortherapie 5
Impact factor:	-
Date of publication:	2020
Number of citations:	1
(Google Scholar, 20.09.2023)	
DOI:	-
PubMed-ID:	-
ISBN:	978-3-96562-030-8



# Special features of cellular respiration in *Viscum album*

## Besonderheiten der Zellatmung in *Viscum album*

Lucie Schröder, Jennifer Senkler and Hans-Peter Braun

### Zusammenfassung

**Hintergrund:** Die mitochondriale Atmungskette, insbesondere die an ihr beteiligten Enzymkomplexe I-IV, werden als unbedingte Voraussetzung für die Zellatmung angesehen. In ihrer Gesamtheit katalysieren diese Proteinkomplexe den Elektronentransport von organischen Verbindungen auf molekularen Sauerstoff (der dadurch zu Wasser reduziert wird). Der NADH Dehydrogenase Komplex (Komplex I) ist dabei als besonders wichtig anzusehen, da er als Haupteintrittsstelle für Elektronen in die Atmungskette fungiert. Defekte innerhalb dieses Proteinkomplexes haben bekanntermaßen gravierende Auswirkungen in Menschen, Tieren, Pilzen und Pflanzen. Überraschenderweise haben jüngste Untersuchungen an der Weißbeerigen Mistel (*Viscum album*) ergeben, dass der mitochondriale Komplex I in dieser Pflanze fehlt. Dabei handelt es sich um das erste berichtete Beispiel überhaupt, dass ein mehrzelliger Organismus natürlicherweise ohne Komplex I auskommen kann. Bisher ist unklar, wie die Zellen der Weißbeerigen Mistel dennoch lebensfähig sind, da die mitochondriale Atmungskette eine Voraussetzung für die Bildung des Adenosintriphosphats (ATP) in den Mitochondrien ist. Fast alle Lebensprozesse werden direkt oder indirekt durch ATP angetrieben. Wie kann der Energiestoffwechsel in *Viscum album* dennoch funktionieren?

**Methoden:** Mitochondrien aus Blättern der Weißbeerigen Mistel wurden mithilfe einer differentiellen Zentrifugation und einer Dichtegradientenzentrifugation aufgereinigt. Die Proteinkomplexe der Mitochondrien wurden nachfolgend durch Behandlung mit einem milden

Detergens aus den mitochondrialen Membranen herausgelöst. Schließlich wurden die mitochondrialen Proteine und Proteinkomplexe mittels einer Blau-nativen Gelelektrophorese aufgetrennt und massenspektrometrisch analysiert.

**Ergebnisse und Schlussfolgerungen:** Die Atmungskette der Weißbeerigen Mistel ist in ungewöhnlicher Weise umgestaltet. Die Komplexe III und IV bilden einen stabilen Superkomplex aus. Ferner kommen zahlreiche sogenannte alternative Oxidoreduktasen vor. Auf diese Weise wird eine zwar verminderte, aber insgesamt ausreichende Funktionalität der Atmungskette gewährleistet. Darüber hinaus sind möglicherweise andere subzelluläre Kompartimente daran beteiligt, die verringerte ATP-Bildung der Mitochondrien zu kompensieren. Die Atmungskette der Weißbeerigen Mistel weist somit außergewöhnliche Merkmale auf. Diese Einblicke erweitern unser Wissen um die biochemischen Besonderheiten der Weißbeerigen Mistel um ein neues Kapitel.

**Schlüsselwörter:** *Viscum album*, Zellatmung, Mitochondrien, Atmungskette, ATP Biosynthese.

## Summary

**Background:** Cellular respiration depends on the enzymes of the mitochondrial respiratory chain, particularly on the so-called complexes I-IV. Together, these protein complexes catalyze the transfer of electrons from reduced organic compounds onto molecular oxygen (which is reduced to water). The NADH dehydrogenase complex (complex I) is of special importance because it is the main site for electron insertion into the respiratory chain. Complex I deficiencies cause drastic complications in humans, animals, fungi and plants. Recent investigations in European mistletoe (*Viscum album*) surprisingly revealed that this species lacks mitochondrial complex I. This is the very first example of a multicellular organism that naturally can exist despite a major truncation of the respiratory chain. How is this compatible with cellular life? Indeed, intactness of the mitochondrial respiratory chain is of prime importance for

the efficient generation of adenosine triphosphate (ATP) which drives many cellular processes. How is energy metabolism maintained in *V. album*?

**Methods:** A procedure was developed for purifying mitochondria from *V. album* leaves, which is based on differential centrifugation and density gradient centrifugation. Membrane bound proteins and protein complexes are solubilized by a mild non-ionic detergent. Mitochondrial proteins and protein complexes are finally separated by native gel electrophoresis and identified by mass spectrometry.

**Results and conclusions:** The respiratory chain of *V. album* is rearranged in a very sophisticated way. The complexes III and IV form a stable respiratory supercomplex and numerous so-called alternative oxidoreductases occur. As a consequence, the respiratory chain maintains a basic but reduced functionality. Furthermore, other subcellular compartments seem to compensate for reduced ATP formation by the mitochondria. In conclusion, energy metabolism in *V. album* follows unique routes, which may contribute to the extraordinary biochemical properties of this species.

**Keywords:** *Viscum album*, cell respiration, mitochondria, respiratory chain, ATP formation.

## Introduction

Plants are photoautotrophic organisms. Photosynthesis, the formation of energy-rich organic compounds from simple inorganic compounds driven by light energy, is in the very center of the plant energy metabolism. In its quantitative most relevant mode, carbon dioxide and water are converted into carbohydrates in a process that is linked to the liberation of oxygen. However, besides photosynthesis, plant cells also carry out cellular respiration, the oxidation of organic compounds, which is coupled to the formation of adenosine triphosphate (ATP). Main products of cellular respiration are carbon dioxide and water. On a global scale, about 50% of the atmospheric carbon fixed by photosynthesis is directly re-liberated into the atmosphere by cellular

respiration. Photosynthesis takes place in the chloroplasts and cellular respiration in the mitochondria. Mitochondria and chloroplasts tightly interact. Indeed, the processes of photosynthesis and cellular respiration are metabolically linked in plant cells on several levels (Braun 2020).

Cellular respiration is a central process in nearly all eukaryotic cells. On a molecular scale, it is based on three steps: (i) import of organic compounds into the mitochondria and their oxidation, e.g. by the enzymes of the citric acid cycle. Many of the occurring reactions are coupled to the formation of “reducing equivalents”, e.g. nicotinamide adenine dinucleotide (NADH) and flavin adenine dinucleotide (FADH<sub>2</sub>). (ii) Re-oxidation of the reducing equivalents by the enzymes of the respiratory electron transfer chain (ETC). These enzymes are located in the inner mitochondrial membrane, which, in contrast to the outer mitochondrial membrane, forms invaginations called “cristae”; electrons are finally transported by the ETC onto molecular oxygen (O<sub>2</sub>), which is converted into water. Respiratory electron transport, which is an exergonic process, is linked to formation of a proton gradient across the inner mitochondrial membrane. (iii) In the last step, this proton gradient drives the formation of ATP from adenosine diphosphate (ADP) and phosphate. This reaction is catalyzed by the ATP synthase complex, which also is located in the inner mitochondrial membrane. The whole process is called “Oxidative Phosphorylation” (OXPHOS), because formation of ATP by phosphorylation of ADP is coupled to the consumption of oxygen. The enzymes of the ETC and the ATP synthase complex altogether are called the OXPHOS system.

The OXPHOS system is likewise present in the mitochondria of nearly all eukaryotes. It consists of the four enzyme complexes of the ETC (the complexes I to IV) and the ATP synthase complex (complex V). Complex I is a NADH-ubiquinone oxidoreductase. It is the main site of electron insertion into the ETC and much contributes to the formation of the proton gradient across the inner mitochondrial membrane. Complex II is a FADH<sub>2</sub>-ubiquinone oxidoreductase, which does not contribute to the proton gradient. Complex III, the cytochrome c reductase, transfers

electrons from ubiquinol (the reduced form of ubiquinone) onto a small protein called cytochrome c. Finally, complex IV, the cytochrome c oxidase, transfers electrons from cytochrome c onto molecular oxygen. Electron transport by the latter two protein complexes also contributes to the proton gradient across the inner mitochondrial membrane.

The OXPHOS system is highly conserved in animals, fungi and plants, which reflects its outstanding importance for cellular energy metabolism. Indeed, no multicellular species has ever been reported to lack any of the five protein complexes of the mitochondrial OXPHOS system. However, recent genetic findings indicated that *Viscum album* might be an exception (Petersen et al. 2015, Skippington et al. 2015, Skippington et al. 2017). *V. album* has a very remarkable life cycle. It is an obligatory hemiparasitic flowering plant that grows on branches of various trees. It is supplied with water, minerals and organic compounds by its host but at the same time can synthesize energy-rich compounds by its own photosynthesis. However, the energy metabolism of *V. album* is largely unknown so far.

What is the nature of the genetic findings pointing to an unusual cellular respiration of *V. album*? According to the endosymbiont theory on mitochondrial origin, mitochondria descend from free-living bacteria. One key proof for this theory is the presence of a genome in the mitochondria of present-day cells. Mitochondrial genomes have features resembling bacterial genomes. However, during evolution, the mitochondrial genomes became very much reduced. Today, only a few mitochondrial proteins are encoded by the mitochondrial genome, whereas most proteins are encoded by the genome of the cell nucleus, synthesized on cytoplasmic ribosomes and afterwards transported into the mitochondria. Several of the genes still present on the mitochondrial genome encode protein subunits of the complexes I to V of the OXPHOS system.

Surprisingly, it has been discovered that some genes encoding OXPHOS subunits are lacking on the mitochondrial genome of *Viscum* species

(Petersen et al. 2015, Skippington et al. 2015, Skippington et al. 2017). Particularly, genes encoding subunits of mitochondrial complex I are absent. It never has been reported before that a multicellular species lacks the genes encoding complex I-subunits in the mitochondrial genome. How can this finding be interpreted? Three hypotheses have been discussed: (i) the complex I genes might have been overlooked in the mitochondrial genome due to sequence divergence. Indeed, it has been found that the mutation rate of the mitochondrial genome is exceptionally high in *Viscum* (Skippington et al. 2015). (ii) The genes encoding complex I subunits have been transferred to the nuclear genome. This has occurred for numerous other mitochondrial genes during evolution. However, it has not occurred for a set of complex I genes, which encode especially hydrophobic subunits, in any multicellular species investigated so far. (iii) *V. album* has no complex I. This hypothesis seemed to be rather unlikely, because, as mentioned above, complex I is the main site for electron insertion into the respiratory chain.

We here investigated cellular respiration in *V. album*.

## Material and methods

Isolation of mitochondria from *V. album* turned out to be challenging; it did not work using standard protocols for purifying mitochondria from plants. Particularly, various viscous compounds, which not only occur in the berries, but also in stems and leaves, formed aggregates, which co-sedimented with organelles upon centrifugation. These had to be removed between the different centrifugation steps. A procedure for purifying mitochondria from *V. album* leaves is given in Senkler et al. 2018 (detailed information on all methods is provided at [https://www.cell.com/current-biology/fulltext/S0960-9822\(18\)30379-8](https://www.cell.com/current-biology/fulltext/S0960-9822(18)30379-8)).

## Results

Transmission electron microscopy of ultra-thin leaf sections was employed to obtain insights into shape and ultrastructure of *V. album* mitochondria. The leaf cells include numerous mitochondria, which have a rounded shape (Fig. 1). Compared to other plants, invaginations of the inner mitochondrial membrane are less pronounced. *V. album* mitochondria include ribosomes, indicating that protein biosynthesis can take place inside these organelles.

Next, the composition of the OXPHOS system was analyzed (Senkler et al. 2018). Mitochondrial membranes from *V. album* leaves were carefully solubilized using the non-ionic detergent digitonin. For reference, analyses were carried out in parallel for the model plant *Arabidopsis thaliana*. The OXPHOS system of *A. thaliana* is well defined (reviewed in Braun 2020). Mitochondrial proteins and protein complexes of both species were subsequently separated by Blue native polyacrylamide gel electrophoresis (BN PAGE). BN PAGE allows the separation of proteins under native conditions; protein complexes remain intact. The molecular masses of the OXPHOS complexes differed considerably between *A. thaliana* and *V. album*. Therefore, second gel dimensions were carried out under non-native conditions for identifying the separated protein complexes based on their subunit compositions.

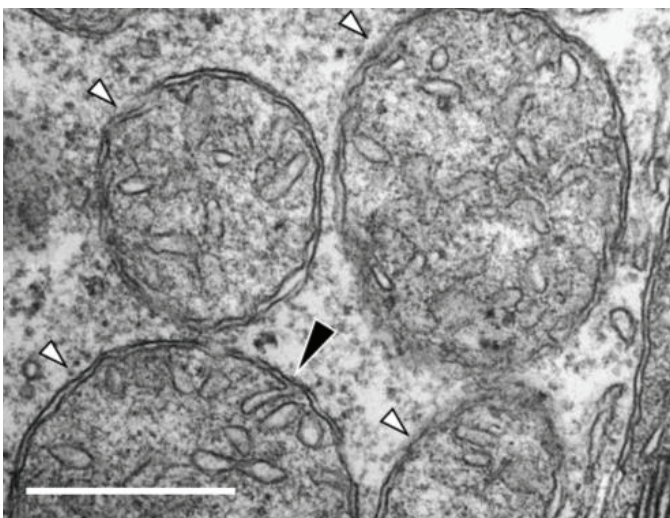


Fig. 1: Transmission electron microscopy (TEM) image of part of a *V. album* leaf cell. White arrowheads, mitochondria; black arrowhead, invagination of the inner mitochondrial membrane. The scale bar corresponds to 0.5  $\mu\text{m}$ . Image taken from Senkler et al. 2018, modified.

The following insights were obtained: In contrast to the OXPHOS system of *A. thaliana*, which consists of the complexes I to V, the OXPHOS system of *V. album* is reduced. On the two-dimensional (2D) gels, only the complexes III and IV are visible. Interestingly, they form a very stable supercomplex, which is not observed in *A. thaliana*. The complexes I, II, V are not visible on the 2D gels. In addition, a supercomplex composed of the complexes I and III, which is present in the mitochondria of *A. thaliana*, is absent in *V. album*. To search for protein complexes of low abundance, proteins visible on the 2D gels were systematically analyzed by mass spectrometry. Based on this experimental approach, subunits of the complexes II, III, IV and V were identified in the mitochondrial fraction of *V. album*. However, the complexes II and V are of comparatively low abundance. No traces of complex I subunits could be detected. To exclude that complex I still has been overseen, a highly sensitive NADH dehydrogenase *in-gel* activity assay has been carried out. In *A. thaliana*, this assay revealed a strong complex I signal. In contrast, no traces of complex I activity could be detected in *V. album*. We conclude that complex I indeed is absent in the mitochondria of *V. album*.

How can cellular respiration function in *V. album* in the absence of complex I? To further investigate mitochondrial functions in *V. album*, protein fractions were analyzed by shot-gun proteome analyses using liquid chromatography coupled to quantitative mass spectrometry (Senkler et al. 2018). More than 400 proteins could be identified. The results gave insights into central mitochondrial metabolism. All enzymes of the citric acid cycle were identified. Furthermore, so-called alternative respiratory oxidoreductases were identified, like the alternative oxidase (AOX) and alternative NAD(P)H dehydrogenases. These enzymes are part of the ETC system in plants. However, in contrast to the “classical” ETC enzymes, these enzymes do not contribute to the proton gradient across the inner mitochondrial membrane. The alternative oxidoreductases are especially abundant in *V. album*. In the absence of complex I, electron insertion into the ETC therefore can be mediated by alternative NAD(P)H dehydrogenases and



complex II. However, based on this OXPHOS mode, ATP formation should be significantly reduced, which was confirmed by oxygen-uptake measurements using isolated *V. album* mitochondria.

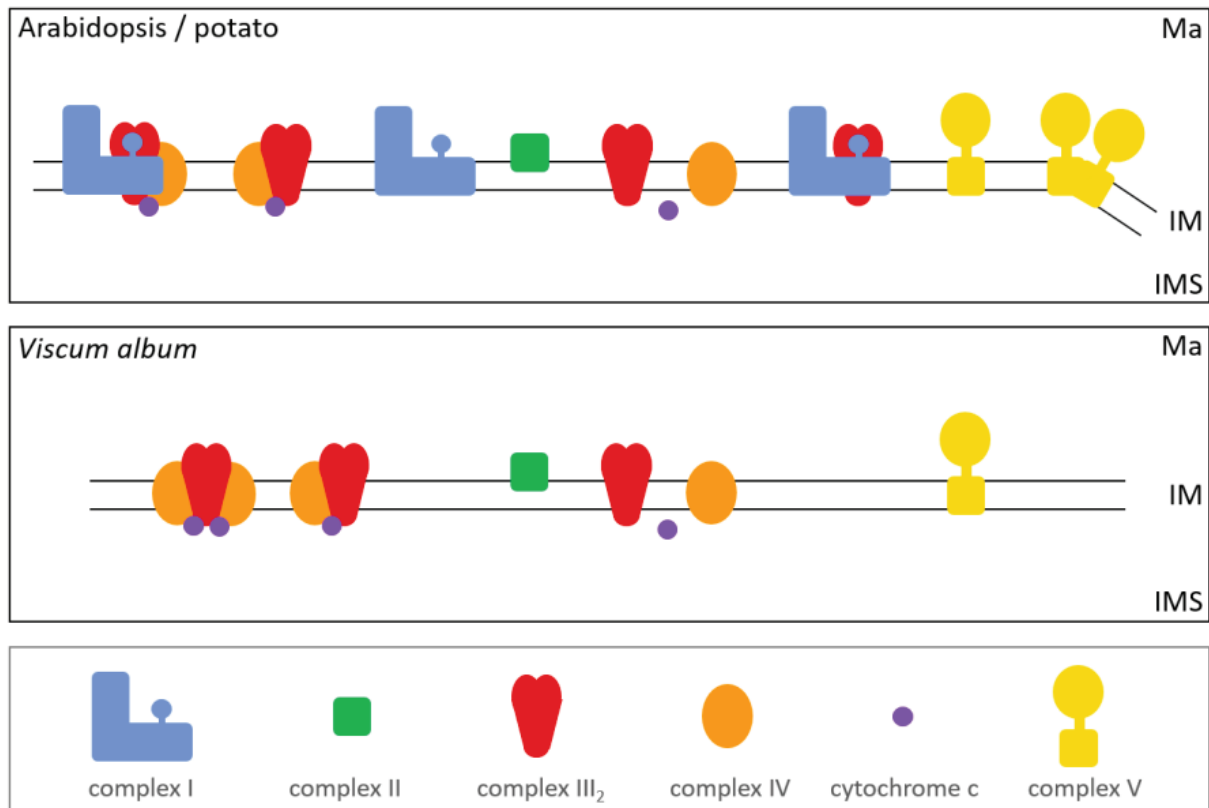


Fig. 2: The protein complexes and protein supercomplexes of the Oxidative Phosphorylation system in the model plants *Arabidopsis thaliana* and potato (top) and *Viscum album* (bottom). The identities of the complexes are given below the two boxes. Ma, mitochondrial matrix; IM, inner mitochondrial membrane; IMS, mitochondrial intermembrane space. Alternative oxidoreductases are also part of the OXPHOS system in all three species but are omitted from the figure.

In summary, the OXPHOS system of *V. album* is reduced because it surprisingly lacks mitochondrial complex I (Fig. 2). This is the first example of a multicellular species that can live in the absence of this prominent OXPHOS complex. Still, OXPHOS is functional in *V. album*, which is based on several rearrangements of the OXPHOS system: The complexes III and IV form a remarkably stable supercomplex, which should allow especially efficient electron transport between these two protein complexes. Furthermore, alternative oxidoreductases are abundant in *V. album*. Finally, cristae formation is reduced in *V. album*.

This correlates with comparatively low abundance of the ATP synthase complex (complex V), which is known to form dimers that contribute to bending the inner mitochondrial membrane and thereby induce cristae formation. Indeed, ATP synthase dimers were not observed in *V. album* (Senkler et al. 2018).

## Discussion

*V. album* has a very special life cycle. It differs in many respects from the life cycles of other flowering plants. Also, on the molecular level, *V. album* has remarkable features. Its mitochondrial OXPHOS system is rearranged. Complex I is not synthesized in *V. album*, which saves a significant amount of energy, since its biosynthesis is expensive. It is by far the largest protein complex of the ETC. About 50 subunits form part of this protein complex, which are encoded by nuclear and mitochondrial genes in all other multicellular species. However, absence of complex I comes with a price: mitochondrial ATP synthesis is less efficient in *V. album*. How can *V. album* survive with less mitochondrial ATP? This currently is not known. Results of Senkler et al. (2018) have been nicely confirmed and complemented by another study (Maclean et al. 2018) and commented by Busch (2018) and Da Fonseca-Pereira et al. (2018). *V. album* might need less ATP, because it has a comparatively slow growth rate and reduced sink organs. Furthermore, energy-rich compounds might be provided by the host tree. However, absence of complex I has not been found in any other parasitic or hemi-parasitic plant so far (Petersen et al. 2020). Finally, *V. album* might compensate reduced mitochondrial ATP formation by increased formation of ATP in other cellular compartments. Indeed, glycolysis was found to be enhanced in *V. album* (Maclean et al. 2018). Furthermore, the chloroplast ATP synthase complex is very abundant in *V. album* (Senkler et al. 2018). The energy biology of *V. album* might hold further surprises and should be further investigated.

## Conflict of interest

We hereby confirm that there are no known conflicts of interest associated with this publication and there has been no significant financial support for this work that could have influenced its outcome.

## References

- Braun HP: The Oxidative Phosphorylation system of the mitochondria in plants. *Mitochondrion* 2020; in press.
- Busch KB: Respiration: Life without complex I. *Current Biology*. 2018; 28: 616–618.
- Da Fonseca-Pereira P, Silva WB, Araujo WL et al.: How does European Mistletoe survive without complex I? *Trends in Plant Science*. 2018; 23: 847–850.
- Macleán AE, Hertle AP, Ligas J et al.: Absence of complex I is associated with diminished respiratory chain function in European mistletoe. *Current Biology*. 2018; 28: 1614–1619.
- Petersen G, Cuenca A, Møller IM et al.: Massive gene loss in mistletoe (*Viscum*, Viscaceae) mitochondria. *Sci Rep*. 2015; 5: 17588.
- Petersen G, Anderson B, Braun HP et al.: Mitochondria in parasitic plants. *Mitochondrion*. 2020; 52: 173–182.
- Skippington E, Barkman TJ, Rice DW et al.: Miniaturized mitogenome of the parasitic plant *Viscum scurruloideum* is extremely divergent and dynamic and has lost all nad genes. *Proc Natl Acad Sci U S A*. 2015; 112: E3515–3524.
- Skippington E, Barkman TJ, Rice DW et al.: Comparative mitogenomics indicates respiratory competence in parasitic *Viscum* despite loss of complex I and extreme sequence divergence, and reveals horizontal gene transfer and remarkable variation in genome size. *BMC Plant Biol*. 2017; 17: 49.
- Senkler J, Rugen N, Eubel H et al.: Absence of complex I implicates rearrangement of the respiratory chain in European mistletoe. *Current Biology*. 2018; 28: 1606–1613.

Lucie Schröder, Dr. Jennifer Senkler, Prof. Dr. Hans-Peter Braun  
Institute of Plant Genetics, Leibniz Universität Hannover  
Herrenhäuser Str. 2, 30419 Hannover  
Correspondance: [braun@genetik.uni-hannover.de](mailto:braun@genetik.uni-hannover.de)

## 2.5 The *Viscum album* Gene Space database

Lucie Schröder<sup>1</sup>, Oliver Rupp<sup>2</sup>, Micheal Senkler<sup>1</sup>, Nils Rugen<sup>1</sup>, Natalija Hohnjec<sup>3</sup>, Alexander Goesmann<sup>2</sup>, Helge Küster<sup>3</sup>, Hans-Peter Braun<sup>1</sup>

<sup>1</sup> Plant Proteomics, Institute of Plant Genetics, Leibniz Universität Hannover, Herrenhäuser Str. 2, 30419, Hannover, Germany.

<sup>2</sup> Institute of Bioinformatics and Systems Biology, University of Giessen, Germany

<sup>3</sup> Plant Genomics, Institute of Plant Genetics, Leibniz Universität Hannover, Herrenhäuser Str. 2, 30419, Hannover, Germany.

Type of authorship:	First author
Type of article:	Research article
Share of the work:	60 %
Contribution to the publication:	Performed experiments, analyzed data, prepared figures, participated in writing the manuscript
Journal:	Frontiers in Plant Science
Impact factor:	6.627 (2022/2023)
Date of publication:	26.06.2023
Number of citations:	0
(Google Scholar, 20.09.2023)	
DOI:	10.3389/fpls.2023.1193122
PubMed-ID:	37484460



## OPEN ACCESS

## EDITED BY

Ute Vothknecht,  
University of Bonn, Germany

## REVIEWED BY

Tiago Santana Balbuena,  
São Paulo State University, Brazil  
Ilka Wittig,  
Goethe University Frankfurt, Germany

## \*CORRESPONDENCE

Hans-Peter Braun

✉ braun@genetik.uni-hannover.de

RECEIVED 24 March 2023

ACCEPTED 02 June 2023

PUBLISHED 26 June 2023

## CITATION

Schröder L, Rupp O, Senkler M, Rugen N,  
Hohnjec N, Goesmann A, Küster H and  
Braun H-P (2023) The *Viscum album* Gene  
Space database.  
*Front. Plant Sci.* 14:1193122.  
doi: 10.3389/fpls.2023.1193122

## COPYRIGHT

© 2023 Schröder, Rupp, Senkler, Rugen,  
Hohnjec, Goesmann, Küster and Braun. This  
is an open-access article distributed under  
the terms of the [Creative Commons  
Attribution License \(CC BY\)](https://creativecommons.org/licenses/by/4.0/). The use,  
distribution or reproduction in other  
forums is permitted, provided the original  
author(s) and the copyright owner(s) are  
credited and that the original publication in  
this journal is cited, in accordance with  
accepted academic practice. No use,  
distribution or reproduction is permitted  
which does not comply with these terms.

# The *Viscum album* Gene Space database

Lucie Schröder <sup>1</sup>, Oliver Rupp <sup>2</sup>, Michael Senkler <sup>1</sup>,  
Nils Rugen <sup>1</sup>, Natalija Hohnjec <sup>3</sup>, Alexander Goesmann <sup>2</sup>,  
Helge Küster <sup>3</sup> and Hans-Peter Braun <sup>1\*</sup>

<sup>1</sup>Plant Proteomics, Institute of Plant Genetics, Leibniz Universität Hannover, Hannover, Germany,

<sup>2</sup>Bioinformatics and Systems Biology, Justus-Liebig-Universität Gießen, Gießen, Germany,

<sup>3</sup>Plant Genomics, Institute of Plant Genetics, Leibniz Universität Hannover, Hannover, Germany

The hemiparasitic flowering plant *Viscum album* (European mistletoe) is known for its very special life cycle, extraordinary biochemical properties, and extremely large genome. The size of its genome is estimated to be 30 times larger than the human genome and 600 times larger than the genome of the model plant *Arabidopsis thaliana*. To achieve insights into the Gene Space of the genome, which is defined as the space including and surrounding protein-coding regions, a transcriptome project based on PacBio sequencing has recently been conducted. A database resulting from this project contains sequences of 39,092 different open reading frames encoding 32,064 distinct proteins. Based on 'Benchmarking Universal Single-Copy Orthologs' (BUSCO) analysis, the completeness of the database was estimated to be in the range of 78%. To further develop this database, we performed a transcriptome project of *V. album* organs harvested in summer and winter based on Illumina sequencing. Data from both sequencing strategies were combined. The new *V. album* Gene Space database II (VaGs II) contains 90,039 sequences and has a completeness of 93% as revealed by BUSCO analysis. Sequences from other organisms, particularly fungi, which are known to colonize mistletoe leaves, have been removed. To evaluate the quality of the new database, proteome data of a mitochondrial fraction of *V. album* were re-analyzed. Compared to the original evaluation published five years ago, nearly 1000 additional proteins could be identified in the mitochondrial fraction, providing new insights into the Oxidative Phosphorylation System of *V. album*. The VaGs II database is available at <https://viscualbum.pflanzenproteomik.de/>. Furthermore, all *V. album* sequences have been uploaded at the European Nucleotide Archive (ENA).

## KEYWORDS

database development, PacBio sequencing, Illumina sequencing, Complexome profiling, mitochondria, oxidative phosphorylation (OXPHOS), complex I, supercomplex

## Introduction

European mistletoe (*V. album*) is an obligate hemiparasitic flowering plant of the order Santalales. It grows on numerous trees in Europe. The host trees provide *V. album* with water, nutrients and, to a certain extent, with organic compounds. At the same time, *V. album* performs photosynthesis and produces organic compounds itself. In contrast to most angiosperms in Central Europe, it does not discard its leaves in winter and performs photosynthesis all year. The vitality of host trees may be impaired by mistletoe settlement.

*V. album* is known for a very special lifestyle (see Glatzel and Geils, 2009 for review): *V. album* does not germinate in soil but on branches of trees where it becomes connected with the xylem of its host. To ensure spreading, the fruits of *V. album* ripe in winter, when other food resources are scarce for birds. The fruits are very sticky to ensure a stable attachment on branches. The seeds lack a seed coat and consist of an embryo, which can germinate from the fruit without a dormancy phase. Haustoria, which are formed first during germination, are guided *via* negative phototropism to the surface of the branch of the host tree. After connection with the xylem of the vascular system, the haustoria take up water, minerals and organic compounds from the host plants. Afterwards, one pair of shoot segments per year per shoot apical meristem are formed by the *V. album* plant. The typical ball-like shape is achieved after several years by annual realignment of the new shoots, which grow in all directions. In contrast to most other plant species the leaves of *V. album* do not close their stomata during water shortage, which can increase water stress of the host plant. In August/September leaves of the previous year are discarded, without recycling chlorophyll, while the new leaves formed in spring stay attached, to perform photosynthesis in the winter.

Biochemically, *V. album* stands out with its rich content of phenolic acids, phenylpropanoids, flavonoids, triterpenes and phytosterols (Urech and Baumgartner, 2015; Jäger et al., 2021). Furthermore, *V. album* produces specific proteins, the viscotoxins and mistletoe lectins, which act as a biotic defense system. The stickiness of the fruits is provided by special kinds of hemicellulose compounds (Azuma Ji et al., 2000). The development of *V. album* is controlled by an extraordinary distribution of phytohormones. *V. album* extracts have immune stimulating and cytotoxic effects, which are used in medicine (Nazaruk and Orlikowski, 2016).

At the molecular level, *V. album* is less well characterized. The mitochondrial and chloroplast genomes have been sequenced (Petersen et al., 2015a; Petersen et al., 2015b; Skippington et al., 2015; Skippington et al., 2017) and found to lack some of the genes normally present in these organelles, especially those encoding subunits of the mitochondrial NADH dehydrogenase complex and the homologous chloroplastidic NDH complex. The complete absence of these complexes was shown by proteomic studies (Maclean et al., 2018; Senkler et al., 2018; Schröder et al., 2020; Schröder et al., 2022a).

The genome of *V. album* consists of  $2n=20$  chromosomes and is considered to be one of the largest genomes of flowering plants (Zonneveld, 2010; Novák et al., 2020). It consists of almost 100 billion base pairs. More than 50% of the genome sequence of *V.*

*album* consists of highly repetitive DNA (Novák et al., 2020). The genome sequence of *V. album* has not been determined to date but the partial sequence of its Gene Space has recently been presented (Schröder et al., 2022b). The GC content of the gene sequences lies at about 50%, which is exceptionally high for angiosperms.

An initial approach to analyze the *V. album* Gene Space was based on Single Molecule Real-Time (SMRT) sequencing (PacBio sequencing) (Schröder et al., 2022b). A database resulting from this project contains 39,092 gene sequences, from which 32,064 protein sequences were derived. The results enabled the development of a first *V. album* Gene Space database. The completeness of this database was estimated to be in the range of 78%. To further develop this database, a *V. album* transcriptome project has been carried out using the Illumina sequencing approach. Analyses were performed for *V. album* samples harvested in winter and summer, respectively. By combining novel and existing sequencing data, we here present a new *V. album* database including 90,039 sequence entries. The quality of the new database is demonstrated by re-evaluation of published *V. album* proteome datasets.

## Materials and methods

### Isolation of mRNA fractions from *V. album*

Mistletoes (European mistletoe; *Viscum album*), grown on an apple tree (*Malus* sp.) on the campus of Leibniz University Hannover were used as starting material. Various organs (leaves, stems, flower buds) of male and female plants were harvested in summer and in winter, shock-frozen using liquid nitrogen, and stored at  $-80^{\circ}\text{C}$  until use. mRNA isolation and quality evaluation were carried out as described previously (Schröder et al., 2022b).

### Sequence analysis

mRNA fractions were reverse transcribed into cDNA. The summer and winter fractions were analyzed separately using Illumina PE150 (paired-end read) sequencing. cDNA libraries containing 250–300 bp inserts were constructed and sequenced. Quantitative data as well as quality evaluation data of the libraries are given in Table 1.

### Transcriptome assembly

The raw Illumina RNA-seq reads were first trimmed for low-quality and adaptor regions using Trimmomatic (Bolger et al., 2014) (version 0.36, ILLUMINACLIP : ADAPTER.fa:2:20:7 SLIDINGWINDOW:4:15 MINLEN:50). The trimmed reads were assembled using Trinity (Haas et al., 2013) (version 2.11.0) including *in silico* normalization with a target coverage of 50 x. The PacBio IsoSeq reads were included in the assembly using the “–long\_reads” option of Trinity. The assembled transcripts were screened for coding sequences using TransDecoder (Haas and Papanicolaou, n.d.). The potential protein sequences were merged

TABLE 1 Results and quality evaluation of the Illumina sequencing approach of the winter and summer samples of *V. album*.

Sample <sup>a</sup>	Raw reads <sup>b</sup>	Raw data(G) <sup>c</sup>	Error (%) <sup>d</sup>	Q20 (%) <sup>e</sup>	Q30 (%) <sup>f</sup>	GC (%) <sup>g</sup>
winter	120,720,364	18,108,054,600	0.03	97.96	93.99	49.47
summer	121,840,742	18,276,111,300	0.02	98.11	94.34	49.37

<sup>a</sup>sample names.

<sup>b</sup>original sequencing reads counts.

<sup>c</sup>raw reads number multiplied by read lengths, saved in G unit.

<sup>d</sup>average sequencing error rate, calculated by  $Q_{phred} = -10\log_{10}(e)$ .

<sup>e</sup>percentages of bases whose correct base recognition rates are greater than 99% in total bases.

<sup>f</sup>percentages of bases whose correct base recognition rates are greater than 99.9% in total bases.

<sup>g</sup>percentages of G and C in total bases.

with the previously created protein sequences (Schröder et al., 2022b) and redundant sequences were filtered using CD-HIT (Li and Godzik, 2006) (version 4.7, -c 0.95 -aS 0.99). The functional annotation was computed using the best blast hit method on the UniProt/Swiss-Prot (Boutet et al., 2007) and UniProt/TrEMBL (The UniProt Consortium et al., 2023) databases. The TPM values were computed with Salmon (Patro et al., 2017) (version 1.9.0). The completeness of the filtered transcripts was estimated with BUSCO (Seppey et al., 2019) (version 5.0.0) using the viridiplantae database.

## The *V. album* database

The final *V. album* Gene Space II database was created by combining PacBio and Illumina sequencing. It includes 90,039 distinct proteins. The database is accessible at <https://viscumalbum.pflanzenproteomik.de/>. Furthermore, all sequences were submitted to NCBI.

## Re-evaluation of the *V. album* mitochondria complexome

The complexome profiling approach is introduced in Schröder et al., 2022c. Primary complexome profiling data were taken from Senkler et al., 2018. Re-evaluation of the mass-spectrometry (MS) data and annotation of proteins were carried out with MaxQuant (version 2.1.4.0) using the novel VaGs II database. The settings were the same as in Senkler et al., 2018. For heatmap generation, the abundance profiles (based on iBAQ values; Schwanhäusser et al., 2011; calculated by MaxQuant) of all identified proteins were used. These profiles were aligned according to similarity by hierarchical clustering using the NOVA software (version: 0.5.8; Giese et al., 2015). The Complexome Map of the re-evaluated *V. album* mitochondria fractions is available at the ComplexomeMap portal at <https://complexomemap.de/75>.

## Results and discussion

For Illumina analysis, transcripts from leaves, stems and buds of female and male *V. album* plants were isolated, combined and reverse-transcribed into cDNA. Organs were harvested in winter

and summer and corresponding cDNA fractions were analyzed separately. Illumina sequence analysis revealed >120,000,000 reads for the summer and the winter fraction, respectively (Table 1).

## Transcriptome assembly

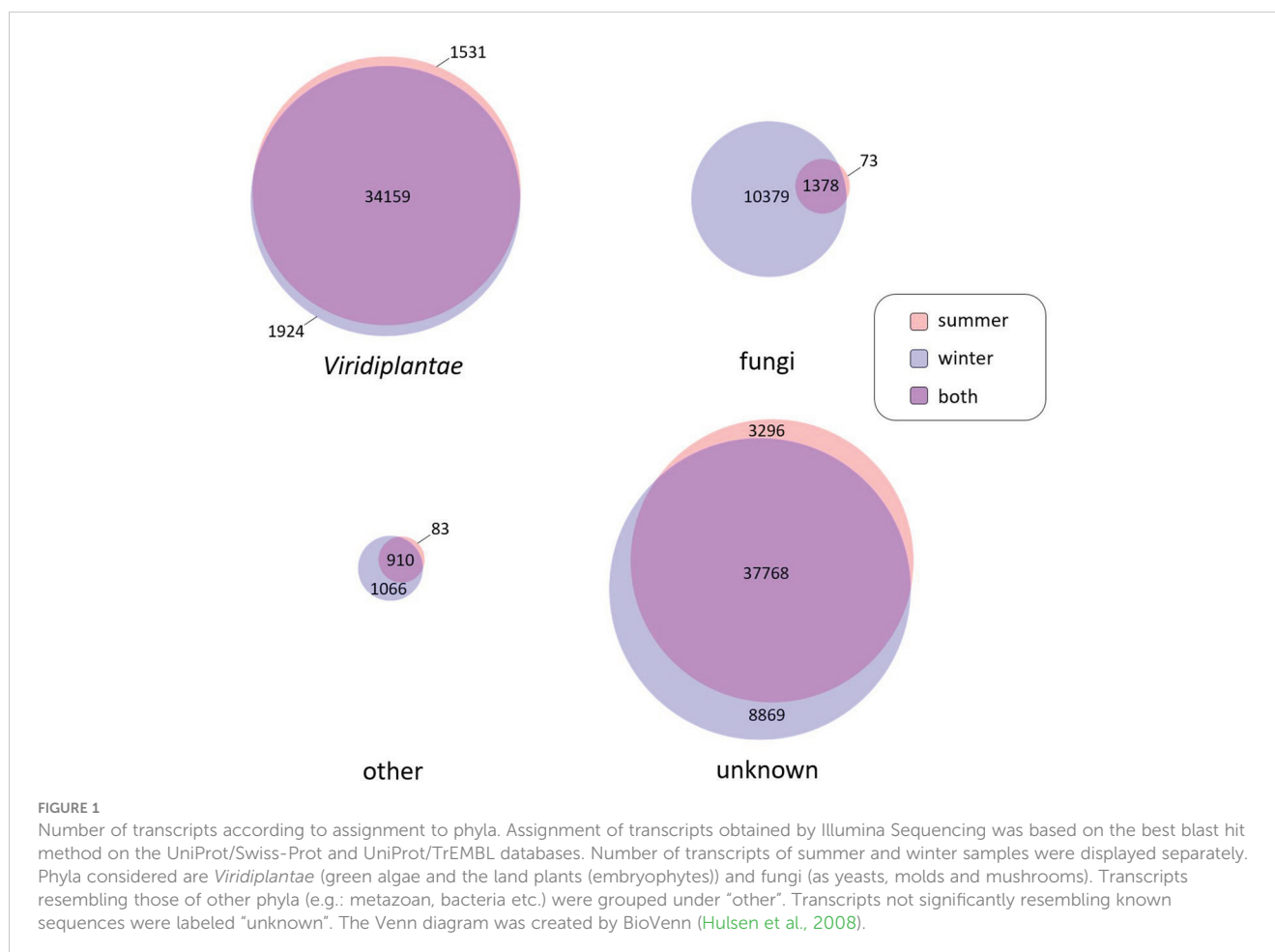
The datasets were processed as described in the Materials and Methods section and assembled using the Trinity software package version 2.11.0 (Haas et al., 2013). The PacBio IsoSeq reads (Schröder et al., 2022b) were included to the assembly using the “-long\_reads” option of Trinity. The Trinity assembly produced 650,594 transcript contigs. TransDecoder predicted potential coding sequences on 144,517 contigs. The clustering with CD-HIT produced 104,405 unique sequences, which were used for further analyses.

## Functional annotation of transcripts and functional evaluation of the *V. album* transcript samples

Functional annotation of the 104,405 transcripts was computed using the best blast hit method on the UniProt/Swiss-Prot (Boutet et al., 2007) and UniProt/TrEMBL (The UniProt Consortium et al., 2023) databases. As a result, 51% of the sequences could be assigned a function. As expected, in most cases the greatest similarity is with sequences from the phylum *Viridiplantae* (green algae and the land plants). However, there are also numerous transcripts which show highest similarity to transcripts from other phyla, especially fungi. No functions could be assigned to many other sequences, which can likely be explained by the fact that no genome sequences of plants more closely related to *V. album* are yet available.

*V. album* organs used for transcript isolation were from plants living in the field. *V. album* leaves are known to be colonized by several endophytic fungi (Peršoh et al., 2010; Kotan et al., 2013, Ariantari et al. 2019, reviewed in Krasnylenko et al., 2020). To investigate the presence of fungal sequences in our database, we evaluated the functional annotation of Illumina transcript sequences according to Phyla for the winter and summer samples (Figure 1). 37,614 of the *V. album* transcripts assigned to *Viridiplantae*. 91% of them (34,159 transcripts) likewise were present in both, the winter and the summer sample. Furthermore, 11,830 transcripts of our





*V. album* samples were assigned to the fungi Phylum (Figure 1). Almost all fungal sequences are from the winter sample, which is probably due to the increased age of the mistletoe leaves (new leaves appear in the spring and are kept in the winter). Only 11% of the fungal sequences occur likewise in the summer and winter samples. Few of the transcripts of our *V. album* samples were assigned to other Phyla than *Viridiplantae* or fungi (Figure 1). Transcripts that could not be functionally annotated were labeled "unknown" (Figure 1). The number of transcripts of this category is similar in the winter and summer samples; also, they show quite a high intersection in terms of their occurrence in the two seasons (76%), similar to the transcripts assigned to *Viridiplantae*. We conclude that these sequences should be predominantly *V. album* transcripts. The relatively high proportion of transcripts of unknown function likely is due to the lack of comparative sequences from related plant species, but also due to the fact that *V. album* has a special way of life, which requires numerous proteins that do not occur in other phyla.

To further analyze the origin of sequences in our *V. album* samples, we quantified all transcripts identified by our Illumina sequencing approach according to their assignment to Phyla (Figure 2). Transcripts per million (TPM) values of transcripts in the summer and winter samples were examined separately. As expected, TPM values are highest for transcripts assigned to

*Viridiplantae* and clearly lower in those assigned to the fungi Phylum. This is particularly visible in the sample harvested in summer. TPM values of unassigned transcripts more resemble the values obtained for transcripts assigned to *Viridiplantae*, which is especially evident in the summer sample. This reconfirms that the transcripts in this category are derived from *V. album* rather than from fungi colonizing *V. album*. The absolute summed up TPM values (summer and winter sample combined) for the four categories are 1,096,579 for *Viridiplantae* (73%), 385,858 for "unknown" (25%), 11,497 for fungi (0.8%) and 17,789 for "others" (1.1%). Thus, about 1% of the transcripts of our *V. album* fractions can be classified as fungal. This should realistically reflect the conditions in the "ecological niche" *V. album*.

## The *Viscum album* Gene Space database II

The previous *V. album* Gene Space database, which was created based on Single Molecule Real-Time (SMRT) sequencing (PacBio sequencing), includes 39,092 entries encoding 32,064 distinct proteins (Schröder et al., 2022b). We now designate this database VaGs I. BUSCO analyses had revealed a completeness of about 78%. Through implementation of the new Illumina sequencing data and

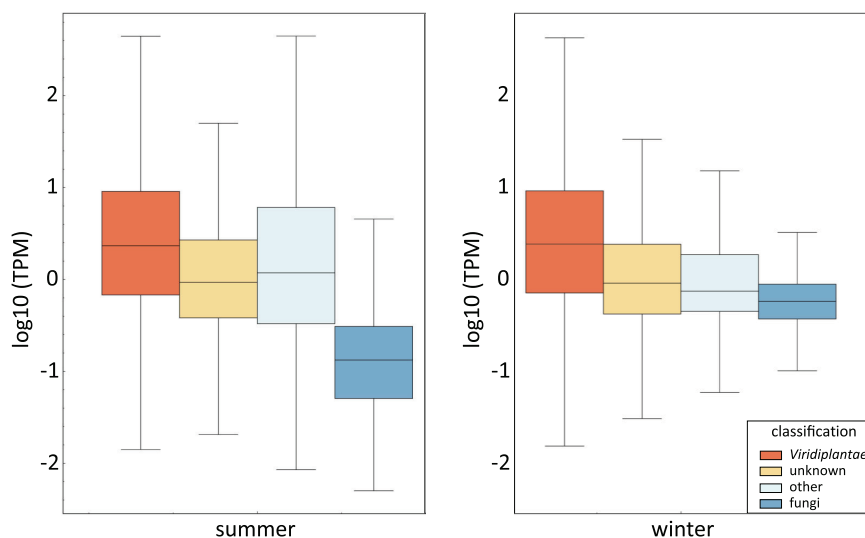


FIGURE 2

Transcript levels within the *V. album* summer and winter samples according to their assignment of phyla. Transcript levels are given in  $\log_{10}$  Transcripts Per Million (TPM). The line within the box shows the median for each dataset. The upper end of the box is the “upper quartile”, which is the median of the upper half of the dataset. The lower quartile (lower end of the box) is the median of the lower half of the dataset. The end of the vertical lines indicate the lowest and highest values of the dataset. The diagram was created by instant clue (Nolte et al., 2018).

improved transcript annotation, we hereby present a novel *V. album* Gene Space database, VaGs II. We decided to remove transcripts that are unambiguously assigned to the Phyla Fungi, Animals, Bacteria and Viruses based on sequence comparisons. VaGs II includes all transcripts assigned to the categories “Viridiplantae” and “unknown”. The total number of distinct transcripts is 90,039. The BUSCO score of VaGs II is 93% (91% complete, 2% fragmented; Figure 3).

A database has been developed that allows all sequences to be viewed (Figure 4). Sequences can be downloaded, proteins can be searched by ID, name, and sequence, and instructions for BLAST searches are given. Furthermore, all *V. album* transcript have been uploaded at the European Nucleotide Archive (ENA) (<https://www.ebi.ac.uk/ena/browser/home>).

## Re-evaluation of complexome profiling data for *V. album* mitochondria using VaGs II

To test the quality of the new VaGs II databank, a published proteomic dataset on *V. album* mitochondria (Senkler et al., 2018) was re-evaluated. This is a complexome dataset which was created as follows: First, mitochondria were isolated from *V. album* and a mild detergent was used to dissolve the mitochondrial membranes. Protein complexes in the resulting solution were separated by Blue-native polyacrylamide gel electrophoresis. A lane of the native gel was then cut from top to bottom into 54 small gel slices, which were individually subjected to label-free quantitative shotgun mass spectrometry for protein identifications. Finally, abundance

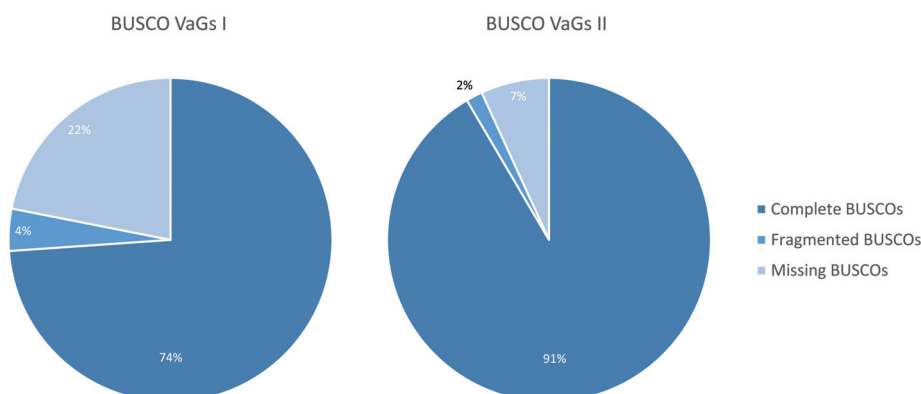


FIGURE 3

Comparison of the completeness of the VaGs I database (Schröder et al., 2022b) and the new VaGs II database as revealed by ‘Benchmarking Universal Single Copy Orthologs’ (BUSCO) analysis (Seppey et al., 2019).

## VaGs II

### *Viscum album* Gene Space Database (2023)



*Viscum album* is known for its very special life cycle, its particular biochemical composition, its unique mode of respiration and its extremely large genome. We here offer the full-length transcriptome of *Viscum album*, consisting of more than 90,000 distinct sequences from our recent project. Both the nucleotide and protein sequences are provided and a functional annotation was computed using the best blast hit method on the UniProt/Swiss-Prot (Boutet et al., 2007) and UniProtTrEMBL (The UniProt Consortium et al., 2023) databases. Further information (e.g. molecular weight, IEP) can be found in the excel file.

### Protein Search

Have a **quick look** to see if we found your protein of interest in our Dataset. Keep in mind that most proteins are not fully annotated yet. We offer homologs from Arabidopsis/TAIR as well as NCBI or Swissprot matches. For more details, please download the database. (links below)

Search Term	Results																	
viscd	<table border="1"> <tr> <td>TRINITY_DN166592_c15_g14_i1   Viscotoxin A   AT1G66100.1</td> <td></td> </tr> <tr> <td>TRINITY_DN68891_c0_g1_i1   Viscotoxin-A3   AT5G36910.1</td> <td></td> </tr> <tr> <td>VaGs38671   Viscotoxin-A3   AT1G66100.1</td> <td> <table border="1"> <tr> <td>VaGs II ID: VaGs38671</td> </tr> <tr> <td>Name: Viscotoxin-A3</td> </tr> <tr> <td>Arabidopsis Homologue: AT1G66100.1</td> </tr> </table> </td> </tr> <tr> <td>VaGs35165   Viscotoxin-A3   -</td> <td></td> </tr> <tr> <td>TRINITY_DN169352_c5_g1_i1   Viscotoxin-A3   AT1G66100.1</td> <td></td> </tr> <tr> <td>TRINITY_DN166592_c15_g26_i3   Viscotoxin-A3   AT1G66100.1</td> <td></td> </tr> <tr> <td>TRINITY_DN170490_c64_g1_i1   Viscotoxin-B   AT1G66100.1</td> <td></td> </tr> </table>	TRINITY_DN166592_c15_g14_i1   Viscotoxin A   AT1G66100.1		TRINITY_DN68891_c0_g1_i1   Viscotoxin-A3   AT5G36910.1		VaGs38671   Viscotoxin-A3   AT1G66100.1	<table border="1"> <tr> <td>VaGs II ID: VaGs38671</td> </tr> <tr> <td>Name: Viscotoxin-A3</td> </tr> <tr> <td>Arabidopsis Homologue: AT1G66100.1</td> </tr> </table>	VaGs II ID: VaGs38671	Name: Viscotoxin-A3	Arabidopsis Homologue: AT1G66100.1	VaGs35165   Viscotoxin-A3   -		TRINITY_DN169352_c5_g1_i1   Viscotoxin-A3   AT1G66100.1		TRINITY_DN166592_c15_g26_i3   Viscotoxin-A3   AT1G66100.1		TRINITY_DN170490_c64_g1_i1   Viscotoxin-B   AT1G66100.1	
TRINITY_DN166592_c15_g14_i1   Viscotoxin A   AT1G66100.1																		
TRINITY_DN68891_c0_g1_i1   Viscotoxin-A3   AT5G36910.1																		
VaGs38671   Viscotoxin-A3   AT1G66100.1	<table border="1"> <tr> <td>VaGs II ID: VaGs38671</td> </tr> <tr> <td>Name: Viscotoxin-A3</td> </tr> <tr> <td>Arabidopsis Homologue: AT1G66100.1</td> </tr> </table>	VaGs II ID: VaGs38671	Name: Viscotoxin-A3	Arabidopsis Homologue: AT1G66100.1														
VaGs II ID: VaGs38671																		
Name: Viscotoxin-A3																		
Arabidopsis Homologue: AT1G66100.1																		
VaGs35165   Viscotoxin-A3   -																		
TRINITY_DN169352_c5_g1_i1   Viscotoxin-A3   AT1G66100.1																		
TRINITY_DN166592_c15_g26_i3   Viscotoxin-A3   AT1G66100.1																		
TRINITY_DN170490_c64_g1_i1   Viscotoxin-B   AT1G66100.1																		

FIGURE 4

The *Viscum album* Gene space database at <https://viscumalbum.pflanzenproteomik.de/>.

profiles along the blue-native gel lane were calculated for all identified proteins. The results were visualized as a heatmap and the profiles of individual proteins were aligned according to similarity. On the resulting heatmap, proteins belonging to the same protein complex form characteristic clusters. It thus is possible to systematically investigate the protein complexes of a biochemical fraction, the 'complexome'. The original data of this experiment still

had to be analyzed using a protein database for the model plant *Arabidopsis thaliana* (Senkler et al., 2018), since a *V. album* database was not available. This allowed the identification of 477 proteins in total. Re-evaluation of the same dataset using the VaGs II database now allowed the identification of 1392 proteins (Figure 5). The newly evaluated mitochondrial complexome of *V. album* is presented as a supplement of this publication

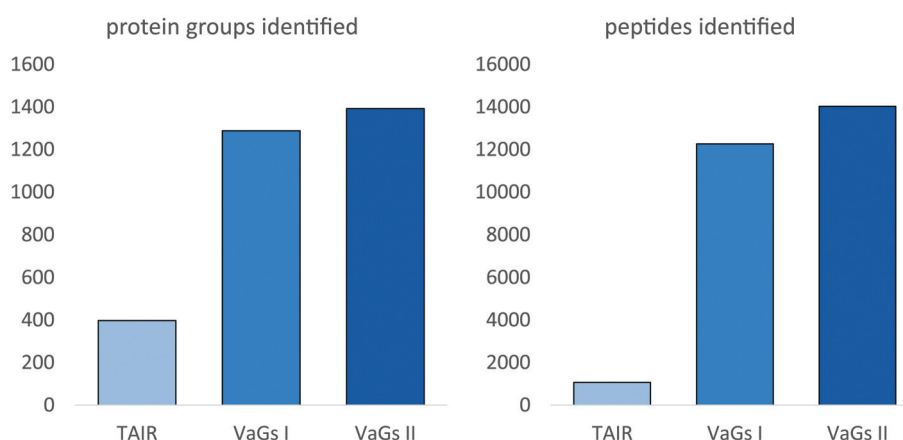
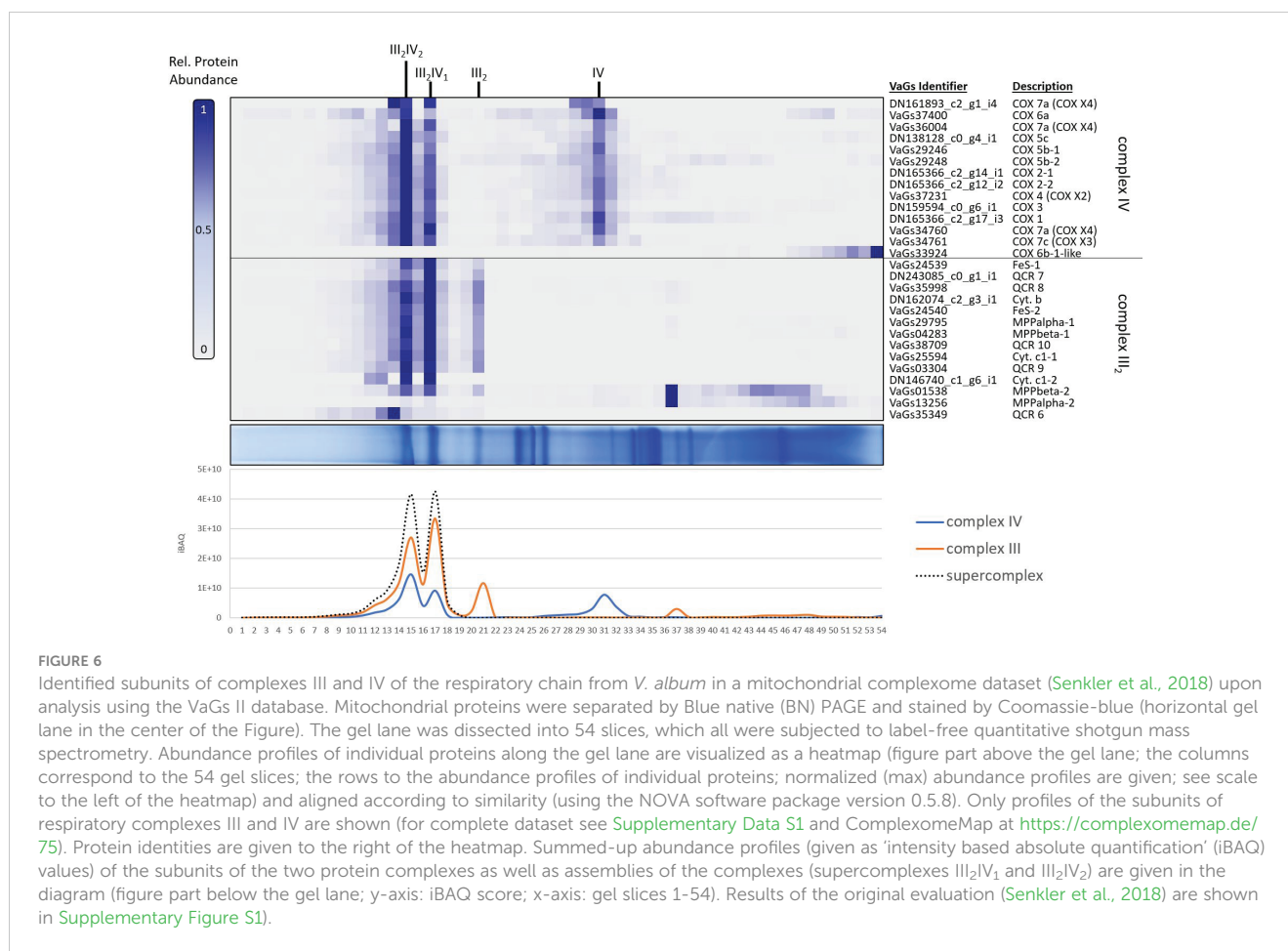


FIGURE 5

Number of identified proteins or peptides in a *V. album* mitochondrial complexome dataset upon data evaluation with TAIR, VaGs I and VaGs II. TAIR10: Arabidopsis protein database provided by The Arabidopsis thaliana Information resource (TAIR), Version 10 (<https://www.arabidopsis.org/>). The mitochondrial complexome dataset is derived from Senkler et al., 2018. The dataset was evaluated by TAIR10 (as in Senkler et al., 2018), VaGs I (Schröder et al., 2022b) and VaGs II (this study).



**FIGURE 6** Identified subunits of complexes III and IV of the respiratory chain from *V. album* in a mitochondrial complexome dataset (Senkler et al., 2018) upon analysis using the VaGs II database. Mitochondrial proteins were separated by Blue native (BN) PAGE and stained by Coomassie-blue (horizontal gel lane in the center of the Figure). The gel lane was dissected into 54 slices, which all were subjected to label-free quantitative shotgun mass spectrometry. Abundance profiles of individual proteins along the gel lane are visualized as a heatmap (figure part above the gel lane); the columns correspond to the 54 gel slices; the rows to the abundance profiles of individual proteins; normalized (max) abundance profiles are given; see scale to the left of the heatmap and aligned according to similarity (using the NOVA software package version 0.5.8). Only profiles of the subunits of respiratory complexes III and IV are shown (for complete dataset see Supplementary Data S1 and ComplexomeMap at <https://complexomemap.de/75>). Protein identities are given to the right of the heatmap. Summed-up abundance profiles (given as 'intensity based absolute quantification' (IBAQ) values) of the subunits of the two protein complexes as well as assemblies of the complexes (supercomplexes III<sub>2</sub>V<sub>1</sub> and III<sub>2</sub>V<sub>2</sub>) are given in the diagram (figure part below the gel lane; y-axis: IBAQ score; x-axis: gel slices 1-54). Results of the original evaluation (Senkler et al., 2018) are shown in Supplementary Figure S1.

(Supplementary Table 1) and is also accessible at the ComplexomeMap portal at <https://complexomemap.de/75>. It offers novel insights into the molecular biology of *V. album* mitochondria. Also, the number of peptides identified in the complexome fractions (gel slices) significantly increased based on VaGs II evaluation, resulting in a better coverage of proteins by peptides.

To further analyze the mitochondrial complexome from *V. album*, as revealed by VaGs II evaluation, we took a closer look at the protein clusters corresponding to respiratory chain complexes III and IV (Figure 6). Complex III is an ubiquinol:cytochrome-c oxidoreductase and complex IV a cytochrome-c:O<sub>2</sub> oxidoreductase. These two protein complexes catalyze the last two steps of the mitochondrial respiratory chain and were found to form two exceptionally stable supercomplexes in *V. album* mitochondria (Senkler et al., 2018). According to current knowledge (Maldonado et al., 2021), complexes III and IV in plants each consist of 10 different subunits (the 10 subunits of complex III, however, all are present in duplicate, as complex III occurs as a functional dimer). In *V. album*, this dimer (III<sub>2</sub>) associates with one or two copies of complex IV; the corresponding supercomplexes are designated III<sub>2</sub>V<sub>1</sub> and III<sub>2</sub>V<sub>2</sub>. Of the total 20 different proteins present in these supercomplexes, all 20 proteins were found in our complexome dataset upon evaluation using VaGs II (Figure 6; compared to only 8

proteins based on the original evaluation, Senkler et al., 2018; see Supplementary Figure S1). 18 of the identified subunits form part of the two supercomplexes, whereas two (QCR6 of complex III<sub>2</sub> and Cox6b from complex IV) are partly detached and migrate in the low-molecular-mass region of the blue native gel, probably because they became detached during membrane solubilization. For some of the proteins, different isoforms are present in *V. album* (e.g. the Cox5b and the  $\alpha$ - and  $\beta$ -MPP subunits, Supplementary Figures S2, S3). The summed-up abundance profiles of the subunits of complex III and of complex IV reveal that the amounts of the two supercomplexes are similar; furthermore, the stoichiometry of the two complexes within the supercomplexes is correctly revealed (Figure 6, bottom).

## Concluding remarks

We present here the *Viscum album* Gene Space database II, VaGs II. Based on our quantitative and qualitative evaluations, we assume that it covers well above 90% of the protein-coding genes of *V. album*. The database has been cleaned with respect to sequences from other organisms, particularly fungi that are known to colonize *V. album* leaves. The database contains 90,039 transcript sequences. In particular, the functional annotation of the sequences was

improved. Moreover, winter and summer samples of *V. album* were studied separately based on Illumina sequencing. Further analysis of these data should provide insights into adaptations of *V. album* to different seasons. VaGs II should provide an important data background useful for further studying the molecular biology of this extraordinary plant.

## Data availability statement

The new VaGs II database is available at <https://viscumalbum.pflanzenproteomik.de/>. In addition, fasta files of thenucleotide or protein sequences can be downloaded. All Illumina and PacBio sequencing datasets and their assembly dataset have been uploaded to the European Nucleotide Archive (ENA) and can be found under the study identifier PRJEB60149. Within this study, the PacBio dataset can be found under the identifiers ERR10970196 and ERR10970197, the Illumina summer dataset under ERR10968077 and the Illumina winter dataset under ERR10968073. The original mass spectrometry proteomics data (Senkler et al., 2018) have been deposited to the ProteomeXchange Consortium via the PRoteomics IDentifications database (PRIDE, Perez-Riverol et al., 2022) partner repository with the dataset identifier PXD008974. The re-evaluated dataset based on an evaluation using the new VaGs II database has been deposited additionally to the ProteomeXchange Consortium via PRIDE and is accessible under PXD041061.

## Author contributions

HPB, HK, and LS initiated and supervised the project. NH isolated mRNA from *V. album* organs. OR, AG, and LS carried out database development and data annotation. NR and LS re-evaluated complexome-profiling data using the new database. MS developed the web portal for the *V. album* Gene Space database. LS and HPB performed data evaluation and interpretation. LS and HPB wrote the manuscript. All authors contributed to the article and approved the submitted version.

## Funding

This research has been supported by the Deutsche Forschungsgemeinschaft, grant BR 1829/16-1, to HPB. The publication of this article was funded by the Open Access Fund of Leibniz Universität Hannover.

## Acknowledgments

Illumina sequencing was carried out by Novogene, Cambridge, UK.

## Conflict of interest

The authors declare that the research was conducted in the absence of any commercial or financial relationships that could be construed as a potential conflict of interest.

## Publisher's note

All claims expressed in this article are solely those of the authors and do not necessarily represent those of their affiliated organizations, or those of the publisher, the editors and the reviewers. Any product that may be evaluated in this article, or claim that may be made by its manufacturer, is not guaranteed or endorsed by the publisher.

## Supplementary material

The Supplementary Material for this article can be found online at: <https://www.frontiersin.org/articles/10.3389/fpls.2023.1193122/full#supplementary-material>

### SUPPLEMENTARY FIGURE 1

Identified subunits of complexes III and IV of the respiratory chain from *V. album* in a mitochondrial complexome dataset (Senkler et al., 2018) upon analysis using the Arabidopsis TAIR10 database (<https://www.arabidopsis.org/>). The same dataset was re-analyzed using the VaGs database (Figure 6).

### SUPPLEMENTARY FIGURE 2

Sequence alignment of *V. album* COX5b-1 and COX5b-2. The COX 5b subunit of the cytochrome c oxidase complex (Complex IV) is present in two isoforms, COX5b-1 and COX5b-2. The proteins are encoded by transcripts VaGs29248 and VaGs29246. Conserved amino acid positions are highlighted in blue. Both proteins form part of the III<sub>2</sub>IV and III<sub>2</sub>IV<sub>2</sub> supercomplexes in the mitochondrial complexome dataset (Figure 4 and Supplementary Data S1).

### SUPPLEMENTARY FIGURE 3

Identified pairs of isoforms of the two subunits of the mitochondrial processing peptidase (MPP) from *V. album* in a mitochondrial complexome dataset (Senkler et al., 2018) upon re-evaluation using the VaGs II database. Both, the  $\alpha$ - and the  $\beta$ -MPP subunits form part of the cytochrome c reductase complex (complex III) in plants (Braun, 2020). The  $\beta$ -subunit is encoded by transcripts VaGs01538 and VaGs04283; the  $\alpha$ -subunit by transcripts VaGs13256 and VaGs29795. The heatmap indicates the abundance profiles of the four proteins along a blue-native gel lane used for the complexome profiling analysis. The positions of complexes III and IV and their supercomplexes are indicated above the heatmap, the molecular masses of standard proteins below the heatmap. One isoform of the  $\alpha$ - and the  $\beta$ -subunit of MPP forms part of the III<sub>2</sub>IV and III<sub>2</sub>IV<sub>2</sub> supercomplexes, respectively. The other two isoforms seem to (partially) form a separate protein complex in the 110-160 kDa range, which might represent a soluble form of the heterodimeric MPP enzyme (detached from complex III). A soluble MPP enzyme has been described for mitochondrial matrix of animals and yeast (Braun and Schmitz, 1995), but possibly also occurs in *V. album*.

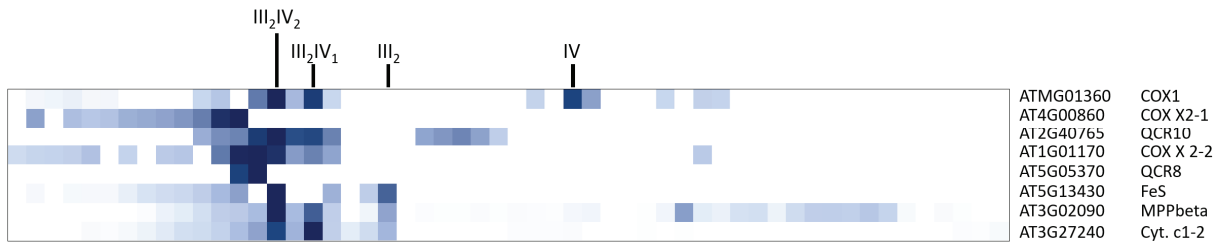
### SUPPLEMENTARY DATA SHEET 1

Heatmap of abundance profiles of the proteins included in the mitochondrial complexome dataset of *V. album* re-evaluated using the VaGs II database.

## References

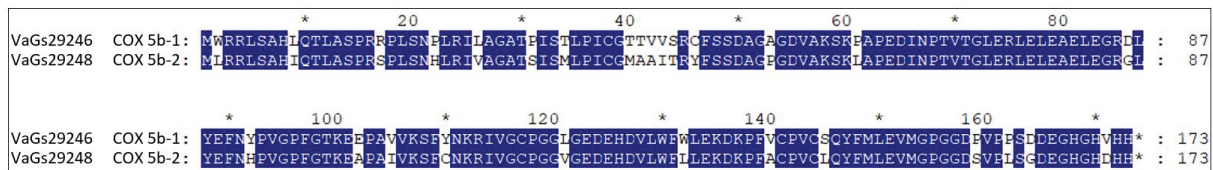
- Ariantari, N. P., Daletos, G., Mándi, A., Kurtán, T., Müller, W. E. G., Lin, W., et al. (2019). Expanding the chemical diversity of an endophytic fungus *Bulgaria inquinans*, an ascomycete associated with mistletoe, through an OSMAC approach. *RSC Adv.* 9 (43), 25119–25132. doi: 10.1039/C9RA03678D
- Azuma Ji, K. N. H., Heux, L., Vuong, R., and Chanzy, H. (2000). The cellulose system in viscum from mistletoe berries. *Cellulose* 7, 3–19. doi: 10.1023/A:1009223730317
- Bolger, A. M., Lohse, M., and Usadel, B. (2014). Trimmomatic: a flexible trimmer for illumina sequence data. *Bioinformatics* 30, 2114–2120. doi: 10.1093/bioinformatics/btu170
- Boutet, E., Lieberherr, D., Tognolli, M., Schneider, M., and Bairoch, A. (2007). “UniProtKB/Swiss-prot,” in *Plant bioinformatics, methods in molecular BiologyTM*. Ed. D. Edwards (Humana Press), 89–112.
- Braun, H. P. (2020). The oxidative phosphorylation system of the mitochondria in plants. *Mitochondrion* 53, 66–75. doi: 10.1016/j.mito.2020.04.007
- Braun, H. P., and Schmitz, U. K. (1995). The bifunctional cytochrome c reductase/processing peptidase complex from plant mitochondria. *J. Bioenerg Biomembr* 27 (4), 423–436. doi: 10.1007/BF02110005
- Giese, H., Ackermann, J., Heide, H., Bleier, L., Dröse, S., Wittig, I., et al. (2015). NOVA: a software to analyze complexome profiling data. *Bioinformatics* 31, 440–441. doi: 10.1093/bioinformatics/btu623
- Glatzel, G., and Geils, B. W. (2009). Mistletoe ecophysiology: host–parasite interactions. *Botany* 87, 10–15. doi: 10.1139/B08-096
- Haas, B. J., and Papanicolaou, A. *TransDecoder (Find coding regions within transcripts)*. Available at: <https://transdecoder.github.io/> (Accessed 3.30.17).
- Haas, B. J., Papanicolaou, A., Yassour, M., Grabherr, M., Blood, P. D., Bowden, J., et al. (2013). *De novo* transcript sequence reconstruction from RNA-seq using the trinity platform for reference generation and analysis. *Nat. Protoc.* 8, 1494–1512. doi: 10.1038/nprot.2013.084
- Hulsen, T., de Vlieg, J., and Alkema, W. (2008). BioVenn – a web application for the comparison and visualization of biological lists using area-proportional Venn diagrams. *BMC Genomics* 9, 488. doi: 10.1186/1471-2164-9-488
- Jäger, T., Holandino, C., Melo, M. N. O., Peñaloza, E. M. C., Oliveira, A. P., Garrett, R., et al. (2021). Metabolomics by UHPLC-Q-TOF reveals host tree-dependent phytochemical variation in *Viscum album* l. *Plants (Basel)* 10 (8), 1726. doi: 10.3390/plants10081726
- Kotan, R., Okutucu, A., Ala Görmez, A., Karagoz, K., Dadasoglu, F., Karaman, İ, et al. (2013). Parasitic bacteria and fungi on common mistletoe (*Viscum album* l.) and their potential application in biocontrol. *J. Phytopathol.* 161, 165–171. doi: 10.1111/jph.12048
- Krasylenko, Y., Sosnovsky, Y., Atamas, N., Popov, G., Leonenko, V., Janošiková, K., et al. (2020). The European mistletoe (*Viscum album* l.): distribution, host range, biotic interactions, and management worldwide with special emphasis on Ukraine. *Botany* 98 (9), 499–516. doi: 10.1139/cjb-2020-0037
- Li, W., and Godzik, A. (2006). Cd-hit: a fast program for clustering and comparing large sets of protein or nucleotide sequences. *Bioinforma. Oxf. Engl.* 22, 1658–1659. doi: 10.1093/bioinformatics/btl158
- Macleay, A. E., Hertle, A. P., Ligas, J., Bock, R., Balk, J., and Meyer, E. H. (2018). Absence of complex I is associated with diminished respiratory chain function in European mistletoe. *Curr. Biol.* 28 (10), 1614–1619.e3. doi: 10.1016/j.cub.2018.03.036
- Maldonado, M., Guo, F., and Letts, J. A. (2021). Atomic structures of respiratory complex III<sub>2</sub>, complex IV, and supercomplex III<sub>2</sub>-IV from vascular plants. *eLife* 10, e62047. doi: 10.7554/eLife.62047
- Nazaruk, J., and Orlikowski, P. (2016). Phytochemical profile and therapeutic potential of viscum album l. *Nat. Prod Res.* 30 (4), 373–385. doi: 10.1080/14786419.2015.1022776
- Nolte, H., MacVicar, T. D., Tellkamp, F., and Krüger, M. (2018). Instant clue: a software suite for interactive data visualization and analysis. *Sci. Rep.* 8, 12648. doi: 10.1038/s41598-018-31154-6
- Novák, P., Guignard, M. S., Neumann, P., Kelly, L. J., Mlinarec, J., Kobližková, A., et al. (2020). Repeat-sequence turnover shifts fundamentally in species with large genomes. *Nat. Plants.* 6 (11), 1325–1329. doi: 10.1038/s41477-020-00785-x
- Patro, R., Duggal, G., Love, M. I., Irizarry, R. A., and Kingsford, C. (2017). Salmon provides fast and bias-aware quantification of transcript expression. *Nat. Methods* 14, 417–419. doi: 10.1038/nmeth.4197
- Perez-Riverol, Y., Bai, J., Bandla, C., Hewapathirana, S., García-Seisdedos, D., Kamatchinathan, S., et al. (2022). The PRIDE database resources in 2022: a hub for mass spectrometry-based proteomics evidences. *Nucleic Acids Res.* 50 (D1), D543–D552. doi: 10.1093/nar/gkab1038
- Peršoh, D., Melcher, M., Flessa, F., and Rambold, G. (2010). First fungal community analyses of endophytic ascomycetes associated with viscum album ssp. *austriacum* its Host *Pinus sylvestris*. *Fungal Biol.* 114 (7), 585–596. doi: 10.1016/j.funbio.2010.04.009
- Petersen, G., Cuenca, A., Möller, I. M., and Seberg, O. (2015a). Massive gene loss in mistletoe (*Viscum, viscaceae*) mitochondria. *Sci. Rep.* 5, 17588. doi: 10.1038/srep17588
- Petersen, G., Cuenca, A., and Seberg, O. (2015b). Plastome evolution in hemiparasitic mistletoes. *Genome Biol. Evol.* 7 (9), 2520–2532. doi: 10.1093/gbe/evv165
- Schröder, L., Eubel, H., and Braun, H. P. (2022c). Complexome profiling of plant mitochondrial fractions. *Methods Mol. Biol.*; 2363, 101–110. doi: 10.1007/978-1-0716-1653-6\_9
- Schröder, L., Hegermann, J., Pille, P., and Braun, H. P. (2022a). The photosynthesis apparatus of European mistletoe (*Viscum album*). *Plant Physiol.* 190 (3), 1896–1914. doi: 10.1093/plphys/kiac377
- Schröder, L., Hohnjec, N., Senkler, M., Senkler, J., Küster, H., and Braun, H. P. (2022b). The gene space of European mistletoe (*Viscum album*). *Plant J.*; 109 (1), 278–294. doi: 10.1111/tj.15558
- Schröder, L., Senkler, J., and Braun, H. P. (2020). “Special features of cellular respiration in viscum album,” in *Die mistel in der tumortherapie* 5. Eds. R. Scheer, et al (Essen: KVC Verlag), pp 3–pp13.
- Schwanhäusser, B., Busse, D., Li, N., Dittmar, G., Schuchhardt, J., Wolf, J., et al. (2011). Global quantification of mammalian gene expression control. *Nature.* 473 (7347), 337–342. doi: 10.1038/nature11848
- Senkler, J., Rugen, N., Eubel, H., Hegermann, J., and Braun, H. P. (2018). Absence of complex I implicates rearrangement of the respiratory chain in European mistletoe. *Curr. Biol.* 28 (10), 1606–1613.e4. doi: 10.1016/j.cub.2018.03.050
- Seppy, M., Manni, M., and Zdobnov, E. M. (2019). “BUSCO: assessing genome assembly and annotation completeness,” in *Gene prediction. methods in molecular biology*, vol. 1962. Ed. M. Kollmar (New York, NY: Humana), 2019. doi: 10.1007/978-1-4939-9173-0\_14
- Skippington, E., Barkman, T. J., Rice, D. W., and Palmer, J. D. (2015). Miniaturized mitogenome of the parasitic plant viscum scurruloideum is extremely divergent and dynamic and has lost all nad genes. *Proc. Natl. Acad. Sci. U S A.* 112 (27), E3515–E3524. doi: 10.1073/pnas.1504491112
- Skippington, E., Barkman, T. J., Rice, D. W., and Palmer, J. D. (2017). Comparative mitogenomics indicates respiratory competence in parasitic viscum despite loss of complex I and extreme sequence divergence, and reveals horizontal gene transfer and remarkable variation in genome size. *BMC Plant Biol.* 17 (1), 49. doi: 10.1186/s12870-017-0992-8
- The UniProt Consortium, Bateman, A., Martin, M.-J., Orchard, S., Magrane, M., Ahmad, S., et al. (2023). UniProt: the universal protein knowledgebase in 2023. *Nucleic Acids Res.* 51, D523–D531. doi: 10.1093/nar/gkac1052
- Urech, K., and Baumgartner, S. (2015). “Chemical constituents of viscum album l: implications for the pharmaceutical preparation of mistletoe,” in *Mistletoe: from mythology to evidence-based medicine*, vol. 4. Eds. K. S. Zänker and S. V. Kaveri (Transl. Res. Biomed. Basel, Karger), pp 11–pp 23. doi: 10.1159/000375422
- Zonneveld, B. J. M. (2010). New record holders for maximum genome size in eudicots and monocots. *J. Bot.* 2010, 527357, 4. doi: 10.1155/2010/527357

Supp. Fig. 1



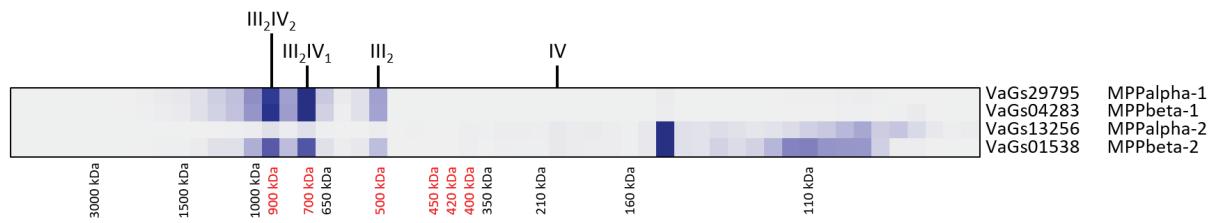
Supp. Fig. S1: Identified subunits of complexes III and IV of the respiratory chain from *V. album* in a mitochondrial complexome dataset (Senkler et al. 2018) upon analysis using the Arabidopsis TAIR10 database (<https://www.arabidopsis.org/>). The same dataset was re-analyzed using the VaGs database (Fig. 6)

Supp. Figure 2



Supp. Figure S2: Sequence alignment of *V. album* COX5b-1 and COX5b-2. The COX 5b subunit of the cytochrome c oxidase complex (Complex IV) is present in two isoforms, COX5b-1 and COX5b-2. The proteins are encoded by transcripts VaGs29248 and VaGs29246. Conserved amino acid positions are highlighted in blue. Both proteins form part of the III<sub>2</sub>IV and III<sub>2</sub>IV<sub>2</sub> supercomplexes in the mitochondrial complexome dataset (Fig. 6 and Supp. data S1).

### Supp. Figure S3



**Supp. Figure S3:** Identified pairs of isoforms of the two subunits of the mitochondrial processing peptidase (MPP) from *V. album* in a mitochondrial complexome dataset (Senkler et al. 2018) upon re-evaluation using the VaGs II database. Both, the  $\alpha$ - and the  $\beta$ -MPP subunits form part of the cytochrome c reductase complex (complex III) in plants (Braun 2020). The  $\beta$ -subunit is encoded by transcripts VaGs01538 and VaGs04283; the  $\alpha$ -subunit by transcripts VaGs13256 and VaGs29795. The heatmap indicates the abundance profiles of the four proteins along a blue-native gel lane used for the complexome profiling analysis. The positions of complexes III and IV and their supercomplexes are indicated above the heatmap, the molecular masses of standard proteins below the heatmap. One isoform of the  $\alpha$ - and the  $\beta$ -subunit of MPP forms part of the  $\text{III}_2\text{IV}$  and  $\text{III}_2\text{IV}_2$  supercomplexes, respectively. The other two isoforms seem to (partially) form a separate protein complex in the 110-160 kDa range, which might represent a soluble form of the heterodimeric MPP enzyme (detached from complex III). A soluble MPP enzyme has been described for mitochondrial matrix of animals and yeast (Braun and Schmitz 1995), but possibly also occurs in *V. album*.



### 3 Appendix

## Danksagung

Lieber Hans-Peter, danke, dass ich bei dir meine Masterarbeit und im Anschluss auch meine Doktorarbeit in dieser großartigen Abteilung schreiben durfte. Das Thema Mistel begleitet mich nun schon so lange, dass es mich wahrscheinlich nie wieder richtig loslassen wird. Auch möchte ich mich für die Möglichkeit, an der ICPMB in Malmö und an der Mistelkonferenz teilnehmen zu dürfen, bedanken. Die Betreuung war super und es war klasse, dich als meinen Doktorvater haben zu dürfen.

Prof. Dr. Thomas Pfannschmidt möchte ich dafür danken sich als mein Korreferent zur Verfügung gestellt zu haben.

Prof. Dr. Helge Küster möchte ich für die tolle Beratung rund ums Thema Genetik und für das zur Verfügung stellen als Korreferent danken.

Ich möchte der gesamten Arbeitsgruppe für die Unterstützung und die schöne Zeit danken.

Insbesondere möchte ich meinen Bürokollegen, die mir immer mit Rat und Tat zur Seite standen, danken. Insgesamt waren wir ein perfekt zusammengestelltes Büro mit drei Experten in jedem Bereich.

Cecile, danke für die großartige Zeit. Zusammen haben wir so viel erlebt: während der Zeit in Schweden, beim Fossilien suchen, auf dem Weihnachtsmarkt, auf der Pflanzenmesse etc.. Du warst immer hilfsbereit und hattest ein offenes Ohr. Die Zeit ohne dich im Büro wird eine große Umstellung, aber ich bin mir sicher, dass du auch in Köln eine gute Zeit haben wirst.

Nils, danke für die gute Beratung zum Thema MS und Probenauswertung, die Gespräche über die neuesten Spiele und dass du mir immer geholfen hast die Süßigkeiten leer zu bekommen.

Jenni, danke für die Betreuung und deine Freundschaft. Bereits während meiner Masterarbeit warst du meine Betreuerin und standest mir immer zur Seite. Ich schätze die Freundschaft mit dir sehr und hoffe mit dir noch sehr oft zur Steine- und Pflanzenmesse gehen zu können.

Christa, danke für die Unterstützung beim Ernten der Misteln, für die unzähligen Sachen die du im Labor für mich gemacht hast und die netten Gespräche.

Michael, danke für die Unterstützung der Datenbank Entwicklung und für das Programmieren verschiedener Tools (Fasta Excel Konverter, pl und Mw calculator und vieles mehr). Ohne dich hätte es wahrscheinlich noch Monate oder Jahre länger gedauert.

Marianne, danke für den Verdau von wer weiß wie vielen Proben.

Holger, danke für die Hilfe bei der Auswertung und Interpretation der MS Daten.

Abschließend möchte ich mich noch bei meinen Eltern für die Unterstützung während meines gesamten Studiums bedanken. Besonders in stressigen Phasen waren sie mein Anker und haben mir Kraft und Zuversicht gegeben.

## 3.1 Curriculum Vitae

### Personal Details

Name: Lucie Schröder  
Date of Birth: March 10, 1993  
Place of Birth: Rathenow, Germany  
Citizenship: German

### School Education

2006-2012 Gymnasium Rathenow  
Abitur, grade: 1.9  
1999-2005 Grundschule Rathenow

### Academic Education

Since October 2018 PhD student  
Institute of Plant Genetics  
Plant Proteomics Department  
Leibniz University Hannover  
Prof. Dr. Hans-Peter Braun

10/2015-03/2018 Master of Science "Plant biotechnology", grade: 1.3  
Leibniz University Hannover, Germany  
Thesis: "Untersuchungen zum oxidativen Phosphorylierungssystem der Mistel (Viscum album)"

04/2017-09/2017 Studies of Biology at Northeastern University of Boston, Massachusetts, US, in the frame of an exchange program with Leibniz University Hannover, Support by a DAAD scholarship

10/2012-09/2015 Bachelor of Science "Plant biotechnology", grade: 2.4  
Leibniz University Hannover, Germany  
Thesis: "Spektrale Untersuchungen von Mikroalgen zur Etablierung einer Kultur in Gewächshausbedachungsmaterialien"

## 3.2 List of Publications

- Schröder L, Rupp O, Senkler M, Rugen N, Hohnjec N, Goesmann A, Küster H, Braun HP (2023)  
The *Viscum album* Gene Space database  
Frontiers in Plant Science, 14  
<https://doi.org/10.3389/fpls.2023.1193122>
- Schröder L, Hohnjec N, Senkler M, Senkler J, Küster H, Braun HP (2022)  
The gene space of European mistletoe (*Viscum album*).  
Plant Journal, 109(1) 278-294  
<https://doi.org/10.1111/tpj.15558>
- Schröder L, Eubel H, Braun HP (2022)  
Complexome Profiling of Plant Mitochondrial Fractions.  
Methods in Molecular Biology, 2363, 101-110  
[https://doi.org/10.1007/978-1-0716-1653-6\\_9](https://doi.org/10.1007/978-1-0716-1653-6_9)
- Schröder L, Hegermann J, Pille P, Braun HP (2022):  
The photosynthesis apparatus of European mistletoe (*Viscum album*)  
Plant Physiology, 190(3), 1896–1914  
<https://doi.org/10.1093/plphys/kiac377>  
First Author Profile Lucie Schröder published at:  
<https://plantae.org/lucie-schroder-plant-physiology-first-author/>
- Schröder L, Senkler J, Braun, H.P. (2020)  
Special features of cellular respiration in *Viscum album*.  
In: Die Mistel in der Tumortherapie 5, Scheer R, et al. (eds.), KVC Verlag, Essen, pp 3-13.  
ISBN: 978-3-96562-030-8
- Schröder L, Fachinger S, Senkler J, Braun, H.P. (2020)  
Composition of the leaf proteome in *Viscum album*.  
In: Die Mistel in der Tumortherapie 5, Scheer R, et al. (eds.), KVC Verlag, Essen, pp 15-17.  
ISBN: 978-3-96562-030-8

### 3.3 Conference abstracts

- Schröder L, Senkler J, Braun HP (2019)  
Special features of cellular respiration in *Viscum album*.  
Phytomedicine, 61  
<https://doi.org/10.1016/j.phymed.2019.09.097>
- Schröder L, Fachinger S, Senkler J, Braun HP (2019)  
Composition of the leaf proteome in *Viscum album*.  
Phytomedicine, 61  
<https://doi.org/10.1016/j.phymed.2019.09.113>

### 3.4 Poster Presentations

- **12<sup>th</sup> International Conference for Plant Mitochondrial Biology (ICPMB)**  
May 22- 27, 2022, Malmö (Sweden)  
Lucie Schröder, Nils Rugen, Jennifer Senkler and Hans-Peter Braun:  
“New insights into the mitochondrial complexome of *Viscum album*”
- **Perspectives in Bioenergetics**  
September 08-10, 2021, (online)  
Lucie Schröder, Jennifer Senkler and Hans-Peter Braun:  
“New Insights into the Oxidative Phosphorylation System of European Mistletoe (*Viscum album*)”
- **7<sup>th</sup> Mistelsymposium**  
November 07-09, 2019, Nonnweiler (Germany)  
Lucie Schröder, Sara Fachinger, Jennifer Senkler and Hans-Peter Braun:  
“Composition of the leaf proteome in *Viscum album*”